

Evaluation of the Candidate High-Level Radioactive Waste Repository at Yucca Mountain Using Total System Performance Assessment

Phase 5

Technical Report

Main-70

Evaluation of the Candidate High-Level Radioactive Waste Repository at Yucca Mountain Using Total System Performance Assessment

Phase 5

1000802

Final Report, November 2000

**EPRI Project Managers
J. Kessler
T. Doering**

DISCLAIMER OF WARRANTIES AND LIMITATION OF LIABILITIES

THIS DOCUMENT WAS PREPARED BY THE ORGANIZATION(S) NAMED BELOW AS AN ACCOUNT OF WORK SPONSORED OR COSPONSORED BY THE ELECTRIC POWER RESEARCH INSTITUTE, INC. (EPRI). NEITHER EPRI, ANY MEMBER OF EPRI, ANY COSPONSOR, THE ORGANIZATION(S) BELOW, NOR ANY PERSON ACTING ON BEHALF OF ANY OF THEM:

(A) MAKES ANY WARRANTY OR REPRESENTATION WHATSOEVER, EXPRESS OR IMPLIED, (I) WITH RESPECT TO THE USE OF ANY INFORMATION, APPARATUS, METHOD, PROCESS, OR SIMILAR ITEM DISCLOSED IN THIS DOCUMENT, INCLUDING MERCHANTABILITY AND FITNESS FOR A PARTICULAR PURPOSE, OR (II) THAT SUCH USE DOES NOT INFRINGE ON OR INTERFERE WITH PRIVATELY OWNED RIGHTS, INCLUDING ANY PARTY'S INTELLECTUAL PROPERTY, OR (III) THAT THIS DOCUMENT IS SUITABLE TO ANY PARTICULAR USER'S CIRCUMSTANCE; OR

(B) ASSUMES RESPONSIBILITY FOR ANY DAMAGES OR OTHER LIABILITY WHATSOEVER (INCLUDING ANY CONSEQUENTIAL DAMAGES, EVEN IF EPRI OR ANY EPRI REPRESENTATIVE HAS BEEN ADVISED OF THE POSSIBILITY OF SUCH DAMAGES) RESULTING FROM YOUR SELECTION OR USE OF THIS DOCUMENT OR ANY INFORMATION, APPARATUS, METHOD, PROCESS, OR SIMILAR ITEM DISCLOSED IN THIS DOCUMENT.

ORGANIZATION(S) THAT PREPARED THIS DOCUMENT

Risk Engineering, Inc.

ORDERING INFORMATION

Requests for copies of this report should be directed to the EPRI Distribution Center, 207 Coggins Drive, P.O. Box 23205, Pleasant Hill, CA 94523, (800) 313-3774.

Electric Power Research Institute and EPRI are registered service marks of the Electric Power Research Institute, Inc. EPRI. ELECTRIFY THE WORLD is a service mark of the Electric Power Research Institute, Inc.

Copyright © 2000 Electric Power Research Institute, Inc. All rights reserved.

CITATIONS

This report was prepared by

Risk Engineering, Inc.
4155 Darley Avenue, Suite A
Boulder, Colorado 80303

Principal Investigators

J. Vlasity
R. McGuire

Authors

J. Kessler, EPRI, Inc.
T. Doering, EPRI, Inc.
J. Vlasity, Risk Engineering, Inc.
R. McGuire, Risk Engineering, Inc.
A. Long, University of Arizona
S. Childs, Kennedy Jenks, Inc.
B. Ross, Disposal Safety, Inc.
F. Schwartz, Ohio State University
D. Shoesmith, University of Western Ontario
J. Massari, Constellation Nuclear Services, Inc.
W. Zhou, Monitor Scientific, LLC.
M. Stenhouse, Monitor Scientific, LLC.
M. Apted, Monitor Scientific, LLC.
E. Sudicky, Groundwater Simulations Group
M. Sheridan, State University of New York at Buffalo

This report describes research sponsored by EPRI.

The report is a corporate document that should be cited in the literature in the following manner:

Evaluation of the Candidate High-Level Radioactive Waste Repository at Yucca Mountain Using Total System Performance Assessment: Phase 5, EPRI, Palo Alto, CA: 2000. 1000802.

REPORT SUMMARY

A successful license application for the candidate spent-fuel and high level waste (HLW) repository at Yucca Mountain depends on a robust demonstration of long-term safety. This report presents EPRI's independent review to identify any conservatisms in the U.S. DOE's Phase 5 Yucca Mountain Total System Performance Assessment (TSPA). The review specifically identifies key facility components, makes recommendations regarding technical development work priorities, and evaluates overall technical suitability of the candidate HLW disposal facility. The report also describes a number of new models used in the TSPA. The information in this Phase 5 TSPA report provides valuable insight in defining important barriers to radionuclide release and the anticipated travel time to the accessible environment, once a release is assumed. Health impacts from such releases are estimated to remain small at all times in the future.

Background

Both regulations limiting the negative impacts of the potential HLW repository as well as the current site recommendation process require a quantitative assessment of total performance. The iterative TSPA process can most wisely be used to refine models and improve databases in order to reduce conservatisms and/or uncertainties. When applied in this manner, the TSPA can guide the allocation of future resources toward repository system components with the greatest impact on overall performance and away from components not affecting performance. The EPA and NRC are issuing new "risk-based" evaluation criteria mandating that applicants show the importance of each system and subsystem used to demonstrate compliance to the EPA's accessible environment standard dose regulations. The Phase 5 TSPA continues to play a crucial role in the compliance demonstration and development of the associated safety case for Yucca Mountain.

Objective

To provide an independent technical review investigating whether or not the DOE's TSPA can be considered conservative and to identify any related technical issues.

Approach

The technical approach includes a number of basic tools—TSPA, Defense-in-Depth, and definition of uncertainties. Through definition of the primary radionuclide barrier, a TSPA helps in understanding the total system and individual component performance contribution. The evaluation reported in this document is based on the DOE's Site Recommendation Characteristics Report (SRCR) design, which includes a "line-loading" of HLW packages in the emplacement drifts to allow the drifts to be spread apart. The drift separation provides a shedding zone where mobilized moisture can drain. The SRCR design has added a number of other new features, such as waste package spacing of 0.10 m, waste packaging with an outer shell of alloy 22, a waste package pallet also made of alloy 22, a titanium drip shield to preclude dripping water on the waste package, an inverted material designed so that moisture will pass through it, and a non-continuous drift support system.

Results

This report presents the results of EPRI's independent technical review of the proposed DOE SRCR design. The EPRI TSPA includes new models based largely on the most recent DOE design for the repository and partially on analysis and process model reports produced for DOE. The new models presented here consider, for example, the combination of drip shield, waste container, and cladding failure that accounts for the new drip shield and container material. One model in particular—EPRI's Integrated Multiple Assumptions and Release Code (IMARC)—has been used to identify key technical components of the Yucca Mountain facility and develop a series of evaluation cases for assumed release scenarios. Also included is a new model of the effect of hydrothermal activity and heterogeneous groundwater flow in the unsaturated zone on internal waste package temperatures as well as the distribution of groundwater capable of dripping into the repository drifts. These changes affect the basic way in which performance calculations are made.

The IMARC-5 calculational cases for the most probable release scenario focus on a dose rate end point calculated over time scales that exceed the time of peak release into the biosphere on the order of several hundred thousand years. This report compares these calculational cases with up-to-date results from the DOE and other government agencies and makes recommendations with respect to the priority of possible design modifications, data collection, and site characterization activities. In addition, the report discusses what constitutes an appropriate safety strategy, reviews the most recent DOE repository safety strategy, illustrates how to develop a safety case for multiple barriers to release, and identifies alternative performance indicators for the repository.

EPRI Perspective

EPRI believes there is much merit to the current repository design compared to the design in place at the time of the Viability Assessment two years ago. EPRI still recommends a balanced approach, with natural and engineered systems working in tandem to demonstrate regulatory compliance. DOE also needs to improve computer modeling of the natural system. The incorporation of another engineered barrier—in this case a titanium drip shield—significantly diminishes the impact of large uncertainty in the amount and distribution of groundwater flow at the repository horizon and increases confidence that doses during the first 10,000 years will remain low. The change of the waste package design was another significant improvement to enhance performance and reduce uncertainty. Overall, EPRI expects that Yucca Mountain will prove itself a suitable spent-fuel and HLW repository, measured against a variety of potential performance criteria. Yucca Mountain development should continue and a license application should be prepared. Related EPRI research includes Yucca Mountain Total System Performance Assessment, Phase 3 (TR-107191) and Alternative Approaches to Assessing the Performance and Suitability of Yucca Mountain for Spent Fuel Disposal (TR-108732).

Keywords

Yucca mountain

High level radioactive wastes

Total system performance assessment

Licensing strategy

CONTENTS

1 INTRODUCTION	1-1
1.1 References	1-4
2 CLIMATOLOGY	2-1
2.1 Introduction.....	2-1
2.1.1 Objectives	2-1
2.1.2 Current Climate at Yucca Mountain.....	2-1
2.1.2 Future Climate at Yucca Mountain Proposed in ANL-NBS-HS-000032 Rev 00 (June 2000).....	2-2
2.2 Discussion of Proposed Future Yucca Mountain Climates in ANL-NBS-HS-000032 Rev 00 (June 2000) and Suggested Alternatives.....	2-2
2.2.1 The “Modern” Climate State	2-2
2.2.1.1 “Monsoon” Conditions.....	2-4
2.2.1.2 Suggested Alternative to “Monsoon” Climate	2-4
2.2.2 Glacial Transition	2-5
2.3 Discussion of ANL-NBS-HS-000032 Rev 00 (June 2000)	2-5
2.3.1 Relevance of Analog Sites to Future Climate	2-6
2.4 Conclusions from the Analysis of the Climate Change Analysis Model Reports.....	2-6
2.5 Implications for the IMARC Code.....	2-6
2.6 References	2-7
3 NET INFILTRATION	3-1
3.1 Introduction.....	3-1
3.1.1 Net Infiltration Calculations at Yucca Mountain.....	3-1
3.1.2 Current Yucca Mountain Project Activity.....	3-1
3.1.3 Objectives	3-3
3.2 Recent Developments in Net Infiltration Modeling.....	3-3
3.2.1 Available Data and Calculations	3-3
3.2.2 Review of Net Infiltration Analysis/Modeling Reports.....	3-3

3.2.2.1 AMR: Future Climate Analysis [USGS 2000b]	3-3
3.2.2.2 AMR: Simulation of Net Infiltration for Modern and Potential Future Climates [USGS 2000a]	3-4
3.2.2.3 AMR: Analysis of Infiltration Uncertainty [CRWMS M&O 2000a].....	3-7
3.2.2.4 Effect of Model Assumptions on Net Infiltration Results	3-8
3.3 EPRI Net Infiltration Calculations	3-9
3.4 Summary	3-10
3.5 References	3-11

4 COUPLED PROCESSES AFFECTING GROUNDWATER DISTRIBUTION AND ROCK	4-1
4.1 Introduction.....	4-1
4.1.1 Near-Field Thermohydrology Introduction	4-1
4.1.2 IMARC5 Inputs.....	4-3
4.1.3 DOE Models.....	4-7
4.1.3.1 Water Drainage and the “Active Fracture” Model	4-8
4.1.3.2 Mountain-Scale Convection	4-9
4.1.3.2.1 Why Mountain-Scale Convection should be Addressed	4-9
4.1.3.2.2 Proposed Modeling Approach	4-11
4.1.3.3 Scanning Curves	4-12
4.1.3.3.1 Description of the Scanning Curve Method	4-12
4.1.3.3.2 Alternative Modeling Approach.....	4-13
4.1.4 Thermohydrology Model Conservatism	4-15
4.1.4.1 Mathematical Stability of DOE’s Models	4-15
4.1.4.2 Conservatism and Non-Conservatism of Assumptions	4-17
4.1.4.2.1 Assumptions Conservative for Temperature and not for Moisture	4-17
4.1.4.2.2 Assumptions Conservative with Respect to Moisture but not Temperature	4-18
4.1.4.2.3 Assumptions for which More Work is Needed to Evaluate Conservatism.....	4-18
4.1.5 Thermohydrology Conclusions and Recommendations.....	4-19
4.2 Near Field Coupled Process Modeling, T-H-C	4-20
4.2.1 Introduction	4-20
4.2.2 The DOE’s Model on Coupled THC Processes	4-22
4.2.2.1 Important Near-Field Processes and Issues	4-22
4.2.2.2 Treatment of Coupling among Processes	4-23

4.2.2.3 Modeling of the Fracture Hydrology System	4-25
4.2.2.4 Modeling of the Chemical System.....	4-25
4.2.2.5 Issue of Spatial Heterogeneity	4-28
4.2.3 Conclusions	4-28
4.3 References	4-29
5 ENGINEERED BARRIER SYSTEM DEGRADATION.....	5-1
5.0 Introduction.....	5-1
5.1 Changes in Waste Package Design since IMARC Phase 4	5-1
5.2 General and Localized Corrosion Modelling Features.....	5-6
5.3 Drip Shield Corrosion.....	5-10
5.4 Waste Package Corrosion	5-17
5.4.1 General Corrosion.....	5-17
5.4.2 Localized Corrosion.....	5-20
5.4.3 Stress Corrosion Cracking.....	5-24
5.5 EBS Corrosion Modeling Input to IMARC5.....	5-31
5.6 Cladding Corrosion	5-35
5.7 References	5-39
6 RADIONUCLIDE MOBILIZATION AND RELEASE FROM THE ENGINEERED BARRIER SYSTEM	6-1
6.1 Review of M&O's Source-Term Model	6-1
6.1.1 M&O's Source-Term.....	6-3
6.1.2 EPRI's Source Term.....	6-7
6.1.3 Comparison of Source-Term Models.....	6-9
6.1.4 Conclusions	6-11
6.2 COMPASS2000: Source-Term Code for EPRI	6-11
6.2.1 New Compartment System.....	6-12
6.2.2 Retention by Barriers to Illustrate "Defense-in-Depth"	6-14
6.2.3 Incorporation of Cladding Degradation Data.....	6-16
6.2.4 EBS Transport Parameters	6-21
Waste Compartment.....	6-21
Corrosion Product Compartment	6-22
Corroded Metal Canister	6-22
Invert	6-22

Diffusion Lengths.....	6-22
6.3 Provision of Solubilities for Key Radioelements	6-23
6.3.1 Background.....	6-23
6.3.2 Geochemical Environment	6-24
6.3.2.1 Aqueous Phase	6-24
6.3.3 Solubility of Radioelements	6-25
6.3.3.1 Conceptual Model.....	6-25
6.3.3.2 The Role of Coprecipitation	6-26
6.3.3.3 Recommendations of Solubility Limits.....	6-26
6.4 Sorption of Radioelements on Corrosion Products from Waste Package Internals	6-29
6.4.1 Background.....	6-29
6.4.2 Geochemical Environment Relevant to Waste Package Internals	6-30
6.4.2.1 Corrosion Products - Solid Phase	6-31
6.4.2.2 Aqueous Phase	6-31
6.4.3 Sorption of Radionuclides on Corrosion Products	6-32
6.4.3.1 Conceptual Model.....	6-32
6.4.3.2 Mechanisms for Sorption on Iron (Hydr)oxides	6-32
6.4.3.3 Recommendations of Specific K_d Values	6-33
6.4.3.4 Other Considerations Relevant to Sorption on Corrosion Products.....	6-35
6.4.3.5 Iron Oxyhydroxides as Colloids.....	6-36
6.5 References	6-36
7 UNSATURATED ZONE AND SATURATED ZONE FLOW AND TRANSPORT	7-1
7.1 Description of the SZ Simulation Domain.....	7-1
7.2 Geologic Constraints on Flow in the SZ	7-2
7.2.1 Geologic Variability.....	7-2
7.2.2 Concept of a Flowing Interval	7-3
7.2.3 EPRI Approach to Modeling the Flowing Intervals.....	7-4
7.3 Modifications to the SZ Flow and Transport Code.....	7-6
7.3.1 Verification of the Modified SZ Code	7-6
7.4 Design of Simulation Trials	7-8
7.5 Sensitivity Analyses	7-10
7.5.1 Variation in the Diffusion Coefficient in the Volcanic Aquifer.....	7-11
7.5.2 Variation in the Size of the Rock Blocks	7-13
7.5.3 Fraction of the Total Section that is Flowing	7-15

7.5.4 Changes to the Boundary Between Volcanic and Alluvial Aquifers.....	7-16
7.5.5 Small Source Dispersion – Single Realization	7-17
7.5.6 Changes in the Vertical Transverse Dispersion Coefficient	7-19
7.5.7 Controls on Maximum Concentration	7-22
7.6 Simulation Parameters for IMARC Runs.....	7-25
7.7 Conservatism in the Concept of a Flowing Interval	7-25
7.7.1 Implications	7-26
7.8 References	7-26
8 BIOSPHERE	8-1
8.1 Introduction.....	8-1
8.2 Biosphere Model Used as Input to the IMARC-5 Calculations.....	8-1
8.3 References	8-8
9 VOLCANISM.....	9-1
9.1 Introduction.....	9-1
9.2 Magma Intrusion Scenario	9-1
9.3 Scenario Evaluation.....	9-1
9.3.1 Analog Sites.....	9-1
9.3.2 Magma Composition	9-2
9.3.3 Dike Intrusion	9-3
9.3.4 Dike Geometry	9-3
9.3.5 Dike Contact Temperature	9-4
9.3.6 Magma Pressure within the Dike	9-5
9.3.7 Rift-Related Eruptions	9-5
9.3.8 Eruption Style.....	9-5
9.4 Conclusion.....	9-6
9.5 References	9-7
10 IMPLEMENTATION OF SUBSYSTEM MODELS INTO THE IMARC-5 CODE	10-1
10.1 Introduction.....	10-1
10.2 Discussion of the Implementation	10-2
Future Climate Change and Net Infiltration	10-2
Focused Flow Factors.....	10-3
Solubility and Alteration Rate	10-3

Matrix Retardation.....	10-3
Waste Container Failures.....	10-4
Fractions of Repository 'Wet'	10-5
Source Term	10-6
Repository Configuration.....	10-6
Conservatism and Optimism in the IMARC-5 Code.....	10-7
10.3 References	10-7
11 IMARC-5 RESULTS AND SENSITIVITY STUDIES	11-1
11.1 Results Using All IMARC Branches	11-1
11.2 Sensitivity Studies Involving a Single Branch.....	11-9
11.3 References	11-19
12 REPOSITORY LICENSING STRATEGY	12-1
12.1 Introduction.....	12-1
12.2 Purpose	12-1
12.3 Regulatory Considerations.....	12-2
12.4 Performance Assessment.....	12-5
12.5 Uncertainty	12-5
12.6 Evaluation Process	12-6
12.7 Defense-In-Depth	12-7
12.8 Review of DOE's Repository Safety Strategy, Revision 3	12-8
12.8.1 Uncertainties	12-9
12.8.2 Defense-In-Depth.....	12-10
12.8.3 Natural Analog Systems.....	12-10
12.9 Analytical Approach	12-11
12.10 Summary of the Essential Elements of an Appropriate Repository Safety Strategy	12-12
12.11 References	12-12
13 BARRIER IMPORTANCE ANALYSIS USING IMARC.....	13-1
13.1 Introduction and Purpose	13-1
13.2 'Traditional' Neutralization Analyses	13-2
13.3 'Hazard Index' Analyses	13-10
13.3.1 Starting Point Assumptions for the IMARC Hazard Index Calculations.....	13-10
13.3.2 Release Scenario.....	13-11

13.3.3 General Description.....	13-11
13.3.4 Presentation of Individual Hazard Index Estimates.....	13-14
⁷⁹ Se (Figure 13-7)	13-14
⁹⁹ Tc (Figure 13-8).....	13-17
¹²⁹ I (Figure 13-9).....	13-19
²⁴¹ Am (Figure 13-10)	13-23
²³⁷ Np (Figure 13-11)	13-23
²³³ U (Figure 13-12)	13-24
²²⁹ Th (Figure 13-13)	13-24
Hazard Index Curves Summed for 22 Radionuclides (Figure 13-14)	13-28
13.4 References	13-29
14 CONCLUSIONS AND RECOMMENDATIONS	14-1
14.1 Suitability of Yucca Mountain as a Permanent Repository	14-2
14.2 Recommendations for Future Work	14-4
14.2.1 General Comments	14-4
14.2.2 Specific Recommendations	14-5
Flow Heterogeneity	14-5
Drip Shield/Container/Cladding	14-5
Solubility/Sorption Data	14-6
Unsaturated and Saturated Zone Fracture/Matrix Coupling and Dilution	14-6
Biosphere/Human Behavior.....	14-6
Volcanism.....	14-7
14.3 References	14-7
A APPENDIX A – CONSERVATISMS AND OPTIMISMS IN THE DOE AND EPRI	
TSPA MODELS	A-1
A.1 Conservatisms and Optimisms Found in DOE’s Current TSPA-SR Models.....	A-1
A.1.1 Future Climate and Net Infiltration.....	A-1
A.1.2 Near Field Processes.....	A-2
Thermal Performance.....	A-3
A.1.3 Engineered Barrier System	A-3
A.1.4 Source Term and EBS transport	A-5
A.1.5 Unsaturated Zone and Saturated Zone Flow and Transport.....	A-5
A.1.6 Biosphere	A-6

A.1.7 Volcanism	A-6
A.2 Conservatism/Optimisms in IMARC-5.....	A-7
A.2.1 Climate Scenarios.....	A-7
A.2.2 Net Infiltration Issues	A-8
A.2.3 Near-Field Coupled Processes Issues	A-8
A.2.4 EBS Drip Shield, Container, and Cladding) Degradation Issues	A-8
A.2.5 Source Term Issues.....	A-9
A.2.6 Unsaturated Zone (UZ) and Saturated Zone (SZ) Flow and Transport Issues.....	A-9
A.2.7 Biosphere Issues	A-10
A.3 Summary of Sensitivity Studies on Waste-Form Saturation and Diffusive Release for Varying Near-Field Rock Lengths	A-10
A.3.1 Sensitivity Cases	A-11
A.3.2 Results with Diffusion-only Transport.....	A-12
Se-79	A-12
Pa-231.....	A-13
Pu-239.....	A-13
Np-237	A-13
A.3.3 Results with Both Diffusion and Advection	A-14
A.3.4 Summary	A-15
A.4 References.....	A-15

LIST OF FIGURES

Figure 1-1 Proposed Repository Layout and Test Facilities.....	1-3
Figure 1-2 Site Recommendation Characteristics Report, Drift Configuration.....	1-4
Figure 4-1.....	4-4
Figure 4-2 WP Surface and Drift Wall Temperatures for 25-yr Ventilation, 0.1-m Spacing, and No Backfill.....	4-5
Figure 4-3 WP Surface and Drift Wall Temperatures for 50-yr Ventilation, 0.1-m Spacing, and No Backfill.....	4-5
Figure 4-4 Percolation Flux vs. Seepage Fraction	4-7
Figure 4-5 Percolation Flux vs. Mean Seepage Flow Rate	4-7
Figure 4-6 Interaction Matrix Showing THC Coupling (Dale, 2000).....	4-21
Figure 4-7 Flow chart of TOUGHREACT for modeling non-isothermal multiphase flow, solute transport, and reactive chemistry (Xu and Pruess, 1998)	4-24
Figure 5-1 21 PWR Commercial SNF Waste Package	5-3
Figure 5-2 Cross-Section of 21 PWR Commercial SNF Waste Package	5-4
Figure 5-3 Waste Package Closure Weld Details	5-4
Figure 5-4 Dripshield Concept. The Figure on the Right Shows the Shield Fitted over the Waste Package which is Resting on an Emplacement Pallet.....	5-5
Figure 5-5 Robust Waste Package.....	5-5
Figure 5-6 Drift Configuration	5-6
Figure 5-7 Titanium (Ti-7) Aqueous General Corrosion Rate Distribution (The Full Data Base of Measured Rates was Used to Calculate the Distribution, but only a Small Number of Rate Values are Shown to Illustrate the Fit)	5-12
Figure 5-8 Outline of the Drip Shield Corrosion Model Used: (1) 10 ± 2.5 nm/year (Normal Distribution); (2) Distribution of Rates in Figure 5-7	5-14
Figure 5-9 Dripshield Failure Time Distributions for Dripping (AGC) and Non-Dripping (HAC) Conditions with and without Hydrogen Induced Cracking (HIC)	5-15
Figure 5-10 Dripshield Failure Time Sensitivity to Hydrogen Absorption Fraction.....	5-16
Figure 5-11 Outline of Waste Package Corrosion Model	5-17
Figure 5-12 Alloy 22 Aqueous General Corrosion Rate Distribution (From Table 26, CRWMS M&O 1999a)	5-18
Figure 5-13 Waste Package Time to Failure from Humid Air/Aqueous General Corrosion	5-19
Figure 5-14 Comparison of Waste Package Failure Times by Localized and General Corrosion (Center – 50 year Ventilation Period).....	5-24

Figure 5-15 Cumulative Probability of Encountering a Flaw as a Function of Distance from Outer Surface of Weld	5-29
Figure 5-16 Size Distribution of Weld Flaws in the Alloy 22 Barrier Welds.....	5-29
Figure 5-17 Time to Failure Distributions for a Waste Package Meeting the Criteria for SCC Susceptibility under Various Scenarios.....	5-31
Figure 5-18 Engineered Barrier System Failure Times for 50 Year Ventilation at the Center and Edge of the Repository	5-33
Figure 5-19 Impact of Ventilation Period Duration on EBS Failure Times	5-34
Figure 5-20 Influence of Reducing the Compressive Layer on the Outer Closure Lid Weld from 12 mm ± 2 mm to 2 to 3 mm on EBS Failure Times.....	5-35
Figure 5-21 Fuel Rod Cladding Failure Distribution	5-38
Figure 6-1 Conceptual description of the current EBS design (adopted from Jolley 1999).....	6-2
Figure 6-2 TSPA program structure and relationship between process models and PA component models.....	6-3
Figure 6-3 Conceptual model system for EPRI source-term COMPASS2000. “↔” represents diffusion transport, and “→” represents advection transport	6-8
Figure 6-4 Illustration of geometry for the compartment system in COMPASS2000. “ r_2 ” is the inner radius of the canisters, “ r_3 ” is the outer radius, L is the length of one waste package, A_{invert} is the invert area, δ_{invert} is the invert thickness, A_{drip} is the area at the top of the drift shield that is open for seepage water to flow into the waste package, δ_{rock} is the rock thickness, and $D_{pin-hole}$ is the pin-hole diameter for the early failure scenario.....	6-13
Figure 6-5 Illustrating retention by barriers: I-129 mass distribution at (a) 120,000 years and (b) 244,000 years. Total inventory is represented as a pie. The containment time is 100,000 years. The alteration time is 3000 years. The cladding gradually degrades and disappears after about 140,000 years of contacting with liquid water	6-15
Figure 6-6 Illustrating retention by barriers: Np-237 mass distribution at (a) 1200 years and (b) 50,000 years. Total inventory is represented as a pie. The containment time is 100,000 years. The alteration time is 3000 years. The cladding gradually degrades and disappears after about 140,000 years of contacting with liquid water	6-16
Figure 6-7 Example of retention by barriers to illustrate “defense-in-depth” for I-129.....	6-17
Figure 6-8 Example of retention by barriers to illustrate “defense-in-depth” for Np-237	6-18
Figure 6-9 Cumulative fractions of failed claddings as a function of time after the waste package fails and becomes wet (Massari 2000)	6-19
Figure 6-10 Cumulative cladding degradation as piece-wise step function of time after containment failure, converted from Figure 6-9 for IMARC calculations.....	6-19
Figure 6-11 EBS release rates of I-129 and Np-237 with cladding credit (with “Mean” curve in Figure 6-9).....	6-20
Figure 6-12 EBS release rates of I-129 and Np-237 without cladding credit taken into account.....	6-21
Figure 7-1 Sketch of the simulation domain in the SZ.....	7-2
Figure 7-2 The flowing interval spacing is defined as the distance from the midpoint of one flowing interval to the next. The typical spacings between the flowing intervals are much greater than the fracture spacings (from CRWMS, M&O, 2000b).....	7-3

Figure 7-3 Comparison of the probability distributions of the log of corrected flowing interval spacing and corrected fracture spacing (from CRMWS, M&O, 2000b)	7-4
Figure 7-4 Comparison of the flow meter survey information among various boreholes. The shaded areas indicate the flowing intervals and the number within the flowing interval represents the percentage of total flow in that interval (from CRMWS, M&O, 2000b)	7-5
Figure 7-5 Comparison of concentration vs time at a point 500 m downgradient from the source for a transverse-dispersivity verification example	7-7
Figure 7-6 Breakthrough concentrations and water flux at the base of the UZ (water table)	7-11
Figure 7-7 Time variation in maximum concentration at the compliance boundary for Series F and S runs as a function of the diffusion coefficient (D_p) of matrix blocks in the volcanic aquifer.....	7-13
Figure 7-8 Time variation in maximum concentration at the compliance boundary for Series F and S runs as a function of the radius of matrix blocks in the volcanic aquifer (r_p).....	7-14
Figure 7-9 Time variation in the maximum concentration at the compliance boundary for Series F and S runs as a function of the effective porosity (θ_e) of the flowing interval in the volcanic aquifer	7-16
Figure 7-10 Time variation in the maximum concentration at the compliance boundary for Series F and S runs as a function of the length of the volcanic aquifer	7-17
Figure 7-11 Isoconcentration contour for Run 01 Series F at $t=1,000,000$ years	7-18
Figure 7-12 Isoconcentration contour for Run 16 with a 50 m x 50 m source at $t=1,000,000$ years.....	7-19
Figure 7-13 Sensitivity of maximum concentration at the compliance boundary to changes in the transverse vertical dispersivity	7-20
Figure 7-14 Isoconcentration contours at $t=1,000,000$ years for Run 17 Series F with a transverse vertical dispersivity of 0.5 m	7-21
Figure 7-15 Isoconcentration contours at $t=1,000,000$ years for Run 18 Series F with a transverse vertical dispersivity of 0.1	7-21
Figure 7-16 Relative concentration profiles for R 01: Series F and R 04: Series S at 1,000,000 years down the flow system at 33 m below the top of the simulation domain.....	7-23
Figure 7-17 Three-dimensional plots of the 0.01 relative concentration isosurface at 1,000,000 years. The upper panel presents results for R 01: Series F. The lower panel presents results for R 04: Series S.....	7-24
Figure 9-1 Temperature profiles across dikes and adjacent host rocks at various non-dimensional times. θ_s is the solidification temperature (fraction of temperature drop for solidification). Diagram from Delaney and Pollard (1982, p. 873).....	9-4
Figure 9-2 Fragmentation (F) vs. dispersal (D) for various types of explosive volcanic products. Diagram from Walker (1973). F represents the fraction of particles less than 1 mm where the deposit is 1/10 of its maximum thickness along the dispersal axis. D represents the area enclosed by an isopach line enclosing the area thicker than 1/100 of the maximum thickness.....	9-6

Figure 10-1 Logic tree for IMARC-5. Example connections are shown here for simplicity. There are 54 branches in total	10-2
Figure 10-2 Configuration of the vertical flow columns through the unsaturated zone	10-6
Figure 11-1 Expected Value of Annual Dose Versus Time 20 km Downstream, Drinking Water Pathway Dose Only.....	11-2
Figure 11-2 Expected Value of Annual Dose Versus Time 20 km Downstream, All Exposure Pathways Included.....	11-3
Figure 11-3 Sensitivity of the Annual Drinking Water Dose from ^{99}Tc to Infiltration Rate	11-5
Figure 11-4 Sensitivity of the Annual Drinking Water Dose from ^{237}Np to Infiltration Rate.....	11-5
Figure 11-5 Sensitivity of the Annual Drinking Water Dose from ^{99}Tc to the Focused Flow Factor	11-6
Figure 11-6 Sensitivity of the Annual Drinking Water Dose from ^{237}Np to the Focused Flow Factor.....	11-7
Figure 11-7 Sensitivity of the Annual Drinking Water Dose from ^{99}Tc to Solubility and Spent Fuel Matrix Alteration Time.....	11-8
Figure 11-8 Sensitivity of the Annual Drinking Water Dose from ^{237}Np to Solubility and Spent Fuel Matrix Alteration Time.....	11-8
Figure 11-9 Sensitivity of the Annual Drinking Water Dose from ^{237}Np to Saturated Zone Matrix Retardation	11-9
Figure 11-10 Sensitivity of the Annual Total Drinking Water Dose to Alternate Source Column Dimensions.....	11-11
Figure 11-11 Sensitivity of the Annual Total Drinking Water Dose to Saturated Zone Velocity.....	11-12
Figure 11-12 Annual Drinking Water Dose for the "Best Estimate" Single Branch: 'Moderate' Infiltration; No Flow Focusing; 'Moderate' Solubility; 3,000-Year Alteration Time; and 'Moderate' Matrix Retardation	11-13
Figure 11-13 Annual Drinking Water Dose for the "Worst Case" Single Branch: 'High' Infiltration; No Flow Focusing; 'High' Solubility; 1,000-Year Alteration Time; and 'Low' Matrix Retardation	11-14
Figure 11-14 Annual Total Drinking Water Dose for the Six Combinations of Infiltration and Flow Focusing.....	11-15
Figure 11-15 Sensitivity of Annual Total Drinking Water Dose to Spent Fuel Matrix Alteration Time	11-16
Figure 11-16 Annual Total Drinking Water Dose for the Nine Combinations of Solubility and Alteration Time.....	11-16
Figure 11-17 Sensitivity of Annual Total Drinking Water Dose to the Intensity of the Future Glacial Climate	11-17
Figure 11-18 Sensitivity of Annual Total Drinking Water Dose to the Spacing Between Flowing Fractures in the Saturated Zone	11-18
Figure 11-19 Sensitivity of Annual Total Drinking Water Dose to the Saturated Zone Matrix Block Diffusion Coefficient.....	11-18
Figure 11-20 Impact on Annual Total Drinking Water Dose of Neglecting Sorption onto Container Corrosion Products.....	11-19
Figure 13-1 Impact on Annual Total Drinking Water Dose of Encountering No Alluvium.....	13-3

Figure 13-2 Impact on Annual Total Drinking Water Dose of Assuming No Cladding Effectiveness	13-5
Figure 13-3 Impact on Annual Total Drinking Water Dose of Assuming No Drip Shield and No Container Effectiveness.....	13-6
Figure 13-4 Impact on Annual Total Drinking Water Dose of Assuming No Cladding, Container, or Drip Shield Effectiveness.....	13-7
Figure 13-5 Impact on Annual Total Drinking Water Dose of Assuming No Drip Shield, Container, or Cladding Effectiveness	13-8
Figure 13-6 Impact on Annual Total Drinking Water Dose of Assuming Increased Container Susceptibility to Stress Corrosion Cracking	13-9
Figure 13-7 Hazard Index Curves for ⁷⁹ Se	13-15
Figure 13-8 Hazard Index Curves for ⁹⁹ Tc.....	13-18
Figure 13-9 Hazard Index Curves for ¹²⁹ I.....	13-20
Figure 13-10 Hazard Index Curves for ²⁴¹ Am	13-21
Figure 13-11 Hazard Index Curves for ²³⁷ Np	13-22
Figure 13-12 Hazard Index Curves for ²³³ U	13-25
Figure 13-13 Hazard Index Curves for ²²⁹ Th.....	13-26
Figure 13-14 Hazard Index for 22 Radionuclides.....	13-27
Figure A-1 Sensitivity study results for Se-79 without advection.....	A-16
Figure A-2 Sensitivity study results for Pa-231 without advection	A-16
Figure A-3 Sensitivity study results for Pu-239 without advection	A-17
Figure A-4 Sensitivity study results for Np-237 without advection.....	A-17
Figure A-5 Sensitivity study results for Se-79 with advection.....	A-18
Figure A-6 Sensitivity study results for Np-237 with advection.....	A-18
Figure A-7 Sensitivity study results for Pu-239 with advection.....	A-19

LIST OF TABLES

Table 3-1 Net Infiltration Estimates for Yucca Mountain, Nevada	3-2
Table 3-2 Year 2000 Net Infiltration Estimates	3-6
Table 3-3 Factors Addressed in Net Infiltration Models	3-7
Table 3-4 Factors Evaluated in Uncertainty and Sensitivity Testing.....	3-8
Table 3-5 Comparison of USGS and EPRI Glacial Climate Characterizations.....	3-10
Table 4-1 Model Mineral Assemblage, Aqueous and Gaseous Species for the Complex Chemical System.....	4-26
Table 5-1 Distribution of Measured Aqueous General Corrosion for Alloy 22	5-18
Table 5-2 Values of Parameters Used in the Waste Package Crevice Corrosion Model (Equation (5-7)) Compared to the Values Used Previously in IMARC 4.....	5-21
Table 5-3 Simplified Distribution of WP Surface Temperature vs. Time.....	5-22
Table 5-4 Distribution of Initial Fuel Rod Cladding Thickness	5-38
Table 6-1 Short Lived Nuclides Considered by M&O's Source-Term.....	6-6
Table 6-2 Comparison of Source-Term Models	6-10
Table 6-3 EBS Transport Parameters.....	6-21
Table 6-4 EBS Diffusion Parameters	6-22
Table 6-5 Previous Values for solubilities (moles/liter) of Key Radioelements (probabilities in parentheses).....	6-23
Table 6-6 Key characteristics of J-13 water (from Efurd et al., 1998).....	6-25
Table 6-7 Recommended Values for Solubility (moles/liter) of Key Radioelements. Revised values are shown in <i>bold italics</i>	6-28
Table 6-8 Elicited Sorption Coefficient (K_d) Distributions (m^3/kg) (from Wilson et al., 1993) ...	6-29
Table 6-9 Recommendations for K_d Values for Specific Elements. Revised values are shown in <i>bold italics</i>	6-34
Table 7-1 Summary of base hydraulic and transport parameters for the SZ, used in Run 01: Series F and Run 04: Series S	7-9
Table 7-2 Summary of K_d and dimensionless K_d values for volcanic units and alluvium in SZ used in Series F and Series S runs	7-10
Table 7-3 Calculated penetration by diffusion.....	7-12
Table 8-1 Dose Conversion Factors for Unit Flux to the Well (from errata in Smith et al. [1996], Table 5-20)	8-3
Table 8-2 Top Three Exposure Pathways Contributing to Peak Total Dose (from errata in Smith et al. [1996], Table 5-21).....	8-4
Table 9-1 Chemical analyses of typical basalts (from Rogers and Hawkesworth, 2000).....	9-2

Table 10-1 Solubility limits employed in IMARC-5 (adapted from Table 6-7)	10-3
Table 10-2 Kd values for sorption onto tuff and alluvium in the saturated zone	10-4
Table 10-3 Fractions of Waste Packages that are Wet.....	10-5
Table 13-1 Hazard Reduction Factors for ^{79}Se	13-17
Table 13-2 Hazard Reduction Factors for ^{99}Tc	13-19
Table 13-3 Hazard Reduction Factors for ^{237}Np	13-23
Table 13-4 Hazard Reduction Factors for ^{233}U	13-24
Table 13-5 Hazard Reduction Factors for the Combined 22 Radionuclides Case.....	13-28
Table 13-6 Assessment of Barrier Action for the 12 Candidate Barriers	13-29
Table A-1 Cases in the Sensitivity Study	A-11
Table A-2 Solubility Data	A-12

1

INTRODUCTION

Significant resources and effort have been expended by EPRI over the past few years in modeling and understanding issues related to high-level radioactive waste disposal. Previous reports (EPRI, 1990; 1992; 1996; 1998) have documented the general model used in the EPRI work and specific inputs to that model for examination of the potential repository at Yucca Mountain, Nevada. Modeling of the potential Yucca Mountain site is an on-going process, and new data are being collected with which to evaluate and modify models of physical processes.

There are several purposes of the current report. The main purpose of this report is to describe the subsystem and total system performance models and present results and analysis of the results. The evaluation is based on the DOE's Site Recommendation Characteristics Report (SRCR) design. This design is called a 'line-loading' of the waste packages in the emplacement drifts. As is seen in Figure 1-1, this allows the emplacement drifts to be spread apart. The separation distance provides a shedding zone where mobilized moisture can drain. Figure 1-2, provides a look inside of the emplacement drifts. The SRCR design has added a number of new features, waste package spacing of 0.10 meters, waste package with an outer shell of Alloy 22, waste package pallet also made of Alloy 22, drip shield to preclude dripping water on the waste package, an invert design that allows moisture to pass through, and a drift support system that is not continuous.

The first part of this report includes presentation of new models based largely on the most recent DOE design of the repository and partially on the Analysis Model Reports (AMRs) and Process Model Reports (PMRs) produced by the Managing and Operating Contractor (M&O) for DOE. For example, the new models presented here consider the combination of drip shield, waste container, and cladding failure that accounts for the new drip shield and the new container material. The cladding model is entirely new for us. We have also included a new model of the effect of hydrothermal activity and heterogeneous groundwater flow in the unsaturated zone on temperatures and the distribution of groundwater capable of dripping into the repository drifts. These changes affect the basic way in which performance calculations are made. Thus, the first part of this report reviews some of the relevant AMRs and describes the new EPRI model, labeled 'IMARC (Integrated Multiple Assumptions And Release Code) Phase 5'. The report also identifies the key technical components of the candidate spent fuel and HLW disposal facility at Yucca Mountain using IMARC Phase 5; makes recommendations regarding the prioritization of the technical development work remaining; and provides an assessment of the overall technical suitability of the candidate High Level Waste (HLW) disposal facility at Yucca Mountain.

A series of calculational cases for the 'normal release' scenario are conducted using IMARC Phase 5. The cases focus on a dose rate end point calculated over times scales that exceed the time of peak release into the accessible environment (biosphere), on the order of several hundred

thousand years. These calculational cases are configured to explore the most recent conceptual models and data regarding future conditions, as well as revised repository design concepts, for the Yucca Mountain Site. Expert judgement is used to evaluate and select data from published sources. Recognizing both current uncertainties and, in some cases, paucity of data, emphasis is placed on selection of “best estimate” values, with higher and lower values representing conservative bounding values. In certain areas, alternative conceptual models are compared as to their impact on overall repository performance. Comparisons of these calculational cases with the most recent results from the DOE and other government agencies are also made. Recommendations are also made with respect to the priority of possible design modifications, data collection and site characterization activities.

The assurance of a successful license application for Yucca Mountain depends on a robust demonstration of long-term safety from a scientifically credible, traceable, and transparent process. Discussion of what constitutes an appropriate safety strategy, along with a brief review of the most recent DOE repository safety strategy, is presented in Chapter 12. Illustrations of how to make a safety case for multiple barriers is provided in Chapter 13.

Many people have contributed to development and application of the EPRI model, and to its documentation in this report. Austin Long of the University of Arizona provided an analysis of the AMR on future climates and wrote Chapter 2. Stuart Childs of Kennedy Jenks, Inc. reviewed some of the AMRs related to surface water effects and infiltration, and wrote Chapter 3. A review of several AMRs related to coupled processes, provided in Chapter 4, was written by Wei Zhou of Monitor Scientific LLC, and Benjamin Ross of Disposal Safety, Inc. Modeling of repository conditions with respect to repository temperature, the fraction of the repository assumed wet, and flow rates through the “wet” portions as a function of time is also documented in Chapter 4 by Benjamin Ross. The containment barrier system model was developed and documented in Chapter 5 by David Shoesmith of University of Western Ontario and John Massari of Constellation Nuclear Services, Inc. A summary of the somewhat revised model of the source term, along with updated information on elemental solubilities and corrosion product sorption coefficients was documented (Chapter 6) by Wei Zhou and Michael Stenhouse of Monitor Scientific LLC. Chapter 7 includes a brief review of the flow and transport models developed by Ed Sudicky of Groundwater Simulations Group, as well as some relevant sensitivity studies on important saturated zone properties. Frank Schwartz, from Ohio State University, also provided updated estimates of hydrologic parameters in Chapter 7. The biosphere dose model used to estimate doses was developed by Graham Smith and others from QuantiSci, Ltd. This model was summarized in Chapter 8. A brief review of some of the M&O work on volcanism was performed by Michael Sheridan of the State University of New York at Buffalo, and is presented in Chapter 9.

Chapter 10 describes the overall structure of the IMARC Phase 5 model and how the subsystem models are integrated. This chapter also provides a general discussion of the assumptions and expert judgment that went into the development of the models. Chapter 10 was written by John Vlasity (Risk Engineering, Inc.) and John Kessler (EPRI). The IMARC Phase 5 calculations were performed at Risk Engineering by John Vlasity. They are reported by John Kessler and John Vlasity in Chapter 11.

A discussion of the considerations that go into the development of a repository safety strategy, along with a brief review of DOE’s Repository Safety Strategy, Revision 3 are provided by

Tom Doering in Chapter 12. Illustrations of how to make a safety case for multiple barriers is provided in Chapter 13, and was produced by John Kessler and John Vlasity. A summary of the general conclusions, and recommendations for future direction, by John Kessler are made in Chapter 14.

Finally, Appendix A includes a description of some of the 'departures from reality' (conservatisms and optimisms) found in both IMARC Phase 5 and in our brief review of the current version of the DOE-sponsored TSPA for Yucca Mountain.

All of these contributors have helped develop the current version of the EPRI model over the past few years, and any measure of success that this model has in providing insights and guidance regarding repository issues is due to their hard work, imagination and cooperation.

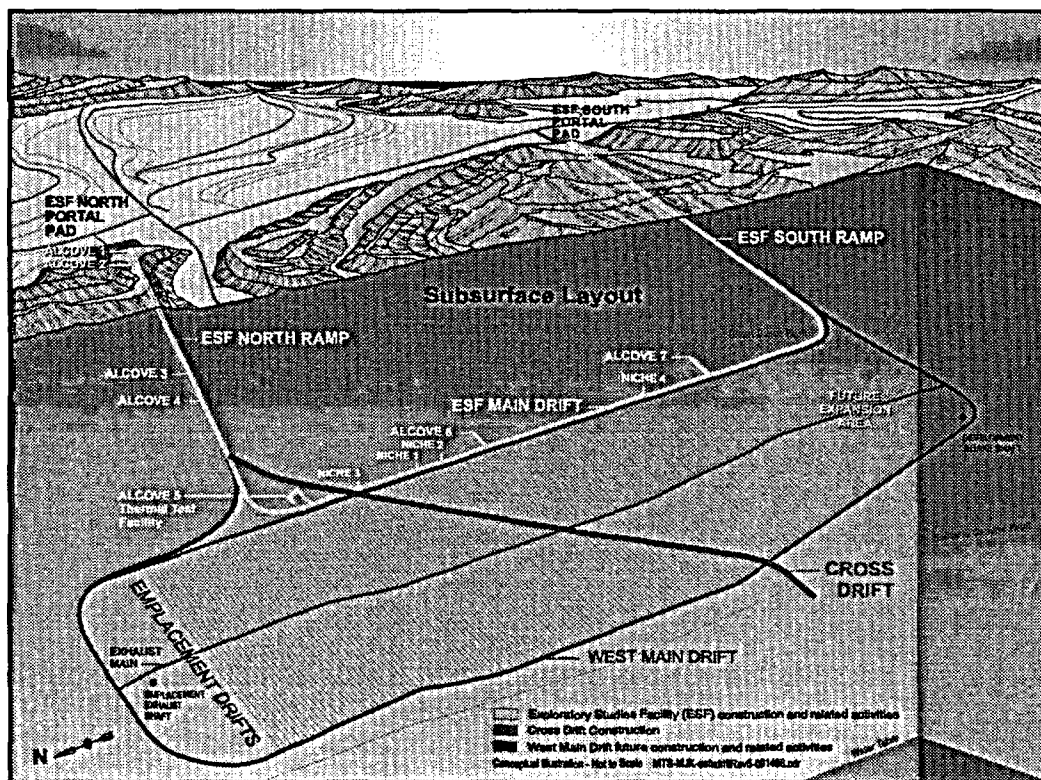


Figure 1-1
Proposed Repository Layout and Test Facilities

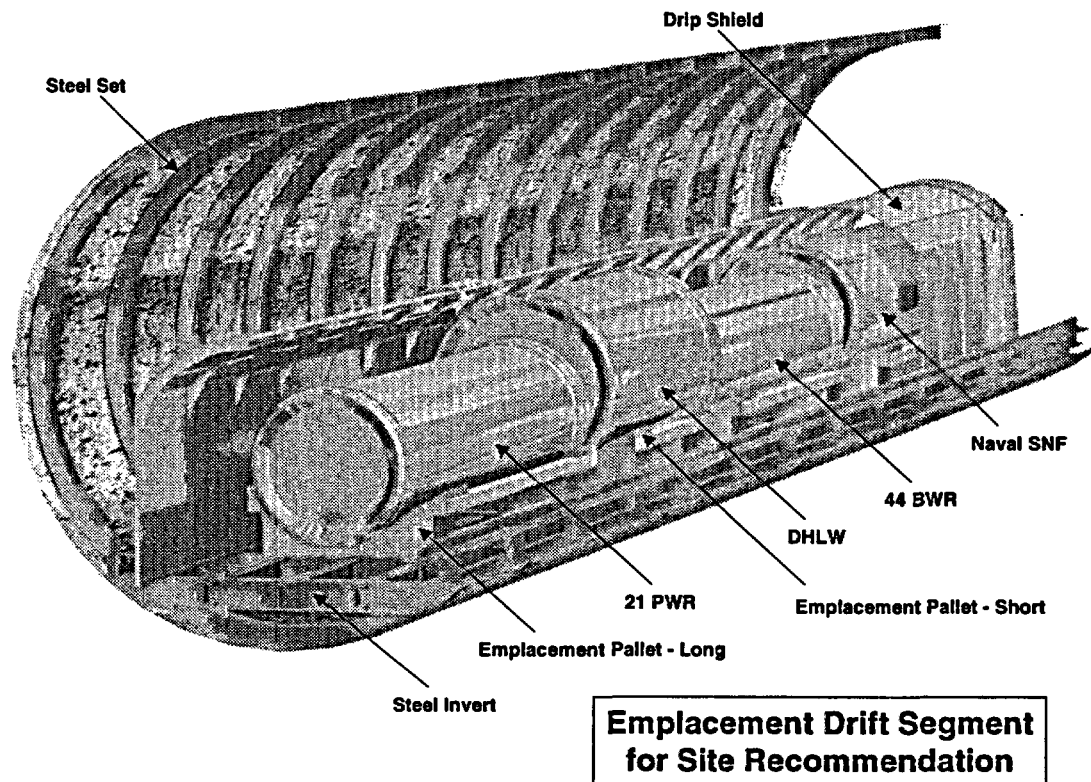


Figure 1-2
Site Recommendation Characteristics Report, Drift Configuration

1.1 References

CRWS M&O (2000). Drift Scale Thermal Analysis. CAL-WIS-TH-000002 Rev. 00.

EPRI (1990). *Demonstration of a risk-based approach to high-level waste repository evaluation*, EPRI NP-7057, Electric Power Research Institute, Palo Alto, October 1990.

EPRI (1992). *Demonstration of a Risk-Based Approach to High-Level Waste Repository Evaluation: Phase 2*, EPRI TR-100384, Electric Power Research Institute, Palo Alto, May 1992.

EPRI (1996). *Yucca Mountain Total System Performance Assessment, Phase 3*, EPRI TR-107191, Electric Power Research Institute, Palo Alto, December 1996.

EPRI (1998). *Alternative Approaches to Assessing the Performance and Suitability of Yucca Mountain for Spent Fuel Disposal*, EPRI TR-108732, Electric Power Research Institute, Palo Alto CA, November 1998.

2

CLIMATOLOGY

2.1 Introduction

This chapter reviews the status of assumed present and future climate at the Yucca Mountain proposed high-level nuclear waste storage facility. The amount, mode and season of precipitation are critical to the amounts of water that penetrate the ground surface to become net infiltration. [EPRI 1996; 1998] As the USDOE Yucca Mountain Project's Total System Performance Assessment (YM TSPA) and modeling effort are nearing completion, defensible estimates of future climates are required to model future infiltration. The recent climate at Yucca Mountain has been hot and very dry, about 150 mm annual precipitation. This has persisted for approximately the past 10,000 years, however, it is unlikely to continue for the next 10,000 years. Below are comments on the climate portion of a draft document from the U.S. Geological Survey [ANL-NBS-HS-000032 Rev 00 (June 2000)].

2.1.1 Objectives

This chapter will review the bases for the proposed future climates and timing suggested in ANL-NBS-HS-000032 Rev 00 (June 2000) in terms of:

1. Likelihood based on current literature, and
2. Appropriateness to estimating net infiltration.

2.1.2 Current Climate at Yucca Mountain

The draft document, "Simulation of Net Infiltration for Modern and Potential Future Climates", ANL-NBS-HS-000032 Rev 00 (June 2000), is the focus of this chapter. The length of on-site weather records was about 30 years, and length of nearby records ranged from 8 to 30 years. The off-site instrumental records were adjusted for elevational differences. Proxy climate records, including tree-rings, lake sediments, pollen and microfaunal species have extended the record of modern climate.

These observations suggest that the present fairly stable warm and dry climate at Yucca Mountain has experienced no major changes for ~10,000 years. However, longer-term proxy geological and paleontological records suggest that this present climate is unusually warm and dry compared to the past several hundred thousand years, and the present climate is unlikely to prevail for the next 10,000 years. The evident cyclicity of past climates indicates an inevitable return to cooler and wetter conditions. Moreover many climatologists suspect that anthropogenic

components in the atmosphere may already have begun altering the climate, and that some of these components will have a significant impact on the Earth's climate for the next few hundred years.

The USGS stochastic precipitation model should provide an excellent representation of the "modern" precipitation, as it evidently includes low-probability, large precipitation events not detected during the field measurement period. The ~200 mm/year figure for "modern" precipitation is higher than the often quoted ~150 mm/year value. This may be influenced by the recent increase of "El Niño" events during the past 150 years. Their Figure 6.23 suggests a range of 160-200 mm/year for the Yucca Mountain spent fuel storage area. Thus, the higher figure may be closer to precipitation expected in the near future.

2.1.2 Future Climate at Yucca Mountain Proposed in ANL-NBS-HS-000032 Rev 00 (June 2000)

The draft document ANL-NBS-HS-000032 Rev 00 (June 2000) focuses on three discrete climate stages assumed to account for the climates expected within the next 10,000 years at Yucca Mountain. These are termed "modern", "monsoon" and "glacial transition". The "modern" climate state is that which exists today; "monsoon" represents a warmer, wetter climate state (compared to modern); and "glacial transition" is a cooler, wetter climate state that is assumed to prevail during most of the next 10,000 years. For the purposes of modeling the radiological impacts of the candidate HLW repository at Yucca Mountain, ANL-NBS-HS-000032 Rev 00 (June 2000) concludes that the "modern" climate state exists from today through 600 years after repository closure. The next climate phase, "monsoon", would extend from 600 years to 2000 years after repository closure. The "glacial transition" phase would extend from 2000 years post closure to the end of the 10,000-year time frame under consideration in the model.

The basis for the projection of future climate characteristics and timing is the pattern of past climates recorded in western United States lakebed deposits, fauna in marine sediments, stable isotopes in polar ice and in particular, extensively dated stable isotope recurring patterns in nearby Devil's Hole vein-filling calcite.

Summary of Proposed Future climate Phases:

Modern	Now (closure) to 600 years post closure
Monsoon	600 to 2000 years post closure
Glacial transition	2000 to 10,000 post closure

2.2 Discussion of Proposed Future Yucca Mountain Climates in ANL-NBS-HS-000032 Rev 00 (June 2000) and Suggested Alternatives

2.2.1 The "Modern" Climate State

ANL-NBS-HS-000032 Rev 00 (June 2000) assumes that the present-day "Modern" Climate State will continue until 600 years post repository closure. This is contrary to a large volume of recent literature and General Circulation Models (GCMs) that predict significant alteration of the

Earth's climate in the next few centuries. One of the models focusing on the Western U.S. originated in the USGS (USGS Circular 1153). The USGS models of North American greenhouse climates, GENESIS and regCM predict 3 to 4 degrees C higher temperature year round for Nevada, and little change in precipitation during the next several hundred years. The forcing function for these changes in climate is the greater absorption of Earth-irradiated infrared energy. The result is warmer air temperatures and more energetic hydrologic cycles.

A recent report: Urban, F. E., Cole, J. E. and Overpeck, J. T., "Influence of mean climate change on climate variability from a 155-year tropical Pacific coral record" *Nature* vol. 407, pp. 989-993 (2000), reveals that the frequency of occurrence of El Niño events has been increasing over this time period, as has the atmospheric CO₂ concentration. During El Niño years the southwestern US receives significantly more winter precipitation. If this trend continues, as some general circulation models predict, the next 600 years ("modern" in the model) will be overwhelmed by the excess temperature predicted in most general circulation models.

A team at the Canadian Centre for Climate Modeling and Analysis, University of Victoria, Canada, recently published a series of three sequential papers [Boer *et al.* 1, Boer *et al.* 2, and Flato *et al.* 2000]. In addition, four papers related to GCMs and Greenhouse effects recently appeared in the same journal [Bouraoui *et al.* 2000; Giorgi and Francisco, 2000; Knutson and Tuleya, 1999 and Liu *et al.* 1999]. Most models adopt a scenario with atmospheric CO₂ levels at twice or three times the pre-industrial level. The most extreme assumes a quadrupling of pre-industrial levels of CO₂. Owing to uncertainties about future mitigation of greenhouse warming, the decades in which the atmospheric CO₂ will reach those levels are uncertain. The Canadian General Circulation Model 1 (CGCM1) assumes a "business as usual" scenario (no interdiction) and predicts that by AD2080 to AD2100 southern Nevada will experience an average winter temperature increase between 5 and 10 degrees C and a summer increase between 3 and 5 degrees C. Precipitation during this time would not change for the summers, but the winter precipitation would increase 50 to 75%. Note that this is quite different from the precipitation assumed in ANL-NBS-HS-000032 Rev 00 (June 2000), and less winter precipitation would be lost by evapotranspiration.

The United States Environmental Protection Agency (EPA) summarizes recent publications which predict water resources impacts of global warming in Chapter 8 of its *Global Warming* publication (ref Chapter 8, North America, EPA web page). The authors of this report examined ten climate models in terms of their predicted impacts on the hydrological cycle. They point out that increasing greenhouse gases could induce an increase in hydrologic variability: more frequent and larger floods and more severe summer droughts. For southern Nevada they quote Nash and Gleick's (1993) report that shows a 10% increase in precipitation during the recent century. If this increase was related to an increase in atmospheric greenhouse gases, this trend will continue into the next century and beyond.

How long will greenhouse conditions persist into the future? This depends on future consumption of fossil fuels, and estimates of CO₂ sequestration, naturally and artificially. The Intergovernmental Panel on Climate Change (IPCC) presents 3 scenarios. In their most optimistic scenario, the atmosphere will return to the present CO₂ level (not the pre-industrial level, but the AD2000 level) by AD2500. Their most pessimistic scenario, the "business as usual" one, atmospheric CO₂ will not return to present levels until AD3000 (~1000 years post closure). The most optimistic scenario brings global temperatures back to present-day levels

by AD2500. Because the present international socio-political climate does not favor immediate CO₂ reductions of either the industrialized or the developing nations, we cannot be optimistic about the optimistic scenario.

The ANL-NBS-HS-000032 Rev 00 (June 2000) authors assert that “Modern” climate conditions will persist until 600 years after repository closure, or until about AD2600. This, however, is the time frame during which the atmospheric CO₂ will likely reach its maximum, possibly as high as 1200ppm, over 4 times the pre-industrial level. This excess of greenhouse gas will almost certainly affect the climate in southern Nevada, and hence the net infiltration.

Although the current GCMs are not in agreement in every aspect of the future greenhouse climate, they are based on first principles of atmospheric physics, and are rapidly improving. To this reviewer’s knowledge, none of them suggests greater summer precipitation, as suggested for the “monsoon” climate mode.

The USGS GCM, RegCM, USGS Circular 1153, has modeled present and future (X2CO₂) climates for the western US, with rather high spatial resolution. The modeled future “greenhouse” climate shows a 4-5°C higher temperature year-round, little change in precipitation year-round. The 2nd generation Canadian coupled general circulation model (CGTCM2) output description is available on-line. (<http://www.cccma.bc.ec.gc.ca/models/gcm2.html>) The model has recently been published, as well (G. J. Boer, G. Flato and D. Ramsden, “A transient climate change simulation with greenhouse gas and aerosol forcing: projected climate to the twenty-first century”, *Climate Dynamics* (2000) vol. 16, pp.427-450). This model predicts an increase in precipitation for the southwest US of about 10%/100 years as the greenhouse effect increases.

2.2.1.1 “Monsoon” Conditions

The authors of ANL-NBS-HS-000032 Rev 00 (June 2000) predict that a “monsoon”-type climate will replace the “modern” climate at Yucca Mountain at 600 years post closure, and extend to 2000 years post closure. The basis for this prediction is an extensive paleoclimate database in the region, and the assumption that climates are cyclic. The authors then select sites where the fossil fauna live today, and assume that the climate supporting the living fauna is the same climate that existed when and where the fossils are found. This works in cases where the designated fauna are known to live only in restricted temperature and precipitation environments.

2.2.1.2 Suggested Alternative to “Monsoon” Climate

It is far from certain that a “Monsoon” climate will begin by AD2600 (600 years post closure). Even if the climates in this area are cyclic, as they are assumed to be in ANL-NBS-HS-000032 Rev 00 (June 2000). A possible future scenario is that the greenhouse warming, responding to rising CO₂ levels to ~4X the pre-industrial level (the “business as usual” scenario), sufficient melting of polar ice occurs to melt much polar ice and raise the sea level by 1.3 meter. Changing ocean circulation patterns would relocate warm water currents, which would change precipitation patterns, and the subtle forces that affect continental climate would change. It is almost certain that climates in the Yucca Mountain area will change in response to global warming, but one can only speculate on how they would change.

A more optimistic future is one in which remedial action reduces the greenhouse gases sufficiently to avoid dramatic climate changes and continued melting of polar ice. In this most optimistic future, global temperature rises only about 1°C, and polar ice reaches a lower equilibrium, but does not completely melt, and ocean circulation patterns remain intact.

Would the “Monsoon” climate mode still lie in the future of Yucca Mountain? The authors of ANL-NBS-HS-000032 Rev 00 (June 2000) make a compelling case for cyclicity of climate in this area. Stable isotopes in ocean sediments, polar ice stratigraphy and Devil’s Hole carbonates all support this idea on long time scales. The longer-period, about 100,000-year cycle changes are well-correlated with orbital eccentricity. All of these well-documented examples, however, have fine structure or shorter time frame isotope variations that are not easily explained. Stable isotope variations appear irregular on shorter time scales. By applying a methodology (the “precession method”), the authors retrieved a correlation between the Devil’s hole stable isotopes and orbital precession. They concluded that the technique and correlation were sufficiently robust to enable prediction of future “monsoon” climate at Yucca Mountain.

However, it is still unclear why the $\delta^{18}\text{O}$ in Devil’s Hole vein-filling carbonate respond to Earth’s orbital eccentricity, which is a relatively weak change in gravitational force (Muller and MacDonald, 1997). Benson *et al.* (2000) make a strong case for synchronicity of the minor climate changes that have occurred, particularly in the southwest US. So even if we do not fully understand the process, empirical relationships can be valid, but still risky.

2.2.2 Glacial Transition

The final model climate block in the 10,000-year future time interval, “Glacial Transition”, begins ~AD4000, or 2000 years post closure. The timing for its initiation is assumed to be controlled by the Earth’s orbital eccentricity.

The authors of ANL-NBS-HS-000032 Rev 00 (June 2000) assumed that the forces that controlled the timing of major climate changes in the past will be effective in maintaining the same timing in the future. Embedded in this assumption is that the features on the Earth that enable the glacial/interglacial cycles will still be present. We do not know for sure what these features are, but they likely involve ocean circulation. Thus, if the existence of a north polar ice cover is important in allowing glaciers to form, and if this cover melts in response to greenhouse warming, the next glacial/pluvial will be delayed significantly. The probability of this scenario is low, but not zero.

2.3 Discussion of ANL-NBS-HS-000032 Rev 00 (June 2000)

Some of the apparent assumptions in ANL-NBS-HS-000032 Rev 00 (June 2000) regarding the relevance of the analog sites to the future climates, and the timing of the climate blocks need to be examined. Clearly, the final consideration is not so much the exact simulation of the natural process in terms of timing and slopes of transitions, but whether the model climates are conceptually correct and sufficiently complex to predict infiltration. Comments below relate to this point.

2.3.1 Relevance of Analog Sites to Future Climate

In the case of the future “Monsoon” climate at Yucca Mountain, the classical monsoon climate features an enhanced summer precipitation. The selected analog sites for “monsoon” do have enhanced summer precipitation. It is not clear from the literature that increased summer precipitation is the expected result of a major increase of carbon dioxide and other greenhouse gases in the atmosphere. Prominent published greenhouse model outputs predict enhanced precipitation in winter seasons, and well in force by AD2100.

2.4 Conclusions from the Analysis of the Climate Change Analysis Model Reports

1. The document ANL-NBS-HS-000032 Rev 00 (June 2000) proposes climates for the Yucca Mountain vicinity for the next 10,000 that are mostly consistent with currently published predictions. An exception is the next several hundred to one thousand years, which more likely will be strongly affected by excess atmospheric CO₂. ANL-NBS-HS-000032 Rev 00 (June 2000) depicts this as a continuation of modern climate. General Circulation Models predict that this early post closure time will be warmer with greater winter precipitation. The intensity of this effect will depend on the success of carbon dioxide abatement.
2. The section in ANL-NBS-HS-000032 Rev 00 (June 2000) justifying the conclusion that the climate at Yucca Mountain responds primarily to Earth’s orbital eccentricity is well argued, but unconventional. We cannot know how global warming will impact the subtle forces that trigger climate change, or how long the system will take to recover from the warm episode. However, the likelihood of glacial/pluvial transition during the next 10,000 years is still finite, and the “Glacial Transition” climate mode should be retained.
3. A more realistic future climate scenario for the Yucca Mountain area would include at least a 2°C increase in temperature and a 10% increase in Winter precipitation extending from closure to at least 500 years, perhaps 1000 years post closure. The suggested “Glacial Transition” should finish out the 10,000-year time period.

2.5 Implications for the IMARC Code

Based on the analysis above, it seems reasonable to maintain the basic climate types adopted in previous IMARC analyses [EPRI, 1998], with certain modifications. We reject the “monsoon” climate proposed by the M&O above, but maintain that a “greenhouse” climate, as described in EPRI [1998] will begin almost immediately. Given the above analysis, it may be that the greenhouse climate will continue for hundreds to perhaps 1,000 years. Since the IMARC code has initial time steps of 1,000 years we therefore assume that the “greenhouse” climate begins at the time of repository closure and continues for 1,000 years. From 1,000 to 2,000 years it is assumed there is a return to a climate state similar to that experienced by Yucca Mountain today, termed the “interglacial” state in EPRI [1996; 1998].

We have also rethought the appropriateness of using multiple, instantaneous climate changes in IMARC. Previous analysis of the “superpluvial” climate states proposed by DOE as part of their

TSPA-VA analyses was previously rejected [EPRI, 1998]. This superpluvial caused what many considered to be spurious, perhaps unrealistic temporary increases in assessed dose rates. Indeed, previous IMARC analyses also show significant variation in future dose rates associated with our multiple climate change events. Many of the climate changes, due to their assumed instantaneous nature, caused such significant changes in estimated doses that climate change effects obscured some important trends that caused difficulty identifying other important features and processes. While we do not wish to underestimate the importance of climate, neither do we wish to obscure important features, events, and processes by climate change details that are somewhat arbitrary in their timing and magnitude, and perhaps unrealistic in their assumed instantaneous nature.

The climate scenario we choose still preserves the basic notions that:

- Greenhouse effects are, indeed, likely to occur for some time into the near future;
- Interglacial (present day) climates are the exception rather than the norm; and
- Glacial climates will predominate in the future, as they have over the past million years or so.

Consequently, we now use the following climate scenario without exception:

- 0 to 1000 years postclosure: “greenhouse” climate as defined in EPRI [1996; 1998];
- 1000 to 2000 years postclosure: “interglacial” (present day) climate also as defined in previous IMARC analyses;
- beyond 2000 years postclosure: “full glacial maximum” as defined in EPRI [1996; 1998].

We have chosen this simplified climate because we found no huge changes in results from carrying along three different future climate scenarios. We also selected the “full glacial maximum” as the long-term climate because this conservatively supplies the highest net infiltration rates resulting in the highest estimated future dose rates.

2.6 References

Benson, Larry, James Burdett, Steve Lund, Michael Kashgarian and Scott Mensing, “Evidence for nearly synchronous northern hemispheric climate change during the first glacial termination” *Nature* in press, 2000.

Benson, Larry, “Records of millennial-scale climate change from the Great Basin of the Western United States *in* Mechanisms of Global Climate Change at Millennial Time Scales, P. U. Clark, R. S. Webb, L. D. Keigwin, eds., Geophysical Monograph 112, American Geophysical Union, 1999 pp. 385-394.

Boer, G. J., G. M. Flato, M. C. Reader and D. Ramsden, “A transient climate change simulation with greenhouse gas and aerosol forcing: experimental design and comparison with the instrumental record for the twentieth century”, *Climate Dynamics* (2000) 16:405-425.

Boer, G. J., G. M. Flato and D. Ramsden, “A transient climate change simulation with greenhouse gas and aerosol forcing: projected climate to the twenty-first century”, *Climate Dynamics* (2000) 16:427-450.

Bourouai, F., G. Vachaud, L. Z., X. Li, H. Le Treut, T. Chen, Evaluation of the impact of climate changes on water storage and groundwater recharge at the watershed scale” *Climate Dynamics* (2000) 15:153-161.

EPA-compiled data on greenhouse effects:

<http://www.epa.gov/globalwarming/publications/reference/ipcc/chp8/america5.html>

EPRI, 1998. Kessler, J. H., McGuire, R. K., Vlasity, J. A., Long, A., Childs, S., Ross, B., Schwartz, F., Shoesmith, D., Kolar, M., Apted, M., Zhou, W., Sudicky, E., Smith, G., Kozak, M., Salter, P., Klos, R., Venter, A., Stenhouse, M., Watkins, B., and R. Little, Alternative Approaches to Assessing the Performance and Suitability of Yucca Mountain for Spent Fuel Disposal, EPRI TR-108732, Electric Power Research Institute, Palo Alto CA, November 1998.

EPRI, 1996. Kessler, J., R. McGuire, J. Vlasity, A. Long, S. Childs, B. Ross, F. Schwartz, D. Bullen, M. Apted, W. Zhou, E. Sudicky, G. Smith, K. Coppersmith, J. Kemeny, and M. Sheridan, Yucca Mountain Total System Performance Assessment, Phase 3, EPRI TR-107191, Electric Power Research Institute, Palo Alto CA, December 1996.

G. M. Flato, G. J. Boer, W. G. Lee, N. A. McFarlane, D. Ramsden, M. C. Reader and A. J. Weaver, “The Canadian Centre for Climate Modeling and Analysis global coupled model and its climate”, *Climate Dynamics* (2000) 16:451-467.

F. Giorgi, R. Francisco, “Uncertainties in regional climate prediction: a regional analysis of ensemble simulations with the HADCM2 coupled AOGCM” *Climate Dynamics* (2000) 16:169-182.

Knutson, T. R., R. E. Tuleya “Increased hurricane intensities with CO₂-induced warming as simulated using the GFDL hurricane prediction system” *Climate Dynamics* (1999)

Ledley, T., E. T. Sundquist, S. E. Schwartz, D. K. Hall, J. D. Fellows, T. L. Killeen, “Climate change and greenhouse gases” EOS, vol. 80, no. 39, 1999, p. 433.

Liu, Z., R. G. Gallimore, J. E. Kutzbach, W. Zu, Y. Golubev, P. Behling, R. Selin, “Modeling long-term climate changes with equilibrium asynchronous coupling” *Climate Dynamics* (1999) 15:325-340.

Muller, R. and G. MacDonald, “Spectrum of 100-kyr glacial cycle: orbital inclination, not eccentricity” in Carbon Dioxide and Climate Change, pp. 8329-8334, National Academy of Sciences, 1997.

3

NET INFILTRATION

3.1 Introduction

Calculations and modeling of groundwater recharge in the vicinity of Yucca Mountain are required to assess the hydrologic condition of the proposed repository site. The primary input of water to the unsaturated zone from the ground surface is net infiltration, water that passes through the surface soil layers and moves downward. This chapter reviews the status of net infiltration measurements and modeling at the Yucca Mountain Project site that support Total System Performance Assessment (TSPA). At this time, the USDOE Yucca Mountain Project's TSPA [CRWMS M&O, 2000d], and the primary data collection and modeling effort for net infiltration [USGS, 2000a] are nearing completion. Therefore, EPRI is updating its TSPA.

3.1.1 Net Infiltration Calculations at Yucca Mountain

Intensive measurements to characterize the Yucca Mountain site have been underway since the 1980's. The studies that are most directly related to net infiltration include characterizations of climate, topography, soils, bedrock geology, and soil and rock physical properties. Related work that has been important to quantifying the net infiltration process includes chloride studies, bore hole neutron logging, chlorine-36 modeling, temperature profile matching, and surface water runoff measurements.

Table 3-1 summarizes net infiltration measurements and model estimates of note. In general, net infiltration estimates have increased during the 1990's. This can be attributed to at least three factors. First, modeling techniques have improved during this period. Also, a vast database of site characterization information is now available so that models are based on fewer assumptions. Finally, a number of lines of evidence have now been used including tracers, direct soil water measurements, runoff data, and temperature profiles. Among the higher values offered are the results of an expert elicitation on the topic [Geomatrix, 1997]. Estimates based on a variety of datasets measured at or near Yucca Mountain generally fall in the range of 2 to 7 mm/year.

3.1.2 Current Yucca Mountain Project Activity

Recently, USDOE has issued Analysis/Model Reports (AMR) to document the technical and scientific efforts that provide a basis for the TSPA - Site Recommendation [CRWMS M&O, 2000d]. These reports provide some new information and complete documentation of the studies performed. Three AMR's are directly related to calculation of potential net infiltration:

Net Infiltration

- Future Climate Analysis [USGS 2000b]. This documents the selection of analogue climates to characterize future climate at the proposed repository site.
- Simulation of Net Infiltration for Modern and Potential Future Climates [USGS 2000a]. This AMR documents the model and datasets used in a) calculation of net infiltration for model calibration, b) estimation of net infiltration for a variety of climates and spatial domains, and c) analysis of uncertainty of model predictions.
- Analysis of Infiltration Uncertainty [CRWMS M&O 2000a]. This report provides results of a partial uncertainty analysis and calculation of weighting factors for use with infiltration model results.

**Table 3-1
Net Infiltration Estimates for Yucca Mountain, Nevada**

DATE	Net Infiltration (mm/year)	Precipitation (mm/year)	Author	Comment
Modern Climate				
1950	0	<203	Maxey and Eakin	Death Valley groundwater recharge estimate
1992	0.9	150.3	EPRI Phase 2	Initial numerical model
1994	1.2		Flint and Flint	Saturated hydraulic conductivity of matrix
1996	0 – 5.4		Fabryka-Martin	Cl ³⁶ mass balance
1996	6.7		Flint et al.	Neutron logs from 90 borings
1996	5.0		Bodvarsson, Ed.	UZ5 temperature profile matching
1996	1.2	154.6	EPRI Phase 3	Improved climate model
1997	10 mean (range: 0.5 – 50)		Geomatrix and TRW	Expert elicitation
1998	7.2	154.6	EPRI Phase 4	Improved runoff model
2000	2.2 – 5.1	188	USGS 2000a	Model calibration for 123.7 Km ² area
2000	7 – 14	170	CRWMS M&O 2000c	Saturated zone chloride data
2000	5	170	CRWMS M&O 2000b	Unsaturated zone chloride data
Glacial / Wetter Climates				
1950	21 – 27	305 – 380	Maxey and Eakin	Death Valley groundwater recharge estimate
1995	11.4 – 32.5	336.3	Lichty and McKinley	Hydrologic/watershed estimates
1996	2.9	194.5	EPRI Phase 3	Improved climate model for Full glacial climate
1998	19.6	194.5	EPRI Phase 4	Improved runoff model for full glacial climate
1998	32.5	300	CRWMS M&O, 1998	Flint et al. 1996 model for Full glacial climate
2000	14	342.8	USGS 2000a	Model calibration for 123.7 Km ² area

3.1.3 Objectives

The overall objective of this chapter is to assess whether the methods EPRI and USDOE uses for TSPA are adequate. Specific objectives to be addressed are:

- Summarize the current status of net infiltration measurements and modeling.
- Review the AMR's that USDOE intends to use to support its TSPA.
- Provide recommendations regarding possible improvements to the EPRI TSPA and the USDOE TSPA.

3.2 Recent Developments in Net Infiltration Modeling

Two key developments in net infiltration modeling occurred between 1998 (CRWMS M&O TSPA-Viability Assessment and EPRI Phase 4) and 2000. First, the primary model used by USDOE was finalized [USGS 2000a]. Second, USDOE released AMRs to document technical work in this area. These documents are part of the TSPA-Site Recommendation process.

3.2.1 Available Data and Calculations

USGS modeling and measurements were used as the basis for TSPA in the Viability Assessment [Gauthier, 1998]. At that time, the model made use of an extensive dataset of field and laboratory observations. Validation of the conceptual and numerical model was based on analysis of neutron borehole logs from 90 locations (Flint et al., 1996). Net infiltration calculated for current conditions was 6.7 mm/year average over the repository footprint area. For an assumed glacial climate averaging 300 mm/year precipitation, net infiltration was 32.5 mm/year.

The USGS model was improved for use in the TSPA-Site Recommendation [USGS 2000a, discussed in the next section]. Average net infiltration for the repository footprint area is now estimated as 4.7 mm/year for modern climate and 19.8 mm/year for the glacial transition climate. Model improvements since 1998 and the future climate analogues selected result in lowered estimates of net infiltration even though the glacial transition and modern climate average precipitation values have increased.

3.2.2 Review of Net Infiltration Analysis/Modeling Reports

Three AMRs are directly relevant to calculation of net infiltration. Each was prepared by a different group but all rely on the USGS net infiltration modeling group for implementation.

3.2.2.1 AMR: Future Climate Analysis [USGS 2000b]

The report describes the rationale and datasets used to quantify monsoon and glacial transition future climates. Modern climate is based on current measurements in the vicinity of Yucca Mountain. The selection of climate datasets is based on average annual precipitation and temperature. Five representative weather station datasets from three geographical areas are used

to characterize glacial transition climate while two stations plus current Yucca Mountain conditions are used for the Monsoon future climate. Climate datasets were selected to characterize lower bound and upper bound estimates for each climate scenario. Table 3-2 shows the range in average precipitation that results from USGS model runs using the chosen climates [USGS 2000a].

The EPRI Phase 4 estimates of average precipitation [EPRI, 1998] do not fall between the upper and lower bound average values chosen by USGS [USGS 2000b]. USGS estimates glacial transition climate average precipitation to range from 206 to 441 mm/year while EPRI uses 195 mm/year. For modern climate, USGS estimates 192 to 277 mm/year while EPRI uses 154.6 mm/year. This results from the datasets and analytical methods used for identifying paleoclimates. The EPRI approach [EPRI, 1998] incorporates paleoecological analysis, geological evidence, and physical principles of meteorology [EPRI, 1992] while the USGS approach is based on ostracode and diatom fossils plus other geological evidence. Other recent paleoclimate research in Southern Nevada has also made extensive use of vegetative indicators including fossil pollen and plant macrofossils [National Research Council, 1992].

The effect of the annual average precipitation difference cannot be determined from current studies because the use of the average value for characterizing climate is likely inadequate. It does not take into account range of annual values, the distribution of winter and summer precipitation, and precipitation characteristics such as storm intensity and duration. These factors are substantially different for the USGS and EPRI approaches (discussed in a later section).

3.2.2.2 AMR: Simulation of Net Infiltration for Modern and Potential Future Climates [USGS 2000a]

This AMR is the culmination of over 10 years of site characterization, data analysis, and modeling of Yucca Mountain conditions. Both the site characterization dataset and conceptual model of net infiltration address climate, vegetation, runoff, and site physical properties (Table 3-3).

An important part of the characterization is an extensive GIS database including a digital terrain map, a soil map, and spatial distribution of a number of measured soil and bedrock properties: hydraulic characteristics, depths, layers, soil texture, and bedrock geology. For TSPA-SR simulations, this information is represented on a 30 m by 30 m grid for the model domain. The largest domain of the model covers 123.7 Km² but calculations are also made for smaller areas: the repository footprint area (4.7 Km²); the area used for simulations of saturated and unsaturated flow from the repository location to the accessible environment (38.7 Km²); and sub-watershed areas used for model calibration.

Model calibration and validation in 1996 was based on matching of predicted and measured net infiltration using soil and bedrock moisture profiles at up to 90 locations and multiple times [Flint et al., 1996]. The matching was done manually and a formal error minimization calculation was not attempted. The final calibration for the model was made by matching regression lines for measured and modeled curves relating net infiltration and annual precipitation. Model results required precipitation in the wash/basin areas to be increased by 30 percent to improve the calibration. In 2000, model validation was refined using watershed runoff data for 5 monitoring

stations at Yucca Mountain. The digital terrain map was used to identify sub-watersheds for each surface water monitoring point and model calculations for two key storm events were made. As in 1996, the model was manually adjusted to optimize its calibration within the acceptable range of values identified in the previous borehole dataset calibration.

Net infiltration calculations for the TSPA-SR are presented in this AMR and are summarized in Table 3-2. The results show strong effects due to within-climate variability in precipitation; between-climate variability in average precipitation; and size of the model domain. In all but one of the climate scenarios (the lower bound modern climate), net infiltration is estimated to be highest for the repository scale model domain. The larger model domains contain more low elevation terrain and have lower estimated net infiltration even though these areas have more washes and drainageways within their boundaries. The net infiltration estimates in Table 3-2 are lower than those offered in 1998, presumably because the runoff calibration resulted in more surface runoff beyond the model domain.

USDOE invested in a detailed characterization and modeling effort to estimate net infiltration for Yucca Mountain conditions. The technical work presented in this AMR is thoroughly done and provides a basis for predicting spatially and temporally averaged net infiltration for modern and future climates. Model output is in a GIS format that could be used in unsaturated zone modeling to evaluate flow to the repository level and below. This AMR (as well as the one described in the next section) does not provide a detailed description of calibration procedures and results other than final output. Therefore, it is not clear whether component processes of water flow are modeled in a physically realistic way.

Net Infiltration

**Table 3-2
Year 2000 Net Infiltration Estimates**

Climate	123.7 Km ² area ¹		38.7 Km ² Area ¹		4.7 Km ² Area ¹ Repository Scale		EPRI 1998 Model Repository Scale	
	Infiltration Mm/year	Precipitation Mm/year	Infiltration mm/year	Precipitation mm/year	Infiltration Mm/year	Precipitation Mm/year	Infiltration mm/year	Precipitation mm/year
Monsoon Climate								
Upper Bound	13.6	412	19.8	415	20.3	422		
Mean	8.6	300	12.2	303	12.5	309		
Lower Bound	3.6	188	4.6	190.6	4.7	197		
Glacial Transition Climate								
Upper Bound	24.6	431	33	434	37.3	441	35.4	
Mean	13.4	310	17.8	318	9.8	323	19.6	194.5
Lower Bound	2.2	201	2.5	202	2.2	206	6.8	
Modern Climate								
Upper Bound	8.8	266	11.1	269	11.6	277	9.6	
Mean	3.6	188	4.6	191	4.7	197	7.2	154.6
Lower Bound	1.2	186	1.3	187	0.4	192	1.1	

¹USGS, 2000a

**Table 3-3
Factors Addressed in Net Infiltration Models**

	USGS, 2000b	EPRI, 1998
Modeling Approach	1 dimensional flow solution	1 dimensional flow solution
	GIS-based spatial treatment	3 hydrologic units
	Sub-daily model time step	Sub-daily model time step
	Multiple year sequential calculations	Multiple year sequential calculations
	Variable model domain	Repository footprint model domain
Soil/Rock Properties	Soil layers, layers, texture	Soil depth, layers, texture
	Spatial variation on 30 m grid	3 hydrologic units
	Measured bedrock hydraulic properties	Estimated soil and bedrock hydraulic properties
	Measured soil hydraulic properties	
Runoff	GIS-based topography	3 hydrologic units
	GIS-based flow routing	Down slope routing of average runoff flow
Climate	Daily Input Data	Daily Input Data
	Stochastic model for future climate	Stochastic model for future climate
	Elevation Corrections	
Vegetation	Snow calculations	
	Cover percentage	Cover percentages for grass, shrubs
	Root depth/distribution	Root depth/distribution

3.2.2.3 AMR: Analysis of Infiltration Uncertainty [CRWMS M&O 2000a]

This AMR was developed to address a perceived shortcoming of the net infiltration model described above. Specifically, the effect of selected input parameters on average net infiltration was unknown. Therefore, an evaluation of 12 factors with uncertain distributions was conducted. The factors evaluated are summarized in Table 3-4. The rationale for selection of parameters to study is not given in the document but the parameters selected were relevant and among the most uncertain.

**Table 3-4
Factors Evaluated in Uncertainty and Sensitivity Testing**

	CRWMS M&O¹	EPRI²
Soil/Rock Properties	Root zone porosity Soil root zone depth Bedrock Root Zone Depth Soil hydraulic properties Bedrock hydraulic properties	Soil matrix texture Soil rock fragment content Soil hydraulic properties
Runoff	Surface flow runoff area	Surface storage of runoff
Climate	Evapotranspiration coefficients (2) Evapotranspiration multiplier Precipitation multiplier Snow melt parameter Sublimation factor	
Vegetation		Cover percentage

¹ Uncertainty Analysis [CRWMS M&O, 2000a]

² Sensitivity Testing [EPRI, 1998]

The result of this uncertainty analysis is a comparison of net infiltration values calculated while varying input parameters with other values calculated without uncertainty [USGS 2000a]. The average values for the uncertainty study are close to but always higher than the USGS values.

The AMR also presents an additional calculation using the uncertainty analysis model runs. USDOE intends to use weighting factors with upper bound, lower bound, and mean climate net infiltration values to develop an overall average net infiltration rate for each climate scenario. The weighting factors are calculated in this AMR. The procedure used is appropriate but no rationale for use of weighting factors is offered.

The uncertainty analysis results presented in this AMR are not particularly useful. They provide limited assurance that model predictions are appropriately made. The analysis offered in the report is very brief; it is likely that USGS may have done more analysis of uncertainty in its model calibration effort than is presented in this AMR. The AMR does recommend that additional study of uncertainty in the selection procedure for potential future climate analogues is warranted. Although this is not a conclusion directly based on AMR analysis, it can be inferred because the variation in net infiltration due to climate is much greater than the effects of variables used in the uncertainty analysis.

3.2.2.4 Effect of Model Assumptions on Net Infiltration Results

The three AMRs directly related to net infiltration calculations provide some assurance that Project net infiltration modeling technique does not introduce a systematic error into estimates.

In part, this conclusion is expected because the output of net infiltration modeling has extensive temporal and spatial averaging incorporated. In fact, the issue that appears to have the largest effect on net infiltration is the selection of climate analogues. There is scientific debate on this topic because multiple lines of geological and paleontological evidence exist. This issue of uncertainty is not well addressed.

3.3 EPRI Net Infiltration Calculations

EPRI's net infiltration modeling has not changed since Phase 4 [EPRI, 1998]. A brief review of model approach is provided below and the approach and results are compared with those of USDOE [USGS, 2000a].

The 1992 net infiltration model is a one-dimensional, finite difference code based on the Richards equation for unsaturated zone water flow. The model incorporates source and sink terms for plant water uptake, surface infiltration, and drainage from the root zone to the deep subsurface (net infiltration). The model requires daily climate information and incorporates sub-daily time steps in order to make a realistic simulation of soil and hydrologic processes.

Model calculations are made for three soil/hydrologic units: shallow soils at the top of Yucca Mountain, moderately deep soils on the side slopes, and deep soils in the basin areas of Yucca Mountain within the footprint of the proposed repository. Average net infiltration for this model domain is calculated by using a spatial average of the three soil/hydrologic units.

Model calculations are made using 122 years of climate input data generated from stochastic models for winter and summer weather patterns (EPRI, 1992). In this way, the variability in net infiltration caused by a) seasonal changes in precipitation and b) antecedent conditions is incorporated in results.

Table 3-3 compares the models used by USGS and EPRI. While numerous specific details of the models differ, both address the same technical issues. The key differences are:

- USGS incorporates an extensive GIS database of physical properties; the EPRI model lumps the model domain into three distinct soil/hydrologic units.
- USGS incorporates treatment of elevational changes in climate and addresses snow fall separate from rainfall; EPRI does not.
- USGS has used two calibration datasets: soil moisture profiles and surface runoff volumes. The EPRI model has had limited calibration.
- The USGS model has been used in an uncertainty analysis. The EPRI model was used to develop a sensitivity analysis of several parameters with unknown distributions (Table 3-4). As with the USGS model [CRWMS M&O 2000a], the EPRI sensitivity analyses demonstrated that the key factor influencing net infiltration results is selection of the climate to characterize future conditions at Yucca Mountain.
- USGS uses climate analogues to model future climate. EPRI uses a climatological method that specifically addresses shifts in winter and summer precipitation patterns. This is considered important because many researchers believe that glacial summers will be

significantly drier than current conditions (NRC, 1992; Spaulding, 1985). Table 3-5 compares glacial climate characterizations used for the two models. The EPRI characterizations follow the recommendations of Spaulding. The USGS analogue climates are characterized by summer climates that are much wetter than either Spaulding or EPRI.

**Table 3-5
Comparison of USGS and EPRI Glacial Climate Characterizations**

Source	Annual % of Modern climate	Winter season % of Modern climate	Summer season % of Modern climate
Spaulding 1985	30-40% wetter	60-70% wetter	40-50% drier
EPRI 1998	26% wetter	66% wetter	48% drier
USGS-Beowawe	46% wetter	6% drier	58% wetter
USGS-Delta	1% wetter	11% drier	48% wetter
USGS-Rosalia	68% wetter	136% wetter	156% wetter
USGS-Spokane	62% wetter	116% wetter	124% wetter
USGS-St John	67% wetter	120% wetter	147% wetter

Net infiltration results for the two models are compared in Table 3-2 for the repository footprint scale. Values are comparable for average net infiltration despite a discrepancy in estimated annual precipitation. This is likely related to the difference in summer precipitation assumed in the two climate characterizations.

3.4 Summary

Measurements and modeling of net infiltration at Yucca Mountain has progressed in the past 10 years. As the change in estimated values shows (Table 3-1), estimated net infiltration has increased since 1992. During that time, conditions at Yucca Mountain have been well characterized and modeling methods have been refined. The USDOE net infiltration estimate for current/modern climate is 4.7 mm/year; the EPRI estimate is 7.2 mm/year. For glacial climate, the USDOE average net infiltration is 19.8 mm/year; the EPRI estimate is 19.6 mm/year.

USDOE released a series of AMRs to document models and measurements used in TSPA. The three AMRs relevant to net infiltration are adequate and serve to document that the factor most in need of further evaluation is future climate. Not only is a reasonable characterization of average climate required, but an evaluation of seasonal distribution and individual storm characteristics is required. In addition, quantification of uncertainty is needed. Given the analyses of future climate available in the scientific literature, it is likely that additional analogue climates should be selected from areas with different winter and summer precipitation patterns.

3.5 References

- Bodvarsson, G.S. and T. M. Bandurraga (eds.). 1996 "Development and calibration of the three-dimensional site-scale unsaturated zone model of Yucca Mountain." Lawrence Berkeley National Laboratory.
- Civilian Radioactive Waste Management Systems Management and Operating Contractor (CRWMS M&O) 2000a. Analysis of Infiltration Uncertainty. ANL-NBS-HS-000027 REV 00. Las Vegas, Nevada: CRWMS M&O. ACC:MOL.20000525.0377.
- CRWMS M&O 2000b. Analysis of Geochemical Data for the Unsaturated Zone. ANL-NBS-HS-000017. Las Vegas, Nevada: CRWMS M&O. Submit to RPC URN-0048.
- CRWMS M&O 2000c. Geochemical and Isotopic Constraints on Groundwater Flow Directions, Mixing, and Recharge at Yucca Mountain, Nevada. ANL-NBS-HS-000021 REV 00. Las Vegas, Nevada: CRWMS M&O. Submit to RPC URN-0060.
- CRWMS M&O 2000d. Total System Performance Assessment – Site Recommendation. Presented to: NRC/DOE Technical Exchange on Total System Performance Assessment (TSPA) for Yucca Mountain. San Antonio, TX. June 6, 2000.
- CRWMS M&O, 1998. "Unsaturated Zone Hydrology Model". Chapter 2 of Total System Performance Assessment-Viability Assessment (TSPA-VA) Analysis, Technical Basis Document. B00000000-01717-4301-00002 REV 01. Las Vegas, NV. CRWMS M&O. ACC: MOL. 19981008.0002.
- Electric Power Research Institute (EPRI), 1998. Alternative Approaches to Assessing Performance and Suitability of Yucca Mountain for Spent Fuel Disposal. Final Report TR-108732. Palo Alto, CA.
- EPRI 1996. "Yucca Mountain Total System Performance Assessment, Phase 3." EPRI TR-107191, Electric Power Research Institute, Palo Alto, CA.
- EPRI 1992. "Demonstration of a Risk-Based Approach to High-Level Waste Repository Evaluation: Phase 2." EPRI TR-100384, Electric Power Research Institute, Palo Alto, CA.
- Fabryka-Martin, J. A., A. V. Wolfsberg, P. R. Dixon, S. Levy, J. Musgrave, and H. J. Turin, 1996. "Summary report of Vhlorine-36 Studies: sampling, analysis and simulation of chlorine-36 in the Exploratory Studies Facility." Los Alamos National Laboratory Milestone report 3783M. Los Alamos, NM.
- Flint, L. E. 1998. "Characterization of Hydrogeologic Units Using Matrix Properties, Yucca Mountain, Nevada." U.S. Geological Survey. Water Resources Investigations Report 95-4035.
- Flint, A. L.; Hevesi, J. A.; and Flint, L. E. 1996. Conceptual and Numerical Model of Infiltration for the Yucca Mountain Area, Nevada. Milestone 3GUI623M. Denver, Colorado: U.S. Geological Survey. ACC: MOL.19970409.0087.

Flint, L. E. and A. L. Flint. 1995. "Shallow Infiltration Processes at Yucca Mountain, Nevada – Neutron Logging Data 1984-93." U.S. Geological Survey. Water Resources Investigations Report 95-4035.

Flint, A. L. and L. E. Flint. 1994. "Spatial Distribution of Potential near Surface Moisture Flux at Yucca Mountain." Proceedings of the Fifth International High Level Radioactive Waste Conference, Las Vegas, NV. April 25-30.

Gauthier, J. 1998. "Climate, Infiltration, and UZ Flow for TSPA-VA." Presentation to the Nuclear Waste Technical Review Board. April 23-24.

Geomatrix Consultants, Inc. and TRW. 1997. "Unsaturated Zone Flow Model Expert Elicitation Project." Prepared for U.S. Department of Energy. May.

Lichty, R. W. and P. W. McKinley. 1995. "Estimates of groundwater recharge rates for two small basins in central Nevada". U.S. Geological Survey Water Resources Investigation Report 94-4104. 31 p.

National Research Council. 1992. "Groundwater at Yucca Mountain. How High Can It Rise?" Final Report of the Panel on Coupled Hydrologic/Tectonic/Hydrothermal Systems at Yucca Mountain. National Academy Press. Washington, D.C.

Spaulding, W. G. 1985. Vegetation and Climates of the Last 45,000 Years in the Vicinity of the Nevada Test Site, South-Central Nevada. U.S.G.S. Professional Paper 1329. 83 p.

U.S. Geological Survey (USGS). 2000a. Simulation of Net Infiltration for Modern and Potential Future Climates AMR. TDP-NBS-HS-000016, Rev. 01. Denver, Colorado: U.S. Geological Survey. ACC: MOL.2000516.0011.

USGS. 2000b. Future Climate Analysis. ANL-NBS-GS-000008 REV 00. Denver, Colorado: U.S. Geological Survey. Submit to RPC URN-0004.

Wilson, M. L. and C. K. Ho. 2000. Unsaturated Zone Flow and Transport. Presentation to DOE/NRC Technical Exchange on Total System Performance Assessment (TSPA) for Yucca Mountain. San Antonio, TX. June 6, 2000.

4

COUPLED PROCESSES AFFECTING GROUNDWATER DISTRIBUTION AND ROCK

4.1 Introduction

This chapter reviews the coupled processes being incorporated in the DOE's and EPRI's TSPA model. This section is made up of two subsections, one subsection will review thermohydrology characteristics of the proposed repository and the second section will comment on the near-field T-H-C coupled processes described in the DOE's SR-TSPA. In each section a review of the DOE's process is provided with a follow on section on suggested modifications.

4.1.1 Near-Field Thermohydrology Introduction

Heat produced by decay of spent fuel is one of the elements of the Yucca Mountain repository that will perturb subsurface conditions. When heating creates temperature gradients, convective flow of fluids will occur. Because the repository will be located in the vadose zone, where water is present in both liquid and vapor phases, water can evaporate or condense as temperatures change and as fluids flow into areas of differing temperature. The combined effects of evaporation, condensation, and convection create a system in which fluid flow and heat transfer influence each other reciprocally. The study of coupled flow and heat transfer phenomena in the subsurface is referred to as thermohydrology.

This chapter will explore the thermohydrologic behavior of the Yucca Mountain repository and the computer models that the DOE is using to simulate thermohydrologic processes. These processes are complex in Yucca Mountain, where the rock contains both fractures and small pores, and fluids behave differently in the two kinds of opening. Because these phenomena had been studied very little before the Yucca Mountain project began, the DOE was not able to simply use a computer model that was already available, measure the rock properties, and run the program with the measured values as inputs. The DOE has therefore made a significant commitment to research in the science of fluid flow and heat transfer through porous fractured rock, to improving computer models of these processes, and to designing the repository to accommodate the direct and indirect effects of heat.

In the last two years, this commitment has increasingly paid off. Uncertainties about fluid flow and heat transfer around a heated repository have been markedly reduced. Some of the more complex coupled processes are better understood, and their effects on repository performance can be modeled more accurately or can be bounded with greater confidence. As a result, the level of complexity needed to model the system has been reduced. This makes possible significant simplifications in systems-level computer models like the EPRI systems performance model. For

more detailed models, like the programs that the DOE is using to predict temperature and fluid flow near the repository, there is a greater ability to understand how assumptions built into the models affect the results. This creates the basis for greatly enhancing the reliability of model predictions.

The principal areas in which uncertainties have been reduced are:

- Scientific research has provided a better understanding of thermohydrology in porous fractured rock.
 - The “active fracture” model of water movement in unsaturated fractured rock explains how water can move through fractures when the rock matrix is not fully saturated, providing a way to model Yucca Mountain in spite of the apparent disequilibrium between fracture and matrix water.
 - Niche seepage tests and the drift-scale heater test support the active fracture model’s rejection of the equilibrium concept of fracture-matrix interactions. The results seem to rule out the scenario in which water vapor condenses above the repository, condensate accumulates into a reservoir of water, and the condensate floods the repository after moisture is wicked back into the rock matrix.
- Changes in repository design have reduced uncertainties about thermohydrology. By increasing the spacing between drifts, the new design ensures that zones in the centers of the pillars between the emplacement drifts will remain below the boiling point at all times. This avoids creation of a continuous layer in which temperature is above boiling and the gas is essentially pure water vapor, as envisioned in earlier design concepts. Such a layer would have obstructed upward movement of noncondensable gases and downward movement of liquid water, creating the possibility of instabilities that would be very difficult to model.
- Changes in repository design have made repository performance less sensitive to thermohydraulic behavior. The waste package will be made of extremely corrosion-resistant alloys and will be protected by a drip shield. Consequently, the adverse effects of any water that might be mobilized when the rock around the repository drift is heated and drip into the drift during the first hundreds or thousands of years after closure will be much less than for the previous design.

These advances make significant simplifications possible in the systems performance model used by EPRI. Accumulation of large amounts of water above the repository has been ruled out. Limits have been placed on the amount of water that could drip into the repository during the first few millennia after emplacement, the “thermal period” during which heat has a strong effect on water movement. Drip shields and redesigned waste packages now protect against such drips, so that water movement during the thermal period has little effect on waste package performance. Consequently, changes in climate and infiltration rate in the first few millennia have little effect on performance, such that only a single climate scenario need be analyzed. For similar reasons, there is no need for a separate analysis of the minority of “cool” waste packages located in parts of the repository where temperatures drop below boiling relatively quickly and water can drip earlier than elsewhere. All waste packages can now be described by a single “typical” temperature curve. The next section of this chapter presents the revised EPRI model inputs.

These developments have also brought DOE much closer to an understanding of the detailed thermohydrologic behavior around the repository. But DOE's models still contain approximations whose effect is not completely understood. Resolving the uncertainties connected with these approximations remains important, despite the design changes that lessen the repository's vulnerability to water that might enter unexpectedly, in order to provide defense in depth. The third section of this chapter seeks to identify the principal uncertainties that remain in the detailed models and suggest methods of eliminating these uncertainties.

The fourth section of the chapter addresses the issue of model conservatism. As discussed above, the revised repository design removes a potentially intractable uncertainty by eliminating the possibility of large-scale chaotic flow. This change is described in detail. The section goes on to list approximations that remain in the DOE's current models and classify them into areas of conservatism and non-conservatism.

Thermohydrologic models predict both temperature and fluid flux, and models are often conservative with respect to one of these variables and non-conservative with respect to the other. The conservatism of each approximation with respect to each of the two variables is therefore assessed separately.

The final section of the section 4.1 summarizes conclusions and recommendations.

4.1.2 IMARC5 Inputs

Inputs to the EPRI systems performance model were updated to reflect changes in repository design and take advantage of advances in modeling by the DOE. Two design changes that have a major impact on thermal modeling in IMARC are shown in Figure 4-1, (1) the "line loading" repository layout in which, pillar centerline temperatures never exceed boiling, and (2) the redesigned waste package which has a very long lifetime. In the redesigned waste package, temperature has very little influence on corrosion once the temperature drops below the boiling point. This weakens the dependence of corrosion rates on time-temperature curves. The only dependence that remains relates to the period when temperatures in the engineered barrier/near field area are above 100°C. With the increased pillar spacing in the new repository layout, each drift feels little effect from heating by neighboring drifts until after temperatures have dropped below boiling. The combined effect of these developments is that temperatures can, to a first approximation, be taken from a single-emplacment-drift model that ignores interactions among the pillars between succeeding drifts.

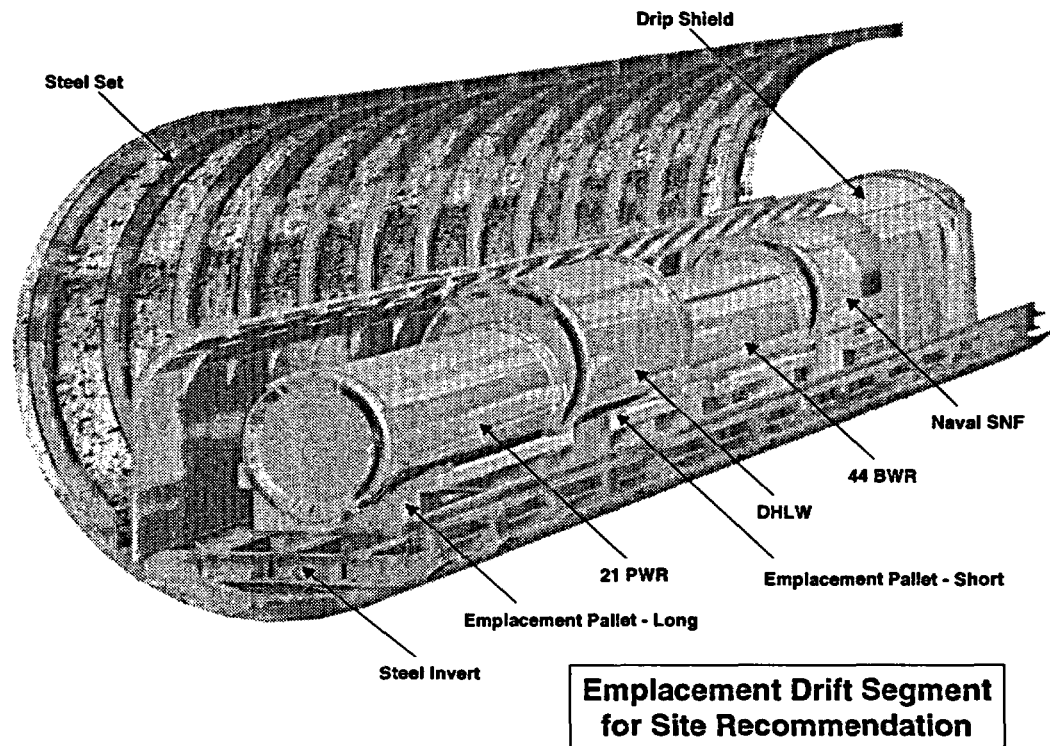


Figure 4-1

Therefore waste-package temperatures used in IMARC-5 were taken from a drift-scale model [CRWMS M&O 2000e]. Temperatures are displayed in Figures 4-2 and 4-3, and in Table 5-3.

Where percolation flux is equal to the infiltration rate, the infiltration rate is the same as used in IMARC-4. Note that at the early times when temperature has a significant influence on corrosion, temperature is insensitive to infiltration. The assumed infiltration rates are as follows. (Infiltration rates used by the DOE [Francis and Itamura, 2000, p. 31] are shown in parentheses.)

Thermal period (until temperature curve drops below boiling) - 0

Current climate:

low infiltration - 1.1 mm/yr (0.6)

baseline - 7.2 mm/yr (6.0)

high infiltration - 9.6 mm/yr (14.6)

Glacial climate:

low infiltration - 6.8 mm/yr (3.0)

baseline - 19.6 mm/yr (24.9)

high infiltration - 35.4 mm/yr (46.7)

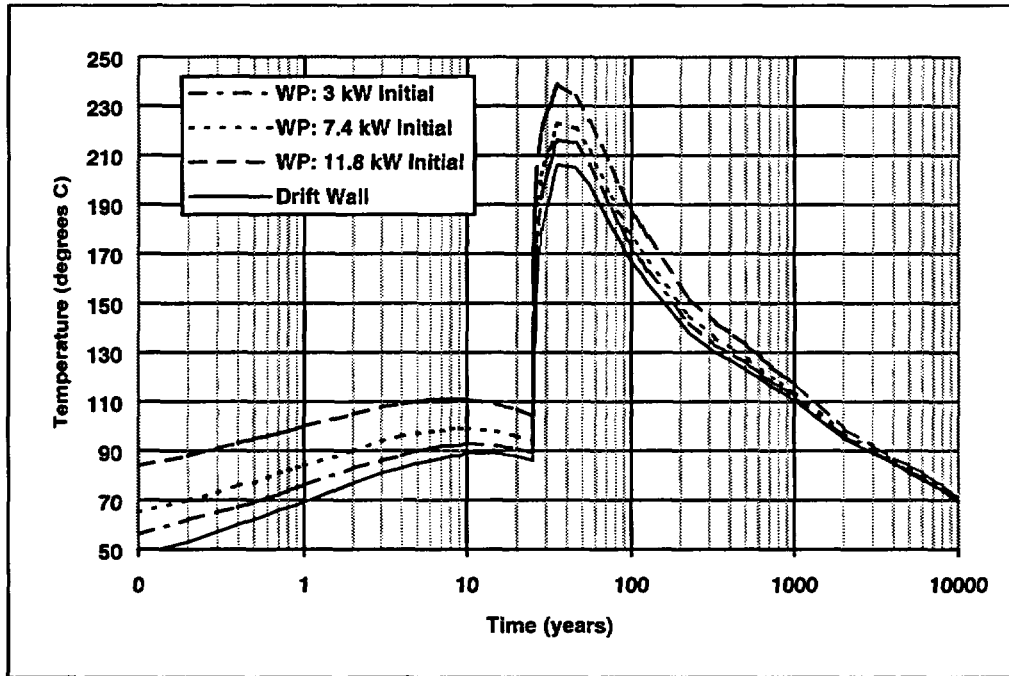


Figure 4-2
WP Surface and Drift Wall Temperatures for 25-yr Ventilation, 0.1-m Spacing, and No Backfill

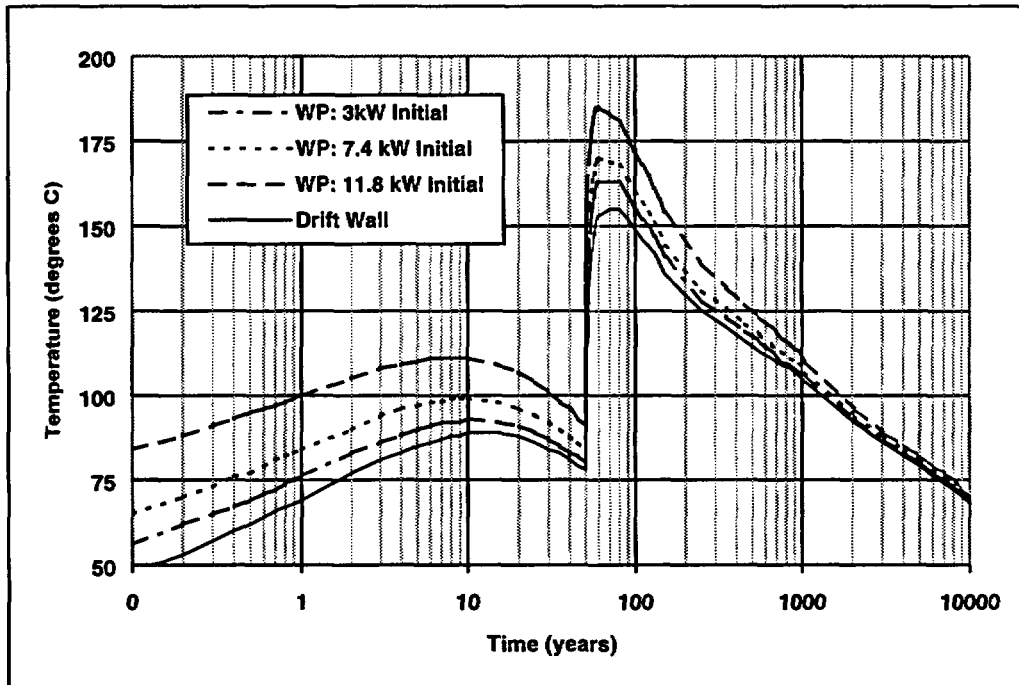


Figure 4-3
WP Surface and Drift Wall Temperatures for 50-yr Ventilation, 0.1-m Spacing, and No Backfill

The flow of liquid water in the unsaturated zone at Yucca Mountain is not uniform; it varies from place to place. This phenomenon is referred to as “flow focusing.” To the extent that it occurs, the water flux at any location in the repository will differ from the average value. This variability is described in terms of a “flow focusing factor”, which is the ratio of the flux in the areas of high flow to the average.

Wilson [2000] provides a detailed analysis of flow focusing based on the active fracture model. He finds that the reasonable range of flow focusing factors is a uniform distribution from 1 to 22. (These are derived as 95% confidence bounds on a more complex distribution that comes from his active fracture model.) In the current version of the EPRI model, two discrete values are chosen, corresponding to Wilson’s bounding values of 1 and 22. A value of “1” means that flow is uniform and that the local percolation rate at any point is equal to the average infiltration rate. A value of “22” means that percolation is concentrated in an area of 4.5% of the repository, where the local percolation rate is 22 times greater than the average infiltration, and that the percolation rate is zero elsewhere. Note that the area of high flow is not a single region, but consists of a large number of relatively small patches distributed throughout the repository footprint.

Within each group of waste packages located in a zones where non zero percolation is assumed, some packages will be wet and some will be dry. Conceptually, we imagine that infiltrating water drips from the hanging wall of the repository drift at discrete points. These drip points are randomly located; their frequency depends on the percolation rate. If a waste package is located under one or more of the drip points, it will be ‘wet’; otherwise, it will be ‘dry’. The probability that a package will be located under one or more drip points, as a function of the local percolation rate, was calculated by Wilson [2000]. Wilson’s results were based on a computer model of water flow in the unsaturated fracture network, which was calibrated against drips that were observed in the ESF niche tests at Yucca Mountain. The same model also gives the water flux past an average wet package.

Figures 4-4 and 4-5 depict the Wilson [2000] curves giving the fraction of wet packages and the water flux past each package. Figure 4-4 shows that the fraction of waste packages that are wet increases rapidly with percolation rate when the local percolation rate is between, roughly, 20 and 500 mm/yr. To the extent that focused changes the local percolation flux within this range, a reduction in the size of the area where flow occurs is compensated by an increase in the fraction of waste packages within that area that get wet. When this occurs, flow focusing does not significantly change the number of waste packages that are wet and therefore has little impact on repository performance. For the glacial baseline infiltration rate of 19.6 mm/yr, the presence or absence of flow focusing has little impact on repository performance. On the other hand, for the “high” and “low” values of 6.8 or 35.4 mm/yr, flow focusing changes the number of wet packages and thus does have an impact on overall performance.

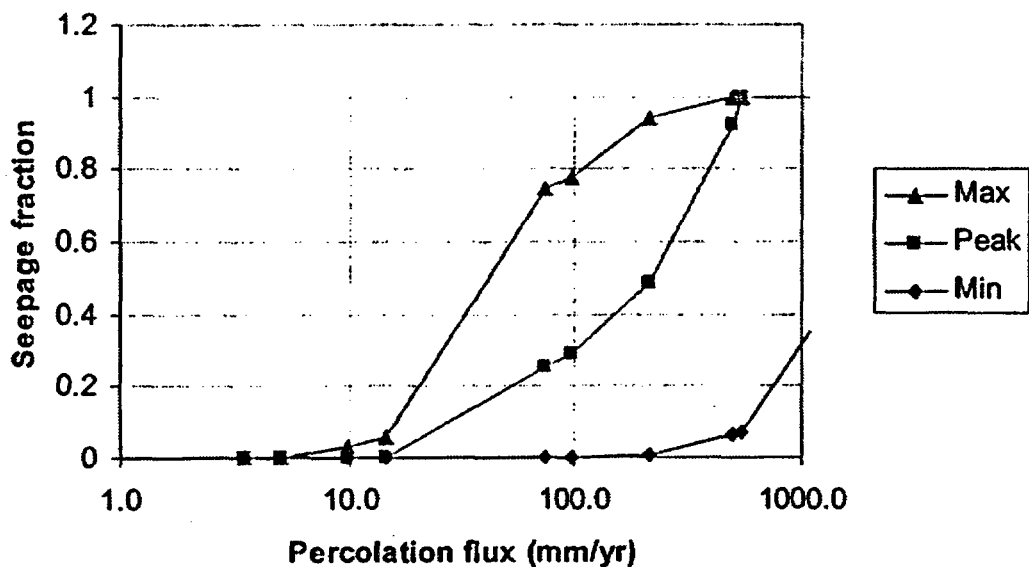


Figure 4-4
Percolation Flux vs. Seepage Fraction

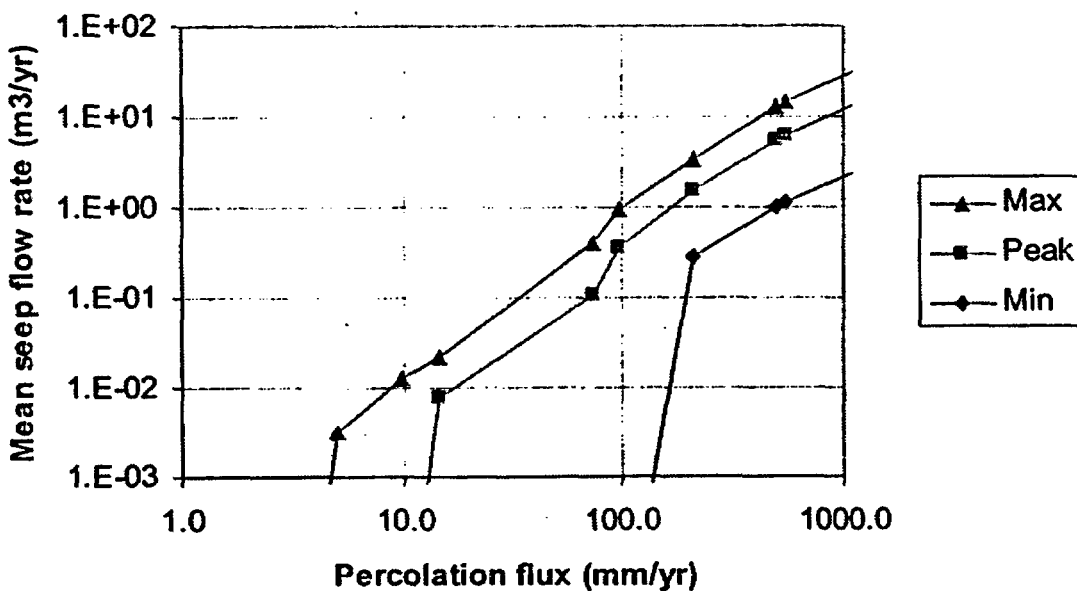


Figure 4-5
Percolation Flux vs. Mean Seepage Flow Rate

4.1.3 DOE Models

The models used by the DOE for detailed predictions of thermohydrologic behavior do not fully reflect recent advances in scientific research and repository design. In particular, these models still contain approximations whose validity has not been fully assessed. Among the most important of these assumptions are:

- Water in partially saturated fractures flows in response to suction forces in the same way as water in pores. This modeling process is considered to be very conservative and should be revised.
- The multi-scale thermohydrologic model does not as yet take account of mountain-scale convective heat transfer and gas flow.
- Because it is not practical to run a single model that spans the range of length scales on which important heat transfer phenomena operate, a “scanning curve” methodology is used to relate models that operate on different scales.

This section discusses the reasons that these approximations seem to be important. It also suggests modeling techniques that could be used to resolve the uncertainties they bring into performance assessment.

4.1.3.1 Water Drainage and the “Active Fracture” Model

The DOE’s Multiscale Thermohydrologic Model (MSTHM) uses an “active fractures” model [Liu et al., 1998] which allows water to flow only in “active” fractures. The distribution of water within the active fractures is controlled by the interplay of gravity and suction forces in the same way as in unsaturated porous media. Pruess [1999] suggests an alternative conceptual model in which gravity alone is the predominant force controlling flow through the fractures. In this model, water moves through fractures like the rivulets of water that run down the windshield of a parked car during a rainstorm.

The rivulets model is supported by several lines of evidence:

- Niche seepage tests. The results of these tests could be simulated with a numerical model only by setting the strength of suction forces to nearly zero [Finsterle and Trautz, 2000].
- The drift-scale heater test. Measurements showed less water above the drift and more water below than had been predicted by numerical models [Liu et al., 2000]. This indicates that gravity is more important vis-a-vis suction than was assumed by the models used in the simulations.
- Geochemical data support the evidence of fast chlorine-36 movement.

The DOE has implemented the active fracture model with numerical models (NUFT and TOUGH) that include an adjustable parameter that determines the strength of suction forces. This “inverse van Genuchten alpha” parameter has units of pressure and corresponds, on a very rough conceptual basis, to the amount of pressure that suction forces exert to draw water into the narrowest portions of the fracture. When this parameter approaches zero, models like NUFT and TOUGH approximates a rivulets model because water is free to run downward through open fractures without being pulled into constricted zones and trapped there.

The Multiscale Thermohydrologic Model used large values of this parameter (on the order of 1000 Pa) which correspond to the ordinary active fractures model in which suction is important. The MSTHM values were obtained indirectly from measured properties of the fractures using a

parallel-plate model; this derivation essentially assumes that suction is important. The large inverse-alpha values thus require further justification even if the active fractures model is correct.

Only the seepage modeling used a small value of the inverse-alpha parameter (50 Pa) which approximates the rivulets model (or at least a version of it). This value was obtained by calibrating the seepage experiments against the model.

Whether the Yucca Mountain behaves as described by the active fracture model or rivulets model can affect repository performance. In the rivulets model, water that condenses when warm moist air flows away from the heat source will drain rapidly toward the water table. Such drainage could remove water from the near field and extend the period during which emplacement drifts remain dry beyond the time of above-boiling temperatures. This effect will be most pronounced if infiltration rates are relatively low.

To help resolve uncertainties about whether the active fracture or the rivulets model better describes flow in unsaturated fractures, DOE should run sensitivity analyses in which the inverse-alpha parameter in the MSTHM is reduced to 50 Pa. This would indicate how strongly the model results depend on the assumption that the active-fracture model describes flow at Yucca Mountain accurately. If there is little dependence, the issue could be considered resolved; if dependence is significant, conservative modeling approaches would be needed unless additional research into unsaturated flow mechanisms could answer the scientific questions.

4.1.3.2 Mountain-Scale Convection

The thermohydraulic analysis presented by Buscheck [2000] does not explicitly model mountain-scale convective gas flow (that is, flow which goes upward through the repository and downward outside the repository footprint). Convection is modeled only on the drift scale, in which gas flows upward near the drifts and downward through the pillars. This choice of scale effectively eliminates convection as a significant factor in determining temperatures, because the formula for the Rayleigh number, the dimensionless parameter controlling thermal convection, implies that the threshold at which convective heat transfer becomes important scales linearly with the size of the convection cell.

4.1.3.2.1 Why Mountain-Scale Convection should be Addressed

Revised waste-package designs that resist corrosion at early times make repository performance less sensitive to temperatures and to water fluxes connected with convective effects. Nonetheless, reasonably accurate modeling of thermal effects is important. A reasonable understanding of repository temperatures and early-time water fluxes provides defense in depth; the safety of the repository should not rest exclusively on the unusual corrosion resistance of package and drip-shield materials. To the extent that mountain-scale convection can significantly alter temperatures, its omission from DOE thermohydrologic models is significant and should be remedied if feasible. Even if convection does not change temperatures appreciably, convective gas flow might move a significant amount of water vapor upward through the repository.

The importance of mountain-scale convective heat transfer is thus related to how its magnitude compares to conduction. Because gas flow depends on rock permeability, the magnitude of convective heat transfer depends on how large the permeability is. A parametric analysis by Ross et al. [1993], which is based on the analytical solution by Zhang et al. discussed above, suggests that with a permeability in the TSw of $5 \times 10^{-11} \text{ m}^2$, convection significantly alters rock temperatures in a Yucca Mountain repository within a few hundred years, and with a permeability of $1 \times 10^{-11} \text{ m}^2$, it alters rock temperatures within 1000 to 2000 years.

The mountain-scale air permeability of the TSw seems to be sufficient to make convection important. While the baseline values of permeability used in the drift-scale thermohydrologic model are around 10^{-12} m^2 in most portions of the TSw [Buscheck, 2000, p. 60], calibrating the unsaturated-zone site-scale model against down-hole measurements of barometric pressure fluctuations yielded values of 10^{-11} m^2 or greater in most of the unit [Bandurraga and Bodvarsson, 1997; Ahlers and Liu, 2000]. The larger values are more relevant to convection analysis because they, unlike the baseline values, are derived from mountain-scale measurements and because the baseline values show an unreasonably small permeability contrast between the TSw and PTn units. Recognizing that larger values of permeability are appropriate in a mountain-scale model [Liu et al., 2000, pp. 30-31], the two-dimensional mountain-scale thermohydrologic modeling used the larger values [Haukwa, 2000, p. 20; Ahlers and Liu, 2000, p. 48]. The results of this modeling [Haukwa, 2000, Figures 45 and 59] show what appear to be regular convection cells developing between 500 and 1000 years after emplacement.

Practical limitations on modeling are a significant barrier to simulation of mountain-scale convection by straightforward discretization of partial differential equations. Scale-dependence requires a model that encompasses the entire mountain (or at least half of it), and three-dimensional effects are significant. However, the gridding must be fine enough to capture the curvature of convection cells. Where temperatures rise above boiling, the existence of wetting fronts makes hard-to-measure parameters important and may introduce additional gridding constraints.

Furthermore, the non-linear relationship between vapor pressure and temperature implies that if there are significant temperature differences between drifts and pillars, the gridding must be even finer in order to depict these temperature contrasts explicitly. For example, if the drift temperature is 125°C and the pillar centerline temperature is 80°C , a coarsely gridded model might calculate a "smeared" temperature of 100°C throughout the pillar. The model would then predict the existence of a zone where soil gas is pure water vapor. Such a zone would block upward convective flow of noncondensable gases. A model gridded finely enough to capture temperature contrasts within the pillar would predict more accurately that noncondensable gases flow upward through the cooler regions of the pillar.

The requirement for a combination of large model domains and fine grids drove DOE to make approximations that have significant limitations when it modeled mountain-scale heat transfer. The multiscale model used a 3-D conduction-only model with a smeared heat source for its mountain-scale modeling; this ignores the largest convection effects. The DOE mountain-scale model succeeded in running a few conduction-convection cases on 2-D north-south cross-sections, but these simulations understate convective cooling because the repository footprint is much shorter in the east-west direction than in the north-south direction. Because convective cooling is most effective near the edge of the repository, a model using a north-south

cross-section will understate the effect of convective cooling in the central portion of the repository. This is where the hottest waste packages are likely to be found.

4.1.3.2.2 Proposed Modeling Approach

The value of incorporating mountain-scale convection in the multiscale thermohydrologic model would be considerable. Such a model is possible if use is made of two recent developments: the shift to a wide-pillar repository design with pillars below boiling, and the development in IMARC-4 of a model [Ross, 1998] for the transition between regimes dominated by convection and heat pipe effects.

As described above, cool pillars provide a pathway for upward flow of noncondensable constituents of soil gas. This flow relieves pressure differences that could develop across a continuous boiling zone from which dry air was excluded. The absence of a strong upward gas-pressure gradient limits the rate at which heat can be transferred by a gravity-driven heat pipe in which condensate descends by gravity flow, evaporates, and flows upward as vapor. Heat pipes then exist primarily as drift-scale phenomena with gas flowing outward in all directions from the boiling zone. Convection dominates on the mountain scale.

With heat pipes decoupled from mountain-scale convection, it becomes possible to model the two phenomena sequentially in the framework of the existing multiscale thermohydrologic model. Approximations are necessary, but it is no longer necessary to eliminate significant couplings entirely. Specifically, one can proceed as follows:

1. Use a drift-scale model (either thermohydrologic or conduction-only) to determine the temperature distribution across a typical pillar at the time of maximum width of the boiling zone.
2. Determine the average of absolute humidity at that time across the cross-section of the pillar.
3. Adjust the curve of vapor pressure of water versus temperature by flattening it out at the maximum value determined from the previous step. (This is similar to a method already employed in the TGIF2 code [Lu and Ross, 1993]. The transition from the steam table values to the flat maximum must be smoothly curved in order to avoid numerical instabilities.)
4. Run a three-dimensional mountain-scale convection-conduction model of the repository, using a smeared heat source and the adjusted vapor pressure curve. This could be done either with TOUGH/NUFT or with TGIF2.
5. In each column that will be simulated in drift-scale modeling, determine the upward gas flux through the repository horizon, as a function of time, from the mountain-scale smeared-source model. Also determine the upward gas flux through the PTn unit.
6. Use drift-scale heat transfer and fluid flow models like those in the current MSTHM model, but change boundary conditions to impose the appropriate upward gas flux. At the bottom of the side of the model, use an imposed-flux boundary with an inward flow (which must change over time) equal to the upward gas flux determined from the mountain-scale model.

Just below the PTn, impose a horizontal flux equal to the difference between the upward flux through the repository horizon and that through the PTn.

This combination of models should give a reasonably accurate representation of both mountain-scale convective heat transfer and drift-scale heat-pipe effects, including dry-out and moisture transfer.

4.1.3.3 Scanning Curves

Another approximation in the MSTHM is the use of a “scanning curve” method to relate models that run on different scales. This technique is used to calculate the temperatures, relative humidities, and other parameters predicted used as inputs to waste package performance studies. The DOE has, as yet, not fully evaluated the adequacy of this approximation, and it deserves further study because so much rests on it.

4.1.3.3.1 Description of the Scanning Curve Method

Heat transfer in the repository occurs on several distance scales. Accurate representation of temperatures inside a drift requires a grid with blocks on a scale of centimeters, and the transfer of heat between drift and pillars requires meter-size grid blocks. But temperatures are also affected by repository-scale heat transfer phenomena that operate on scales of several kilometers in the horizontal direction and hundreds of meters in the vertical. To solve the governing equations of all of these phenomena simultaneously would require a grid kilometers wide with nodes spaced only a few centimeters apart in some areas. Given the complexity of the governing equations for coupled heat and fluid flow, such a grid would have far too many nodes to be solvable with available computing power.

The scanning curve technique used in the multi-scale thermohydrologic model [Buscheck, 2000] attacks the problem of contrasting length scales by running a series of models with the aim of spanning the necessary range of length scales and approximations. The models are as follows:

- A 3-D mountain-scale conduction-only model (SMT)
- A 1-D conduction-only model that simulates heat transfer in a vertical column that is one-half pillar wide (SDT)
- A 2-D convection-conduction model that simulates heat transfer between pillars and drift in a half-pillar-wide vertical column (LDTH)
- A 3-D conduction-radiation model that simulates heat transfer within a drift containing several different kinds of waste packages (DDT).

The LDTH model is the core of the calculation. But it is not able to simulate the largest- and smallest-scale heat transfer mechanisms in the repository. Mountain-scale heat transfer is not addressed because the horizontal boundary conditions of the LDTH assume a repository of infinite area. Heat transfer among the various types of waste packages in the repository is not addressed because the model is two-dimensional and thus assumes the heat source is uniform

along the axis of the drift. These limitations are overcome by using the SMT, SDT, and DDT models to adjust the inputs and outputs of the LDTH model as follows:

1. The thermal loading in the LDTH model is reduced from the “true” value to a value that, when used in the SDT model, gives the same peak temperature as the true value gives for that location in the SMT model.
2. The LDTH model, with the thermal loading computed in Step 1, is used to compute temperature on the drift wall and throughout the pillar as a function of time for each location within the repository.
3. For each time step t , a “pillar-average” temperature T_{pa} is calculated by averaging the temperature profile calculated by the LDTH model across the pillar. Time is rescaled by saying the LDTH-calculated profile describes the pillar temperatures not at time t , but at the time t' when the temperature predicted at the same location by the SMT is T_{pa} . (This rescaling of time is what Buscheck refers to as a “scanning curve.”)
4. The DDT model is used to compute the difference between, on one hand, the temperatures at various locations in the waste packages, the drift, and the drift wall and, on the other hand, either the average drift wall temperature or the average waste package temperature. These differences are functions of “unadjusted” time, using “unadjusted” thermal loading as input. The appropriate difference term is added to the average wall or package temperature calculated by the LDTH model to give the predicted temperature at each location.
5. The LDTH model is used to calculate curves (also called “scanning curves”) which represent the approximate relationships between temperature and relative humidity in the host rock and on the drift wall. These curves are used to obtain host-rock and drift-wall humidity from the temperatures.
6. Additional functional relationships are calculated in order to obtain relative humidities within the drift and percolation rates in both host rock and drift. These relationships involve both time (which is included explicitly to reflect changing infiltration rates) and temperature (which enters explicitly and also indirectly via the host-rock relative humidities calculated in Step 5).

The scanning curve technique is complex. A simpler way to correlate models operating on differing scales is described below. Even if it turns out to be impractical to rewrite the computer code to implement this alternative technique, it can play a role by helping to identify the approximations built into the scanning curve method.

4.1.3.3.2 Alternative Modeling Approach

The Buscheck [2000] technique for connecting models that operate on different length scales uses the same approximation at all times. Models vary according to spatial scale but are the same on all temporal scales. Another way to approach the problem is to vary approximations on temporal scales as well as spatial ones. By simplifying in different ways at early and late times, one can take advantage of the limiting behavior of the system.

In the limit of early time, the heat generated by the waste has not yet penetrated to a significant degree to the center of the pillars. Mountain-scale heat transfer thus has a negligible effect on temperatures. For the period when little heat has moved past the boundaries of a drift-scale model, local temperatures can be calculated with reasonable accuracy by a drift-scale heat-transfer model without need of coupling several models together. (It may be most convenient to account for three-dimensional effects by coupling two drift-scale models.) But in this time period, heat output is changing rapidly, with temperatures sensitive to both the cumulative local heat load and the time history of that load. The early-time model must therefore be transient.

At late times, heat output is changing much more slowly. In this regime, heat transfer in and near the drift becomes, to a close approximation, a quasi-steady-state process. The temperature in and around the waste package is determined by the instantaneous heat output of the waste packages and the mid-pillar temperature. However, mountain-scale effects cannot be ignored as they can at early times because the pillar temperature is affected by mountain-scale heat transfer. Thus, the near-drift heat transfer can be steady-state, but it must be coupled to a transient mountain-scale model.

The current multi-scale model parameterizes the space of possible states of a drift-pillar system in terms of initial thermal loading and time. All submodels run transient analyses with a fixed initial thermal loading. This creates the need to match up differing temperatures calculated by submodels that operate on different spatial scales. To go from mountain scale to drift scale, submodels are matched up by adjusting the time axis. In going from 2D drift scale to 3D drift scale, the submodels are tied together by computing the radiative heat transfer with an inaccurate drift-wall temperature. In both cases, there is a mismatch that introduces some degree of error.

The parameterization in terms of time and initial loading is advantageous at early times, when heat output and temperature change rapidly. Because mountain-scale effects are not important in this time period, little loss of accuracy is caused by matching up different spatial scales. But at late times the time-thermal loading parameterization fails to take advantage of the quasi-steady behavior of the system. An alternative parameterization using instantaneous heat output and pillar-average temperature as independent variables would be more advantageous. The space of states of a drift-scale system would be described by surfaces giving the temperatures at locations in and near the drift as functions of heat output and pillar temperature. This parameterization introduces an error, which approaches zero at late times, resulting from the approximation of the transient local heat transfer problem as steady state.

Parameterizing the system in this way suggests an alternative approach to multi-scale thermohydrologic modeling:

1. Use transient drift-scale models alone at early times, with temperatures determined directly from the drift-scale model and mountain-scale effects ignored.
2. Run transient mountain-scale models at late times to determine pillar-average temperatures as a function of time and location. Run steady-state drift-scale models repeatedly to compute surfaces that give temperatures within the host rock, drift, and packages as functions of pillar-average temperature and instantaneous heat output. Read late-time local temperatures off these functions, using the pillar-average temperature calculated by the mountain-scale model and the known instantaneous heat output of the waste as arguments.

3. For intermediate times, execute both early- and late-time approaches, and compute temperatures as weighted averages that change smoothly between early- and late-time behavior.

There are clear physical arguments for the accuracy of this alternative modeling approach in the limits of early and late times. Without more analysis, it is difficult to say how long the early- and late-time periods are and how large an error the approach introduces at intermediate times. But at a minimum, the known accuracy of the alternative method in the two limits provides a benchmark for gauging the potential for error in the current methodology.

4.1.4 Thermohydrology Model Conservatism

All modeling requires assumptions and approximations. To assess the reliability of a model, it is necessary to identify areas where the model approximations have a significant impact on the results and classify them as conservative or non-conservative. This makes it possible to target efforts at model improvement where they will have a significant impact.

Recent changes in repository design place one essential assumption of DOE's models on a much firmer basis. Like nearly all computer models, the DOE models assume that the differential equations they are solving are stable. This mathematical property is needed to ensure that the solution to the equation corresponds to what really happens. Previous repository designs, in which the entire repository horizon would be heated above boiling, put the thermohydrologic system into a region that is not clearly stable. The current design, in which the emplacement drifts are widely spaced and the central portion of the pillar remains below boiling, avoids this difficulty. This is discussed in the first part of the section.

The remainder of the section catalogs major modeling assumptions and examines their conservatism. Thermohydrologic modeling provides two outputs that affect repository performance separately: water percolation rates and temperatures. An assumption that is conservative with respect to one of these outputs need not be, and in fact usually is not, conservative with respect to the other. In general, assumptions that add water to the system lead to more evaporation and therefore decrease temperature. Thus an assumption that is conservative with respect to temperature is often non-conservative with respect to container wetting and radionuclide transport. Conversely, an assumption that removes water is generally conservative with respect to container wetting and radionuclide transport, but non-conservative with respect to temperature.

4.1.4.1 Mathematical Stability of DOE's Models

Changes in the repository design greatly enhance the mathematical stability of models used by DOE. The current repository design with widely spaced pillars has waste packages spaced closely together along the axis of each drift. With this geometry, the temperature in the central portion of the pillars between the drifts never rises above boiling. This is a change from previous designs, in which the temperature was above boiling throughout the repository horizon, and has important implications for the stability and predictability of fluid flow and heat transfer around the repository.

Viewed from a thermodynamic viewpoint, the heated repository is an example of a system that does not reach equilibrium because a driving force is applied from the outside. In this case, the heat source is the driving force and the temperature difference between the repository zone and the surrounding rock constitutes the departure from equilibrium. The stronger the driving force applied to such a system, the less stable and more chaotic is its behavior. Once the strength of the driving force exceeds a threshold, there occurs a series of discrete transitions from simpler to more complicated energy transport regimes.

A fluid heated from below is a classic example of such a system, first studied many years ago by Lord Rayleigh. As the heat source in such a system is made stronger, the system passes from heat conduction to regular convection cells to oscillating convection cells to turbulent flow. The more complicated regimes are very difficult to predict numerically. Obstacles to accurate modeling include a need for very finely gridded models and the difficulty of addressing stability phenomena in a numerical model. These general considerations apply to Yucca Mountain, with its heat source located beneath a 2000-foot layer of gas-saturated porous medium. Their relevance is shown by results of the mountain-scale coupled-process model for Yucca Mountain, which shows what appear to be convection cells [Haukwa, 2000].

Up to 96°C (the boiling point of water at the repository elevation), the destabilizing factor in the repository system is simply that a less dense fluid lies below a denser fluid. The instability threshold at which a uniform layer of hot warm air heated from below in a porous medium begins to form convection cells was calculated by Zhang et al. [1994]. With Yucca Mountain-like parameters and maximum temperatures just below 96°C, the system is near the threshold or slightly above it and convection is likely to have a significant effect on temperatures. Only if the maximum repository temperature is below a value around 85-95°C (depending mostly on gas permeability), can one be sure of being below the threshold.

Above 96°C, there is a second potential source of instability. Because non-condensable gases are driven out of the above-boiling area, this zone becomes an obstacle to convective gas circulation. The hot gas wants to move up, so it must break up into smaller convection cells. This is a more complex behavior than the simple repository convection cell, and it introduces additional modeling difficulties, such as those resulting from our incomplete understanding of wetting front movement in hot fractured rocks.

To be sure, temperature-driven gas flow will occur in Yucca Mountain whether or not the system exceeds these two thresholds, since the heat source is not infinite in horizontal extent. Gas will rise within the heat source and descend to the sides. Nevertheless, the thresholds are important. For a finite-sized heat source, gas flow will occur no matter what the thermal output, but convection will make a significant contribution to heat transfer only when one of the thresholds is exceeded. When temperatures are determined by conduction alone, or are near the convection threshold, there is no danger of the gas flow being irregular, unstable or chaotic because feedbacks are not important in the system. In such cases, numerical models can be used to predict gas flow and heat transfer, and any mathematically correct solution to the equations can be assumed stable.

A further complication arises because the repository is not a uniform disk. The heat source will be localized in the drifts, and the drift walls will be hotter than the pillars. Nevertheless, these stability considerations will remain applicable at least qualitatively. Because geometric scale

appears in the numerator of the Rayleigh number, the dimensionless number that controls convective instability, the largest-scale circulation is always the most unstable.

It is in this context that the new design, with the central portions of the pillars remaining below boiling, has its main significance to coupled process analysis. The below-boiling zone in the pillars provides a place for non-condensable gases to rise upward within the repository footprint and for liquid water to drain. Consequently, the more complex phenomena connected with above-boiling temperatures occur on the scale of the drift spacing rather than repository scale. This eliminates the trapping of noncondensable gases as a source of instability. As a result, there is little risk that heat transfer in the new repository design will be unstable and intrinsically unpredictable. In this way, the new design eliminates modeling uncertainties that would have been very difficult to address with the previous design.

4.1.4.2 Conservatism and Non-Conservatism of Assumptions

Most assumptions in thermohydrologic modeling can be divided into two categories: (1) those that are conservative with respect to temperature but non-conservative with respect to water flux, and (2) those conservative with respect to water flux but non-conservative with respect to temperature. A few assumptions have not been categorized due to limitations on available information and resources. Significant assumptions are listed below by category. Where the assumption has not been explained and evaluated above, a discussion follows.

4.1.4.2.1 Assumptions Conservative for Temperature and not for Moisture

Major assumptions that are conservative (or realistic) with respect to temperature, but not with respect to water flux are:

- **Use of conduction-only heat transfer on the mountain scale thermal evaluation.**
- **Modeling convection on a north-south cross-section** - The mountain-scale model [Haukwa, 2000] modeled convection along a north-south cross-section. This appears to have been done because the repository drifts run east-west, so that only a north-south cross-section could depict temperature contrasts between drifts and pillars. However, the repository is elongated in the north-south direction, so that the north-south cross-section is much longer than an east-west one would have been. In three dimensions, the center of the repository is much closer to the edge than it appears to be in a north-south section. As a result, the possibility that edge effects will penetrate to the center of the repository is underestimated by the north-south cross-sectional model.
- **Geometric mean of measured fracture permeabilities** - Permeability is a spatially variable parameter. The hydrologic properties analysis adopts the geometric mean of measured fracture permeabilities as the baseline value for modeling, and this is the value used in the MSTHM. But the geometric mean may not be the most appropriate average. In a large block of rock, the operational meaning of permeability is the ratio of flow to pressure (or head) gradient. When flow goes through a set of subparallel fractures, the total flow will be the sum of the flows through individual fractures. The pressure gradient is the same across all the fractures. The permeability value that will correctly predict the flow is the arithmetic mean, which is larger than the geometric mean. Because flow in different unsaturated-zone

fractures at Yucca Mountain appears to be weakly connected, the proper value to use for permeability would appear to be closer to the arithmetic mean than the geometric mean. Use of the geometric mean will therefore tend to underpredict water flows.

- **Surface needle effect** - Water can be forced to seep into drifts when fractures dead-end at a drift with no connections to other fractures that could provide pathways for lateral diversion. This “surface needle effect” is discussed in the seepage modeling report but not included in the numerical calculations. Neglect of the surface needle effect is recognized by the project as being non-conservative with respect to moisture and further work is planned to address it. The surface needle effect does not alter temperatures.

4.1.4.2.2 Assumptions Conservative with Respect to Moisture but not Temperature

Major assumptions that are (or at least seem likely to be) conservative with respect to water flux but not with respect to temperature are:

- **High inverse-alpha value.**
- **Neglect of ventilation dry-out** - Removal of moisture from the host rock by ventilation is mentioned in reports, but not considered in numerical models.
- **Rescaling of time** - The times corresponding to temperature fields calculated by the LDTH model are rescaled at each location to correspond to the temperature decay curve calculated by the SMT model. This rescaling reduces the calculated temperature difference between pillar and drift wall because the calculated package temperatures correspond to a later time when radioactive decay has reduced the heat output. This assumption is thus non-conservative with respect to waste package temperature. It is conservative with respect to moisture because in the real situation the center of the pillar will be cooler than the model predicts and thus will have a greater tendency to drain condensate out of the system.
- **Adjustment of thermal loading** - The thermal loading in the LDTH model is reduced, based on a comparison between the SMT and SDT models. The main value of this step seems to be that it creates a one-to-one correspondence between the SMT and LDTH temperature curves that allows time to be rescaled without leaving any gaps. Like rescaling of time, this assumption reduces the temperature contrast between waste package and pillar, and therefore it is conservative with respect to moisture and non-conservative with respect to temperature.

4.1.4.2.3 Assumptions for which More Work is Needed to Evaluate Conservatism

There are some assumptions for which either the AMRs did not give enough information to evaluate their conservatism, or resource constraints did not permit a thorough evaluation:

- **Latent heat removal by ventilation** - Thermal models include ventilation by simply assuming 70% heat removal during the ventilation period. Ventilation models calculate how much ventilation air is needed to achieve 70% heat removal, considering only sensible heat. Latent heat will also be removed; it is unclear whether the intention is to ventilate the repository at the calculated rates and remove more heat than predicted, or to use the minimum airflow capable of removing 70% of the generated heat. Whether the neglect of latent heat removal by ventilation is conservative or non-conservative depends on whether

ventilation rates will be reduced to keep the heat removal at 70%, or the calculated ventilation rate will be maintained.

- **Thermohydrologic model** - The underlying governing equations for flow and heat transfer in TOUGH and NUFT is the same, yet these models have largely been validated against each other. The impacts of any possible model validation problems are unknown.
- **Neglect of dependence of radiative heat transfer on drift-wall temperature** - A conduction/radiation model is used in the MSTHM to calculate temperature differences within the drift. Since radiative heat transfer, unlike conduction, is not linear in temperature, the magnitude of temperature differences depends on temperature as well as on the heat output of the packages. More details of the modeling are required to evaluate the conservatism of calculating package-drift wall temperature differences for a single drift-wall temperature and then extrapolating directly to other drift-wall temperatures. The procedure appears to give realistic results with regard to moisture, since it was applied primarily within the drift, and moisture movement has very little temperature dependence in the drift where (when there is no backfill) dripping is the major means of water movement.
- **Time-independent RH(T) function at the drift wall** - Time, which affects waste-package heat output, infiltration rate, and (via the temperature history) the size of any dry-out zone around the drift, is ignored by the MSTHM in relating drift-wall humidity to drift-wall temperature. Detailed examination of model results would be needed to evaluate the conservatism of this assumption.
- **Moisture fluxes and host-rock humidities** - Additional functional relationships are used to estimate humidities within the drift and moisture fluxes in both host rock and drift. We have not evaluated the conservatism of these relations due to limitations on available information and resources.

4.1.5 Thermohydrology Conclusions and Recommendations

Advances in science and repository design during the last three years significantly reduce uncertainties about coupled fluid flow and heat transfer at Yucca Mountain. Principal among these are: (1) underground tests confirm that water can drain through fractures even when the rock matrix is not fully saturated, (2) pillar temperatures will remain below boiling and allow upward flow of rock gas, and (3) more corrosion-resistant containers and drip shields make waste package performance less sensitive to direct and indirect effects of repository heating.

These developments put the DOE's thermohydrology modeling in a position to address the entire spectrum of physical processes that are likely to occur in a repository. However, more work is needed to enhance the reliability of modeling results. The following additional calculations are recommended to ensure that all relevant phenomena are considered in the modeling and to check the validity of assumptions and approximations made in the multi-scale thermohydrologic model:

- **Model effects of mountain-scale convection** using absolute-humidity curves adjusted to reflect repository design with "cool" pillars.
- **Perform sensitivity evaluations** using the MSTHM computer code with an inverse-alpha value of 50 Pa.

- Analyze the consequences of evaporation, condensation, and latent heat transfer due to forced and natural ventilation.
- Benchmark TOUGH/NUFT against a code which uses different approximations and governing equations.
- Compare results of scanning curve methodology with calculations in which early-time temperatures are taken directly from drift-scale model, late-time temperatures are computed from a quasi-steady-state drift-scale model with boundary conditions set by a mountain-scale model, and intermediate-time temperatures are obtained by interpolating between these two models.

4.2 Near Field Coupled Process Modeling, T-H-C

4.2.1 Introduction

The “near-field coupled processes” in this context refers to combined thermal, hydrological, and chemical (THC) processes near an emplacement drift.

As envisioned by DOE/M&O, the sequence of events associated with coupled THC processes starts with heating from the waste package, which induces coupled heat and mass transfer, and alters temperature, pressure, relative humidity, water saturations, concentrations of groundwater constituents, and partial pressures of gaseous components near the emplacement drift. Altered rock-water interactions lead to mineral dissolution and precipitation, causing changes in hydrologic properties. In some scenarios, fractures may be plugged, and flow path may be altered.

Because the heating effect from spent nuclear fuel inside of the waste package has the most intensive effect on the host rock near the drift and dissipates gradually with distance from the drift; the basic unit in the near-field THC modeling is the rock immediately surrounding the emplacement drift. The thermal effect is present irrespective of the area mass loading, low or high. In some cases, the modeling domain includes both the surface and water table in order to take into account of effects from boundaries and stratification.

Detailed evaluation of THC coupled processes may be important to TSPA, because of the possibility of changes to parameters incorporated into source-term calculations, which is the center part of a TSPA. For example, THC modeling impacts source-term calculations directly by influencing the rate, time-variation, and chemical composition of groundwater flowing through the waste form and EBS.

Coupled THC process modeling impacts DOE/M&O source-term calculations indirectly by providing information to sub-process modeling. These sub-processes include:

- engineered barrier (drip shield, waste package, and cladding) degradation,
- waste form dissolution, and
- geochemical interactions between the influx water and EBS materials.

Source-term parameters, such as water contact time, dissolution rates, radioelement sorption coefficients and solubilities, can then be obtained by detailed modeling of these sub-processes.

Figure 4-6 shows an Interaction Matrix format of the near-field THC coupled processes expressed by the DOE (Dale, 2000). This figure demonstrates that the near-field coupled processes have been extensively considered by the DOE researchers although the interaction matrix can be made more detailed and transparent. Also shown in the matrix is the mechanical process (M). The coupling between M and THC may also be potentially important. In particular, heating tends to close pre-existing fractures within the heated volume of rock, and the corresponding decreases in compressive stress tend to open fractures outside the heated region.

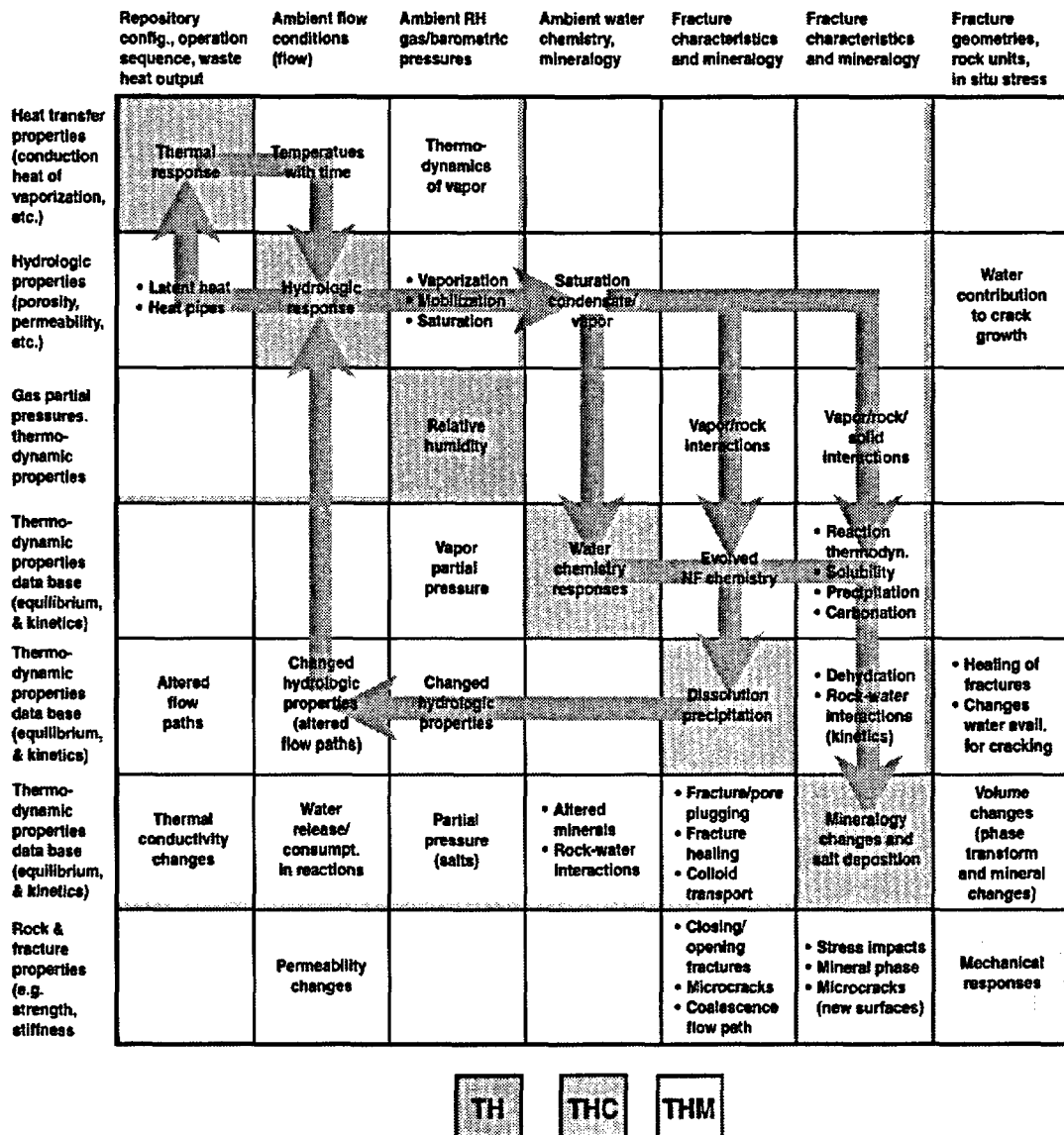


Figure 4-6 Interaction Matrix Showing THC Coupling (Dale, 2000)

In the following sections, review comments on DOE's work (Dale, 2000; CRWMS M&O, 2000) will be presented. Although the DOE also attempted coupling of THC with M, the main focus in this review is the THC coupling. The review will focus on the approach used to couple the processes and the degree of conservatism of the DOE's model.

4.2.2 The DOE's Model on Coupled THC Processes

4.2.2.1 Important Near-Field Processes and Issues

Potentially important near-field THC processes include:

1. heat conduction via partially saturated rock, and convection by flowing fluids,
2. fluid (water-gas two phase) flow,
3. water phase change,
4. water vapor and air binary diffusion,
5. transport of aqueous and gaseous species,
6. chemical reactions of minerals and species,
7. effects of temperature and flow on reaction-transport,
8. mineral dissolution and precipitation,
9. changes in porosity and permeability due to dissolution/ precipitation,
10. flow and transport in fractures,
11. flow and transport in matrix, and
12. interaction between fractures and the matrix.

All of these processes have been included in the project's model. Important related issues include:

- climate change, and
- spatial heterogeneity.

Climate change has been taken into account in the project's model by incorporating time-dependent infiltration rates. Spatial heterogeneity is considered in the uncertainty discussion, but is not explicitly included in the model.

4.2.2.2 Treatment of Coupling among Processes

Simulations of coupled THC processes are conducted by TOUGHREACT (Dale, 2000; Xu and Pruess, 1998), which is a computer simulation code based on TOUGH2 with reactive-transport module included. TOUGH2 was developed to simulate coupled heat and mass transfer, i.e., Processes 1-4 listed above, with built-in equation-of-state for water. Hence, TOUGH2 is used to model thermal-hydrological processes (TH), but is not capable of modeling THC without modification. TOUGH2 and NUFT were developed to simulate ground water movement in soils. These computer codes have been used in a number of land fills and low level waste evaluations. For either computer code no detailed benchmarking and verification of the numeric models has been performed as other nuclear grade computer codes are put through. It is unfortunate but the limited benchmarking of these two computer codes simply consist of comparing the results from one code to the other. This is not a true benchmark, since NUFT and TOUGH 2 are derived from the same computer code. It is therefore recommended that a detailed verification effort be implemented to ensure that the codes are verified before License Application.

TOUGHREACT (another laboratory off shoot from the same basic computer code) was developed to handle coupled THC processes. In this context, the chemical process (C) represents another two coupled sub-processes: reaction and transport. Coupling of reaction and transport is treated by a sequential iterative approach (Steeffel and MacQuarrie, 1996). In this approach, interactions between porosity changes due to precipitation/dissolution and transport have been taken into consideration.

The coupled reactive-transport module is further coupled with TH in TOUGH2 to form TOUGHREACT according to the flowchart shown in Figure 4-7. In Figure 4-7, reaction-transport sub-flowchart (denoted as "C" thereafter) is enclosed in a dashed box, which covers Processes 5, 6, and 8 listed in the previous sub-section. It can be seen that coupling between C and TH is carried out by the following interactions:

- temperature distribution from TH to C,
- flow velocities from TH to C, and
- update physical parameters from C to TH.

The above three interactions are the most important aspects in THC coupling (referring to the previous sub-section, these interactions cover Processes 7 and 9, respectively). In this way, computation starts with TH calculation, feeding results to C. When the C computation is completed, the results are fed back to TH for the next time-step calculation.

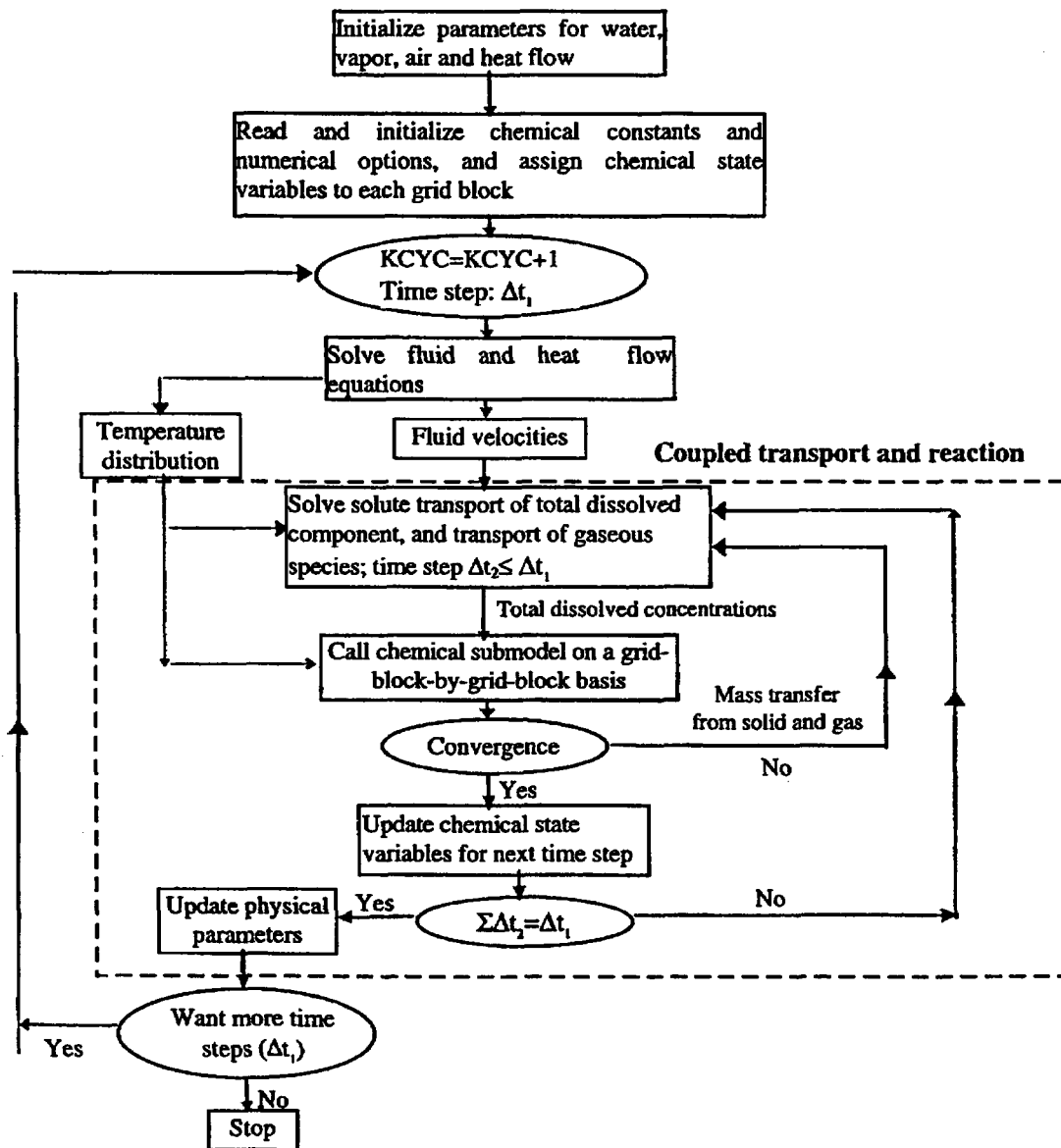


Figure 4-7
Flow chart of TOUGHREACT for modeling non-isothermal multiphase flow, solute transport, and reactive chemistry (Xu and Pruess, 1998)

It is concluded that the three computer code family will provide insight into the behavior of the coupled processes. Although, it is strongly recommended that a standard nuclear industry validation of the computer codes be undertaken. Simply comparing the three computer codes against each other is wrong, since all three codes use the same basic structure and algorithms. The basic DOE's approach of coupling THC processes seems reasonable. This implies that modeling results will be unaffected by the coupling approach, provided that the programming implementation is correct. This does not warrant, however, that the project's results are correct. Other issues, e.g., spatial heterogeneity and chemical modeling, also contribute to the credibility of the THC coupled results, as discussed later.

4.2.2.3 Modeling of the Fracture Hydrology System

The DOE employs a dual permeability method to handle separate flow and transport in fractures and the matrix within the near field. With this approach, each gridblock is separated into two continua: one for the fracture and one for the matrix, each of which is characterized by its own pressure, temperature, liquid saturation, water and gas chemistry, and mineralogy. Each continuum has its own material and transport properties. Interaction of the two continua is usually governed by parameters such as fracture spacings (Zhou and Apted, 1995).

The DOE's processes seems appropriate with regards to the matrix and fracture properties and an appropriate discretization in time and space, the dual permeability method is "a sufficiently accurate approximation of the real world for the spatial scales of interest" (Dale, 2000, p. 3-20).

4.2.2.4 Modeling of the Chemical System

The DOE has simulated coupled THC with its Drift Scale Test (DST) in order to compare the simulated results with the collected data from DST. Furthermore, the same approach is used to simulate long-term near-field THC coupled effects in host rock near an emplacement drift. Two rock-water chemical systems are considered:

- The *complex* chemical system (referred to Case 1 full chemistry in CRWMS M&O 2000) as shown in Table 4.x.1, and
- The *less complex* chemical system (referred to Case 2 simplified chemistry in CRWMS M&O 2000), representing a smaller set of species and minerals (calcite, gypsum, silica phases) that captures many basic aspects of the DST water and gas chemical evolution, such as the pH and gas-phase CO₂ concentrations, but neglects Al, Fe, and F-bearing aqueous species and minerals.

Both systems have been simulated (Dale, 2000; CRWMS M&O 2000). Comparing calculations against the DST, the computational results obtained for the *less complex* system agreed better with observed results than those calculations for the *complex* system. The effect of dissolution/precipitation on hydrological properties (porosity and permeability) is found insignificant. Based on these results, the project abstracts THC coupled process modeling results using the *less complex* system, and concludes that the TH coupling, instead of THC coupling, system is sufficient in determining the near-field environment.

**Table 4-1
Model Mineral Assemblage, Aqueous and Gaseous Species for the Complex Chemical System**

Species	Minerals
Aqueous:	
H ₂ O	Calcite
H ⁺	Tridymite
Na ⁺	α-Cristobalite
K ⁺	Quartz
Ca ⁺²	Amorphous Silica
Mg ⁺²	Hematite
SiO ₂	Fluorite
AlO ₂ ⁻	Gypsum
HFeO ₂	Goethite
HCO ₃ ⁻	Albite
Cl ⁻	Microcline
SO ₄ ⁻²	Anorthite
F ⁻	Ca-Smectite
	Mg-Smectite
Gas:	Na-Smectite
CO ₂	K-Smectite
	Illite
	Kaolinite
	Sepiolite
	Stellerite
	Heulandite
	Mordenite
	Clinoptilolite
	Volcanic Glass

Source: CRWMS M&O 2000, Table 7

Regarding the project's approach used in geochemistry modeling and the abstraction strategy, the reviewers have the following comments:

1. The DOE uses a form of the kinetic rate law for mineral dissolution and precipitation that is not pH-dependent. The pH-dependence of many of the reactions considered in the model are known, however, so the rationale for this decision is unclear. Variations in pH should be expected during boiling and condensation as a result to exsolution and dissolution, respectively, of CO₂. The total range in pH for Cases 1 and 2 calculated by the DOE is roughly between 7 and 10 (Figures 30 and 31, respectively). Experimentally determined dissolution rates of aluminosilicate minerals may vary by several orders of magnitude over this pH range.

2. The DOE states that the *complex* model does not agree with the field experiments (DST) because the kinetic models are overpredicting reaction rates. This observation is consistent with limited field observations suggesting that actual reactions rates are slower, by up to three orders of magnitude, compared to rates calculated on the basis of experimental measurements alone. The reason for this, however, may have more to do with poor estimates of reactive surface areas in the field than with any intrinsic uncertainties in the laboratory measurements. If so, this suggests that DOE's methodology for estimating reactive surface areas yield values that are far too high. Furthermore, misapprehension of the actual factors that are uncertain could cause the project to misapply valuable time and resources in future R&D studies. The apparent inability (not just by DOE, but by geochemical modelers in general) to accurately estimate reactive surface areas in real geologic systems may be a fundamental limitation in applying coupled THC models to predict chemical changes in the Yucca Mountain environment. It would be useful for the DOE to address this limitation, and discuss how this limitation might be overcome (e.g. using uncertainty/ sensitivity analyses added to the base-case THC simulations) in future modeling exercises
3. The importance of chemistry in THC coupling lies in the feedback between mineral dissolution/ precipitation reactions and associated effects on porosity and permeability. The project's results suggest that such effects are unimportant for both the *complex* (full chemistry) and *less complex* (simplified chemistry) systems. The reviewers consider this as reasonable. In real geosystems, strong effects on porosity/permeability can be found, e.g., in many geothermal systems. The lifetime of these hydrothermal conditions, however, is much longer (10^4 to 10^5 years) than conditions relevant to Yucca Mountain (10^3 to, at most, 10^4 years, depending on heat loading strategy).
4. It remains questionable whether TH coupling is adequate for Yucca Mountain, or whether THC coupling is also required. To help address this question, it would be useful for the project to compare calculated changes in fluid chemistry due to boiling/ condensation with the natural variability of porewater compositions at Yucca Mountain. A distinct possibility (especially for the *less complex* system) is that the calculated changes lie within the range of compositions existing in the Yucca Mountain host rocks. Furthermore, if changes in hydrogeologic conditions can be shown to be insignificant, and if associated changes in groundwater chemistry are insignificant compared with natural variations in groundwater chemistry, the project will be in a stronger position to defend as reasonable its argument that only TH coupling needs to be considered to describe the near-field environment.
5. It is difficult to understand the full rationale of why DOE/M&O adopts the *less complex* (simplified chemistry) system over the *complex* (realistic chemistry shown in Table 4-1) system simply because the former model produces results that agree better with the field experiments (lasting only 20 months). This *less complex* system is then used to evaluate THC evolution over 10,000 years. More effort should be contributed to addressing why the *complex* system results agree so poorly with the field experiments, improving the model accordingly, and using it to support the TSPA.

Based on the above observations, it is difficult to judge the conservatism of DOE's model. Overall, however, the reviewers consider their model as they stand to need additional work to ensure proper quantification of conservatives.

There are major differences between the *complex* and *less complex* results. Most notably, both calculated pH and dissolved carbonate concentrations are significantly greater for the *complex* system. Both these parameters could elevate actinide (and other radionuclides) solubilities compared with the *less complex* system. The DOE should adopt a more regress evaluation model, which should be based on a more realistic geochemical model of reacting minerals and species. The DOE's rationale for using the *less complex* (simplified geochemistry) system is that predictions are better based on comparisons with the field experimental (DST) evidence. The DOE acknowledges that the more complex system may be better for the long term (i.e. greater than 20 months), which will open the project to significant criticism and expressions of lack of confidence by independent peer reviewers and regulatory agencies. It is suggested that the more complex model process be implemented for License Application. For Site Recommendation the DOE's models will provide sufficient insight.

4.2.2.5 Issue of Spatial Heterogeneity

Spatial heterogeneity has been identified as a factor contributing to uncertainties, but not explicitly modeled in DOE's coupled process study. When considering the feedback between mineral dissolution/ precipitation and associated changes in porosity and permeability, spatial heterogeneity may become potentially important.

In particular, excluding spatial variation in fracture's aperture may exclude fracture plugging as a consequence of mineral precipitation. Fracture plugging has been identified by DOE as a potential consequence of the near-field THC coupling, as noted in Figure 4-6. Their modeling results, however, have excluded this consequence because their model is based on average and homogeneous rock properties. Fractures are well-known to have variable aperture, with the smaller opening greatly influencing water flow, colloid filtration, and other processes. Once fracture plugging occurs, flow path may be altered, which may further lead to altered rate and time-variation of water influx into the emplacement drift.

If the plugging happens near the apex of the drift, excluding this effect may lead to over-estimating the rate of groundwater flowing into the drift. Other than the apex location, plugging may have significant effects on colloid filtration if included in performance assessment calculations, and in this case, ignoring this effect would be overly conservative.

4.2.3 Conclusions

The DOE's PMR and AMR on near-field coupled process model and abstraction are reviewed. This involves direct coupling between thermal and hydrological (TH) processes, and indirect coupling between TH and chemical (C) process. Important interactions and feedback between TH and C are included. The approach used for coupling processes seems reasonable for Site Recommendation. As additional data is gathered the models should be updated and a more regress modeling process put into place.

Some concerns are raised in the DOE's model. Although these concerns are not related to the coupling of processes, they contribute to the credibility of the coupled THC modeling results. These are:

- In chemical modeling, the kinetic rate law for mineral dissolution/ precipitation used in DOE's model is not pH dependent.
- Reactive surface areas estimated by DOE's methodology may be too high.
- The DOE failed to compare calculated changes in fluid chemistry due to boiling/ condensation with the natural variability of porewater compositions at Yucca Mountain. This comparison is considered important because this gives rationale whether the THC or TH system should be used to support TSPA.
- The reason why the DOE adopts the simplified chemical system, rather than a more realistic system, is unclear and unconvincing.
- It is unclear why DOE excludes spatially varying fracture properties, as this may exclude fracture plugging effect near the drift.

In summary, concerning DOE's chemical modeling, their model may need to be updated to account for the chemical processes from low to higher thermal loads. It is believed that additional understanding will cause the model to become more conservative. The model as it stands today, adopts a simplified chemical system that may yield lower solubilities than the one found in nature's chemical system. Concerning DOE's exclusion of spatially varying fracture properties, which may result in fracture plugging, their model may be conservative because fracture plugging impacts water influx, colloid filtration, etc.

In both cases, the rationale for their modeling choices is not presented clearly. Information available from the reviewed documents is not sufficient to judge the credibility of their coupled THC modeling results, although their coupling approach is sound.

In order to fully realize the potentially important impacts of THC coupling on TSPA by IMARC, it may be necessary to

- further discretize the near field to consider local plugging effects on flow, and
- incorporate time-dependent variation in important source-term parameters such as flow rate and groundwater composition.

In addition, since most or all of the computer codes that model the natural system have been generated within a small community of laboratories and have only been benchmarked against each other, a standard verification process is needed before any License Application argument can be made. Simply benchmarking each computer code against each other, when they all derive from the same code is unsatisfactory.

4.3 References

CRWMS M&O 2000e. Drift Scale Thermal Analysis. CAL-WIS-TH-000002 REV 00.

C. F. Ahlers and H. H. Liu, Calibrated properties model, OCRWM Report MDL-NBS-HS-000003, March 2000.

T. M. Bandurraga and G. S. Bodvarsson, Calibrating matrix and fracture properties using inverse modeling, in G. S. Bodvarsson, T. M. Bandurraga, and Y. S. Wu, The site-scale unsaturated zone model of Yucca Mountain, Nevada, for the Viability Assessment, E. O. Lawrence Berkeley National Laboratory Report LBNL-40376, June 1997, Chapter 6.

T. Buscheck, Multiscale thermohydrologic model, OCRWM Report ANL-EBS-MD-000049, April 2000.

S. Finsterle and R. C. Trautz, Seepage calibration model and seepage testing data, OCRWM Report MDL-NBS-HS-000004, January 2000.

N. D. Francis and M. T. Itamura, Features, events, and processes in thermal hydrology and coupled processes, OCRWM Report ANL-NBS-MD-000004, May 2000.

N. D. Francis and D. Sassani, Abstraction of drift-scale coupled processes, OCRWM Report ANL-NBS-HS-000029, March 2000.

C. Haukwa, Mountain-scale coupled processes (TH) models, OCRWM Report MDL-NBS-HS-000007, March 2000.

H. H. Liu, Conceptual and numerical models for UZ flow and transport, OCRWM Report MDL-NBS-HS-000005, March 2000.

H. H. Liu, C. F. Ahlers, and M. A. Cushey, Analysis of hydrologic properties data, OCRWM Report ANL-NBS-HS-000002, March 2000.

H. H. Liu, C. Doughty, and G. S. Bodvarsson, An active fracture model for unsaturated flow and transport in fractured rocks, *Water Resources Research*, vol. 34, pp. 2633-2646 (1998).

N. Lu and B. Ross, Mountain-scale modeling of transient, coupled gas flow, heat transfer and carbon-14 migration, in *Proc. Site Characterization and Model Validation, Focus '93*, Las Vegas, Nevada, 1993, pp. 103-109.

K. Pruess, A mechanistic model for water seepage through thick unsaturated zones in fractured rocks of low matrix permeability, *Water Resources Research*, vol. 35, pp. 1039-1051 (1999).

B. Ross, Interaction between convection and countercurrent flow in a gravity-driven heat pipe, in R. McGuire et al., Alternative approaches to assessing the performance and suitability of Yucca Mountain for spent fuel disposal, Electric Power Research Institute Report TR-108732, November 1998, Appendix D.

B. Ross, Y. Zhang, and N. Lu, Implications of stability analysis for heat transfer at Yucca Mountain, *Proc. High Level Radioactive Waste Management*, Las Vegas, Nevada, 1993, vol. 1, pp. 584-89.

E. Sonnenthal and N. Spycher, Drift-scale coupled processes (DST and THC seepage) models, OCRWM Report MDL-NBS-HS-000001, March 2000.

C.-F. Tsang and G. Li, Seepage model for PA including drift collapse, OCRWM Report MDL-NBS-HS-000002, February 2000.

M. L. Wilson, Abstraction of drift seepage, OCRWM Report ANL-NBS-MD-000005, March 2000.

Y. Zhang, N. Lu, and B. Ross, Convective instability of moist gas in a porous medium, *Int. J. Heat Mass Transfer*, vol. 37, pp. 129-138, 1994.

CRWMS M&O, (2000) Drift-Scale Coupled Processes (DST and THC Seepage) Models, MDL-NBS-HS-000001 REV 00.

Dale, W., (2000), *Near-Field Environment Process Report*, TDR-NBS-MD-000001 REV 00.

Steeffel, C.I. and MacQuarrie, K.T.B., (1996) "Approaches to Modeling of Reactive Transport in Porous Media", in *Reactive Transport in Porous Media*, Editors: P.C. Lichtner, C.I. Steefel, and E.H. Oelkers, *Reviews in Mineralogy Volume 34*. pp. 83-129.

Xu, T. and K. Pruess, (1998), *Coupled Modeling of Non-Isothermal Multi-Phase Flow, Solute Transport and Reactive Chemistry in Porous and Fractured Media: 1. Model Development and Validation*, LBNL-42050.

Zhou, W. and M. J. Apted, "Flow and Transport Simulation in Yucca Mountain Using Dual-Porosity Model," in *the Proceedings of the Sixth Annual International Conference on High Level Radioactive Waste Management*, Las Vegas, Nevada, April 40 - May 5, 1995, pp. 160-162.



5

ENGINEERED BARRIER SYSTEM DEGRADATION

5.0 Introduction

A key component of the multibarrier arrangement proposed for the Yucca Mountain repository is the combination of a drip shield and the corrosion-resistant waste package. This engineered combination coupled with the inherent defense provided by the wastefrom cladding is expected to compliment in a major fashion the natural barrier provided by the mountain itself. The major advantage of waste disposal within Yucca Mountain is anticipated to be the limitation of the availability of groundwater to cause the corrosion of the metal barriers (drip shield, package, cladding) and the spent fuel wastefrom and the subsequent transport of radionuclides. This natural geological advantage can then be enhanced by design of the repository lay-out and the geometry of waste package emplacement as described in previous sections.

In this section models are described to predict the corrosion performance of the drip shield, the waste package, and the spent nuclear fuel cladding. The primary purpose of these models is to determine the total period of protection of the wastefrom from the time the waste is emplaced in the repository to the time when it is exposed to groundwater and release of radionuclides can commence. Failure of the engineered barrier is defined as the time when the drip shield and waste package have failed, and the decay heat of the waste form is sufficiently reduced so as to allow water entry. The distribution of failure times produced is then taken as input to the source term model within IMARC. The cladding failure distribution is treated as a separate input to the COMPAS source term model used in IMARC, and is used to define the fraction of the waste form that is subject to alteration and transport at a given time following breach of the waste package.

5.1 Changes in Waste Package Design since IMARC Phase 4

Since the publication of IMARC Phase 4, the design of the waste package has changed significantly. At that time, the reference waste package design employed a dual wall arrangement in which a 2-cm thick Alloy 22 inner barrier was encapsulated within a 10-cm thick carbon steel outer barrier. This design offered the advantages of combining a corrosion allowance material (carbon steel) with a corrosion-resistant material (Alloy-22), a combination with no expected common mode of corrosion failure. The primary purpose of the outer barrier carbon steel was to provide predictable corrosion protection to cover the period when waste package surface temperatures were high enough that the inner barrier Alloy-22 might be susceptible to localized corrosion. Beyond this period, Alloy-22 was expected to degrade only very slowly by general corrosion.

While model calculations predicted that a carbon steel outer barrier could serve this function, a couple of issues remained unresolved, and even though these were deemed to be of very low probability, design changes were implemented. Primary among these was the possibility of producing acidic Fe^{III} conditions, via carbon steel corrosion under aerated conditions, at occluded sites between the inner and the outer barrier materials. Although thought to be a scenario with a low probability, the limited test data available for nickel alloys suggested such a development could promote crevice corrosion of the inner package wall. A second unresolved issue was the potential to produce wedging stresses as a consequence of the accumulation of iron oxide corrosion products in the gap between the outer and inner walls, and the fear that these stresses could be severe enough to promote stress corrosion cracking (SCC) of the Alloy-22.

In view of these uncertainties it was deemed judicious to remove the carbon steel and to avoid the formation of unnecessary crevices, while maintaining the advantages of a dual barrier design utilizing two different materials with no common corrosion failure mode. Through a series of iterations the concept of a single-walled package* of 2-cm thick Alloy-22 protected by a 15 mm thick drip shield fabricated from titanium Grade-7 evolved. Since Alloy-22 is most susceptible to corrosion under extreme oxidizing conditions while titanium alloys require extreme reducing conditions, this combination of materials should be capable of providing excellent corrosion performance over all anticipated repository conditions. It is this design which is considered in the development of the models presented in this section. A sketch of this package is shown in Figures 5-1 and 5-2. Figure 5-3 shows the key features of the dual lid design and closure welds. Figure 5-4 shows a schematic of the waste package/drip shield arrangement within a repository drift. Figures 5-5 and 5-6 provide an isometric view of the waste package and the drift emplacement mode now being proposed by the DOE.

* The waste package is actually designed with an inner wall of NG stainless steel (5-cm thick). However, the purpose of this wall is to provide structural stability and its function as a potential corrosion barrier is ignored.

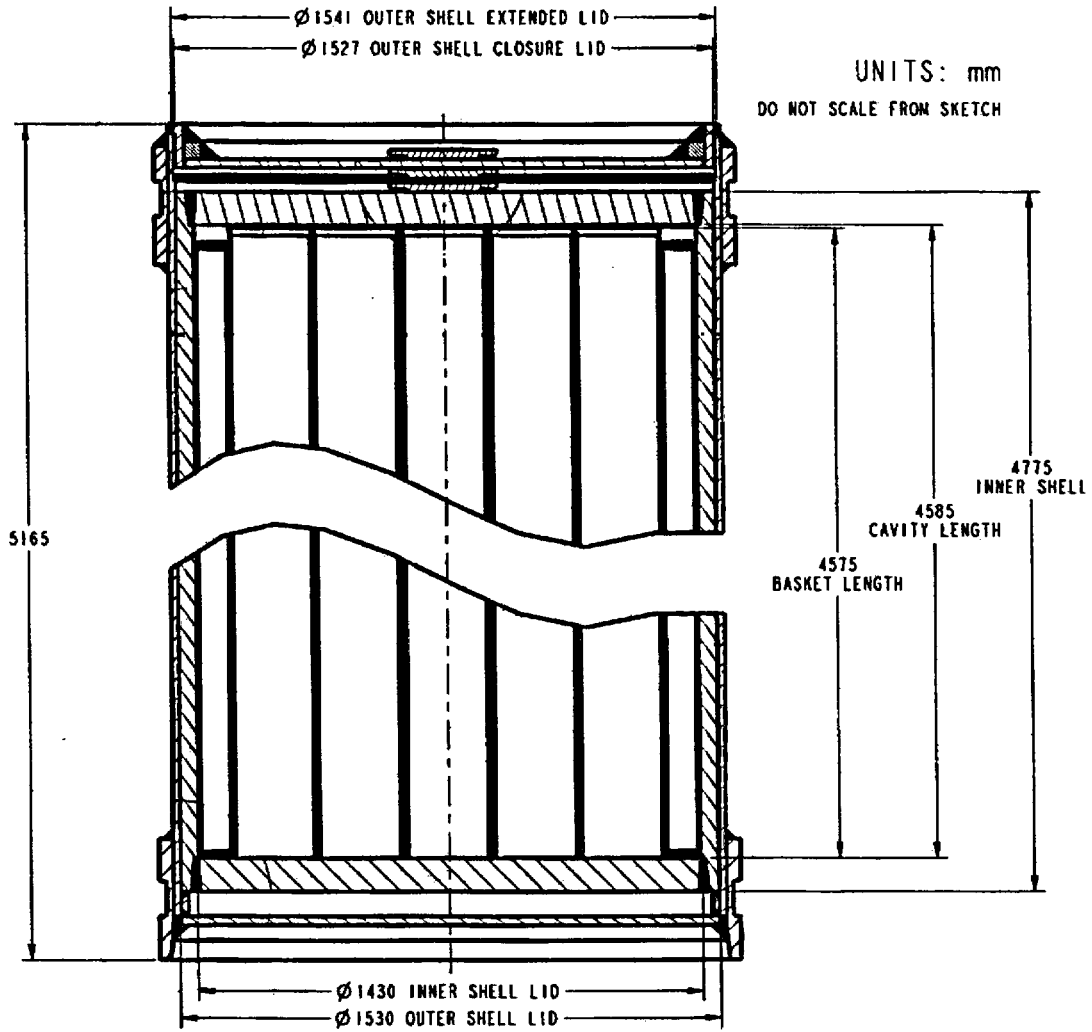


Figure 5-1
21 PWR Commercial SNF Waste Package

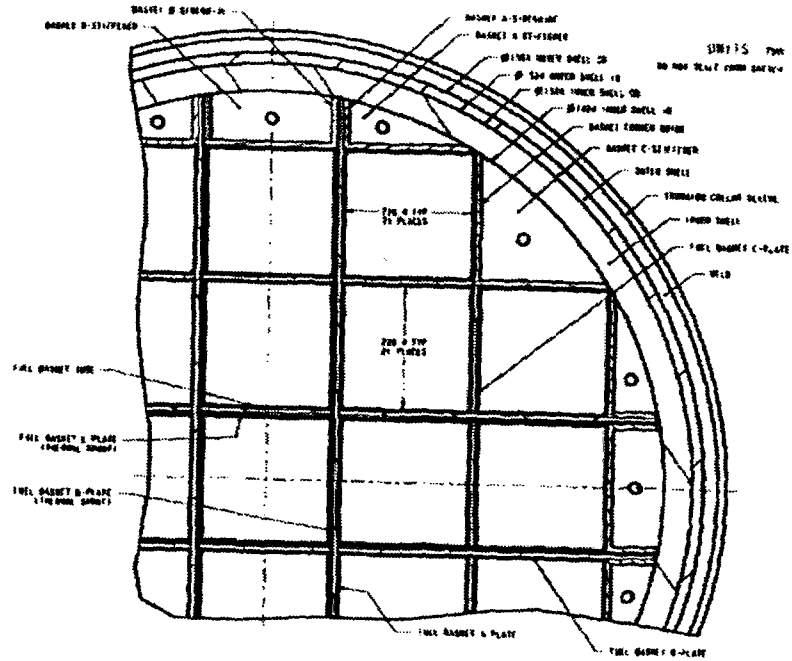


Figure 5-2
Cross-Section of 21 PWR Commercial SNF Waste Package

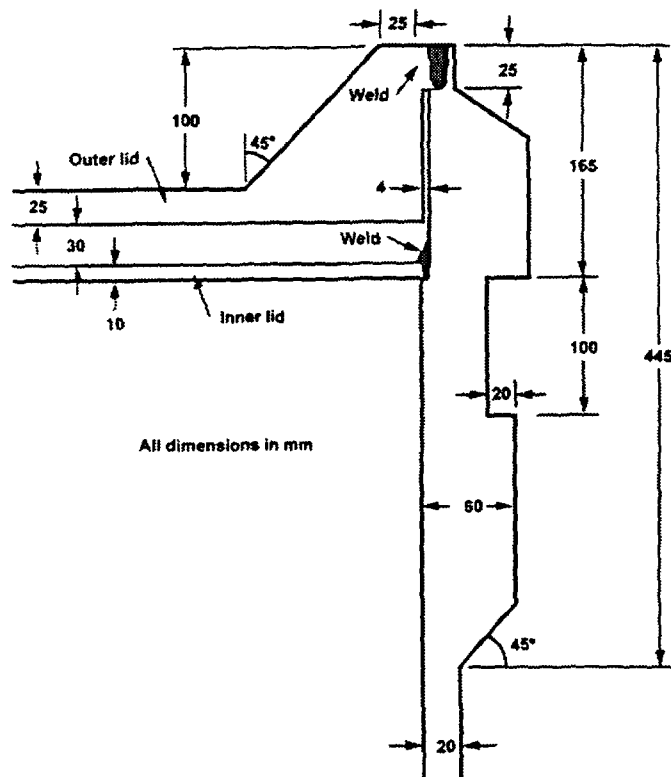


Figure 5-3
Waste Package Closure Weld Details

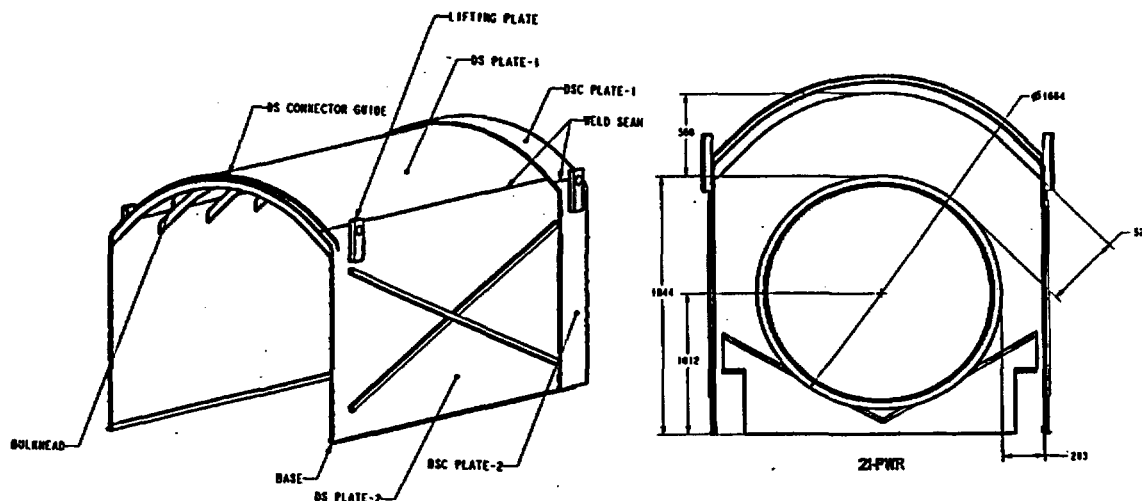


Figure 5-4
Dripshield Concept. The Figure on the Right Shows the Shield Fitted over the Waste Package which is Resting on an Emplacement Pallet

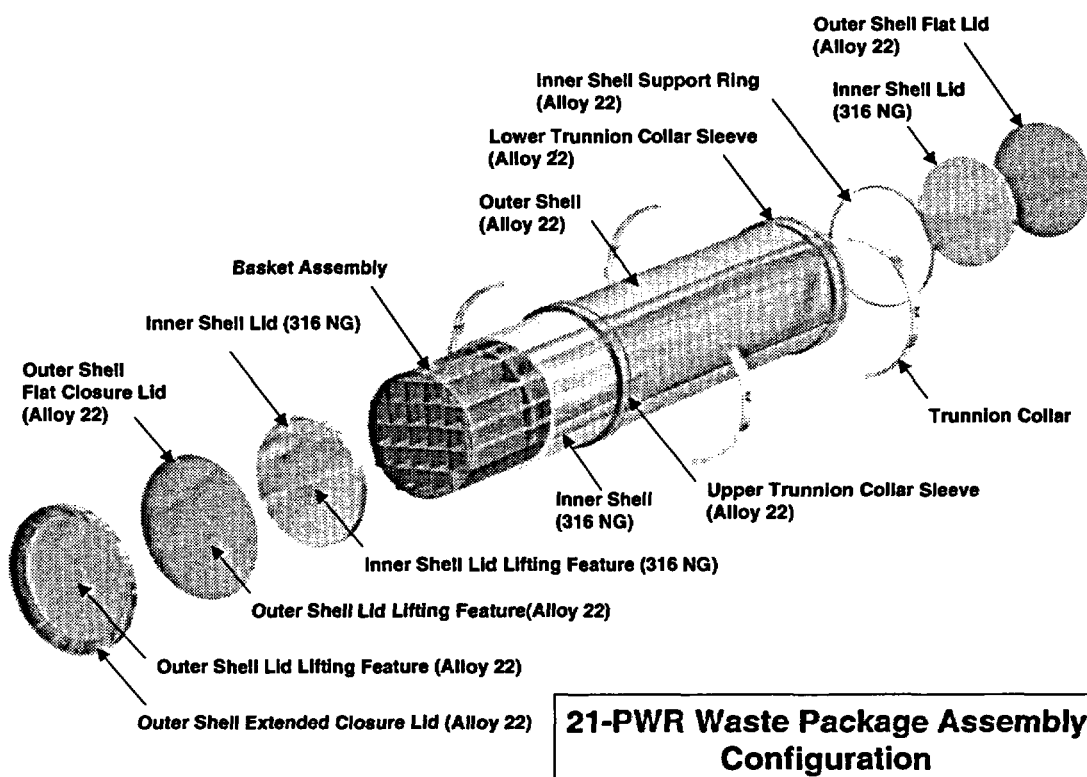


Figure 5-5
Robust Waste Package

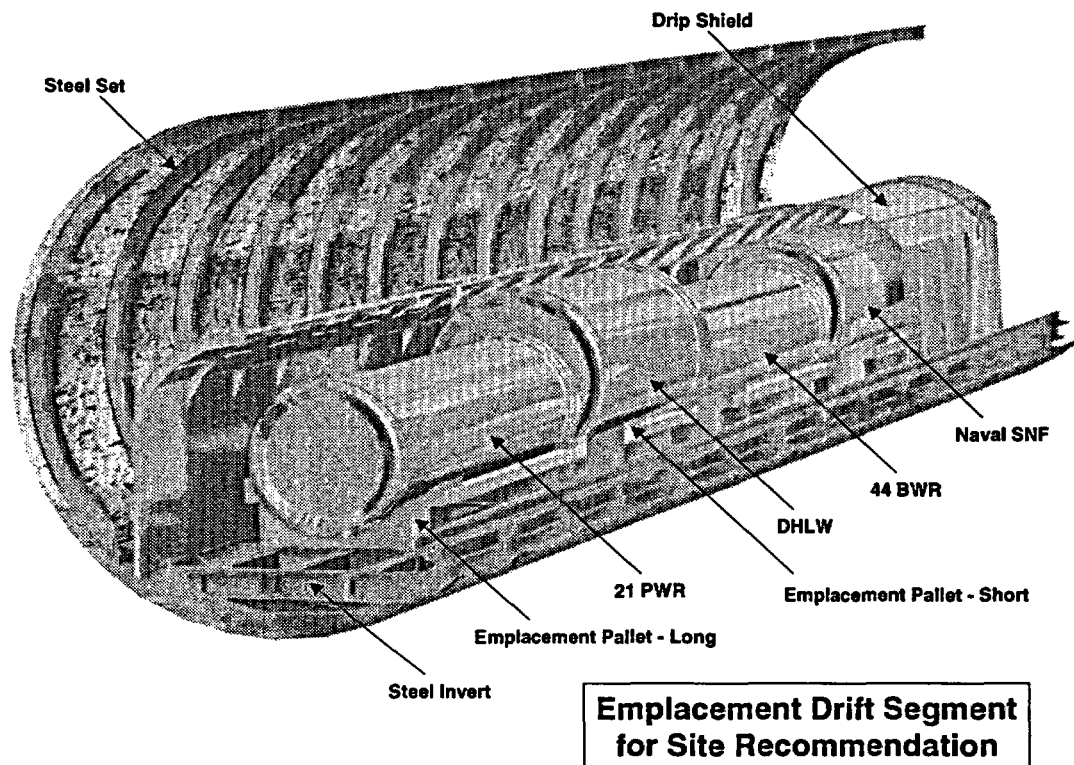


Figure 5-6
Drift Configuration

5.2 General and Localized Corrosion Modelling Features

The corrosion of the drip shield and waste package, here designated DS/WP when considered as a combination, will be controlled by the thermal hydraulic conditions within the repository, the seepage flux model into the repository, and the composition of the groundwater as influenced by the dripping-evaporative cycles occurring on the DS/WP.

Within the proposed repository design and geometry of package loading (the EDA II design incorporating line loading of the waste packages), a dryout zone will initially develop around the repository drift. Under these conditions the relative humidity within the drifts will be very low and any corrosion of the DS/WP will be by dry atmospheric oxidation. Such a process will produce a thin strongly adherent oxide film of only a few nanometres thickness.

Consequently, insignificant corrosion damage is to be expected over the period of the few hundred years that dry conditions will be maintained (CRWMS M&O 1999a, Welsch and Pramod 1996). Consequently, in calculating times to failure of the DS/WP, this period of dry oxidation can be ignored. If no dry-out period existed, and the metal surfaces were wet from the time of emplacement, passivity would be maintained by the rapid formation of an oxide film under aqueous conditions.

Eventually, as waste packages cool, this dry out zone will shrink, and water will return to the drift. Once sufficiently humid conditions are established on the DS/WP surfaces, degradation will commence in the form of a humid air or aqueous corrosion process. Which of these two processes occurs will depend on the amount of water condensed onto the metallic surface. A humid air process is assumed to occur when only a small amount of condensed water is present, whereas aqueous corrosion requires the presence of bulk water (2-5 monolayers, CRWMS M&O 2000a, Leygraf 1995). In our model, it is assumed that humid air conditions can be established on all corrodable surfaces within the repository while the establishment of aqueous conditions requires that groundwater, in the form of seepage drips, contact the surface. This assumption is consistent with assumptions made in USDOE models and clearly defines that the primary function of the drip shield will be to protect the waste package from seepage drips leading to the evaporative cycles which will establish potentially aggressive aqueous conditions. Since such evaporative cycles cannot occur in the absence of the groundwater species supplied by seepage drips, this assumption is realistic.

In IMARC4, the differentiation between humid air and aqueous corrosion was made on the basis of thresholds in the repository relative humidity (RH). Thus, if $RH > 70\%$ it was assumed that humid air corrosion was possible, while, for aqueous corrosion to start, the RH had to rise to $> 90\%$. This meant that the two processes occurred consecutively, not simultaneously. This was a necessary separation since for carbon steel, humid air corrosion rates were distinctly different to the rates for "fully submerged" aqueous conditions. The influence of evaporative cycles leading to the elevation of the boiling point of water was not considered in the establishment of these threshold RH values and their relationship to waste package surface temperatures. This led to the assumption that aqueous conditions were established on the waste package once the surface temperature fell to 100°C , the approximate boiling point of pure water.

Since the publication of that model a substantial amount of experimental effort has been expended on determining the consequences of such evaporative cycles on aqueous chemistry and its influence on the relationship between RH and waste package surface temperature. Despite these studies the specification of a contact water composition, threshold relative humidity (RH_{thres}) and associated surface temperature is not a straightforward task. The value of RH_{thres} will depend on the nature of the hygroscopic salts introduced into the repository either as soluble groundwater species or as aerosols and dust transported in air during the early period of forced ventilation.

The value of RH_{thres} at which aqueous conditions can be established will be determined by the deliquescence point of the salt mixture formed during evaporative cycles. As discussed in CRWMS M&O 2000a, the environment likely to be produced on the drip shield and waste packages is still not defined with certainty, but will comprise a mixture of hygroscopic salts with a wide range of deliquescence points. J-13 water, a well water with chemistry typical of that of saturated zone waters at Yucca Mountain, will be representative of the water likely to seep into the waste emplacement drifts (CRWMS M&O 2000a). During evaporative concentration, laboratory studies show that HCO_3^- , Ca^{2+} , Mg^{2+} and, eventually F^- and SO_4^{2-} should be removed by precipitation leading to a solution dominated by Na^+ , K^+ , Cl^- and NO_3^- (CRWMS M&O 2000b). Within this mixture, NaNO_3 is the most deliquescent solid, and capable of sustaining aqueous conditions at a relative humidity of 50% at its boiling point of 120.6°C (sea level). Consequently, since the composition of the actual ground water expected to contact the waste package is not presently known and, anyway, is likely to vary from site to site, it has been conservatively

assumed that the RH_{thres} is determined by the deliquescence point of this salt. Implicit in this assumption is that all other salts with lower deliquescence points are removed from the groundwater prior to the concentration process on the DS/WP surface. Since nitrate is generally a non-aggressive ion on passive materials the establishment of such a solution would eliminate any susceptibility of Alloy 22 to localized corrosion. However, when constructing corrosion models it is assumed that the environment formed by evaporative cycles will be sufficiently aggressive to cause localized corrosion since it will not be a pure NaNO_3 solution and will contain aggressive anions such as Cl^- .

Based on laboratory tests (CRWMS M&O 2000a, 2000b) this threshold relative humidity is related to temperature according to the following polynomial fit,

$$RH_{\text{thres}} = 3.5932 \times 10^{-5} \times T(^{\circ}\text{C})^3 + 5.9649 \times 10^{-3} \times T(^{\circ}\text{C})^2 - 0.45377 \times T(^{\circ}\text{C}) + 81.701 \quad (R^2 = 0.9854) \quad \text{Eq. 5-1}$$

This relationship allows us to specify a threshold temperature for the establishment of an aqueous environment under dripping conditions, a key model parameter in determining the possible susceptibility of Alloy-22 to localized corrosion (see below). This threshold temperature, assuming aqueous conditions are established at $RH = 50\%$, the deliquescence point for NaNO_3 , is 120°C . Since, the real solution will contain a mixture of anions and cations with a lower deliquescence point, the actual temperature at which aqueous conditions can be established will be lower than this. This assumption that aqueous conditions can be established at 120°C is conservative, since it shortens the dry-out period when oxidation of the metals will be negligible and lengthens the period over which aqueous corrosion processes can occur. However, as the calculations in this chapter will show, assuming a lower threshold temperature value has a very minor impact on predicted waste package lifetimes.

Such a groundwater concentration process will not occur in the absence of seepage drips onto the DS/WP surfaces. Consequently, under the generally prevailing humid air conditions, it is likely that this threshold relative humidity (50%) will be even more conservative. However, in view of the uncertainties in the environment on DS/WP surfaces (establishment by dust and aerosol deposits in the absence of seepage drips) it is judicious to assume the same RH_{thres} for humid air (no seepage drips) and aqueous (seepage drips) conditions. A similar bounding assumption is made in the USDOE model. Implicit in this assumption is that deposition of dust and aerosols cannot cause localized corrosion. This seems very reasonable.

A second common assumption with the USDOE model that we have made is that if the localized corrosion of Alloy-22 is to occur, it will only do so on those packages which sustain seepage drips leading to the aggressive aqueous conditions produced by evaporative cycles. A further assumption, specific to our model but not incorporated into the USDOE model, is that the general corrosion rate on drip shields exposed to seepage drips will be higher than on those free of drips. The basis for this assumption will be discussed in more detail below. This differentiation in corrosion performance requires that the fraction of drip shields likely to experience seepage drips must be specified as well as that fraction of these shields which are defective and allow dripping onto the waste package.

The need to specify a threshold relative humidity and surface temperature, as well as the number of drip shields and waste packages subjected to seepage drips, represents a coupling of the engineered barriers corrosion processes to the thermal hydrology of the repository. However, in some other important aspects, it is possible to decouple the DS/WP performance from repository conditions. In IMARC Phase 4, in the absence of experimental results to demonstrate otherwise, it was necessary to assume that all corrosion processes, whether general or localized, were thermally activated. This necessitated the use of the Arrhenius relationship to calculate the temperature dependence of corrosion rates, which were hence predicted to be high when aqueous conditions were first established at high temperatures. As a consequence, in IMARC4, waste package performance was strongly coupled to the evolution of waste package surface temperature with time.

In the interim an extensive test program conducted in the Long Term Corrosion Test Facility (LTCTF) at Lawrence Livermore National Laboratory has shown that the general corrosion rates for both Ti-7 (drip shield) and Alloy-22 (waste package) are effectively independent of not only temperature but also the specific test solution composition (CRWMS M&O 1999a). Since the range of tests solutions simulated most of the concentrated environments anticipated in the repository, these results make it possible to use a single data set of corrosion rates in modelling DS/WP performance. The absence of an overall temperature dependence for general corrosion suggests that the reaction might involve two activated reaction steps, which exert opposite effects on the overall temperature dependence. A possibility is that an increase in metal oxidation rate with temperature (leading to an increase in rate) is counterbalanced by an increase in oxide thickness with temperature (which would lead to a decrease in corrosion rate).

Also, the lack of a corrosion rate dependence on temperature means that the exact form of the DS/WP surface temperature profiles is no longer a determinant of corrosion performance. As will be discussed in more detail below, only two points on the surface temperature-time profiles are required (see the section on Waste Package Corrosion and the values in Table 5-3);

- (i) the time at which aqueous conditions are first established (i.e. t_{AQ} = the time when $T_{aq} = 120^{\circ}\text{C}$);
- (ii) the time when the temperature attains the threshold value for susceptibility of Alloy-22 to localized corrosion (t_{CC}).

The time period between these two temperatures ($t_{CC} - t_{AQ}$) then represents the window within which the waste package is potentially susceptible to localized corrosion. Two temperatures can then be used to establish a criterion for susceptibility of the waste package to localized corrosion:

- (i) For $t_{AQ} > t_{CC}$, the initiation of localized corrosion, in the form of an under-deposit crevice corrosion process at drip sites on the waste package surface, is assumed possible;
- (ii) If $t_{AQ} < t_{CC}$, then the waste package will be immune to localized corrosion, and only general corrosion can occur. Condition (ii) would be expected for waste packages emplaced around the outer perimeter of the repository and possibly for all waste packages if a sufficient period of enforced repository ventilation is employed before final closure. This criterion is identical to the one used in IMARC Phase 4 to determine the susceptibility of Alloy-22 to localized

corrosion, although the values for T_{AQ} and T_{CC} are different. The criterion is also different to that used in the USDOE model.

In the USDOE model, whether or not localized corrosion will occur on either the drip shield or the waste package is determined from electrochemical tests in which open circuit corrosion potentials (E_{CORR}) and threshold potentials for localized corrosion (E_{CRIT}) were determined in a range of simulated exposure environments as a function of pH and temperature. Whether or not localized corrosion is assumed to occur is then based on polynomial fits to the relationships between potential and pH or temperature and the universally accepted electrochemical criterion which states that if

$$E_{CORR} > E_{CRIT} \quad \text{Eq. 5-2}$$

then localized corrosion will occur (CRWMS M&O 1999a, CRWMS M&O 1999b). Since, in the test program conducted, this criterion is met localized corrosion is predicted not to occur on either the drip shield or the waste package. Effectively, the use of this criterion eliminates localized corrosion from consideration, although it is stated that it could simply be included by relaxing this criterion. In the IMARC model, localized corrosion is not excluded in this fashion.

5.3 Drip Shield Corrosion

The selection of Ti-7 for the fabrication of the drip shield limits the feasible corrosion processes to general corrosion and, possibly, hydrogen-induced cracking (HIC). A wealth of corrosion test data shows that localized processes such as pitting or crevice corrosion require either extreme anodic polarization or temperatures in excess of 200°C, respectively (Shoesmith and Ikeda 1997, Schutz and Thomas 1987), both unattainable conditions within the repository. Recent test results from the LTCTF at Lawrence Livermore National Laboratories in test environments consistent with those anticipated at Yucca Mountain showed no evidence for localized corrosion (CRWMS M&O 1999a).

Under the oxidizing conditions expected to prevail within Yucca Mountain the slow general corrosion of Ti-7 would be expected to be supported by reaction with dissolved O_2 under both humid air and aqueous conditions,



Since this process does not lead to the production of hydrogen, we would not expect it to be accompanied by the absorption of hydrogen into the alloy, a process which must occur if the material is to be eventually rendered susceptible to HIC.

However, if under dripping conditions, evaporative processes lead to the formation of concentrated solutions, a salting-out effect could lead to very low concentrations of dissolved O_2 contacting the drip shield, especially at high temperatures. Under these conditions, general corrosion of Ti-7 could be supported by reaction with H_2O ,



a hydrogen-producing reaction which could lead to the absorption of hydrogen into the alloy depending on the permeability of the oxide film present on the alloy surface.

A review of available information on the permeability of oxide-covered titanium to hydrogen (Shoosmith and Ikeda 1997) shows that hydrogen absorption is not observed until potentials are quite negative (~ -0.6 V vs SCE) in 30°C artificial seawater). For these low temperatures it was possible to rationalize that this threshold was a consequence of the need to induce redox transformations in the oxide (Ti^{IV} | Ti^{III}) which were accompanied by hydrogen absorption. However, for temperatures above 65°C it is possible that oxide recrystallization and the introduction of minor fractures in the oxide could allow hydrogen absorption uncoupled to oxide redox transformations (Noel 1999).

Kim and Oriani (1987) showed that some hydrogen absorption can occur on Grade-12 titanium (Ti-12) exposed to concentrated brine solutions under natural corrosion conditions even at 25°C. Measurements at 100°C showed this absorption rate to be effectively independent of temperature. It is significant that the measured corrosion potentials were quite negative, -0.4 to -0.6 V (vs the saturated calomel electrode (SCE)), consistent with the presence of an oxide which could be permeable to hydrogen. While these results were obtained on Ti-12, an alloy known to more readily absorb hydrogen than other Ti alloys (Lunde and Nyborg 1993), similarly negative corrosion potentials were measured on Ti-7 in the LCTCF tests at LLNL.* (CRWMS M&O 2000c).

These results suggest that the uniform corrosion of the Ti-7 drip shield in concentrated solutions could be accompanied by some hydrogen absorption into the substrate alloy. Consequently, it is judicious to incorporate into our model the possibility of failure by HIC. Since concentrated solutions are only likely to develop due to evaporative cycles under dripping conditions it is assumed that general corrosion rates, leading to more extensive hydrogen absorption, will be greater for that fraction of the drip shields subjected to dripping.

The failure of the drip shield is, hence, assumed to occur by one of two possible corrosion processes;

1. wall penetration by general corrosion;
2. failure by HIC once the hydrogen concentration exceeds a critical value.

The corrosion rates used in our model are those based on weight loss measurements on specimens exposed in the LTCTF at LLNL. These rates comprise the most extensive database of general corrosion rates available and were measured in exposure environments chosen to simulate the anticipated environment within Yucca Mountain (CRWMS M&O 2000c). The rates measured fit a Weibull cumulative distribution function

$$f(t) = 1 - \exp\left[-\left\{\frac{t - \theta}{\alpha}\right\}^\beta\right] \quad \text{Eq. 5-5}$$

* These negative E_{CORR} values were obtained in electrochemical polarization tests and may not be representative of the more positive E_{CORR} values anticipated after extended natural corrosion exposure.

where α , β , and θ represent the scale, shape, and location (distribution minimum value) parameters respectively (all > 0) and $t \geq \theta$ (Modarres 1993, p. 77). The resulting Weibull parameters from a least-squares fit are $\alpha = 31.785$, $\beta = 0.807$ and $\theta = 6$. Figure 5-7 shows the 10 (8 nm/year), 50 (25), 90 (100) and 100 (350) percentile values from the LTCTF tests and the resulting Weibull cumulative distribution function.

This distribution is based on a large database which shows the rates to be independent of solution concentration (J-13 to 1000 x J-13), pH over the range 2.7 to 8.0, and temperature over the range 60°C to 90°C. Since the range of conditions tested is very varied it is reasonable to assume that this independence of rate would apply over a wider range of environmental conditions.

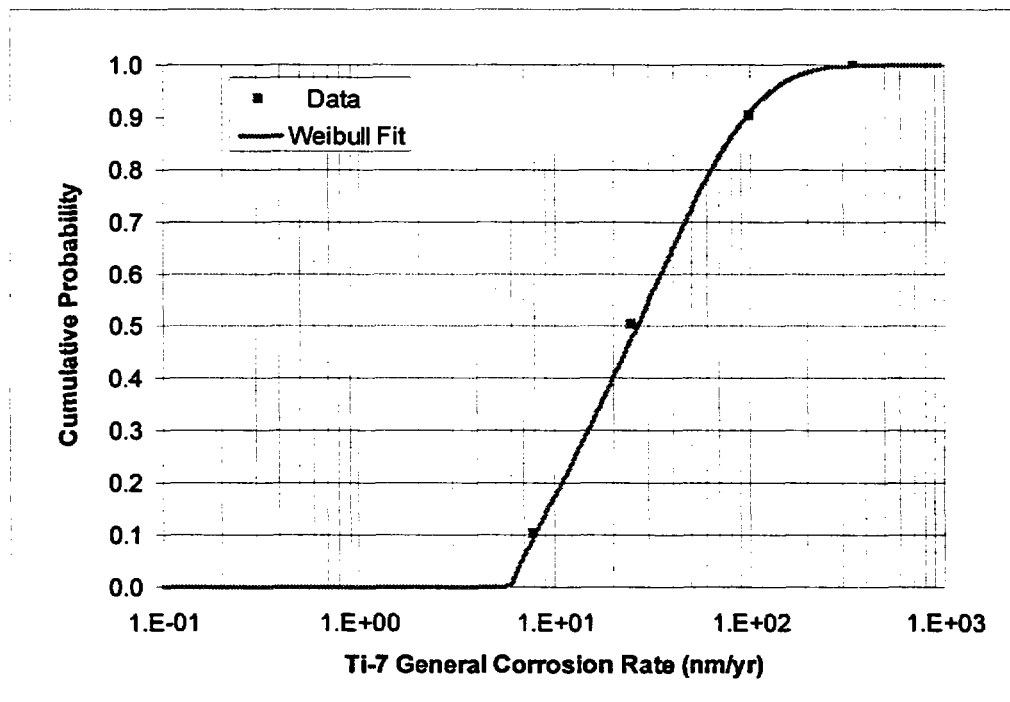


Figure 5-7
Titanium (Ti-7) Aqueous General Corrosion Rate Distribution (The Full Data Base of Measured Rates was Used to Calculate the Distribution, but only a Small Number of Rate Values are Shown to Illustrate the Fit)

These values are consistent with other published values. Mattsson and Olefjord (1990) measured rates in the range 0.5 to 4 nm/year on Ti-2 (commercially pure Ti) and Ti-7 in compacted bentonite clays saturated with saline solutions (95°C), Blackwood et al. (1988) rates of 15 to 20 nm/year on Ti-2 in various acidic (values from < 0 to 3) and alkaline (14) solutions at $\sim 40^\circ\text{C}$, and Kim and Oriani (1987) rates of 40 to 60 nm/year on Ti-12 (0.8 wt % Ni; 0.3 wt % Mo) in saturated brines. These last authors also found only a marginal increase in rate between 25°C and 108°C (the boiling point of the brine). A similar absence of a temperature dependence was observed for Ti-7 in aggressive saturated brines, the rate increasing by only a factor of ~ 2 (from 30 nm/year to 70 nm/year) over the temperature range 90°C to 170°C (Accary 1985, Smailos et al. 1986).

On the basis of this observed independence of corrosion rate on temperature, we have used temperature-independent rates in our model. However, since the literature values of corrosion rate (Kim and Oriani 1987) suggest that the rate may be higher in extremely concentrated saline solutions, we have chosen to use the full database of corrosion rates from the LTCTF for shields exposed to seepage drips and a reduced data set of lower rates for those shields not exposed to drips. For the non-dripping condition, a normal distribution of rates with a mean value of 10 nm/year, a standard deviation of 2.5 nm/year and truncation values of 7 and 25 nm/year is used. These rates effectively bracket the values measured by Mattsson and Olefjord (1990) and Blackwood et al. (1988), for solutions not approaching saturation. In the more conservative USDOE model, the full data set was used irrespective of whether dripping occurred on the shield or not.

To determine the probability of failure by HIC we have used the approach discussed in detail in Shoesmith et al. (2000). Hydrogen absorption is assumed to occur at a linear rate which is directly proportional to the uniform corrosion rate, and failure to occur once the absorbed hydrogen concentration exceeds a critical value. The amount of hydrogen absorbed (H_A) as a function of time is related to the general corrosion rate (R_{GC}) by the expression

$$H_A = 4 \times 10^6 f_H R_{GC} t [M_{Ti} (d_0 - R_{GC} t)]^{-1} \quad \text{Eq. 5-6}$$

where H_A is in $\mu\text{g/g}$, f_H is the fractional efficiency for hydrogen absorption (i.e., the fraction of hydrogen produced by the corrosion reaction (4) which is absorbed into the alloy), R_{GC} is in mm/year, M (= 47.9) is the atomic mass of Ti, and d_0 (= 15 mm) the drip shield wall thickness. The value for f_H was uniformly distributed between 0 and 0.04 based on a published values for neutral solutions under cathodic conditions (Okada 1983). Using a lower limit of 0 acknowledges that hydrogen absorption may not occur if sufficiently oxidizing conditions prevail.

This model for hydrogen absorption can be considered very conservative since it assumes that all the hydrogen absorbed during general corrosion will remain in the residual wall thickness and will not be consumed by the consumption of titanium as general corrosion progresses through the drip shield wall. Titanium hydride is unstable with respect to titanium oxide under anticipated vault conditions (Beck 1973). Hence a credible case can be made, especially for temperatures $\leq 80^\circ\text{C}$ when hydrogen transport into the bulk of the metal will be slow (Schultz and Thomas 1987), that significant hydrogen levels will not accumulate in the Ti-7 drip shield as a consequence of general corrosion. Within our model this is equivalent to assuming the absorption efficiency, f_H , is equal to zero. By assuming that all the hydrogen absorbed is retained within the alloy ($f_H \leq 0.04$), it is also implicitly assumed that all absorbed hydrogen is immediately dispersed throughout the drip shield. This constitutes a very conservative assumption, since it is highly likely that absorbed hydrogen will be retained at the surface through which it is absorbed and hence consumed (i.e., re-released) as the corrosion process proceeds.

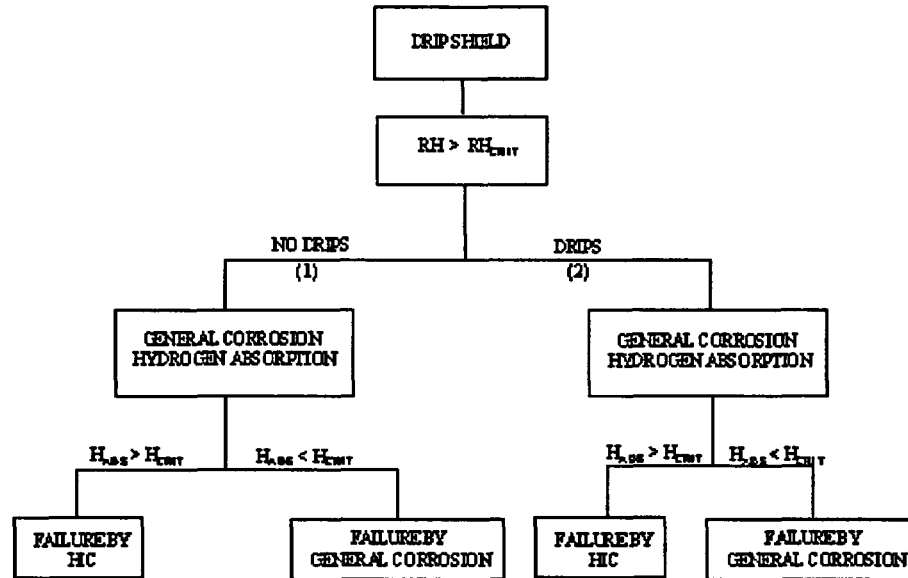


Figure 5-8
Outline of the Drip Shield Corrosion Model Used: (1) 10 ± 2.5 nm/year (Normal Distribution); (2) Distribution of Rates in Figure 5-7

The critical hydrogen concentration is defined as the value, H_{CRIT} , above which the fracture toughness of the material is first observably influenced by the presence of absorbed hydrogen. Failure is then assumed to occur instantaneously (Shoemith et al 2000). This threshold approach is very conservative since there are grounds to believe that titanium alloys can sustain much higher hydrogen levels without failure (Schutz and Thomas 1987). For the critical hydrogen concentration we have used a normal distribution about a mean value of $1000 \mu\text{g/g}$ with a standard deviation of $200 \mu\text{g/g}$. This value was based on the measurements of Ikeda and Quinn (1998) who found no influence of hydrogen on the fracture toughness of Ti-16 (an alloy containing 0.06 wt % Pd, compared to the ~ 0.2 wt % in Ti-7) up to this concentration. We would expect this threshold value to be at least this value for the Ti-7. An outline of the drip shield corrosion model is given in Figure 5-8.

The same approach to modelling HIC is used by the USDOE, but with a much more conservative value of $H_{CRIT} = 400 \mu\text{g.g}^{-1}$ (CRWMS M&O 2000d) and a constant value of absorption efficiency, $f_H = 0.02$. On the basis of sensitivity calculations they then concluded that a large margin of safety existed for the drip shield against HIC in the first 10^4 years of emplacement. In our analysis, by using a uniform distribution for f_H coupled to a normal distribution of H_{CRIT} and a Weibull distribution of general corrosion rates as shown in Figure 5-7, we introduced a low probability that a very small number of drip shields could fail by HIC at times $< 10^4$ years. We believe this small conservatism is necessary since neither model (EPRIs or the USDOE) takes into account the possibility that local hydrogen absorption by the drip shield could occur due to galvanic contact between the Ti-7 shield and carbon steel when the drift support structure collapses. Such galvanic couples are expected to be short-lived and local but could lead to additional hydrogen absorption while they last. It is unlikely that this will be a significant effect, but, to date, no meaningful data is available to quantitatively assess the consequences.

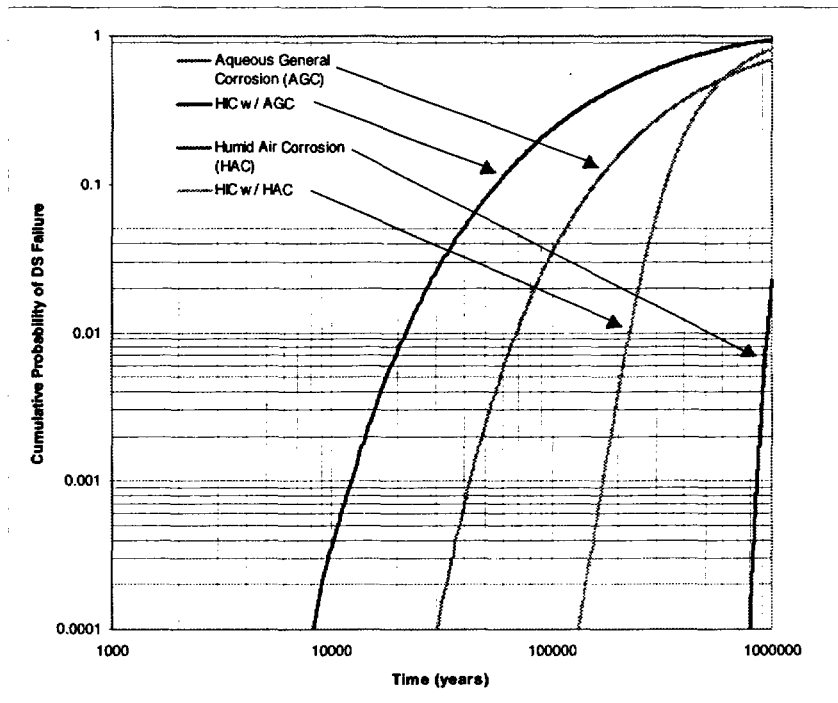


Figure 5-9
Dripshield Failure Time Distributions for Dripping (AGC) and Non-Dripping (HAC)
Conditions with and without Hydrogen Induced Cracking (HIC)

Using this approach our model predicts the distribution of failure times plotted in Figure 5-9. The drip shield failure distribution presented in Figure 5-9, as well as the remaining drip shield, waste package, EBS, and cladding failure distributions presented in this chapter, were developed through Monte Carlo sampling of the uncertain parameters in the model. Typically, 300,000 realizations were utilized. Using a cumulative probability of 0.0001 (i.e. 1 in 10,000 shields assuming one shield covers one waste package) as a level of comparison, no drip shield unexposed to seepage drips will fail in $< 100,000$ years. If hydrogen is assumed not to accumulate in the alloy in the absence of dripping then no failures would occur in $\leq 800,000$ years. Assuming that general corrosion will proceed more rapidly under dripping conditions then, with hydrogen absorption and accumulation, no shield would fail in ≤ 8000 years. Without hydrogen absorption lifetimes would be extended to $\geq 30,000$ years.

Figure 5-10 provides the results of a sensitivity evaluation of the effects of varying the hydrogen absorption fraction, f , in order to simulate the possible effect of galvanic coupling with fallen steel sets. For this sensitivity, f was varied from 0.02 to 0.08, while H_{CRIT} remained normally distributed as described above.

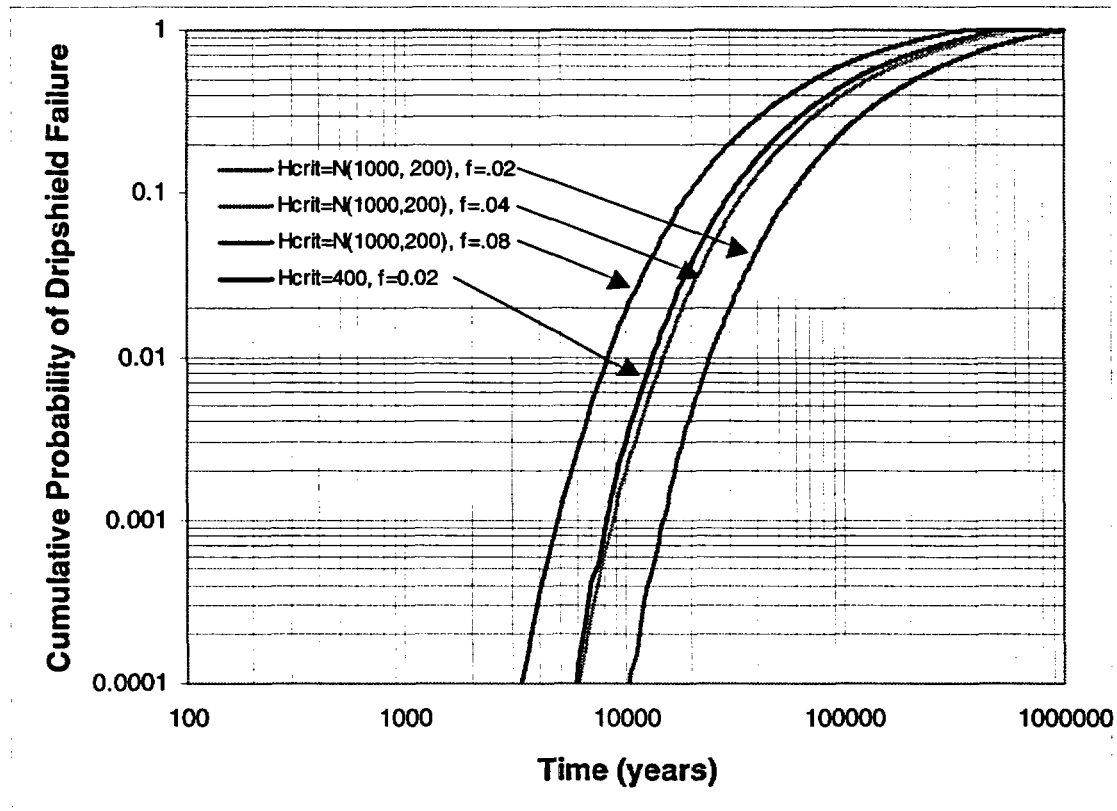


Figure 5-10
Dripshield Failure Time Sensitivity to Hydrogen Absorption Fraction

For many reasons the efficiency of an iron/steel-titanium galvanic couple will be limited:

- (i) the contact area between the two metals will be small and the anode to cathode area (area of steel and titanium, respectively) low;
- (ii) conditions in the repository will be oxidizing, making it less likely that a galvanic couple will sustain the reduction of water necessary for hydrogen absorption. Even small concentrations of cations such as Fe^{III} , likely to be produced under these oxidizing conditions, would be sufficient to reinforce passivation (Schutz and Thomas 1987);
- (iii) while temperatures are high ($> 80^{\circ}C$), the intermittent nature of aqueous conditions will allow only limited periods for hydrogen absorption;
- (iv) titanium has a high tolerance for hydrogen and substantial concentrations must be achieved before any degradation in fracture toughness is observed (Shoesmith et al. 2000, Ikeda and Quinn 1998).
- (v) for galvanic contact at temperatures below $80^{\circ}C$ hydride formation is likely to be confined to the surface of the Ti-7 and the hydrogen to be subsequently removed by general corrosion once the galvanic process stops.

This scenario for hydrogen absorption due to galvanic coupling is presently not included in USDOE models (CRWMS M&O 2000d) although it is anticipated that a revised version will address the issue.

5.4 Waste Package Corrosion

Our model includes three possible processes that could lead to waste package failure;

1. general corrosion;
2. localized corrosion in the form of an underdeposit process or a creviced contact between the waste package and the support pedestal.
3. SCC.

An outline of our waste package corrosion model incorporating these processes is shown in Figure 5-11.

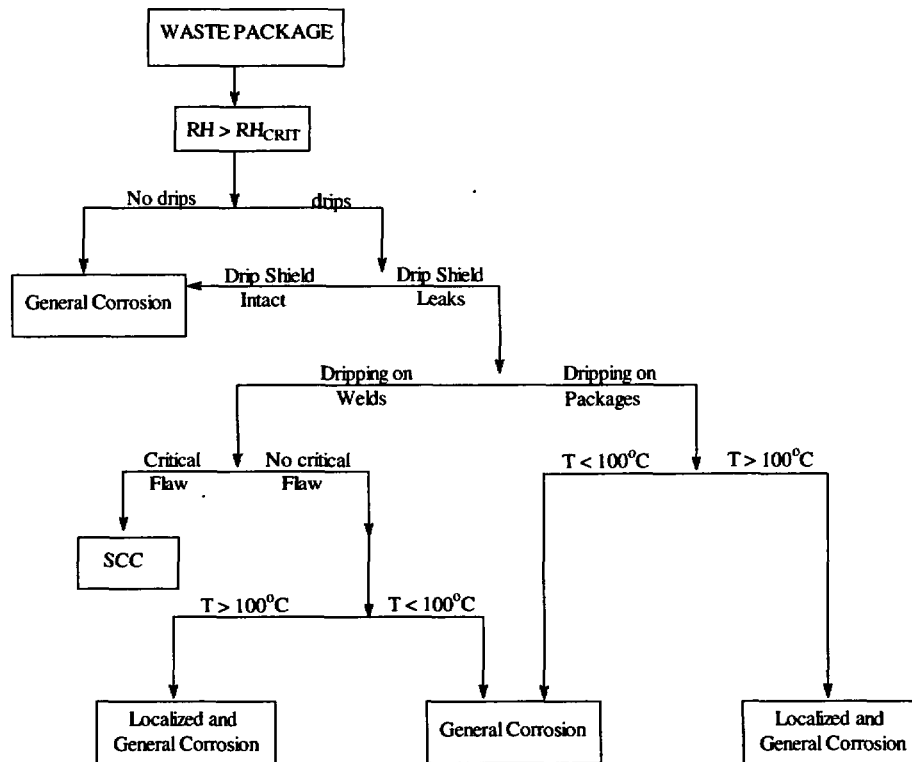


Figure 5-11
Outline of Waste Package Corrosion Model

5.4.1 General Corrosion

In the absence of seepage drips and the accompanying evaporative cycles it is assumed that only general corrosion can occur. The rates used in our model are those generated after two years of

testing in the LTCTF and LLLNL (Table 26, CRWMS M&O 1999a). Figure 5-12 shows a Weibull cumulative distribution function ($\alpha = 40.381$, $\beta = 0.984$ and $\theta = 0$) fitted to a number of points from this table. These points are summarized in Table 5-1 below. These values are consistent with values measured by Accary et al. (1985) and Smailos et al. (1986) for the C-4 Alloy in saturated brines.

**Table 5-1
Distribution of Measured Aqueous General Corrosion for Alloy 22**

Percentile	Corrosion Rate (nm/yr)
0	0
5.2	2.07
10	4.21
50.4	26.64
90	97.99
95.2	112.54
97.6	143.08
99.2	250.56
100	730.77

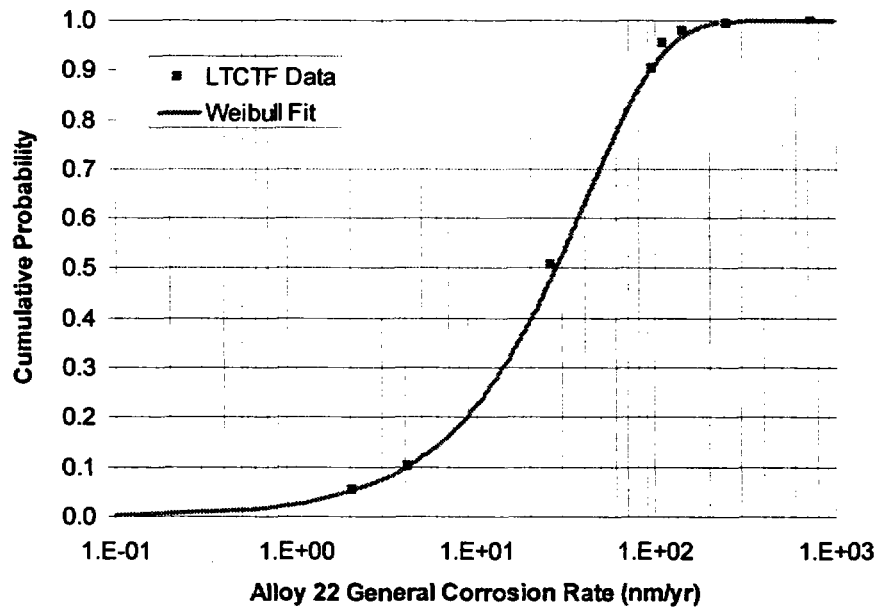


**Figure 5-12
Alloy 22 Aqueous General Corrosion Rate Distribution (From Table 26, CRWMS M&O 1999a)**

As in IMARC Phase 4, the general corrosion rate is assumed to be constant over the lifetime of the package wall. The rationale for adopting such a model has been discussed elsewhere (Shoesmith and Kolar 1998, Shoesmith et al. 1995a). However there are two significant differences in modelling approach compared to IMARC Phase 4. In the present model no Arrhenius temperature dependence of the rate is included, consistent with the observations in the LTCTF tests. These tests were conducted at temperatures of 60°C and 90°C, but the results of Accary (1985) and Smailos et al. (1986) show that, even in extremely aggressive saturated brines, the rate increase for the general corrosion of the inferior alloy C-4 between 90°C and 170°C was only a factor of ~3. Consequently, we would expect a negligible increase in rate between 90°C and 120°C, the highest temperature at which aqueous conditions can be established under repository conditions, and feel this justifies our decision not to include a temperature dependence. Also, the rates used under dripping conditions are the same as those for non-dripping conditions. Previously, we included a multiplication factor of 50 (for the 50 percentile value) to account for the possibility of an increase in rate at the lower pH values expected to develop in acidified crevices between Alloy 22 and the carbon steel barrier. The LTCTF data shows this was not justified, no significant difference in corrosion rates being observed between pH = 2.7 and neutral conditions.

It is worth mentioning at this juncture that this decoupling of the general corrosion rates from the repository environment makes the general corrosion performance of the waste package independent of repository design features such as the period of ventilation and the spacing between waste packages. Figure 5-13 shows the time to failure distribution developed from the model discussed above for a waste package subject to dripping or humid air conditions sufficient to create a water film on the surface of the package.

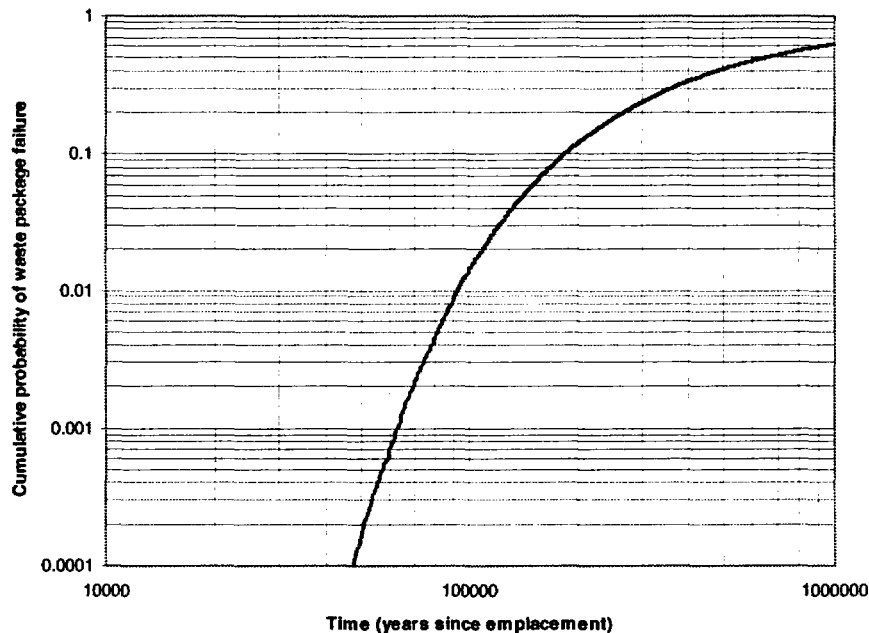


Figure 5-13
Waste Package Time to Failure from Humid Air/Aqueous General Corrosion

The prediction that such lifetimes will be achieved rests on the assumption that corrosion rates will remain constant over many tens to thousands of years. Obviously, experimental evidence to support such a claim is unavailable for these timescales, but industrial experience in various aggressive environments over the past 50 years or more shows changes in these passive materials is often immeasurable. An example would be the performance of titanium in heat exchanger applications, most of which involve exposure of the material to hot seawater. Over a 25 year operating period it has been reported that no corrosion failures have been experienced in over 61,000 km of titanium tubing (Schutz and Scaturro 1988, Schutz and Covington 1981, Adamson and Schutz 1987). As a consequence, TIMET (Henderson, Nevada) has sufficient confidence to place a 40 year warranty on titanium desalinators/surface condensers (Schutz and Covington 1981).

While one would not expect all passive materials to behave identically, there is some evidence to support claims that passive systems are capable of dynamically re-healing themselves. For Ni-Cr-Mo alloys, the class to which Alloy-22 belongs, passivity would be expected to be congruently dynamic, since there is no evidence to support a contention that dealloying might occur until transpassive conditions are achieved at potentials around 0.9 to 1.0 V (vs. SCE) (Bojinov et al. 2000). Such conditions do not appear unachievable under natural corrosion conditions. For titanium alloys, the available evidence points to a different long term passive evolution process. Very sensitive electrochemical impedance spectroscopy measurements show that minor film fracture events are rapidly resealed, probably by the accumulation of insoluble material within the fractures (Pan et al. 1996, Azumi et al. 2000).

5.4.2 Localized Corrosion

In IMARC Phase 4 the expected site of localized corrosion was the crevice between the Alloy-22 inner barrier and the failed outer carbon steel barrier. Within such a site it was feared that acidic conditions could develop due to carbon steel corrosion processes leading to the initiation of crevice corrosion. With the present single wall design such a crevice will not exist and the probability of crevice corrosion should be substantially lower, the only credible site for a crevice being underneath a deposit formed by the combination of seepage drips and the accompanying evaporative cycles. Consequently, as indicated in Figure 5-11, the drip shield must fail and dripping occur directly on the waste package for it to experience localized corrosion.

Since the last IMARC model was published a considerable amount of corrosion testing of Alloy-22 has been undertaken (Gruss et al. 1998, CRWMS M&O 1999a, CRWMS 1999b). Despite this, definitive proof that crevice corrosion will not occur under Yucca Mountain conditions has proved elusive. None of the crevice corrosion experiments conducted in the LTCTF showed any signs of localized corrosion and the repassivation potentials measured by Gruss et al. (1998) were > 900 mV (vs. Ag/AgCl), a potential unattainable under natural corrosion conditions. However, Scully et al. 1999 (referenced in CRWMS M&O 1999a) have observed crevice corrosion under electrochemically polarized conditions in chloride-dominated solutions ($5.0 \text{ mol.L}^{-1} \text{ LiCl}$ + small concentrations of NO_3^- and SO_4^{2-}) at 80 to 95°C. While such chloride-dominated solutions are not anticipated in Yucca Mountain, the residual uncertainties over the groundwater compositions achievable by evaporative cycles (CRWMS M&O 2000a) make it judicious not to rule out the possibility that such a process may occur, while acknowledging that it is a very unlikely possibility.

To model crevice corrosion we have chosen to use the same penetration growth law used in IMARC Phase 4, but have modified the parameter values to reflect recent improvements in mechanistic understanding. The wall penetration growth law used has the form

$$d_{cc} = Bt^n \quad \text{Eq. 5-7}$$

where d_{cc} is the maximum penetration depth ($\mu\text{m}/\text{year}$), B is a crevice growth constant and n is the time exponent, expected to have a value to 0.5 if the growth process is limited only by diffusive or resistive effects within the local corrosion site. An extensive discussion of the general applicability of this law to a number of metal/alloy systems has been presented elsewhere (Shoesmith and Kolar 1998). This growth law is used in conjunction with the temperature threshold value (T_{cc}) for the onset of crevice corrosion discussed above and outlined in Figure 5-14 (with $T_{cc} = 100^\circ\text{C}$; see below).

Table 5-2 summarizes the values used in the penetration growth law, equation (5-7), in the present model compared to the previous IMARC model.

Table 5-2
Values of Parameters Used in the Waste Package Crevice Corrosion Model (Equation (5-7))
Compared to the Values Used Previously in IMARC 4

Parameter	Value	
	IMARC 4	Present Model
T_{cc} ($^\circ\text{C}$)	80	100
n	0.5	0.1 to 0.5 (uniform distribution)
B	(5%) 5 (50%) 55 (95%) 100	5 55 100

The threshold temperature of 80°C used previously was chosen as a conservative value based on critical crevice corrosion temperatures measured in chloride-dominated (4% NaCl) acidic ($\text{pH} = 2$) solutions containing 0.1% Fe^{III} ions (Haynes 1987a). For a waste package design with a carbon steel outer barrier over an Alloy-22 inner barrier these data were the most appropriate available. Even so, the measurements indicated that the threshold temperature for Alloy-22 was 102°C , and 80°C was chosen as a conservative value since only a single set of measurements was available. For the present package design, these threshold temperature values are no longer as appropriate since acidic Fe^{III} conditions are no longer anticipated, and the most recent electrochemical and immersion test results obtained in the LTCTF at LLNL (CRWMS M&O 1999a) offer justification for raising T_{THRES} to 100°C or higher. Electrochemical polarization experiments in saturated saline solutions at 120°C showed no evidence for film breakdowns under non-creviced conditions and only under extreme polarization ($> 1000 \text{ mV}$ vs Ag/AgCl) could crevice corrosion be forced to initiate in 4 mol.L^{-1} NaCl at room temperature. While this test program cannot be considered complete, the evidence that crevice corrosion will only be

sustainable on Alloy-22 under extreme conditions of temperature and salinity is becoming compelling, and further testing is most likely to eliminate the possibility altogether.

Table 5-3 below summarizes the simplified distribution of waste package surface temperatures used in the corrosion modeling. Times after emplacement when the surface temperatures of waste packages of varying initial heat output have cooled to 120°C and 100°C are given. This information was obtained from CRWMS M&O 2000e, Tables 6-7 and 6-18 for the 25 year and 50 year ventilation times, respectively. These cases assumed a waste package spacing of 0.1 meters and no backfill, and calculations utilized a 3-D pillar model of an infinite repository in the lateral direction. As such, they provide temperatures representative of the center of a finite repository. It was assumed that packages at the edge of the repository were 25°C cooler for the purpose of estimating the times when such packages would reach the surface temperatures of interest. The percentage of waste packages with the indicated initial heat output is based on a simplification of the information on the number of various types of waste packages and their initial heat output provided in Tables 5-6 and 5-7 of CRWMS M&O 2000e.

**Table 5-3
Simplified Distribution of WP Surface Temperature vs. Time**

Approx. Initial WP Heat Output	Time (years) T = 120°C		Time (years) T = 100°C		Delta-time (years)		% WPs	Cumulative WPs
	Center	Edge	Center	Edge	Center	Edge		
25 year ventilation period								
3 kW	658.3	210.7	1775.0	525.0	1116.7	314.3	2.27%	2.27%
7.4 kW	725.0	225.0	1848.5	575.0	1123.5	350.0	38.03%	40.30%
11.8 kW	875.0	295.0	1969.4	700.0	1094.4	405.0	59.70%	100.00%
50 year ventilation period								
3 kW	425.0	136.7	1511.5	310.0	1086.5	173.3	2.27%	2.27%
7.4 kW	483.3	147.5	1588.5	370.0	1105.1	222.5	38.03%	40.30%
11.8 kW	650.0	210.0	1764.3	500.0	1114.3	290.0	59.70%	100.00%

A problem with assigning appropriate values to the crevice growth constant, B, and the time exponent, n, in equation (5-7) is the absence of a database of these values and a thorough understanding of the mechanism of initiation, propagation and repassivation on Alloy-22. In IMARC4 a value of n = 0.5 was adopted based solely on a single measured value of n = 0.46 for the crevice corrosion of the highly susceptible Ti-2 alloy. The adoption of this value was tantamount to assuming that the localized corrosion of Alloy 22 is limited only by diffusive or resistive effects within the active localized corrosion site. This ignores those metallurgical features designed into the alloy to enforce its repassivation, as well as inhibit the initiation, of crevice corrosion.

The presence of Mo in Alloy 22 inhibits active metal dissolution and, hence, promotes repassivation (Newman 1985, Clayton and Olefjord 1995). A similar limitation on the propagation of crevice corrosion on other alloys designed to resist localized corrosion

(e.g., Ti-12 (Shoesmith et al. 1995b) has been observed. This suggests that, except under artificially stimulated electrochemical conditions as applied by Scully et al. (referenced in CRWMS M&O 1999a), Alloy-22 should only incur a relatively small amount of crevice corrosion damage if such a process in fact initiates. Empirically, enforced repassivation would lead to an "n" value much less than 0.5 in equation (5-7). Based on this rationale, we have used a uniform distribution of "n" between 0.1 and 0.5, Table 5-2.

For the growth constant, we have kept the values used in the previous IMARC model. These values were a composite set compiled from the available test data for the C Alloy series (C-4, C-276, C-22), with the data for the C-4 alloy being the primary source. Since subsequent corrosion testing has not yielded measured values for the crevice growth constant, B, we have taken these values, measured in aggressive 10% FeCl₃, to be the only available source. By accepting the values measured for the C-4 Alloy we are assuming that the major differences in resistance for this series of alloys will be in their ability to reenforce repassivation (encapsulated in the value of n) rather than in their propagation rates (embodies in the value of the growth constant B).

We have also taken B to be independent of temperature, based on experience with Ti alloys designed to resist crevice corrosion; e.g. Ti-12. For this alloy, the propagation of crevice corrosion has been shown to be limited by metallurgical features, the thermally-activated increase in propagation rate being counterbalanced by the thermally-activated increase in repassivation rate. This leads to an independence of the observed rate on temperature (Shoesmith et al. 1995b). With no dependence on temperature, the value for B was sampled in the corrosion modeling process from a Weibull distribution with an $\alpha = 54.085$, $\beta = 1.285$, and $\theta = 0$.

Our model for crevice corrosion is considerably less conservative in some regards but more conservative in others than the model used by the USDOE. As in our model, they assume that localized corrosion will only occur as a consequence of dripping directly onto the waste package through a failed drip shield. Their criterion for initiation is not based on a temperature threshold but a potential threshold measured electrochemically as described above (equation 5-2). Based on these measurements it is predicted that crevice corrosion will not initiate, a less conservative conclusion than used in this IMARC model. However, the USDOE model for crevice propagation, if it were to initiate, is extremely conservative. It is assumed that the penetration rate will be linear with time, equivalent to assuming a value of $n = 1$ in equation (5-7). Such a value ignores any ability of metallurgical features to reinforce repassivation. Based on assumed linear rates measured under extremely aggressive test conditions they adopted rates ranging from 12.7 $\mu\text{m}/\text{year}$ (0 percentile) to 1270 $\mu\text{m}/\text{year}$ (100 percentile). With a linear time dependence these rates suggest failure by crevice corrosion would occur in ~ 12 to 1200 years if initiated.

Figure 5-14 assesses the consequences of including a localized corrosion model by showing the distribution of predicted failure times for general and general-plus-localized corrosion for the first 100,000 years of emplacement. As can be seen, localized corrosion has a minor impact on the distribution due to the short time span in which it can occur; i.e., the model predicts that the accumulation of localized corrosion damage will be rapid but short-lived. What is clear from this calculation is that further measures to reduce the surface temperature of the waste package, such as an increased period of ventilation or an increase in the space between packages, would be of minor value.

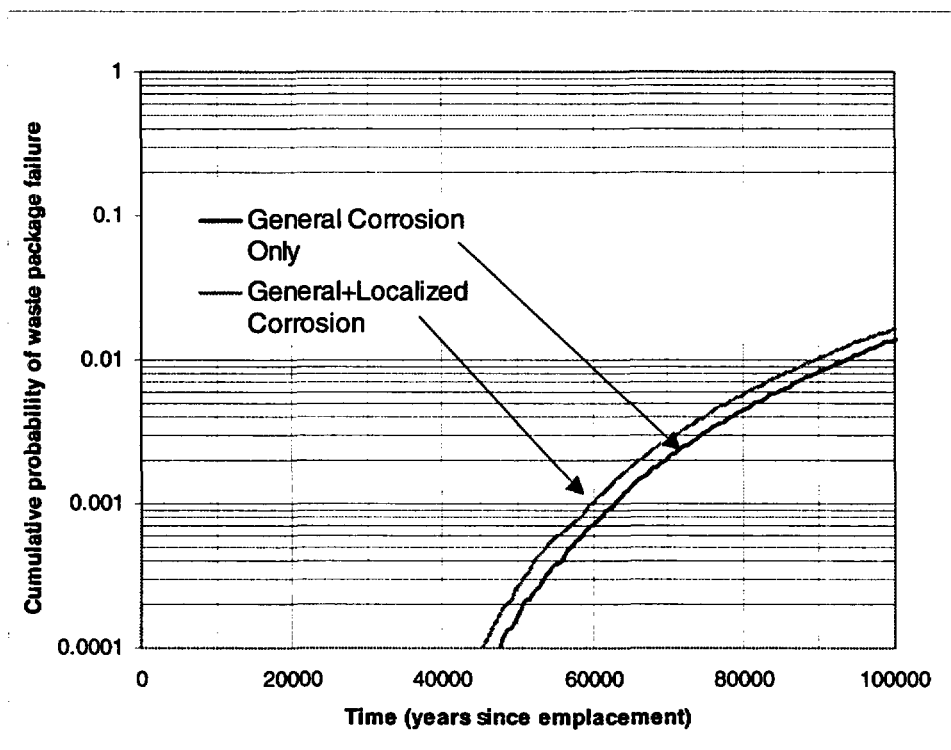


Figure 5-14
Comparison of Waste Package Failure Times by Localized and General Corrosion
(Center – 50 year Ventilation Period)

5.4.3 Stress Corrosion Cracking

As indicated in Figure 5-14, we assume that SCC can only occur in region of the welds. Additionally, since all fabrication welds used in manufacturing the waste package can be fully annealed prior to the emplacement of the waste, they will not be subject to residual stresses high enough for SCC to occur (CRWMS M&O 2000f, 2000g). Consequently, in common with the USDOE model, we assume that only the closure lid weld of the waste package can develop residual stresses high enough to cause SCC, since this weld must be made with the waste in place, a condition which disqualifies a subsequent full package anneal.

If cracks are to initiate and propagate in structural components via SCC, then three basic conditions must be met simultaneously; (i) the material must be metallurgically susceptible; (ii) the environment must be sufficiently corrosive; and (iii) a source of tensile stress must be present. While it cannot be demonstrated unequivocally that one of these conditions will not be met under Yucca Mountain conditions, very convincing arguments can be made that the combination of the natural features of the mountain and the engineered design of the drip shield and waste package make it highly improbable that failure by SCC will occur.

As with localized corrosion, it is difficult to make the argument that Alloy-22 will be immune to SCC. Tests conducted in acidic 5% NaCl brine (pH = 2.7) (Roy et al. 1998) and in basic aerated concentrated saline solutions (pH ~13.4, 110°C) (CRWMS M&O 2000x) both showed that crack

growth could be sustained in Alloy 22 at least for some period of time. While the development of acidic environments at Yucca Mountain now seems a very remote possibility, the development of basic solutions via evaporative processes does not, with saline solutions with pH values greater than 12, appearing possible (CRWMS M&O 2000a).

As a consequence, no argument can be made that environments sufficiently aggressive to sustain SCC will not occur. However, the probability that such an environment will contact the potentially susceptible final closure weld is considerably reduced by the properties of the mountain and the design of the engineered barriers. As outlined in Figure 5-11, the repository drift must experience drips and the drip shield must fail at a drip site before groundwater can contact the waste package and, via evaporative concentration, produce a sufficiently aggressive environment. Even then the probability that the drip will directly contact the weld (P_w) will be low and can be assumed given by the probability of a drip contacting the waste package (P_{wp}) multiplied by the ratio of the exposed weld area (A_w) to the total waste package surface area (A_{wp}); i.e.

$$P_w = P_{wp}(A_w/A_{wp}) \quad \text{Eq. 5-8}$$

Equation 5-8 can be considered conservative since the closure welds are protected from direct dripping when containers are emplaced horizontally.

Finally, the probability that the final closure weld will be subjected to the necessary stresses can be significantly reduced by a combination of design features and localized stress relief procedures. The design of this closure weld is shown in Figure 5-3. The dual lid construction and chosen lid thicknesses mean that 35 mm of Alloy-22 must be penetrated before failure by SCC can be said to have occurred. Also, it is planned that both the outer and inner lid welds will be annealed by induction coil heating and laser peening, respectively.

Stress analyses of this design to determine stress distributions and stress intensity factors (using finite element procedures) show that only the influence of hoop stress leading to the growth of a radial crack is a likely cause of SCC (CRWMS M&O 2000f). These calculations also show that, after stress mitigation, the stress intensity factor profile in the inner lid will be negative for the first 5 mm of thickness, and even at the 3σ limit (assuming a normal distribution) will not exceed a low value of $8 \text{ MPa}\cdot\text{m}^{1/2}$ throughout the remaining wall thickness. A similar analysis of the outer lid weld suggests the outer 12 ± 2 mm of total weld thickness (25 mm) will be immune to SCC.

These immune outer weld layers would have to be removed by general or localized corrosion processes before SCC could initiate. This means that, irrespective of whether one or both lids were susceptible to SCC at the same radial location, between ~ 12 mm and 19 mm of wall thickness would have to be removed by corrosion first. Based on the rates for general corrosion discussed in previous sections this could take tens to hundreds of thousands of years.

A final feature of the dual lid design which reduces the probability that SCC could fail both lids at the same site is the low probability that two radially-oriented flaws of the required critical size will occur at the same location, one in the outer and the other in the inner weld.

Two distinct models have been considered for the SCC of the waste package closure weld (CRWMS M&O 2000f, 2000g); the Stress Intensity Threshold Model (STM) and the Slip Dissolution/Film Rupture Model (SDM). According to the STM (Jones and Ricker 1987, Sprowls 1987), there exists a threshold stress intensity factor (K_{ISCC}) such that crack growth will only occur in a pre-existing crack having a stress intensity factor (K_I) greater than this value. If K_{ISCC} is exceeded no attempt to model the crack growth rate is attempted since failure is assumed to be effectively instantaneous.

By contrast, the SDM assumes that there is a finite probability that a pre-existing crack can grow at even low values of K_I and that no justifiable threshold value of stress intensity factor can be defined. In this model the crack growth rate is calculated for a given crack tip environment, corrosion potential and metallurgical condition based on the theory of slip dissolution and film rupture (Ford and Andresen 1988, Andresen and Ford 1994). In this theory the crack growth rate is calculated for a series of film rupture-crack tip metal dissolution events. The extent of metal dissolution (proportional to the crack growth rate, V_i) is calculated from electrochemical oxidation transients following induced film ruptures and the frequency of film rupture is calculated from the ratio of the fracture strain of the film to the strain rate at the crack tip. Assuming constant load conditions, this theory can be expressed by the equation

$$V_i = A(K_I)^n \quad \text{Eq. 5-9}$$

in which A and n are constants specific to the material and the corrosive environment at the crack tip. The USDOE have evaluated both models and chosen to use the SDM. When the STM was used in scoping calculations using Roy's measured value of K_{ISCC} (Roy et al. 1998) of $30 \text{ MPa}\cdot\text{m}^{1/2}$ * and the computed values of K_I from finite element calculations, SCC was predicted not to occur in either closure weld (CRWMS M&O 2000g). However, since only a single value of K_{ISCC} was available, this conclusion was judged insufficiently reliable to eliminate SCC as a potential failure process.

When applying the SDM, crack growth was assumed possible at a stress equal to a value uniformly distributed between 20 to 30% of the yield stress (CRWMS M&O 1999b, 2000g). This value was used with a maximum incipient flaw size of $50 \mu\text{m}$ to define the value of K_I in equation (5-9). This is a conservative value since it is an upper bound but its use does not influence the crack penetration time significantly. Using the relationship between A and n developed for stainless steel, a value of A was calculated using a uniform distribution of n between 0.75 to 0.84. Since susceptibility to SCC decreases as n increases, the arbitrary choice of a lower bounding value of 0.75 is a significant conservatism, especially since the upper bounding value of 0.84 was obtained from a crack growth measurement made under aggressive conditions (basic saturated saline solution (pH ~13.4, 110°C) (CRWMS M&O 2000f).

By contrast, we have chosen to use the STM in our model but with a much lower value of $K_{ISCC} = 8 \text{ MPa}\cdot\text{m}^{1/2}$ compared to Roy's measured value of $30 \text{ MPa}\cdot\text{m}^{1/2}$. We chose this value based on a consideration of bounding calculations using the SDM (CRWMS M&O 2000g) and consider it to be conservative. This calculation is based on the bounding values of n and a range of K_I values which can be anticipated in the closure lid welds. The results are plotted in

* Actually, a normal distribution around $33 \pm 1.8 \text{ MPa}\cdot\text{m}^{1/2}$ was used.

Figure 11 of CRWMS M&O 2000y, and show that once a crack initiates penetration of the lid will be relatively rapid in geological time. For the 25 mm thick outer lid using the lower boundary value of $n = 0.75$, the value of K_I must drop below $\sim 8 \text{ MPa}\cdot\text{m}^{1/2}$ before weld penetration times are predicted to exceed 10^3 years. Compared to the estimated induction period of $> 10^4$ years required for the corrosion penetration of the stress-relieved outer weld layer, this constitutes a relatively quick. We have taken this as justification for using the STM with a $K_{ISCC} = 8 \text{ MPa}\cdot\text{m}^{1/2}$. This value of K_{ISCC} is substantially lower than Roy's measured value and would require only a small flaw to achieve.

We also assume that the inner lid weld will not experience SCC because the three simultaneous criteria for SCC to occur (i.e. metallurgical susceptibility, aggressive environment, sufficient stress) will be extremely difficult to satisfy. Exposure of the inner weld will not occur quickly and, hence, the development of an environment sufficiently aggressive to sustain SCC will be difficult. Many years of corrosion ($\geq 10^4$ years) will be required to remove the 11-mm thick stress-relieved layer of the outer weld. Assuming this is followed by immediate penetration of the residual outer weld thickness by SCC, the temperature on the inner weld surface will have decayed to $\sim 30^\circ\text{C}$ to 50°C before it contacts a wet environment. Subsequently, it would be necessary to corrode away the 5 mm-thick outer layer of the inner weld for which K_I is negative before SCC was possible (CRWMS M&O 2000g). This would also require $\geq 10^4$ years, by which time the weld temperature would be $\leq 40^\circ\text{C}$ and the likelihood of establishing an environment aggressive enough to support SCC very remote.

A second argument in support of ignoring SCC of the inner lid weld comes from the calculation of K_I as a function of the projected radial crack depth in the inner lid weld (Figure 8, CRWMS M&O 2000g). This profile shows K_I to be negative to a depth of ~ 5 mm and, even at the 3σ limit, never exceeds a value of $\sim 9 \text{ MPa}\cdot\text{m}^{1/2}$ throughout the remaining wall thickness. This is only marginally greater than our threshold value for $K_{ISCC} = 8 \text{ MPa}\cdot\text{m}^{1/2}$. Considering our value of K_{ISCC} is significantly lower than the measured value of $30 \text{ MPa}\cdot\text{m}^{1/2}$, it is reasonable to assume a sufficient stress intensity to support SCC is a remote possibility.

In summary, we can specify our SCC model as follows, Figure 5-11. Only those welds subject to dripping and, hence, evaporative concentration processes will develop a sufficiently aggressive environment to sustain SCC. Once dripping on a weld occurs the outer stress-relieved layer of 12 ± 2 mm thickness will begin to corrode. If dripping starts while $T \geq 100^\circ\text{C}$ then corrosion will proceed by both general and localized processes. If $T < 100^\circ\text{C}$, only general corrosion will occur. Corrosion must then proceed until this layer is removed. Since we assume the thickness of this stress-relieved layer is uniformly distributed, the time to remove it will be similarly distributed. Then, the probability of instant penetration of the remaining 13 ± 2 mm of weld thickness by SCC will be the probability that a surface breaking flaw exists of sufficient depth to produce $K_I > K_{ISCC} = 8 \text{ MPa}\cdot\text{m}^{1/2}$ at the crack tip.

The information on the frequency and size distribution of weld flaws utilized in this analysis was obtained mainly from CRWMS M&O 2000h, [Section 6.2.1]. This document utilized available information on flaw size and existence frequencies in nuclear piping and vessel welds to make estimates for the Alloy 22 barrier of the waste package. Since the USDOE document was focused primarily on surface breaking flaws due to an earlier project assumption that only those types of flaws would be of concern for SCC, information on the through-wall distribution of

flaws was obtained from Khaleel et al. 1999 (Table 5, Case 10) for an uninspected 25.4 mm stainless steel weld. This distribution is provided in Figure 5-15, and as can be seen, it indicates that 90% of flaws would be encountered within the outer half of the weld. This may result from the fact that it is based on data from V-groove welds. Since the waste package lid closure welds may have a more uniform through-wall width, a sensitivity analysis utilizing a uniform flaw location distribution has also been performed, and is discussed below.

The size distribution for flaws in the welds is shown in Figure 5-16, and is essentially the same as that used in CRWMS M&O 2000h. The distributions take into account the thickness of the weld, the welding method (TIG assumed), and the type of non-destructive examinations performed. For the waste package shell welds, radiographic, dye-penetrant and ultrasonic examinations are assumed, while for the lid closure welds, only ultrasonic examination is assumed. As can be seen from Figure 5-16, the majority of flaws remaining in a weld after inspection have a depth of only a few millimeters. This is primarily a result of their typically being below the limits for rejection, or simply below the size limit where they can be reliably detected by NDE methods.

A flaw occurrence frequency for the shell welds of 2 flaws per waste package was used based on the information given in CRWMS M&O 2000h. For the lids however, the flaw occurrence frequency of 13.8 flaws per meter for a 1 inch uninspected stainless steel weld from Khaleel et al. 1999 (Table 5, Case 10) was utilized. The flaw frequency was adjusted to account for the ultrasonic inspection of the lids in the same manner as was done in CRWMS M&O 2000h. This yielded an estimate of 25 flaws per outer Alloy 22 lid and 18 flaws per inner Alloy 22 lid.

As mentioned above, only flaws in the waste package lid that are radially oriented are considered of concern for SCC. Shcherbinskii and Myakishev (1971) measured the angles of defects with respect to the direction of welding in steel steam pipe welds between 16 and 60 mm thick that had been welded by either automatic or manual methods. It was found that orientation of flaws could be represented by a normal distribution centered on the weld direction with a standard deviation of 4.93. Such a distribution results in an infinitesimally small probability of a flaw being oriented normal to the direction of welding. However, a flaw need not be exactly radial to be subject to sufficient hoop stress to be of concern for SCC. Therefore, a probability of 0.01 of a flaw being radially oriented has been conservatively utilized. This corresponds to a 13° angle from the direction of welding on the above-mentioned distribution. Based on the above mentioned flaw frequencies, this results in 25% of waste packages having a radial flaw in the outer lid.

In addition to considering the flaws as potential sites for SCC, the weld flaws can also be viewed as localized reductions in the thickness of the waste package barrier. Therefore, the general and localized corrosion modeling of the package also considered weld flaws when predicting waste package failure time. This was done simply by sampling the size distribution for the shell or lid by the number of flaws expected per package for that weld, and reducing the effective thickness of the barrier by the size of the largest flaw.

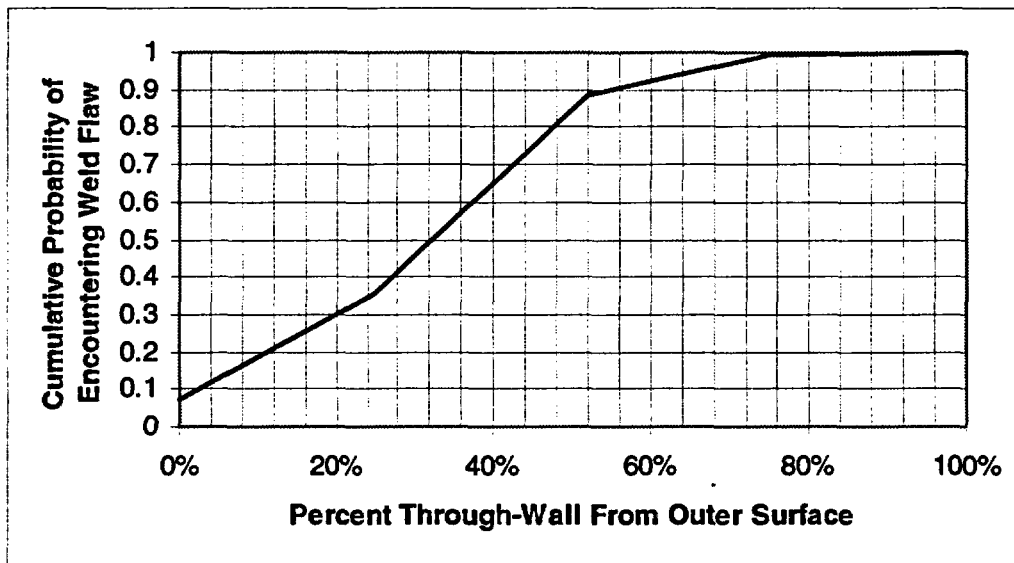


Figure 5-15
 Cumulative Probability of Encountering a Flaw as a Function of Distance from Outer Surface of Weld

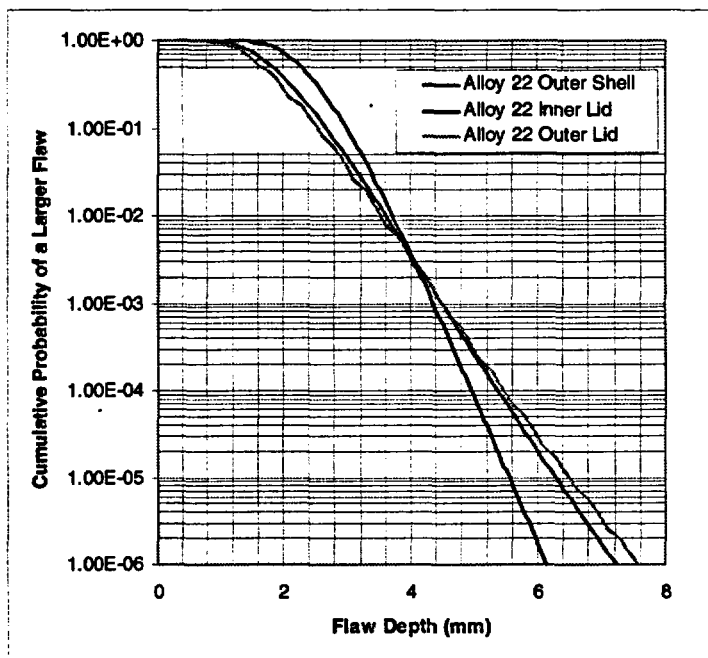


Figure 5-16
 Size Distribution of Weld Flaws in the Alloy 22 Barrier Welds

Figure 5-17 provides the resulting distribution for waste package failure times that include consideration of the effects of SCC for packages that meet the criteria for susceptibility (exposure to dripping water and the presence of a radial flaw in the outer closure weld). For the base case, SCC played little role in waste package failure. The combination of the outer and inner lids (25 mm and 10 mm respectively) never fails before the shell fails by general or

localized corrosion (although the outer lid does fail before the shell in many cases). Several factors combine to cause this effect, including: 1) a large (10 to 14 mm) surface compressive layer on the outer weld, 2) a mean flaw depth of less than 2 mm, 3) ~80% of flaws occur in the compressive layer (thus prohibiting SCC failure) based on the nuclear piping data, and 4) the small aperture size of the outer Alloy 22 lid SCC failure prohibits the inner lid from experiencing an environment that would promote SCC. This clearly emphasizes the advantage gained by using a dual lid design and stress mitigation techniques on the closure welds.

To examine the sensitivity of the model to the assumption that such a compressive layer could be achieved, a calculation was performed in which the thickness of the compressive layer was reduced to 2-3 mm. This would be the layer thickness expected if laser peening, as opposed to induction coil heating, were used to mitigate stresses in the outer, as well as the inner, closure lid weld. Such a reduction might also occur if the stress relief process were improperly done. The reduced thickness of the compressive layer causes the outer lid to fail much more rapidly due to SCC. However, as can be seen from the distribution in Figure 5-17, the inner lid, which is still considered immune to SCC due to an inability to get the necessary aggressive groundwater species to it, still provides considerable protection.

Another sensitivity case was run to examine the effect of utilizing a uniform flaw location distribution, as opposed to the one shown above in Figure 5-16. No other parameters were altered from the base SCC case. A uniform distribution may be more applicable for a narrow groove weld (such as that used for waste package closure) than one developed from data on V-groove welds. However, the results in Figure 5-17 show that this assumption has little impact on the waste package failure distribution.

A sensitivity case was also run to quantify the degree of defense-in-depth provided by the inner Alloy-22 barrier lid. All parameters from the base SCC case were retained, but the inner lid was assumed not to be present. The result was that the cumulative probability of waste package failure reached 10^{-4} at 31,000 years (15,000 years earlier). The mean time to failure occurred at 551,000 years (100,000 years earlier than base case), and the total fraction of packages failed at 1,000,000 years was only 5% greater. This shows that exclusion of the inner lid results in only a modest reduction in waste package performance if the outer lid performs as expected.

The true measure of the inner lid's defense-in-depth value is seen in the final sensitivity case, which coupled removal of the inner lid with a 2-3 mm compressive stress layer in the outer lid. The resulting distributions shows that 1% of waste packages with radial flaws (25%) that are exposed to direct dripping would fail within 1,000 years due to SCC in the outer Alloy-22 lid. This large number of early failures is not unexpected for such an extreme sensitivity case, as Figure 5-15 indicates that ~7% of weld flaws are outer surface breaking, and Figure 5-16 indicates that ~5% of these flaws would extend below a 2-3 mm compressive stress layer. Since this is all that is required to cause SCC in the current model, failure of the outer lid is almost instantaneous for a small fraction of packages meeting the criteria for SCC. Consideration of the fact that a flaw must extend a certain minimum distance into the tensile stress layer of the weld (e.g. $K_I > 8 \text{ MPa}\cdot\text{m}^{1/2}$), and use of a uniform flaw location distribution would eliminate some of the conservatism from the model and likely lower the fraction failed at 1,000 years by at least an order of magnitude. However, this conservative model still serves to illustrate the defense-in-depth that is provided by the inner Alloy-22 lid against improper stress-relief (which is also a small probability event), or higher than expected flaw occurrence rates in the outer

Alloy-22 lid. In addition, the inclusion of a drip-shield in the design of the EBS, and the consideration that the fuel's decay heat will prevent water entry for several thousand years, provides additional layers of defense-in-depth.

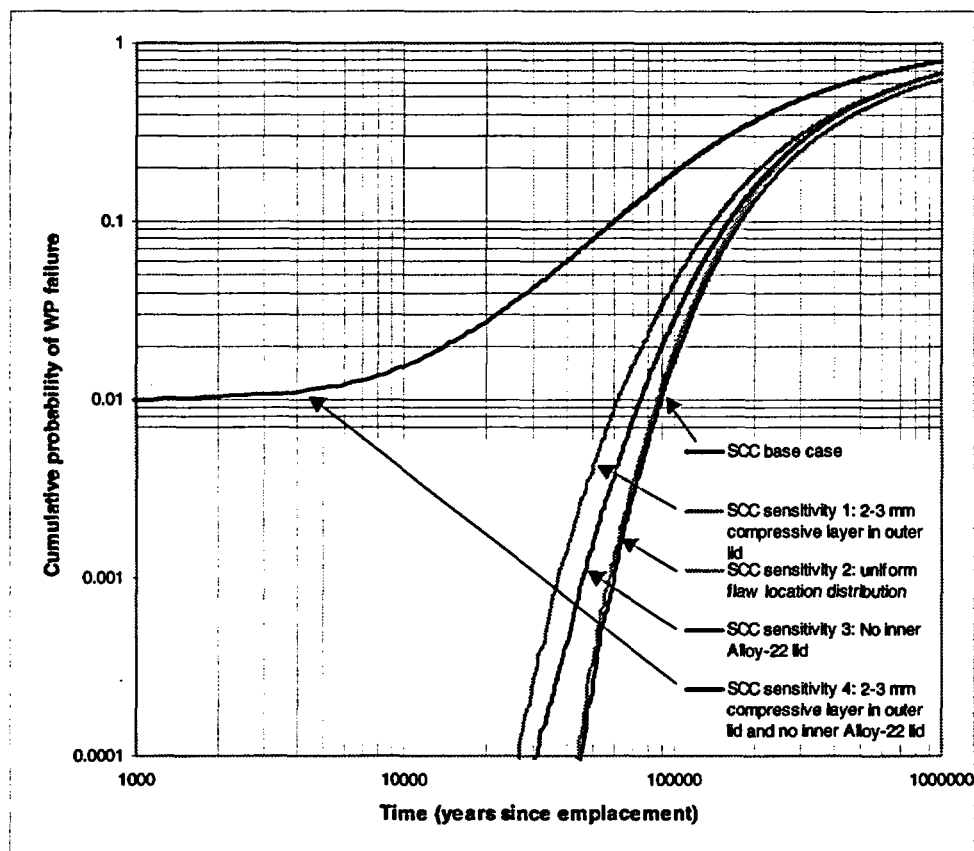


Figure 5-17
Time to Failure Distributions for a Waste Package Meeting the Criteria for SCC Susceptibility under Various Scenarios

5.5 EBS Corrosion Modeling Input to IMARC5

This section summarizes the engineered barrier system failure time distributions that will be utilized as input to the IMARC5 performance assessment model. For IMARC5, failure of the engineered barrier system is defined as the time when water first enters a package that is located under a dripping fracture. This occurs when the following three criteria are met:

1. the drip shield has failed,
2. the WP has failed, and
3. the waste package decay heat has dropped to the point where the presence of liquid water is possible within the failed waste package.

The third item was considered as part of the IMARC5 model based upon the information provided in CRWMS M&O 2000i (Section 6.3). However, since the combined drip shield and waste package failure times were in excess of 10,000 years for the cases considered, the effect of decay heat preventing water entry into the waste package at times < 10,000 years was not evident in the EBS failure distributions. However, it should be recognized that this is another example of defense-in-depth provided by the repository design.

Figure 5-18 provides the EBS failure distributions for the IMARC5 base case. The base case was run for a 56 MTU/acre repository with a 50 year ventilation period, using the temperature points given in Table 5-3 to define the establishment of aqueous conditions ($T = 120^{\circ}\text{C}$) and the susceptibility to crevice corrosion ($T = 100^{\circ}\text{C}$). Waste package locations at the center and edge of the repository were considered. However, as can be seen from Figure 5-18, the results were nearly identical for both locations. Therefore, for the remaining sensitivity analyses, only the central location will be considered.

In addition to physical location, initial condition of the drip shield was also varied. CRWMS M&O 2000h (Figure 6.2-11) provides estimates of the probability that the drip shield would be improperly emplaced, resulting in a gap of unspecified size over a waste package, as a function of the drip shield length. For a drip shield with a length of 6 meters, there will be slightly less than one connection between adjacent drip shields per waste package. Based on CRWMS M&O 2000h, this yields a probability of 10^{-4} per waste package of a drip shield emplacement error. Consideration of the effects of rockfall could increase this probability to 1.5×10^{-3} , as CRWMS M&O 2000o (p. 3) indicates that 14 dripshields may be subjected to rockfalls in excess of their 6 tonne design basis during the first 10,000 years. Such an impact is expected to result in deformation of the drip shield and cracking in the vicinity of the stiffeners, but would not directly affect the waste package. The crack aperture would be narrow and expected to accumulate deposits leading to its resealing.

For conservatism, it has been assumed that a waste package under a failed drip shield would essentially be unprotected from dripping. For such packages, the 10^{-4} probability of water entry is reached at approximately 43,000 years, as opposed to 63,000 years. The mean time to water entry is 636,000 years for a waste package under a misplaced dripshield, as opposed to approximately 1,000,000 years for a properly placed dripshield. Package failure occurred primarily as a result of general and localized corrosion for packages under a misplaced dripshield, while only general corrosion was responsible for package failure for packages under a properly placed drip shield. Due to the failure time of the drip shield by corrosion, only packages that were under a misplaced drip shield would be subject to aqueous conditions while between the temperature range for localized corrosion of 120°C to 100°C . For reasons discussed previously, the base case model for SCC resulted in no cases where the lids failed prior to the shell. This was due to the fact that even after consideration of weld flaws, general/localized corrosion processes were still required to remove an amount of material that was generally greater than the thickness of the shell.

The difference between the two sets of curves in Figure 5-18 defines the maximum influence of localized corrosion on waste package lifetime as well as illustrates the advantage to be gained from proper emplacement of the drip shield. A key observation is the lack of sensitivity of package lifetimes to location within the repository; i.e., center vs edge. This reflects the temperature independence of the corrosion models and also illustrates the conservatism inherent

in the localized corrosion model (equation 5-7, Table 5-2). The period of susceptibility to localized corrosion varies by a factor of 5 to 10 depending on waste package heat output and location, Table 5-3. This has a negligible effect on waste package lifetimes since the accumulation of localized corrosion damage, in the unlikely event that it occurs, will be rapid but of short duration.

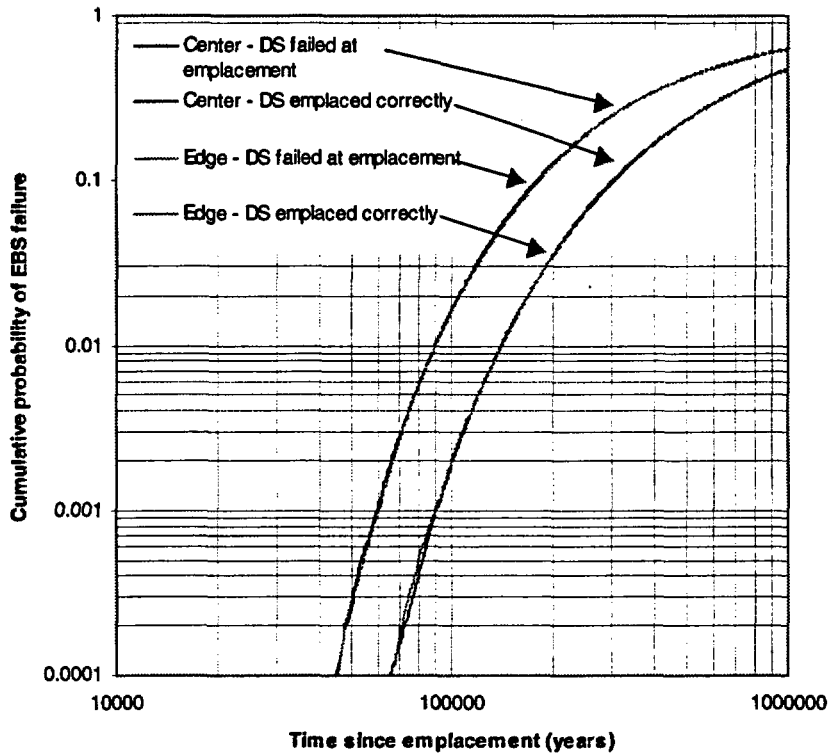


Figure 5-18
Engineered Barrier System Failure Times for 50 Year Ventilation at the Center and Edge of the Repository

Several sensitivity cases were run to examine how various parameters affect the performance of the engineered barriers in the IMARC5 model. Figure 5-19 shows a comparison of the results for 25 and 50 years of ventilation for the repository center. As can be seen, there is essentially no effect caused by this variation. This is because the change in ventilation time has little effect on the duration of time that the waste package surface is within the temperature range required for localized corrosion to occur. The only effect of reducing ventilation time to 25 years is to shorten the time to reach 120°C, and establish aqueous conditions, by a few hundred years.

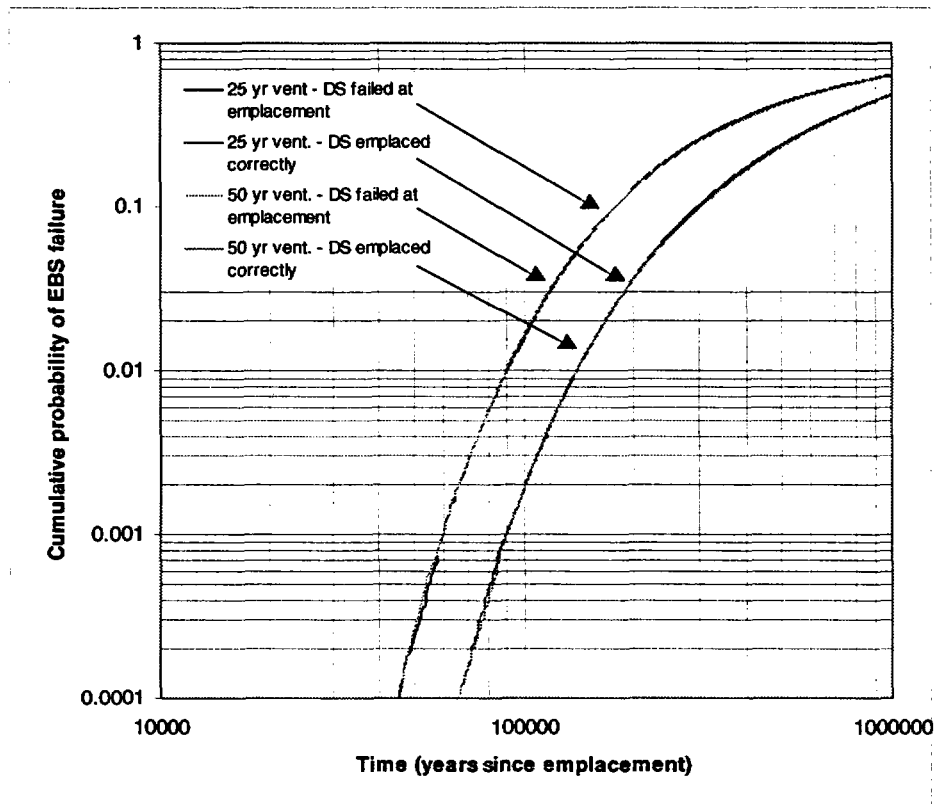


Figure 5-19
Impact of Ventilation Period Duration on EBS Failure Times

Figure 5-20 provides the results for a sensitivity case that considered increasing the susceptibility of the waste package to SCC by reducing the thickness of the compressive stress layer in the outer lid closure weld to 2-3 mm. Due to the defense-in-depth provided by the inclusion of the drip shield in the EBS design, only a modest reduction in performance of the engineered barrier system is seen (the 10^{-4} probability of failure for the EBS occurs at ~46,000 years). While the 10^{-4} EBS failure time for packages under misplaced dripshields is under 30,000 years, this distribution is conditional on the presence of a radial flaw in the package at the location under a failed dripshield, which has a probability of $\sim 2.5 \times 10^{-5}$. In addition, if the compressive stress layer thickness of 12 ± 2 mm by heat treatment is retained in the design, a further reduction in this probability would be required to account for failure by this process. Thus, with the degree of defense-in-depth that has been built into the EBS design, it is not expected that even perturbations that could increase the susceptibility of a small number of packages to SCC would significantly affect the overall performance of the EBS.

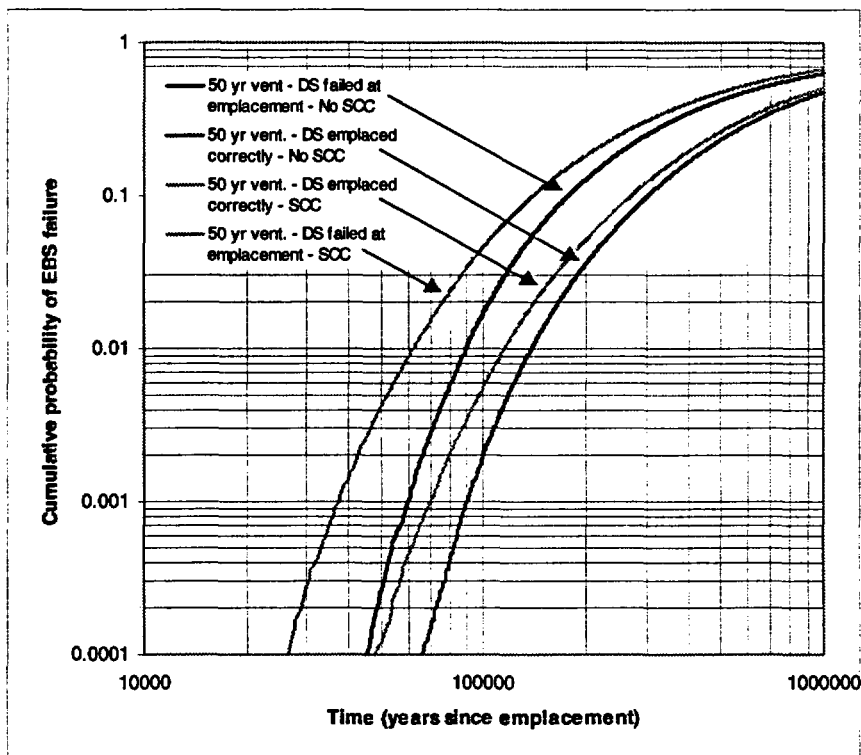


Figure 5-20
Influence of Reducing the Compressive Layer on the Outer Closure Lid Weld from 12 mm \pm 2 mm to 2 to 3 mm on EBS Failure Times

5.6 Cladding Corrosion

Extensive detailed analysis of the potential modes of failure of fuel cladding have been undertaken and documented (CRWMS M&O, 2000j, 2000k, 2000l, 2000m, 2000n, 2000p).

Prior to sealing within the waste package and emplacement in the repository, these modes include failures during reactor operation and subsequent failures by creep and iodine-induced SCC during dry storage and shipping to the repository, when temperatures of 350°C may be achievable (CRWMS M&O 2000n). Since free iodine concentrations within fuel rods are expected to be negligible, creep failure is the dominant failure mode anticipated during storage and transport. Subsequently, there is the possibility that rod failures will occur by creep within sealed waste packages prior to package failure in the repository.

Whether or not such in-package failures can occur can be directly related to the waste package surface temperature achieved in the repository, which itself is indicative of the maximum cladding temperature achievable within the waste packages. The accepted criterion is that the cladding temperature must not exceed 350°C if the rod creep strain is not to exceed the creep failure strain criterion. The analysis in CRWMS M&O 2000n shows that in-package creep failures will be negligible if the waste package surface temperature does not exceed 250°C after emplacement in the repository (CRWMS M&O 2000n, Figure 8). Since such temperatures will

not be achieved, the possibility of additional creep failures after waste package sealing can be ignored.

Thus, in the USDOE model, on first failure of the waste package in the repository, the number of fuel rods already failed and, hence, in a state to allow fuel wetting and the immediate commencement of radionuclide release from the waste form will be the sum of those failed in reactor and those failed in subsequent dry storage and transport to the repository. According to the latest assessments (CRWMS M&O 2000n (to be revised)) these failures can be represented by a triangular distribution with a best estimate of 2.44% of rods failed with a lower limit of 1.05% and an upper limit of 4.64%. In the cladding model within COMPASS, the IMARC source term model, only the best estimate value is eventually used with no distribution.

Any subsequent failures will depend on cladding corrosion once the waste package is breached and water enters. The IMARC model used to calculate these failures differs considerably from that used by the USDOE. Neither model succeeds in totally capturing the complete scientific essence of the complex cladding corrosion/failure process. However, while differing in conceptual scientific detail they are both predicated on the common, and reasonable, assumption that the fraction of rods failed by corrosion as a function of time will be linearly dependent on the rate of water ingress into a failed waste package.

Based on a review of the localized corrosion of zirconium and its alloys (CRWMS M&O 2000 m), the USDOE model assumes that cladding corrosion will proceed by reaction of zirconium with fluoride introduced in seepage drips into the failed waste package. It is conservatively assumed that any fluoride which enters a waste package will contact a 10-mm length of cladding to cause corrosion to failure at that site on a single rod. The 10 mm length is taken to be the lateral dimension likely to be affected by contact of a seepage drip, and each F^- ion is assumed to cause corrosion by converting the protective oxide (and underlying alloy) to a non protective fluoride (ZrF_2). Once failure at this site has occurred, the cladding breach is assumed to begin unzipping, and hence exposing an increasing area of fuel at a rate dictated by the alteration rate of the fuel. Meanwhile the concentration of F^- due to seepage drips is assumed to begin the degradation of another fuel rod via the identical process. In this manner, fluoride fails one rod after another in a continuous sequence until all rods have failed. Subsequently, the rod unzipping process proceeds longitudinally from the initial failure site leading to an increased area of exposed fuel as unzipping proceeds.

The key feature of this model is that all F^- which enters the waste package causes corrosion making the failure rate of fuel rods directly proportional to the inventory of F^- entering the waste package and, hence, to the total volume of seepage water into the failed package. The model can be considered conservative for a number of reasons:

- (i) The assumption that all F^- entering the package causes corrosion;
- (ii) the assumption that F^- leads to consecutive rod failures rather than a slower simultaneous failure of a number of rods;
- (iii) the assumption that all rods will experience seepage drips leading to fluoride corrosion.

An alternative scenario for cladding failure is used in IMARC5, and acknowledges the susceptibility of zirconium and its alloys to localized corrosion processes such as pitting in oxidizing saline conditions. A wealth of evidence exists to show that the critical potentials for film breakdown on zirconium alloys are low, in the range 0.1 to 0.3 V (vs SCE), a potential possibly achievable in the presence of relatively small concentrations of oxidants such as Fe^{III} . This is acknowledged in the Analysis Model Report (CRWMS M&O 2000m) and in a number of literature articles (Maguire 1984, Yau and Maguire 1990, Hornkjol 1988, Greene et al. 2000).

Given the iron content of the internal structure of the waste package, and the fact that the fuel bundles remain forever a heat source with respect to their surroundings, it becomes a difficult argument to claim that seepage drips, evaporative processes and the accumulation of dissolved oxidizing metal ion species from steel corrosion processes can never lead to the formation of a sufficiently aggressive environment to initiate pitting of cladding. However, it is reasonable to assume that the development of such sites will be confined to those failed waste packages which experience drips. Within these packages it is possible that a trickle down/evaporative process of seepage water will occur during which the accumulation of dissolved metal cations (Fe^{III}), the concentration of groundwater anions (e.g. Cl^-), and the formation of an acidified environment, could occur. This could lead to the establishment of a small number of localized corrosion sites on the cladding. While such sites could lead to the rapid failure of the cladding, the consequences of such failures should not be drastic. The aperture produced in the cladding will be small, and at least partially blocked by corrosion products, and should not, therefore, lead to a major exposure of fuel for dissolution.

Presently, insufficient information on the development of such environments within a failed waste package exists to predict the probability that such sites will exist. Consequently, we have chosen to use a model which assumes that corrosion of the Zircaloy cladding will be general in nature, but not specifically driven by contact with fluoride. In the absence of specific low temperature values for general corrosion rates for zirconium and its alloys, it has been assumed that the corrosion rates will be similar to those measured for titanium alloys in the LTCTF at LLNL (CRWMS M&O 2000c). This assumption is based on the similar properties of the oxides on these two materials, both metal cations being in the +4 oxidation state and both oxides exhibiting negligible solubility over a wide pH range. Thus, to calculate cladding corrosion rates for dripping conditions, the distribution of rates plotted in Figure 5-7 has been used. In the absence of drips a failure rate of 10 ± 5 nm/year with a normal distribution was used. These rates were used with a distribution of initial cladding thicknesses (shown in Table 5-4) based on the 1999 historical and projected waste stream number of various PWR and BWR assembly types (CRWMS M&O 1999c, Tables B-1 and B-2) and information on the cladding thickness for each assembly type (DOE 1992, Appendix 2A). These thicknesses were then reduced by 57% of the existing oxide thickness produced in-reactor. The thickness of the oxide layer was taken to be normally distributed with a mean of 54 μm and a standard deviation of 29 μm (CRWMS M&O 2000j, p. 30). Figure 5-21 shows the resulting cladding failure distribution for both dry and dripping conditions, with the mean initial failure fraction discussed above.

Table 5-4
Distribution of Initial Fuel Rod Cladding Thickness

Initial Cladding Thickness (mm)	Probability of Thinner Cladding
0.569	0
0.572	0.310
0.615	0.380
0.635	0.455
0.660	0.457
0.673	0.513
0.711	0.562
0.749	0.589
0.762	0.596
0.813	0.960
0.864	0.979
0.902	0.983
0.914	0.985
0.940	0.997
1.016	0.998
1.168	1.000

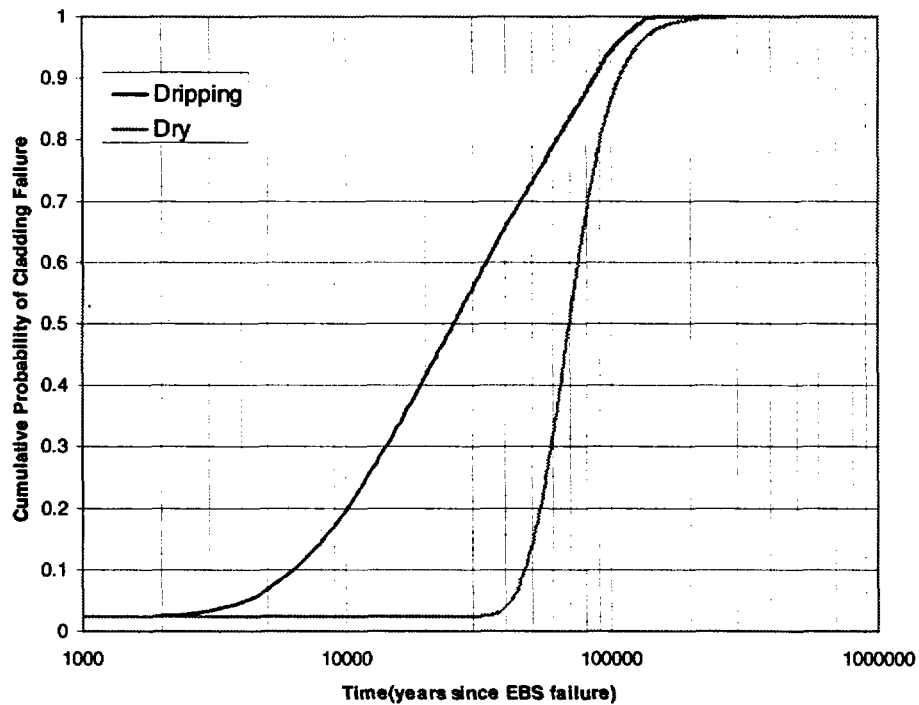


Figure 5-21
Fuel Rod Cladding Failure Distribution

5.7 References

Accary, A. 1985. Corrosion behavior of container materials for geological disposal of high level radioactive waste: Report of the Commission of European Communities, EUR 9836 EN.

Adamson, W.L. and R.W. Schutz. 1987. Application of titanium in shipboard seawater cooling systems. *Naval Engineers Journal*, 74(2), 124-134.

Andresen, P.L. and F.P. Ford. 1994. Fundamental modeling of environment cracking for improved design and lifetime evaluation in BWRs. *International Journal of Pressure Vessels and Piping* 59(1-3), 61-70.

Azumi, K., N. Yasui and M. Seo. 2000. Changes in the properties of anodic oxide films formed on titanium during long-term immersion in deaerated neutral solutions. *Corrosion Science*. 42, 885-896.

Beck, T.R. 1973. Electrochemistry of freshly-generated titanium surfaces – I. Scraped-rotating-disk experiments. *Electrochimica Acta* 33(8), 1143-1149.

Blackwood, D.J., L.M. Peter and D.E. Williams. 1988. Stability and open circuit breakdown of the passive oxide film on titanium. *Electrochimica Acta* 33(8), 1143-1149.

Bojinov, M., G. Fabricius, P. Kinnunen, T. Laitinen, K. Makela, T. Saario and G. Sundholm. 2000. The mechanism of transpassive dissolution of Ni-Cr alloys in sulphate solutions. *Electrochimica Acta*, 45, 2791-2802.

Clayton, C.R. and I. Olefjord. 1995. Passivity of austenitic stainless steels, *In Corrosion Mechanisms in Theory and Practice*, P. Marcus and J. Dudar (editors), 175-199, Marcel Dekker Inc., New York, NY.

CRWMS M&O 1999a. General Corrosion and Localized Corrosion of Waste Package Outer Barrier. ANL-EBS-MD-000003 REV 00.

CRWMS M&O 1999b. WAPDEG Analysis of Waste Package and Drip Shield Degradation. ANL-EBS-PA-000001 REV 00.

CRWMS M&O 1999c. 1999 Design Basis Waste Input Report for Commercial Spent Nuclear Fuel. B0000000-01717-5700-00041 REV 01.

CRWMS M&O 2000a. Environment on the Surfaces of the Drip Shield and Waste Package Outer Barrier. ANL-EBS-MD-000001 REV 00.

CRWMS M&O 2000b. Engineered Barrier System: Physical and Chemical Environment Model. ANL-EBS-MD-000033 REV 00.

CRWMS M&O 2000c. General corrosion and localized corrosion of the drip shield. ANL-EBS-MD-00000 4 REV 00.

CRWMS M&O 2000d. Hydrogen induced cracking of the drip shield.
ANL-EBS-MD-00000 6 REV 00.

CRWMS M&O 2000e. Drift scale thermal analysis. CAL-WIS-TH-000002 REV 00.

CRWMS M&O 2000f. Stress corrosion cracking of the drip shield, the waste package outer barrier, and the stainless steel structural material. ANL-EBS-MD-000005 REV 00.

CRWMS M&O 2000g. Abstraction of models of stress corrosion cracking of drip shield and waste package outer barrier and hydrogen induced corrosion of drip shield.
ANL-EBS-PA-000004 REV 00.

CRWMS M&O 2000h. Analysis of Mechanisms for Early Waste Package Failure.
ANL-EBS-MD-000023 REV 01.

CRWMS M&O, 2000p Clad degradation – FEPs screening arguments.
ANL-WIS-MD-000008 REV 00.

CRWMS M&O 2000i. Water pooling-evaporation in a waste package.
CAL-EBS-NU-000009 REV 00.

CRWMS M&O, 2000j. Initial cladding condition ANL-EBS-MD-000048 REV 00.

CRWMS M&O, 2000k. Clad degradation - dry unzipping. ANL-EBS-MS-000013 REV 00.

CRWMS M&O, 2000p. Clad degradation – wet unzipping. ANL-EBS-MD-000004 REV 00.

CRWMS M&O, 2000m. Clad degradation – local corrosion of zirconium and its alloys under repository conditions. ANL-EBS-MD –000012 REV 00.

CRWMS M&O, 2000n. Clad degradation – summary and abstraction.
ANL-WIS-MD-000007 REV 00.

Ford, F.P. and P.L. Andresen. 1988. Development and use of a predictive model of crack propagation in 304/316L, A533B/A508 and Inconel 600/182 Alloys in 288°C water. *In* Proceedings of the Third International Symposium on Environmental Degradation of Materials in Nuclear Power Systems – Water Reactors. Traverse City, Michigan, August 30 – September 3, 1987. G.J. Theus and J.R. Weeks (editors), 798-800, NACE International, Houston, TX.

Greene, C.A., C.S. Brossia, D.S. Dunn and G. Cragolino. 2000. Environmental and electrochemical factors on the localized corrosion of Zircaloy-4. Paper 210, CORROSION 2000, NACE International, Houston, TX.

Gruss, K.A., G.A. Cragolino, D.S. Dunn and N. Sridhar. 1988. Repassivation potential for localized corrosion of Alloys 625 and C22 in simulated repository environments. Paper 149, CORROSION 98, San Diego, CA, NACE International, TX.

Haynes International Inc. 1987. Hastelloy Alloy-22, Haynes Product Brochure H-2019C, Haynes International Inc., Kokomo, Ind. NNA 910419.0002.

Hornkjol, S. 1988. Pitting corrosion of zirconium and hafnium. *Electrochimica Acta*, 33, 289-292.

Ikeda, B.M. and M.J. Quinn. 1998. A preliminary examination of the effects of hydrogen on the behaviour of Grade-16 titanium at room temperature. Ontario Hydro Report No. 06819-REP-01200-0078-R00.

Jones, R.H. and Ricker, R.E. 1987. Stress corrosion cracking. Metals Handbook Ninth Edition, Volume 13, Corrosion, 145-163, ASM International, Metals Park, OH.

Khaleel et al 1999, "Flaw Size Distribution and Flaw Existence-Frequencies in Nuclear Piping" in *Probabilistic and Environmental Aspects of Fracture and Fatigue*. PVP-386. American Society of Mechanical Engineers.

Kim, Y.J. and R.A. Oriani. 1987. Brine Radiolysis and Its Effect on the Corrosion of Grade-12 Titanium, *Corrosion* 43, 92-97.

Leygraf, C. 1995. "Atmospheric Corrosion" Chapter 12 in *Corrosion Mechanisms in Theory and Practice*. P. Marcus and J. Oudar, editors, New York, Marcel Dekker, NY.

Lunde, L. and R. Nyborg. 1993. Hydrogen absorption of titanium alloys during cathodic polarization. Paper No. 5. NACE International, Houston, TX.

Maguire, M. 1984. The pitting susceptibility of zirconium in aqueous Cl⁻, Br⁻, and I⁻ solutions. In *Industrial Applications of Titanium and Zirconium: Third Conference; ASTM STP 830*, R.T. Webster and C.S. Young (editors), *American Society for Testing and Materials*, 175-189.

Mattsson, H. and I. Olefjord. 1990a. Analysis of oxide formed on Ti during exposure in bentonite clay-I. The oxide growth. *Werkstoffe and Corrosion* 41(7) 383-390.

Modares, M. 1993. *What Every Engineer Should Know About Reliability and Risk Analysis*. New York, New York, Marcel Dekker, Inc.

Newman, R.C. 1985. The dissolution and passivation kinetics of stainless alloys containing molybdenum, *Corrosion Science* 25(5), 331.

Noel, J.J. 1999. The electrochemistry of titanium corrosion. Ph.D. Thesis, University of Manitoba, Manitoba, Canada.

Okada, T. 1983. Factors influencing the cathodic charging efficiency of hydrogen by modified titanium electrodes. *Electrochimica Acta* 28(8), 1113-1120.

Pan, J. D. Thierry and C. Leygraf. 1996. Electrochemical impedance spectroscopy study of the passive oxide film on titanium for implant application. *Electrochimica Acta*, 41, 1143-1153.

Roy, A.K., D.L. Fleming, D.C. Freeman and B.Y. Lum. 1998. Stress corrosion cracking of Alloy-22 and titanium Grade-12 using double-cantilever-beam technique. UCRL-JC-132145. Lawrence Livermore National Laboratory, Livermore, CA.

Schultz, R.W. and D.E. Thomas. 1987. Corrosion of titanium and titanium alloys. *In Metals Handbook, Ninth Edition, Volume 13, Corrosion*, ASM International, Metals Park, OH, 669-706.

Schutz, R.W. and M.R. Scaturro. 1988. Titanium: an improved material for shipboard and offshore platform seawater systems. *In Proceedings of U.K. Corrosion '88, Brighton, U.K., October 3-5*, 285-300.

Schutz, R.W. and L.C. Covington. 1981. Titanium applications in the energy industry. *In Proceedings of the Annual Meeting of TMS, February 1981, Chicago, IL, The Metallurgical Society of AIME, Warrendale, PA*, 1-19.

Shcherbinskii, V. G. and Myakishev, V. M. 1971, *Statistical Distribution of Welding Defects with Respect to Azimuth*, Consultants Bureau, Plenum Publishing Corporation, New York, New York.

Shoesmith, D.W. and B.M. Ikeda. 1997. The resistance of titanium to pitting, microbially induced corrosion and corrosion in unsaturated conditions. Atomic Energy of Canada Ltd. Report, AECL-11709, COG-96-557-1.

Shoesmith, D.W. and M. Kolar. 1998. Waste package performance. *In Alternative approaches to assessing the performance and suitability of Yucca Mountain for Spent Fuel Disposal*, J. Kessler (editor), EPRI Report TR-108732, 5-1 to 5-67.

Shoesmith, D.W., B.M. Ikeda, M.G. Bailey, M.J. Quinn and D.M. LeNeveu. 1995b. A Model for predicting the lifetimes of Grade-2 titanium nuclear waste containers. Atomic Energy of Canada Ltd. Report, AECL-10973, COG-94-558.

Shoesmith, D.W., F. King and B.M. Ikeda. 1995a. An assessment of the feasibility of indefinite containment of Canadian Nuclear fuel wastes, Atomic Energy of Canada Ltd. Report, AECL-10972, COG-94-534.

Shoesmith, D.W., J.J. Noel, D. Hardie and B.M. Ikeda. 2000. Hydrogen absorption and the lifetime performance of titanium nuclear waste containers. *Corrosion Reviews* 18 (4-5), 331-359. Freund Publishing House, London, UK.

Smailos, E., W. Schwartzkopf and R. Koster. 1986. Corrosion behaviour of container materials for disposal of high-level wastes in rock salt formations. Nuclear Science and Technology, Commission of the European Communities, Luxembourg, EUR 10400 EN.

Sprowls, D.O. 1987. Evaluation of stress-corrosion cracking. *Metals Handbook Ninth Edition, Volume 13, Corrosion*, 245-282, ASM International, Metals Park, OH.

Welsch, G. and D.D. Pramod, Editors. 1996. *Oxidation and Corrosion of Intermetallic Alloys*. West Lafayette, Indiana: Purdue University.

Yau, T.L. and M. Maguire. 1990. Control of localized corrosion of zirconium in oxidizing chloride media. *In Advances in Localized Corrosion*, H.S. Isaacs, U. Bertocci, J. Kruger and S. Smailowska (editors), 311-319, NACE International, Houston, TX.



6

RADIONUCLIDE MOBILIZATION AND RELEASE FROM THE ENGINEERED BARRIER SYSTEM

6.1 Review of M&O's Source-Term Model

The purpose of this report is to review the latest development and issues associated with DOE's source-term model. "Source-term" is defined as the model calculation that estimates the release of radionuclides from engineered barrier system (EBS) into the geosphere (Zhou et al. 1994)¹. Analysis of EBS performance and radionuclide confinement is a key part of the Total System Performance Assessment (TSPA) program that quantitatively assesses the combined performance of both natural environment and artificial barriers.

By this definition, a source-term model encompasses the following FEPs (Features, Events, and Processes) for the current US geological disposal concept (see Figure 6-1):

- Failure of the drip shield,
- Failure of metal canisters,
- Water liquid contact and flow through waste form and the EBS,
- Cladding degradation,
- Spent-fuel matrix alteration,
- Mobilization and transport of radionuclides through the EBS.

The basic unit for source-term modeling is a single waste package plus any surrounding engineered materials. Barriers in this context may include corrosion products within the canister, the metal canister, the invert, and a portion of host rock according to the current disposal concept (see Figure 6-1). These barriers are the physical components through which radionuclides can be transferred. Complex, coupled interactions among transport, radioactive decay, and geochemical reactions will control the rate of release of radionuclides through these barriers.

¹ The EBS can be a vital component in a geological repository in confining radionuclides. As noted by SKB with respect to their KBS-3 design concept: "The primary function of the rock is to provide stable mechanical and chemical conditions over a long-period of time so that the long-term performance of the EBS is not jeopardized." (SKB, 1992, TR 92-20, page xvii). In other words, one of the important geosphere's roles is to protect the functional integrity of the EBS.

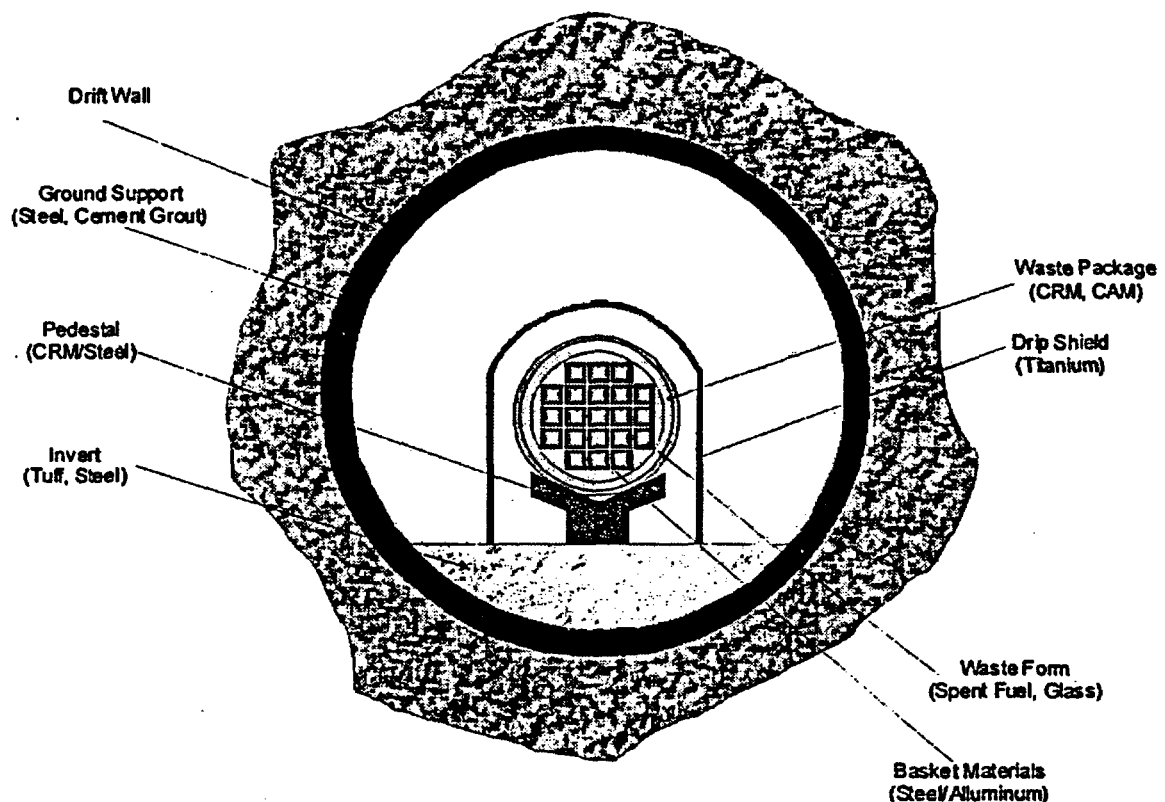


Figure 6-1
Conceptual description of the current EBS design (adopted from Jolley 1999)

In source-term modeling, however, it is neither necessary nor practical to explicitly and fully model all the interactions among the coupled processes. For example, extended containment by a combination of barriers, such as the Alloy 22 container, Ti-drip shield and zircaloy cladding, can delay contact between water and spent fuel (i.e., the initiation of source-term) until the temperature perturbation has essentially been dissipated. Also, there will be no liquid water contact until the EBS temperature is lower than boiling point. These constraints exclude strongly coupled thermal processes.

There are other reasons for omitting coupled process models in source-term calculations. For example, because concentrations of released radionuclides in the EBS pore water are much lower than concentrations of groundwater constituents, the effect on groundwater chemistry due to the presence of radionuclides can be ignored. In the context of groundwater chemistry, one only needs to consider its effect on radioelement sorption and solubility.

Figure 6-2 shows the schematic TSPA program and its relation with sub-process modeling. As can be seen from Figure 6-2, the modeling of coupled THCM processes (thermal, hydrological, chemical, and mechanical) is, however, of importance to the estimation of containment time (i.e., the delay between repository closure and initiation of source-term). The

location, rate, frequency and chemical character of seepage water is central to containment assessments.

Thus, for the expected evolution of conditions at Yucca Mountain, modeling of drip-shield, canister, and cladding performance will likely be a sensitive function of coupled THCM processes. Assuming extended containment by three barriers (10,000 years), the evolution of waste form performance is expected to occur at a time of minimal THCM impacts. In such a case, waste-form performance can be abstracted into relatively simple (but not too simple) models un-impacted by coupled-process modeling.

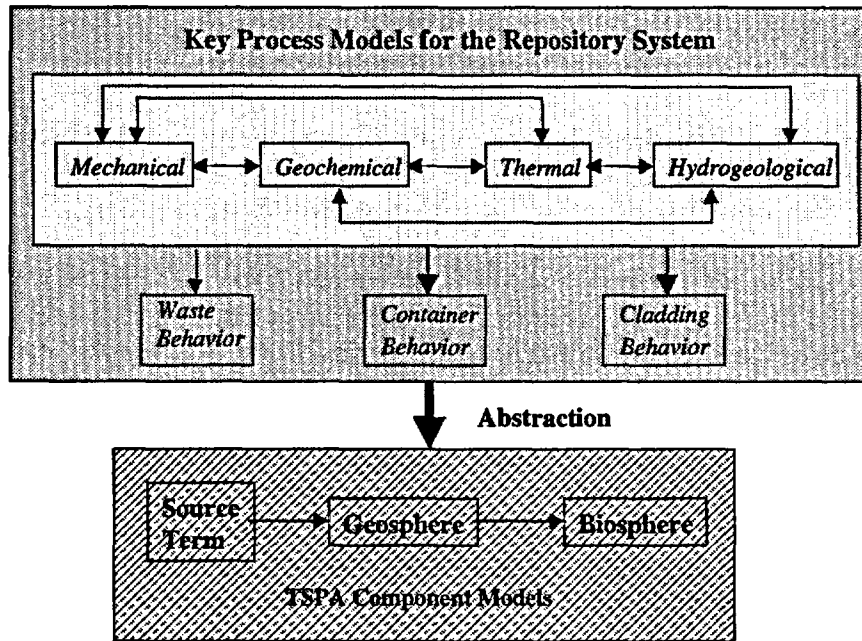


Figure 6-2
TSPA program structure and relationship between process models and PA component models

The following sub-sections evaluate and compare the current source-term models by the M&O and EPRI. Although complete documentation of the M&O's source-term is lacking, it seems apparent that a number of key FEPs are absent (e.g., radioactive decay and in-growth and sorption during transport within the EBS). It is not merely the fact that EPRI's source-term model includes these FEPs, but also the fact that all international source-term models include such FEPs. The concern is that the M&O's source-term has been abstracted to a simplistic level that potentially important FEPs for attenuating release are not included.

6.1.1 M&O's Source-Term

In the Yucca Mountain Project, the "source-term" is referred to as the mobilization of radionuclides from confinement in the waste form (Stockman, 2000; Chesnut, 2000). This is further decoupled from the EBS transport modeling analysis although the waste-form and the EBS are one continuous physical entity. Nevertheless, the same connotation of source-term

defined previously will be maintained here. This means, review of M&O's source-term covers M&O's *Waste Form* and *EBS transport* process and analysis modeling reports (Stockman, 2000; Chesnut, 2000; Gross, 2000; and MacNeil, 2000).

Rigorous modeling of release and transport within the waste package could not be found from these documents. In presenting the bathtub scenario (a release scenario which is later screened out), mass balance analysis is presented in Gross (2000, pp. 68-70) for determining radionuclide concentrations within, and advective release from, the waste package. With minor modifications, this analysis is said to also apply to the flow-through scenario that assumes seepage water flowing through the waste package and EBS. Radioactive decay and in-growth are not shown in this analysis. It is not clear that the analysis is merely a demonstration of conceptual model for treating advection from the waste form, or radioactive decay has been neglected.

In addition to advective release through groundwater flowing through a breached waste package, the M&O's source term model considers a diffusion-only release scenario. The modeler (Gross 2000) assumes a continuous pathway between the waste package and invert for diffusive release from the waste package. Rigorous modeling supporting this assumption, however, cannot be found from the document. It seems that M&O's approach is to decouple the waste package release and transport in the invert. This approach is reasonable for advective release from the waste package such as bathtub and flow-through scenarios. For diffusive release, decoupling of the two physically connected components (if neglecting supporting materials between the waste package and invert) requires proper boundary conditions at the interface between the two components. This information, however, is also missing in the reviewed document. It would be conservative, however, to assume excellent connection of diffusive pathways inside the waste package, and between the waste package and the invert. For example, it is assumed water diffusing in through an opening in the container immediately (i.e., within the same time step) comes into contact with the waste form, then diffusive releases may be seriously overestimated. If, immediately after release from the waste form, it is assumed the radionuclides diffuse out another opening in the waste package in the bottom of the container, which is in intimate contact with the invert (i.e., pedestals and other engineered features preventing intimate contact with the invert are neglected), then yet more conservatism may be introduced.²

In summary, the FEPs considered in the M&O's source-term model include:

- Waste form dissolution,
- Cladding degradation,
- Water contact (1 mm thin film on the entire waste form surface is assumed) and flowing through the EBS,³

² This latter conservatism is likely to be large at earlier times when the pedestals and other engineered features are still likely to be maintaining separation between the container and the invert. At later times, when the pedestal has failed, the potential magnitude of this particular conservatism will be lessened.

³ This film thickness is likely conservative for diffusive release scenarios in areas with no advection (i.e., pure diffusive release). In such a case, the water film will be a function of the relative humidity, but should be much smaller than one millimeter. Furthermore, assuming a film thickness of 1 mm for all surfaces is likely to be conservative even for the advective case.

- Solubility limit within the waste package,
- Decay and in-growth considered within the waste form (this is not shown in the in-package mass balance equations but is listed in the included FEPs [Stockman, 2000]),
- Diffusive release of radionuclides through stress corrosion cracking on the metal canister,
- Advective release of radionuclides from corroded patches on the metal canister,
- Diffusive and advective transport through the invert, and
- Colloid transport.

The following FEPs have been neglected in the M&O's source term:

- In-package corrosion product as a transport barrier,
- Sorption in the EBS (except for sorption on colloids),
- Solubility in the EBS,
- Radioactive decay and in-growth in the EBS,
- Evaporation of liquid water within the waste package during period after waste package temperatures descend below boiling. The effect of this mechanism would be to delay liquid water contact with the waste form,
- Tortuosity in effective diffusion coefficient, and
- Dispersion in the invert.

Inclusion of any of these FEPs would tend to make a more realistic, less conservative source-term analysis. This issue is further discussed as follows:

1. The corrosion product formed after the basket materials corroded presents an extra barrier to dissolved radionuclides escaping out of the waste package. This barrier function arises from the sorption capabilities, as well as limited surface area for transport. Ignoring this barrier may overestimate EBS release rates of radionuclides (EPRI 1998).
2. Ignoring sorption in invert transport is an over-conservative assumption, which has been studied by both IMARC (EPRI 1998) and the M&O (MacNeil 2000). The M&O's treatment on sorption on colloids, however, also tends to overestimate the release because high sorption coefficients have been used and sorption onto some colloids is assumed to be highly reversible.
3. Ignoring solubility-limits in invert transport is a slightly conservative assumption. Invert is composed of rock gravels with low volumetric moisture content (0.066 – 0.071, [MacNeil 2000]). In this case, it is likely that some radionuclides, especially the nuclides with low solubility and relatively short-lived parents (Zhou et al. 1988), reach their share of element solubility.⁴

⁴ In Zhou, et al., (1988) an analysis for a two-member decay chain with advection only in a 1-D pathway was conducted. Solubility limits for both members were imposed at the source end. Precipitation of the daughter nuclide was predicted.

4. Ignoring radioactive decay and in-growth during the transport through invert is conservative for short-lived nuclides. Sensitivity analysis on invert transport has shown that the break-through times range from 10^2 to 10^3 years (MacNeil 2000). For short-lived nuclides considered by M&O (Stockman 2000) listed in Table 6-1 below, most of them will decay within the invert before reaching the geosphere, except for those nuclides in secular equilibrium with their parent nuclides (e.g., Ac-227 with parent Pa-231). Fortunately, these nuclides do not contribute to long-term safety concerns. It should be noted, however, the break-through times were obtained without considering sorption. With sorption and solubility-limit effects in the invert being considered, the break-through times can be considerably longer. In this case, many long-lived nuclides may also decay within the EBS.

Table 6-1
Short Lived Nuclides Considered by M&O's Source-Term

Nuclide	Half Life [yrs]	Comment
Ac-227	21.77	Daughter
Am-241	432	Primary
Cs-137	30	Primary
Ni-63	100	Primary
Pb-210	22.3	Daughter
Pu-238	87.7	Primary
Sr-90	28.8	Primary

Note, the short-lived primary nuclides can be assumed "pre-decayed" by adding their inventories into their daughter inventories (e.g., Am-241's inventory can be added into Np-237's inventory).

5. Extended evaporation of water liquid inside the waste package by residual waste heating may be possible well the after peak thermal period. This may delay water contact time, hence, delay mobilization and release of radionuclides, and reduce EBS release rates. Ignoring this effect may overestimate EBS releases. Furthermore, it is probably a key FEP to consider for scenarios involving early loss of containment.
6. The M&O's source-term uses an upper bound Archie's law (Gross, 2000; MacNeil, 2000) in determining effective diffusion coefficient in the invert:

$$D_{eff} = D_{free} \epsilon S \quad \text{Eq. 6-1}$$

That is, the effective diffusion coefficient is proportional to porosity and water saturation, but is not dependent on tortuosity. Ignoring tortuosity in porous material and surface diffusion (Conca and Wright 1992) in gravel invert may overestimate release from the EBS.

7. Ignoring dispersion in the invert is reasonable as the path length (0.6 m) for transport in the invert is not long enough to contribute significant impact.

6.1.2 EPRI's Source Term

Before comparing the M&O and EPRI source-term models, a brief review of the EPRI source-term model code, COMPASS (now COMPASS2000), is presented here. A detailed description of COMPASS2000 can be found in Section 6.2. Figure 6-3 shows the COMPASS2000 source-term model system. This specific compartment model is the conceptualization of the recent US disposal concept developed by DOE/M&O for Yucca Mountain.

In COMPASS, a compartment modeling approach is used, in which the resolution of spatial discretization is made just small enough to represent all the EBS features without introducing numerical artifacts. Compared with a more detailed finite-difference method, the compartment modeling approach has a lower spatial resolution, or a coarser discretization. In TSPA calculations, however, uncertainties arising from limited knowledge on data and future conditions overwhelm the demand for spatial resolution (Glassley 2000). Rather, flexible geometry and fast computation offered by the compartment model are desirable features for a large scale probabilistic assessment, providing flexibility in comparing alternative conceptual models and EBS designs, as well as ensuring the capability for robust sensitivity analysis.

Each box in Figure 6-3 represents an EBS or near-field component, or compartment, in the current disposal concept. There are six compartments in the newest COMPASS2000:

1. The *Waste* compartment represents spent-fuel that undergoes alteration once there is contact with liquid water. Alteration could occur due to dry oxidation, but this has been neglected. Cladding protection is part of this compartment. Cladding degradation controls the release of gap/grain boundary inventories, as well as the amount of waste matrix exposed to liquid water. In COMPASS2000, radionuclides in the gap/grain-boundary are assumed to dissolve into liquid water congruently with the cladding degradation. Radionuclides in the UO_2 matrix are assumed to dissolve in liquid water with the convolution of cladding degradation and the UO_2 matrix alteration.
2. The *Corrosion Product* compartment represents basket materials inside the waste package that are assumed to have been relatively quickly degraded into a porous layer of oxyhydroxides upon contact with water. This compartment is included to explore potential retardation effects of those radionuclides that sorb onto oxyhydroxides.
3. The *Canister* compartment represents the metal canister that undergoes general corrosion after contacting with water liquid. Early, localized breach is included as an option for sensitivity studies of early failure impact by using a pin-hole mass transfer model, in which the canister compartment is reduced to a pin-hole compartment.
4. The *Invert* compartment represents crushed tuff with some steel materials placed below the waste package.
5. The *Near-Field Rock* compartments (including rock matrix and fractures) represent a small portion of the host rock. These compartments serve as a necessary boundary condition for calculating EBS transport. In light of dilution of radionuclides within a large rock mass, concentrations in the near-field rock are expected to be considerably lower than in the EBS.

Hence, zero concentrations in these compartments are assumed. This is, however, a conservative assumption. If radionuclide removal from the EBS edge by fracture flow is not efficient, this treatment may overestimate radionuclide EBS release rates. Furthermore, a certain degree of conservatism in the release rate calculation may also arise for not explicitly modeling the near-field rock as a dual-porosity/ dual-permeability system.

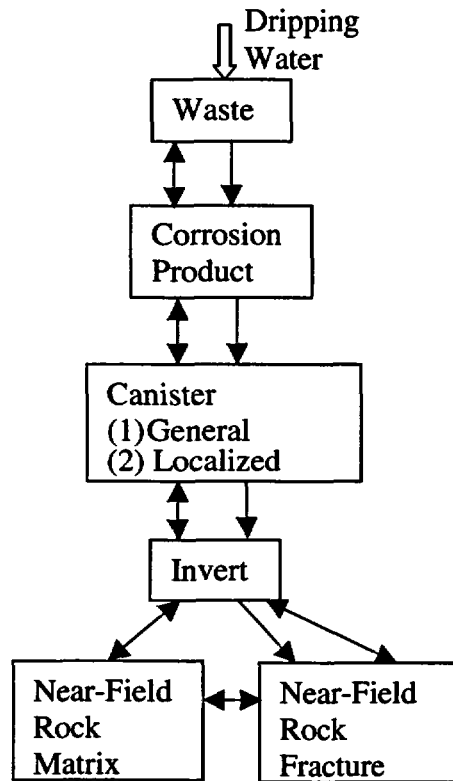


Figure 6-3
Conceptual model system for EPRI source-term COMPASS2000. “↔” represents diffusion transport, and “→” represents advection transport

Each compartment is treated as a “mixing tank” where radionuclide concentrations are assumed to be uniform. Mass balance for each nuclide is established in each compartment in terms of total amount of the nuclide, including aqueous, precipitated, and sorbed nuclides. Transport of the nuclide from and to the neighboring compartments is by diffusion and advection of aqueous concentrations. The mass balance takes into account radioactive decay and in-growth. The total mass is partitioned into aqueous, sorbed and precipitated components according to a linear, reversible equilibrium sorption model and elemental solubility sharing. Physical and transport parameters in each compartment that affect radionuclide concentrations and transport include:

- Density (for sorption),
- Porosity,
- Water saturation,
- Total volume,

- Interface area with neighboring compartments,
- Path length for diffusion, and
- Diffusion coefficient (including tortuosity).

In the waste compartment, the mass balance equation contains the source of radionuclides that are released from dissolution of the waste form. Radionuclides residing in gaps and grain boundaries are released instantly and proportionally to the fraction of cladding that has degraded. Radionuclides in the waste matrix are released congruently with the convolution of the matrix alteration and cladding degradation according to a model implemented in the previous IMARC project (EPRI 1996).

The transport pathway is shown in Figure 6-3. Detailed mathematical equations are given in the IMARC Phase 3 report (EPRI 1996). The time-dependent fluxes from the invert compartment into the near-field rock compartments are delivered to the geosphere transport model.

COMPASS2000 handles time-dependent seepage fluxes into the open waste package, as well as time-dependent cladding degradation rates. Waste matrix alteration rate, sorption coefficients, solubilities, EBS transport parameters (porosity, density, water saturation) and waste canister opening area, are assumed to be constant over time, although COMPASS2000's architecture is able to handle time-dependent parameters. In the current EPRI IMARC calculations, the water contact time is a result of combined probabilities of the following events:

- Breach of drip shield,
- Waste canister failure,
- Cladding failure, and
- Evaporation rate due to decay heat no longer exceeds the heat of vaporization from the influx of seepage water.

6.1.3 Comparison of Source-Term Models

To further evaluate M&O's source-term model, Table 6-2 compares the source-term models used by both M&O and EPRI IMARC.

**Table 6-2
Comparison of Source-Term Models**

Issues/Processes	EPRI	M&O
Delayed wetting due to evaporation	Included	<i>Excluded</i>
Waste matrix alteration	Included	Included
Cladding credit	Included	Included
Solubility limit inside waste package	Included	Included
Colloid transport	<i>Excluded</i>	Included
Solubility limit in barriers	Included	<i>Excluded</i>
Sorption in barriers	Included	<i>Excluded</i>
Decay/in-growth inside waste package	Included	Included
Decay/in-growth in barriers	Included	<i>Excluded</i>
Waste canister as a barrier	Included	Included
Invert as a barrier	Included	Included
Diffusive transport	Included (treated as a continuum from the waste to the EBS edge)	Included (waste canister is decoupled from the EBS)
Advective transport	Included	Included
Effective diffusion coefficients in barriers	Conca and Wright's results for invert; Tortuosity factor of 0.1 times the upper bound of Archie's law for other barriers.	Upper bound of Archie's law.
In package chemistry evolution	<i>Excluded</i>	Included
Chemistry evolution in barriers	<i>Excluded</i>	Included

It should be noted that, in EPRI's COMPASS2000, conceptual model equations for each of the included FEPs have been described in detail in EPRI (1996) and the next Section. In the M&O's source-term model, it is not clear how the included FEPs are treated. These are simply shown in the included FEP lists. Conceptual model equations associated with these FEPs could not be found from the reviewed reports (Stockman, 2000; Chesnut, 2000; MacNeil, 2000; and Gross, 2000). This is important information that should be included in the key M&O reports.

Furthermore, in the M&O's process modeling reports and assessment modeling reports associated with source-term, it can be seen that tremendous effort has been placed in determining seepage fluxes, in-package chemistry, thermal processes, and waste package and waste form degradation. These are important processes that should be studied in detail. Relatively speaking, less effort has been contributed to the radionuclide mobilization and transport in the near field. The reviewed reports do not present essential equations for calculating radionuclide release rates from the EBS.

6.1.4 Conclusions

The M&O's source term model is reviewed and compared with EPRI's model. The common grounds of the two models include:

- Waste matrix dissolution,
- Cladding credit,
- Seepage flowing through the waste package and near-field system,
- Solubility limit within waste package, and
- Diffusion and advection transport throughout the invert.

There are also some important differences between the two models:

- Inclusion of barrier components,
- Sorption in barriers,
- Diffusion coefficients,
- Evolution of EBS chemical conditions,
- Delayed wetting due to evaporation, and
- Decay and in-growth in the EBS.

The M&O's process and assessment modeling reports related to the source-term cover many issues and processes that are important to the release of radionuclides from the EBS. Modeling of these processes provides important parameters for radionuclide mobilization and transport in the near field. Compared with the effort spent on studying these processes, however, less effort has been contributed to modeling of radionuclide mobilization and transport within the EBS. Sufficient information is difficult to obtain for more in-depth model evaluation. The presented information suggests that the current M&O's source-term model is over-conservative.

6.2 COMPASS2000: Source-Term Code for EPRI

COMPASS2000 is developed based on modification of COMPASS. It is a compartment model for evaluating radionuclide release from and transport through the EBS (see Section 6.1.2). The motivation for modification is to meet the requirement of EPRI IMARC calculation for the year 2000. These requirements are:

1. To be consistent with the current EBS design adopted by DOE/M&O,
2. Retention by barriers to illustrate "defense-in-depth", and
3. Incorporating new cladding degradation data.

These modifications will be described below.

6.2.1 New Compartment System

Figure 6-1 (shown in the previous section) shows the current EBS design adopted by the Yucca Mountain Project. The figure shows that the waste package is placed in an open drift. The key differences between the current and previous designs are:

- The waste-package is covered by a drip shield,
- The waste package materials are now an outer layer of Alloy 22 surrounding an inner layer of stainless steel (rather than an outer layer of carbon steel surrounding an inner layer of Alloy 22), and
- The invert is crushed host rock with steel instead of concrete.

Mobilization of radionuclides is initiated by the following sequential events:

- Water dripping,⁵
- Failure of the drip shield,
- Failure of the waste canister,
- Liquid water contact,
- Degradation of the cladding, and
- Dissolution of the spent-fuel matrix.

Inside the metal canister, there are basket materials that are composed of steel and aluminum (see Figure 6-1). Once in contact with water, these materials degrade to a layer of corrosion product. The metal canister may fail by either general corrosion or early, localized corrosion followed by general corrosion (see Section 5). The failed barriers open ways for radionuclides to escape. However, because of limited surface areas for transport and sorbing capabilities, these barriers also provide resistance to radionuclide transport. The invert material also plays a barrier role to escaping radionuclides in EBS.

Hence, the new compartment system corresponding to the new EBS design includes the following components as shown in Figure 6-2 (shown in the previous section):

- The “Waste” compartment represents the void volume in the vicinity of the waste form that first receives dissolved nuclides,
- The “Corrosion Product” compartment represents the porous material that is formed after the basket materials are corroded,
- The “Canister” compartment represents the failed metal canisters,
- The “Invert” compartment represents the gravel-like material under the waste package, and

⁵ The current IMARC conceptualization ignores diffusive release from the EBS in zones without active dripping. While this is a non conservative assumption, it is felt not to be significantly non conservative. IMARC studies presented in Appendix A investigate the degree of non conservatism. It is felt that the current M&O model of diffusive release is very conservative.

- The “Near-Field Rock Matrix” and “Near-Field Rock Fracture” compartments represent host rock in the vicinity of the drift to serve as the boundary condition to the transport equations.

Two scenarios can be specified for the “Canister” compartment:

1. General corrosion, and
2. Localized failure.

In the first scenario, the metal canister degrades to a layer of corrosion product. The second scenario corresponds to early breach of the metal canister due to, for example, a manufacturing defect. A small fraction of all canisters may experience this type of failure (Farmer 2000; Section 5 of this report). This scenario is followed by general corrosion, which is the first scenario. This feature is added into the new source-term code only for sensitivity analysis to study the impact of the early, but limited release.

In both scenarios, water is assumed to flow through the compartments if there is water entering the open drip shield. The flow rate is determined by:

$$Q_{drip} = A_{drip} \times q \quad \text{Eq. 6-2}$$

where Q_{drip} is the flow rate of water entering the waste package [m^3/yr], A_{drip} is the opening area for water to enter the waste package [m^2], and q is the infiltration rate [m/yr]. Use of A_{drip} allows various scenarios to be considered. [Backfill no longer included in the current design.]

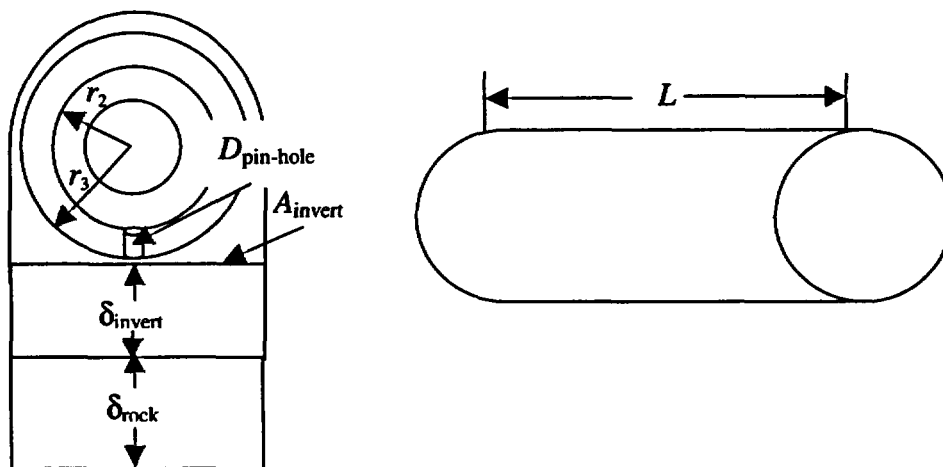


Figure 6-4
 Illustration of geometry for the compartment system in COMPASS2000. “ r_2 ” is the inner radius of the canisters, “ r_3 ” is the outer radius, L is the length of one waste package, A_{invert} is the invert area, δ_{invert} is the invert thickness, A_{drip} is the area at the top of the drift shield that is open for seepage water to flow into the waste package, δ_{rock} is the rock thickness, and $D_{pin-hole}$ is the pin-hole diameter for the early failure scenario

In the early failure scenario, it is assumed that the breach in the upper portion of the canister is the same as in the lower portion. Hence, the amount of water entering the waste package per unit time is limited by the opening, or pin-hole, area. That is,

$$Q_{drip} = \max(A_{pin-hole}, A_{drip}) \times q \quad \text{Eq. 6-3}$$

where $A_{pin-hole}$ is the pin-hole area [m²].

The transport mechanisms in the COMPASS2000 compartments include diffusion and advection as shown in Figure 6-2. COMPASS2000 allows “no advection” (or diffusion only) scenario, which corresponds to “zero infiltration” scenario or “no dripping” scenario.⁶ In this case, transport of radionuclides is by diffusion-only assuming that a continuous pathway exists.

The diffusion coefficient in the “Invert” compartment is determined by the following equation (Conca and Wright, 1992):

$$\log_{10} D = 2.14 \log_{10} S - 1.5 \quad \text{Eq. 6-4}$$

where D is the effective diffusion coefficient in the invert (m²/yr) and S is water saturation in the invert.

Equation (6-4) is the default diffusion coefficient in the invert. This, however, can be overridden by giving a value in the input file with the keyword “INVERT” in the “DIFFUSION” data block.

Geometry parameter input in COMPASS2000 is illustrated in Figure 6-3. The mathematical model for COMPASS2000 is the same as COMPASS, described in EPRI (1996).

6.2.2 Retention by Barriers to Illustrate “Defense-in-Depth”

In COMPASS, mass balance is computed at every time-step and is reported at the end of the calculation. The purpose is to check physical and mathematical models employed in the code and computational accuracy. This mass-balance actually illustrates radionuclide retention by barriers.

The Retention-by-Barriers illustration is to study the function of individual components of the EBS by tracing the “fate” of radionuclides. For a given nuclide with a given initial inventory, the amount of nuclide at a given time is determined by its half-life. These nuclides can only either stay in the waste-form, be retained by the EBS, or escape outside the EBS (in the geosphere or biosphere).

Taking I-129 as an example, the amount of I-129 at 1200 years after the emplacement is shown in Figure 6-5 (a) as a pie. In this example, the containment time is 10⁵ years, and the waste matrix alteration time is 3000 years, which are median values used in IMARC. The rate of seepage water flowing through the waste package is 7.3 m³/yr, also a median value used in IMARC. The moderate cladding degradation data are used (see next section), in which the cladding gradually degrades and completely disappears after 140,000 years of contacting with

⁶ In the current implementation of IMARC, the “no advection” option was not exercised.

water. Transport parameters are presented in Section 6.2.4. This figure shows that, at 120,000 years, 65% of the I-129 are still in the waste matrix (shown as the magenta slice in the pie in Figure 6-5 (a)). The rest are either in the EBS (the yellow slice) or out of the EBS ("Outside", the light blue slice). At this time, nuclides escaping the EBS are about 34% of the inventory and only little amount of I-129 remains within the EBS (about 1%) due to high solubility and non-sorbing.

Figure 6-5(b) illustrates what happens to I-129 at 244,000 years. The pie representing the inventory at this time is slightly smaller than that at 120,000 years due to radioactive decay. The distribution of I-129 is different from that at 120,000 years. The amount of I-129 held up in the EBS is down to less than 1% of the inventory. There is no I-129 in the waste form after the matrix is completely altered. The amount of I-129 escapes to the outside is more than 99% of the inventory.

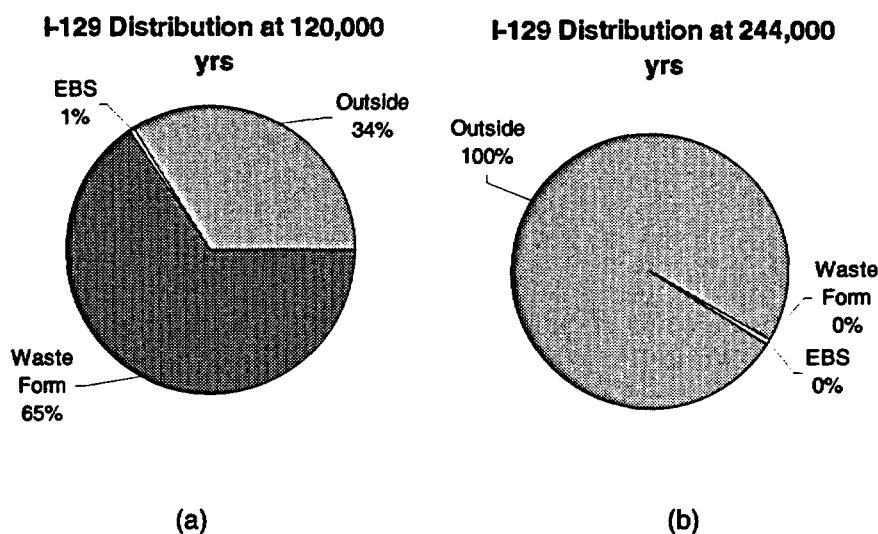


Figure 6-5
Illustrating retention by barriers: I-129 mass distribution at (a) 120,000 years and (b) 244,000 years. Total inventory is represented as a pie. The containment time is 100,000 years. The alteration time is 3000 years. The cladding gradually degrades and disappears after about 140,000 years of contacting with liquid water

In this example, the soluble, non-sorbing I-129 is not retained effectively by the EBS. As an opposite example, Figure 6-6 illustrates Np-237 mass distribution in the same system and at the same times.

At 120,000 years, the amount of Np-237 within the waste form is about 65% of the inventory. It can be seen that, at 120,000 years, only 8% Np-237 has escaped out of the EBS (comparing 34% for I-129 at the same time). At 244,000 years, 40% of Np-237 is still retained within the EBS due to sorption ($0.001 \text{ m}^3/\text{kg}$ in both corrosion product and the invert) and solubility limit ($3 \times 10^{-5} \text{ mol/l}$) (comparing this with <1% for I-129 at the same time).

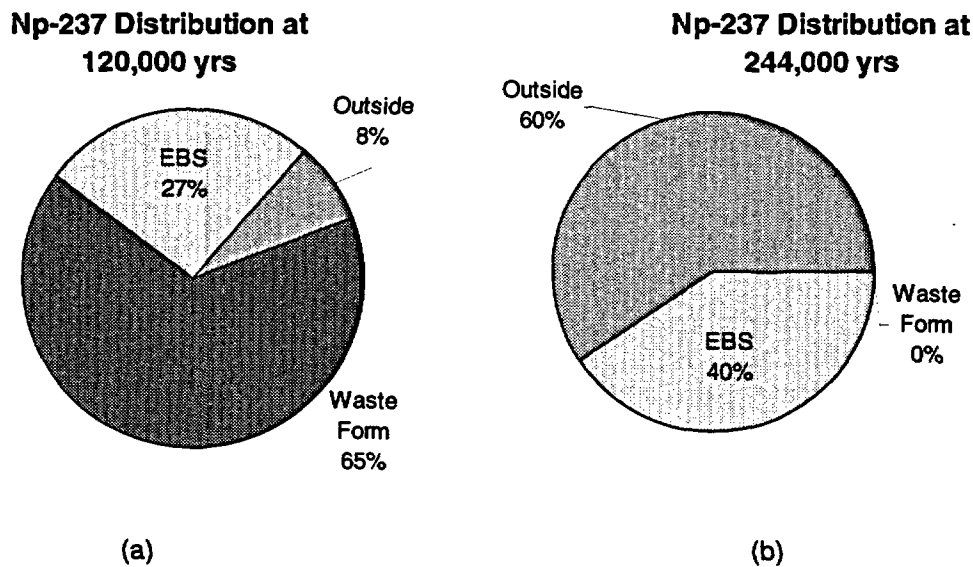


Figure 6-6
 Illustrating retention by barriers: Np-237 mass distribution at (a) 1200 years and (b) 50,000 years. Total inventory is represented as a pie. The containment time is 100,000 years. The alteration time is 3000 years. The cladding gradually degrades and disappears after about 140,000 years of contacting with liquid water

The “Inventory” gives total amount of nuclides at a given time. These nuclides should be either in the waste-form (“Waste-Form”), in the barriers (“EBS”), or out of the barriers (“Out-of-EBS”). Therefore, the following equation holds at any time:

$$M_{Waste-Form}(t) + M_{Near-Field}(t) + M_{Outlet}(t) = M_{Inventory}(t) \quad \text{Eq. 6-5}$$

where $M(t)$ is the amount of nuclide [mol].

Figures 6-7 and 6-8 are an example of the plot of retention by barriers for I-129 and Np-237. The spiky behavior of I-129 curve is explained in the next section.

6.2.3 Incorporation of Cladding Degradation Data

In previous IMARC calculations, cladding is assumed to completely fail at the time the canister fails. Hence, even though cladding may only fail partially and degrade slowly with time, its protection of spent-fuel integrity was not taken into account. “Cladding credit” is now being added into this IMARC iteration. COMPASS has a built-in cladding degradation model developed previously (EPRI 1996). In order to realistically model the source and to incorporate new cladding degradation modeling results (see Chapter 5.), COMPASS2000’s cladding model is obtained by slightly modifying the existing COMPASS cladding model. The new cladding model considers the cladding credit in delaying release of radionuclides residing both in the gap/grain boundary (instant release fraction) and in the UO_2 matrix.

The cladding degradation curves are shown in Figure 6-9. These curves give the cumulative fraction of failed cladding as a function of time after the waste canister fails and waste package is contact by water. Once input to COMPASS2000, the times of the curve are convolved with the canister failure time (assumed to be the time at which the drip shield fails, the canister fails, and water liquid is present within the waste package). At each simulation time step, the total released amount of the i th radionuclide residing in the gap and grain boundaries is given by:

$$q_{g,i} = M_{g,i}(t) \times f_c(t) \tag{Eq. 6-6}$$

where $M_{g,i}(t)$ is the i th radionuclide's gap/cladding inventory at time t [mol], and $f_c(t)$ corresponds to the fraction of cladding assumed failed at time t on Figure 6-9.

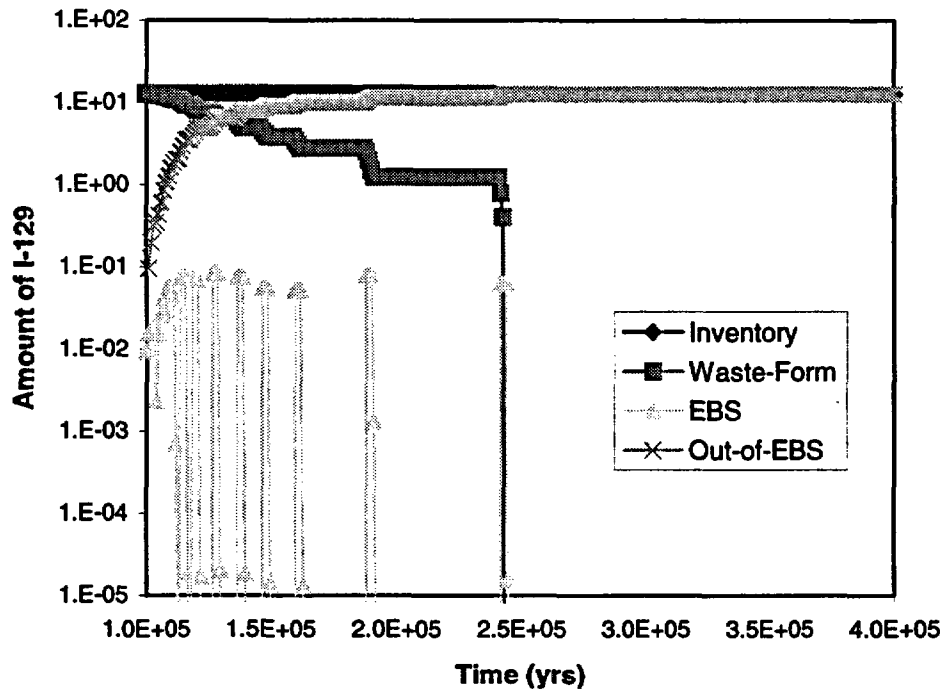


Figure 6-7
 Example of retention by barriers to illustrate “defense-in-depth” for I-129

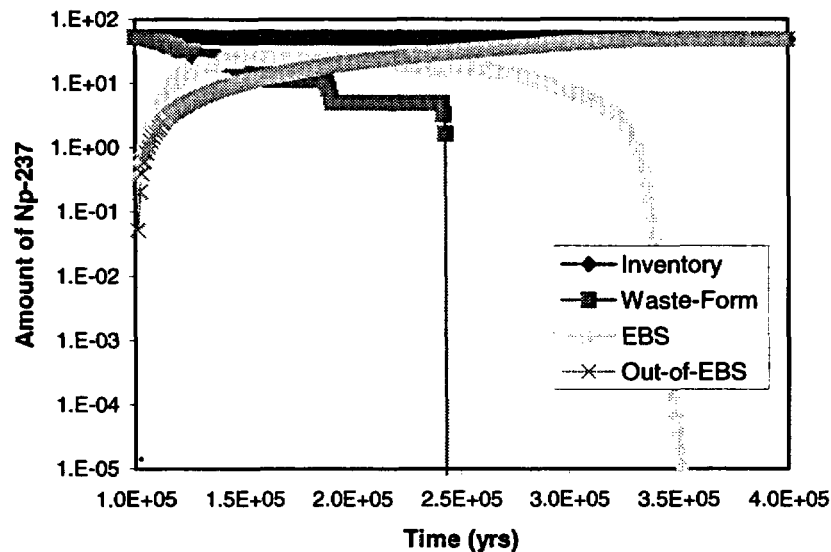


Figure 6-8
Example of retention by barriers to illustrate “defense-in-depth” for Np-237

In calculating the release from waste matrix, the cladding failure curve is convoluted with the matrix alteration, as described in EPRI (1996).

To enhance computational speed, these cladding degradation curves are converted into piece-wise step functions shown in Figure 6-10.

Figures 6-11 and 6-12 compares the EBS release rates for I-129 and Np-237 with and without cladding credit. In this example, the alteration time of 3000 years is used. The containment time is 100,000 years. It can be seen that the peak release rate- with the cladding credit for I-129 is one order of magnitude lower than that without the cladding credit. The release of I-129 is distributed over the course of about 140,000 years rather than all focused over the first 3,000 years. For Np-237, no significant differences between the two figures can be observed because solubility and sorption control the EBS release and transport.

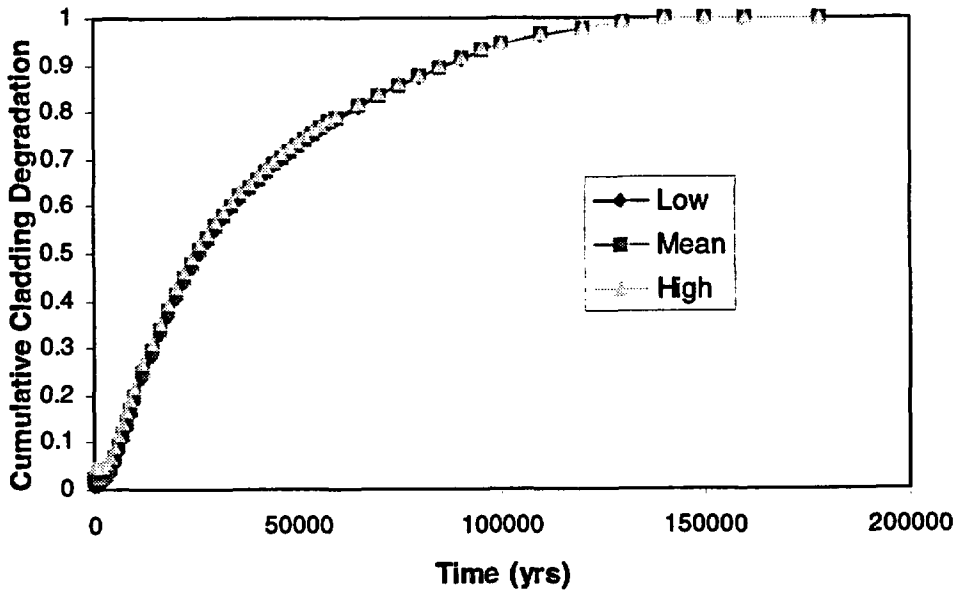


Figure 6-9
Cumulative fractions of failed claddings as a function of time after the waste package fails and becomes wet (Massari 2000)

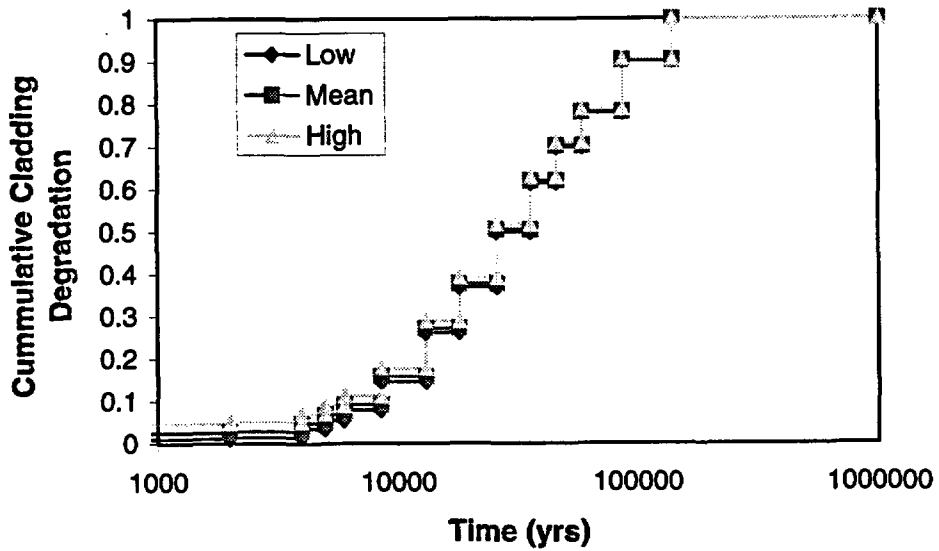


Figure 6-10
Cumulative cladding degradation as piece-wise step function of time after containment failure, converted from Figure 6-9 for IMARC calculations

Note, a spiky behavior for I-129 flux can be observed at later times from Figure 6-11. This is caused by the piece-wise step function conversion of cladding degradation curves (see Figures 6-9 and 6-10). For soluble and non-sorbing I-129, the transit time (the time required to migrate from the waste-form to the EBS edge) is much shorter compared with the time durations used for piece-wise step function of cladding degradation. In other words, once mobilized from the waste-form, I-129 arrives at the EBS edge quickly. Then, the I-129 release rate falls because there are no more nuclides being mobilized from the waste-form and existing within the EBS until the next time duration. When more cladding degrades and more waste matrix is exposed to water, more nuclides are available for transport and release, and the release rate of I-129 rises again.

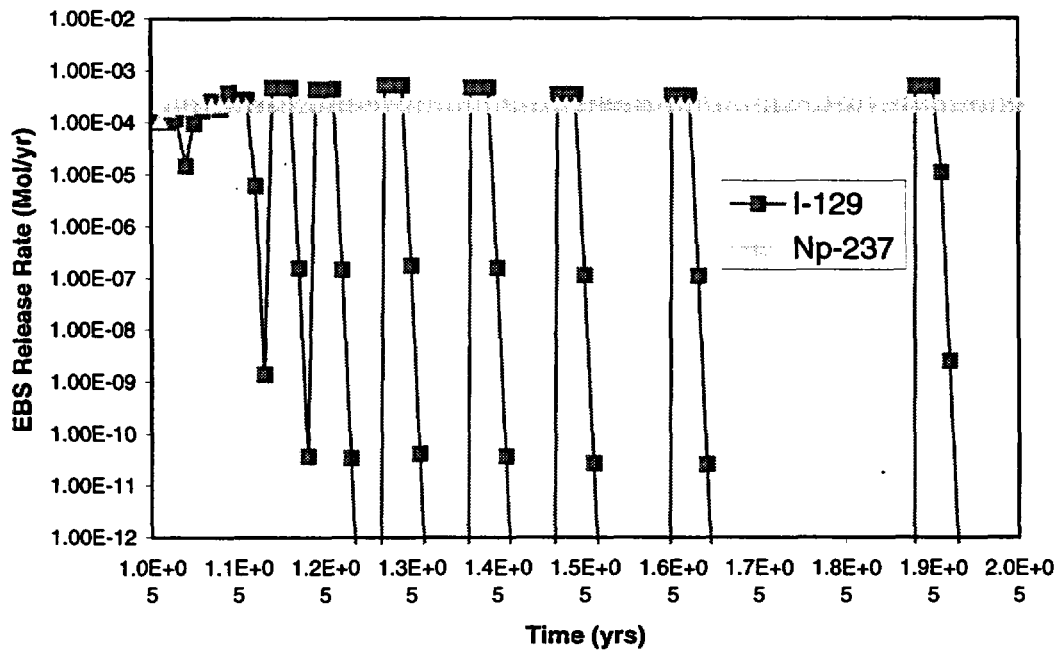


Figure 6-11
EBS release rates of I-129 and Np-237 with cladding credit (with "Mean" curve in Figure 6-9)

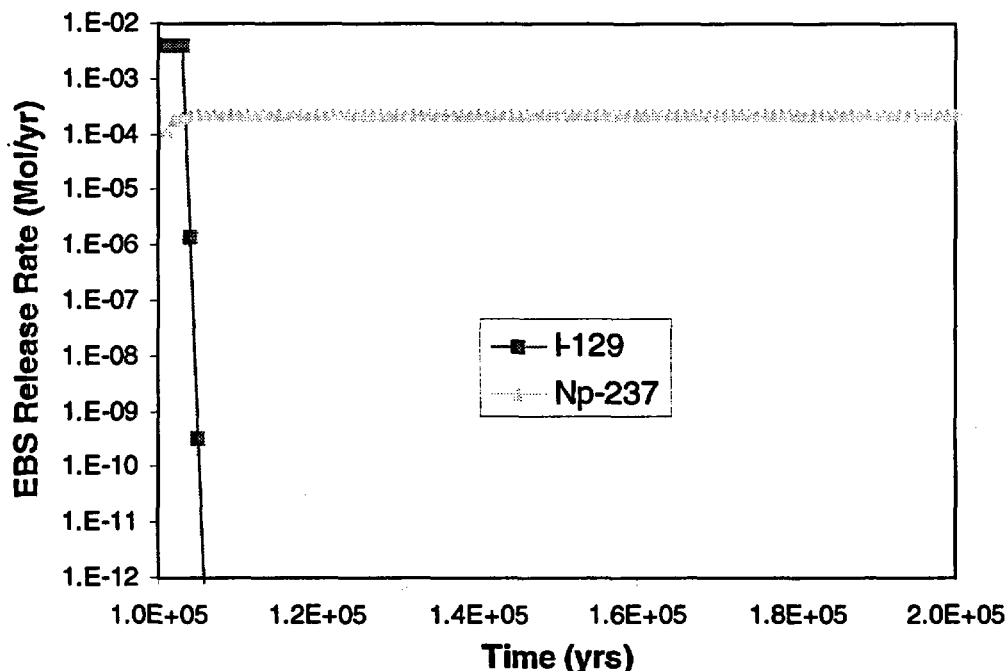


Figure 6-12
EBS release rates of I-129 and Np-237 without cladding credit taken into account

6.2.4 EBS Transport Parameters

A source-term model involves many parameters that can be obtained from design, process modeling calculations, or literature. Many parameters are discussed elsewhere (e.g., alteration times, water contact times, sorption coefficients, solubilities, etc.). In this sub-section, parameters related to EBS transport are presented. These are EBS densities, porosities, water saturations, and diffusion lengths. Table 6-3 shows the parameters for the current IMARC calculations.

Table 6-3
EBS Transport Parameters

	Waste	Corrosion Products	Corroded Canister	Invert
Porosity	0.239	0.42	0.42	0.545
Saturation	0.2	0.35	0.35	0.13
Density [kg/m ³]	0.0	5260	3047	2530

Waste Compartment

The porosity is the ratio of the void volume inside the waste package that is available to receive dissolved radionuclides, to the total volume inside the waste package (provided by Massari 2000). Water saturation is an assumed value, but is likely to be very conservative for almost all plausible scenarios. This is because the COMPASS model calculates the solubilities

and fluxes based on the saturation values in each of the compartments. Setting the saturation in the container compartment is 20% is effectively assuming water fills 20% of the entire cavity inside the container. For a flow-through scenario, like the one being used here, it may be that the container saturation should be less than 1%. For a diffusion-only scenario, where containers are assumed filled with only humid air, the effective saturation will be a fraction of one percent. This conservatism is likely to cause the release rate of potentially solubility-limited species (e.g., Np, U, Pu, and maybe Se) to be overestimated since more water is assumed available into which dissolution can occur, than would actually be expected.

Corrosion Product Compartment

In deriving parameters for the corroded basket materials, the AlOOH has been ignored so the corrosion product is characterized by properties of Fe₂O₃, due to its assumed predominance. The porosity and density are based on 58% packing factor for the granular iron, i.e., 58% of the volume occupied by the oxide is filled (Massari 2000). Water saturation is an assumed value.

Corroded Metal Canister

In deriving porosity and density for this compartment, it has been assumed that properties of this compartment are represented by those of stainless steel. The rationale for choosing porosity and density values is the same as for corrosion product. Water saturation is an assumed value.

Invert

The invert parameters are obtained from M&O's report (MacNeil 2000).

Diffusion Lengths

The diffusive length of a compartment is defined as the distance from the center of the compartment to the interface of the two contacting compartments. This parameter is related to the geometry parameters of the system, which, in turn, are related to the EBS design parameters. Table 6-4 shows diffusion lengths (*d*), effective diffusion coefficients (*D_{eff}*) and the ratio of the two for the EBS compartments.

**Table 6-4
EBS Diffusion Parameters**

	Corrosion Product	Canister	Invert
<i>D_{eff}</i> [m ² /yr]	4.645×10 ⁻⁴	4.645×10 ⁻⁴	4.02×10 ⁻⁴
<i>d</i> [m]	0.046	0.025	0.303
$\frac{d}{D_{eff}}$ [yr/m]	100.0	52.63	1000.0

The third row in the above table (the ratio of the diffusion length and diffusion coefficient) represents the mass transfer resistances of these compartments. Because these compartments are connected in series (see Figure 6-3), the overall mass transfer rate by diffusion is controlled by the compartment that has the maximum resistance (an analogy from electric circuit). Table 6-4 tells that the invert controls the overall diffusive mass transfer rate for radionuclides migrating from the waste form to the EBS edge.

6.3 Provision of Solubilities for Key Radioelements

6.3.1 Background

The objective of this section is to provide values for the solubilities of key radioelements in the near field based on a review of relevant information in the literature. The starting point for this review is the set of solubilities (with probabilities) provided previously as input data (see Table 6-5) for the IMARC code (Apted et al., 1998). Radioelement values are expressed in moles/liter throughout this report and any revisions are based on relevant new information acquired from the literature. In this context, an important source of information and data reviewed is the recent report by Runde (2000).

Table 6-5
Previous Values for solubilities (moles/liter) of Key Radioelements
(probabilities in parentheses)

Element	Solubilities (moles/liter)		
	Low Value (5% probability)	Median Value (90% probability)	High Value (5% probability)
Se	1E-03	1E-02	7E+00
Tc	3E-07	1E-03	1E+01
Cs	9E-06	3E-03	1E-02
I	3E+00	1E+01	2E+01
Pb	1E-08	3E-07	1E-05
Ra	1E-10	1E-08	1E-06
Ac	1E-10	1E-08	1E-07
Th	1E-10	3E-09	1E-06
Pa	6E-07	6E-06	1E-04
U	1E-05	3E-05	2E-04
Np	6E-07	6E-06	1E-04
Pu	1E-10	1E-08	6E-07
Am	2E-09	1E-08	1E-06

6.3.2 Geochemical Environment

The geochemical environment within the repository is discussed by Nowak (2000) and Jolley (1999). As the radioactive components of spent fuel decay, the initial high temperature and low humidity conditions will eventually give way to temperatures below 100°C and a relative humidity above 85%. Over the early history of the repository, the processes which are likely to occur within the drift will include evaporation/ condensation, salt precipitation and redissolution, resulting in groundwater brine formation (Nowak, 2000). Presumably for this reason, various studies and experiments have been conducted by the M&O using groundwater compositions ranging from ~0.01x to ~1000x that of J-13.

As temperatures within the drift decrease sufficiently, water will seep into the drift onto the backfill, both by dripping (gravity) and by capillary flux. Eventually, groundwater will breach the drip shield and reach the surface of waste packages. Waste packages will then degrade sufficiently for groundwater to infiltrate the waste package and contact the fuel rods. Water contact with the fuel matrix may be further delayed by the fuel cladding, although this "containment" will also eventually degrade and allow water/moisture to contact the fuel matrix. At this stage, release of the mobile fraction of radionuclides in spent fuel is possible.

Redox conditions within the drift are assumed to be oxidizing at all times (Mariner, 2000). Jolley (2000) notes that within the repository, the rate of steel corrosion could dominate reactions involving what free oxygen is present, thereby creating a temporary reducing environment until the mild steel is consumed or stops corroding. On the other hand, radiolysis will have the effect of increasing *Eh* such that conditions at the waste form surface will be oxidizing.

6.3.2.1 Aqueous Phase

As discussed in Jolley (1999), ambient groundwater compositions can be defined either by analyzed values of water from the saturated zone (e.g. well J-13), or from analyses performed on porewater extracted from unsaturated zone rock samples. Harrar et al. (1990) concluded that J-13 water could be used as a reference water for the unsaturated zone. Table 6-6 contains a summary of the key characteristics of the J-13 water. The J-13 water is characterized by a fairly low ionic strength, with carbonate and hydroxide the principal complexing anions. Kaszuba and Runde (1999) state that the *Eh* of J-13 waters varies between 0.10 and 0.43 V.

Measurements of groundwater compositions from the saturated zone indicate a predominantly dilute sodium bicarbonate with high concentrations of aqueous silica (Benson et al., 1983; Harrar et al. 1990).

Waters from the unsaturated zone tuffaceous rocks have pH values in the range 6.4 to 7.5 (Yang et al., 1990; Yang 1992). Some constituents (Ca^{2+} , K^+ , Mg^{2+} , SO_4^{2-} , Cl^- and dissolved salts) have higher concentrations than found in samples from the saturated zone, but the HCO_3^- content of the unsaturated zone was found to be less than that in the saturated zone samples (Peters et al., 1992).

Table 6-6
Key characteristics of J-13 water (from Efurd et al., 1998)

Species	Concentration (mM)	Species	Concentration (mM)
Na ⁺	1.96	F ⁻	0.11
K ⁺	0.136	Cl ⁻	0.18
Li ⁺	0.009	NO ₃ ⁻	0.16
Ca ²⁺	0.29	SO ₄ ²⁻	0.19
Mg ²⁺	0.072	SiO ₂	1.07
Mn ²⁺	0.00002	Alkalinity	2.3 mequiv/l
Fe ^{2+/3+}	0.0008	Total carbonate	2.81
Al ³⁺	0.0010		
pH	7.0	Eh	430±50 mV *

*: remeasurement and value used by Efurd et al. (1998) for solubility calculations.

6.3.3 Solubility of Radioelements

6.3.3.1 Conceptual Model

The solubility of a radioelement depends on its speciation in solution and on the solid phase, which is considered to be the solubility-limiting phase. In providing recommendations for solubility values, the solubility-limiting phase is taken to be a non-colloidal pure solid – typically an amorphous oxide/hydroxide or a crystalline oxide (see also the discussion of iron oxyhydroxides as colloids in Section 6.4.3.5). Rai and Ryan (1982) noted the increase in crystallinity of a precipitate with time, described as “Ostwald ripening”, due to the higher solubility (more positive free energy) of materials in a finely divided state. Thus, the solubility of the amorphous phase is typically greater than the solubility of the corresponding crystalline phase.

Although thermodynamic considerations dictate that the amorphous oxide will eventually convert to the crystalline material, Rai and Ryan (1982) have shown that (alpha) radiolytic effects oppose the crystallization process. Such a process will impact particularly on the nature of the solid phase of actinides (amorphous vs. crystalline).

In addition, it should be noted that incorporation of trace radioelements in the dominant U-bearing alteration solid by solid solution substitution, rather than formation of separate, compositionally pure solids for each radioelement as discussed above, is a more credible

conceptual model for establishing solubility limits for radioelements. Some success has been achieved with this approach in the Swedish repository program (Bruno et al., 1996).

6.3.3.2 The Role of Coprecipitation

As indicated above, a coprecipitation/solution model involving elements and other (less soluble) secondary phases within the waste package or the host rock is likely to yield radioelement solubility limits which are substantially lower than values obtained using pure radioelement solid phases.

As one example, Bruno et al. (1991) emphasized the need to develop a coprecipitation/solid solution model to better estimate trace element concentrations in a region of iron (hydr)oxide formation. Failure to include the role of co-precipitation or solid solution of radionuclides in Fe oxyhydroxides in performance assessment models was shown to result in major overestimated concentrations (by several orders of magnitude) of trace elements (Bruno et al., 1991). This issue may be a significant technical (over) conservatism in current Yucca Mountain assessments that should be further tested and evaluated.

Apart from Fe oxyhydroxides, secondary phases may include ferric phosphates, carbonates and secondary uranyl minerals. Experimental evidence indicates that uranium coprecipitates with Fe(III) oxyhydroxides (Bruno et al., 1995). On the other hand, Combes et al. (1992) showed that retardation of Np(V) by goethite was due to adsorption rather than coprecipitation. If coprecipitation is a significant process, which is likely in the case of most elements, then the solubility of a radioelement will be governed by the solubility of the secondary phase.

Coprecipitation with sparingly soluble hydroxides, preferably Fe(III) hydroxides, is frequently used in analytical chemistry for the separation of trace elements. The amorphous intermediates that are formed by condensation of mononuclear to polynuclear hydroxo complexes offer a high specific surface area with hydroxyl groups as reactive sorption sites for many species of trace elements. Coprecipitation of trace elements with Fe(III) hydroxide or Fe(III) phosphate, is often used as an effective procedure in the preparation of drinking water (Lieser, 1995). Thus, coprecipitation must be considered as a significant retardation process, whether by direct radioelement precipitation, or by adsorption of radioelements on precipitated material.

6.3.3.3 Recommendations of Solubility Limits

The recommendation of solubility limits for key radioelements are shown in Table 6-7. Where experimental work is used in support of values quoted, the appropriate reference is included. In experimental work, preference is given to solubility measurements carried out using Yucca Mountain waters, especially J-13 water. In the absence of experimental data, reasoned argument and chemical analogs are reported to justify solubility values.

In reviewing solubility data in the literature, the same issues discussed in Apted et al. (1998) apply equally here and it is worth restating them:

The context in which solubility recommendations are made for performance assessment calculations, e.g. whether for scoping purposes or for compliance issues, will have an impact on the values recommended.

- Solubilities are very much dependent on environmental conditions, especially groundwater chemistry and whether oxidizing or reducing conditions prevail. Under reducing conditions, several radioelements (U, Tc, Se) will display significantly lower solubilities than under the oxidizing conditions at Yucca Mountain.
- Stable elements must be factored into calculations of shared solubility limits. The elements, Ni, Zr, Se, Pd and Sn are present in spent nuclear fuel and/or structural parts (Vieno and Nordman, 1996). Similarly, for elements which comprise several long-lived radionuclides whose mass contributions are significant, e.g. U-238, U-233 and U-235, all nuclide contributions must be taken into account when considering solubility limits.
- The procedures by which solubility measurements are carried out may well influence the values obtained, *viz.*
 - supersaturated solutions using pure solid phases with time-invariant, solubility concentration measurements; expected to yield upper concentration (solubility) limits; solid phase may not necessarily be relevant to actual secondary phase formed from dissolution of nuclear waste forms and, therefore, may yield too high a solubility limit.
 - steady-state concentration limits obtained in long-term dissolution tests; expected to yield a lower concentration (solubility) limit; steady-state conditions may not be reached, in which case, the solubility limit obtained is too low.

In keeping with previous estimates, solubility limits are provided as low (5% probability), median (90% probability) and high (5% probability) values. However, the generation of probability distributions for solubility and sorption parameter values is a highly subjective procedure and it is questionable whether such values can be validated. Much more appropriate to this author are best estimates combined with a conservative value representative of adverse conditions or perturbations that might occur in a given environment.

Table 6-7
 Recommended Values for Solubility (moles/liter) of Key Radioelements. Revised values are shown in *bold italics*

Element	Solubility Values (moles/liter)			Comments/References
	Low (5% Probability)	Median (90% Probability)	High (5% Probability)	
Se	1E-03	1E-02	7E+00	No change; selenium expected to be highly soluble.
Tc	1E-08	1E-03	1E+01	Median and high values – no change; low value based on measurements by Eriksen et al. (1992); redox potential key variable.
Cs	9E-06	3E-03	1E-02	No change
I	3E+00	1E+01	2E+01	No change
Pb	5E-09	5E-06	5E-05	Median and high values based on measurements by Marani et al. (1995); low value based on data review by Marani et al. (1995).
Ra	1E-10	1E-06	1E-05	Median and high values based on calculations by Runde (2000) relevant to Yucca Mountain waters; low value no change.
Ac	1E-10	1E-09	3E-06	Am conservatively used as chemical homolog; Ac solubilities may be lower (x10) due to less radiation damage of solid phase.
Th	1E-10	3E-09	1E-06	No change.
Pa	6E-07	3E-05	6.5E-04	Np used as chemical homolog.
U	1E-05	4E-05	5E-04	Values based on measurements by Sandino and Bruno (1992); only slight changes to median and high values.
Np	6E-07	3E-05	6.5E-04	Median and high values based on measurements by Efurud et al. (1998); pH7 and pH6 respectively.
Pu	1E-10	2E-08	1E-06	Median based on measurements by Efurud et al. (1998), pH7; high value based on measurements by Nitsche et al. (1992), pH 8.5.
Am	1E-10	1E-09	3E-06	Median based on measurements by Nitsche et al. (1992); high based on measurements by Nitsche et al. (1992), for slightly higher carbonate water; low value arbitrarily set 10x lower.

6.4 Sorption of Radioelements on Corrosion Products from Waste Package Internals

6.4.1 Background

The objective of this section is to address the potential for sorption of radionuclides on corrosion products generated from the corrosion of waste package internals. In addition, this report provides values to the IMARC code for the associated distribution coefficient (K_d) for a range of radioelements, based on relevant information available from literature studies.

The possibility of sorption of radionuclides on iron oxides by the Yucca Mountain Project was first entertained in TSPA-93 (Wilson et al., 1993, page 9-11). "Iron oxide" was added to the list of "rock types" to take into account the possibility of sorption of radionuclides on corrosion products from the degradation of (carbon steel) containers (see Table 6-8).

Table 6-8
Elicited Sorption Coefficient (K_d) Distributions (m^3/kg) (from Wilson et al., 1993)

Element	Minimum K_d Value (m^3/kg)	Maximum K_d Value (m^3/kg)	Probability Distribution
Am, Sm, Zr, Nb, Ac, Th	1	5	uniform
Pu	1	5	uniform
U, Se	0.1	1	uniform
Np, Pa	0.5	1	uniform
Ra	0	0.75	exponential
Pb	0.1	1	uniform
Cs	0	0.25	exponential
Sn	0	5	uniform
Ni ¹	-0.1	3	log-normal
Sr	0.02	0.05	uniform
C	0.1	0.3	uniform
Cl, Tc, I	0	0	—

¹: distribution coefficients defined in logarithmic space.

Although distribution coefficient values were reported, sorption on container corrosion products was not factored into the 1993 TSPA calculations. Note that the basis for the elicited values shown in Table 6-8 was not provided by Wilson et al. (1993).

Thus the conservative approach typically has been to ignore any retardation caused by sorption on corrosion products. The implications of such sorption can readily be evaluated by comparison of the performance of the EBS with and without corrosion products as one compartment within COMPASS for retardation.

Since TSPA-1993, the design of the waste package for disposal at Yucca Mountain has been modified and carbon steel is no longer a component material of the waste container. Despite this design modification, large quantities of carbon steel will exist in the planned repository, not only as engineering components of repository construction and tunnel supports, but within the waste package itself as internal elements, mainly making up the lattice holding spent fuel assemblies in place.

Evaluation of corrosion products of mild steel tend to focus on iron because of the greater quantity of iron, and corrosion products of iron, formed from the degradation processes. Where corrosion products are formed in place, i.e. at the surface of the original carbon steel, interaction of radionuclides with these corrosion products will remove them from solution. Interactions will occur via reversible sorption/desorption and possibly irreversible coprecipitation.

The association of radionuclides with secondary iron phases by sorption and coprecipitation has been investigated in natural analogue studies, such as at the Osamu Utsumi uranium mine, Poços de Caldas (Cross et al., 1991). At this site, enrichment of certain trace elements (Cs, Ni, Pd, and Se) by up to a factor of 300 was observed with iron oxyhydroxides on the oxidizing side of a natural redox front, providing the association occurs in natural groundwater conditions. From a consideration of radionuclide inventories with iron content in the Swiss HLW repository, McKinley et al. (1992) concluded that radionuclide associations with iron corrosion products were quite capable of immobilizing the entire inventory of most safety relevant nuclides via a combination of sorption and coprecipitation.

The focus of this section is on the sorption of radionuclides on corrosion products formed *within* the waste package, predominantly from the corrosion of carbon steel lattice.

6.4.2 Geochemical Environment Relevant to Waste Package Internals

A brief overview of geochemical conditions was provided in Section 6.3.2. Once the container has been breached and water enters the waste package, the mild steel internals will begin to degrade by general corrosion.

If the cladding does not provide long containment, there may be only slight corrosion of the mild steel prior to radionuclide release. Those radionuclides which are predicted to be released from spent fuel immediately on contact with water would not be retarded by sorption on corrosion products under this circumstance. More likely, however, is that protection by cladding will delay nuclide release until after significant corrosion of the mild steel internals.

Geochemical conditions within the drift are expected to provide a suitable environment for the corrosion of steels and alloy components of the repository, resulting in significant amounts of iron oxides (hematite or goethite) throughout the repository (Jolley, 1999). However, as noted above, the focus here is on corrosion products formed predominantly from corrosion of the carbon steel lattice within the waste package.

In discussing the development of the in-package chemical environment, Brady (2000) assumes that the water that infiltrates waste packages can be represented by J-13 well water, i.e. there is minimal contact/interaction between incoming groundwater and repository backfill or deposited salts, prior to entering a waste package.

Predictions from EQ3/6 calculations are that the mineralogy of waste packages degrading into solution within the repository will be dominated by clay minerals and a number of oxides, including hematite (Brady, 2000). Together with $\text{UO}_3 \cdot 2\text{H}_2\text{O}$, hematite makes up the volumetrically dominant secondary phases.

6.4.2.1 Corrosion Products - Solid Phase

The nature of the specific iron corrosion products formed will depend on whether ambient conditions are oxidizing or reducing. Initially in the repository, corrosion of iron outside the waste packages will occur under both oxidizing and unsaturated conditions, resulting in a mixture of oxides/hydroxides/oxy-hydroxides of iron – generally abbreviated to iron (hydr)oxides.

Gdowski and Estill (1996) studied the corrosion of carbon steel in humid, oxidizing conditions. Their results indicate that the major products of aqueous electrochemical corrosion consist of an inner oxide of Fe_3O_4 and an outer oxide of a powdery Fe_2O_3 and/or $\text{Fe}_2\text{O}_3 \cdot \text{H}_2\text{O}$. In this case, iron oxides, principally Fe_3O_4 and Fe_2O_3 , are expected to dominate the corrosion products formed during degradation of carbon steel. In the presence of an abundant supply of oxygen, iron would be expected to exist in a more oxidized form, as Fe_2O_3 or FeOOH or $\text{Fe}(\text{OH})_3$, depending on saturation conditions.

Thus, clearly a mixture of iron (hydr)oxides will exist as a result of steel corrosion. The stability of iron (hydr)oxides is (Stumm and Morgan, 1981):

Amorphous $\text{Fe}(\text{OH})_3$ < goethite (FeOOH) < hematite (Fe_2O_3)

However, the kinetics of transition from goethite to hematite is slow (Krauskopf, 1979), so that goethite may well be the dominant phase.

With respect to physical characteristics, corrosion products of carbon steel have been characterized generally as fine, gel-like particles which have a greater specific volume than the uncorroded metal (Raman and Nasrazadani, 1990).

6.4.2.2 Aqueous Phase

The essential characteristics of the aqueous phase were discussed in Section 6.3.2.1, and presented in Table 6-6. With regard to redox conditions, we reiterate that Kaszuba and Runde (1999) state that the Eh of J-13 waters varies between 0.10 and 0.43 V, a wider range than that shown in Table 6-6; in either case, conditions are considered oxidizing.

6.4.3 Sorption of Radionuclides on Corrosion Products

6.4.3.1 Conceptual Model

Sorption is incorporated in transport equations via the retardation parameter, R , viz.

$$R = 1 + \rho_b K_d / \theta$$

where ρ_b = bulk density of solid phase [g/ml or kg/m³]; and θ = moisture content [-].

The extent of sorption is represented by K_d , distribution coefficient, equal to the ratio C_s/C_l , where C_s is the concentration of radioelement on solid phase [mol/g or mol/kg], and C_l the concentration of radioelement in liquid phase [mol/ml or mol/m³].

6.4.3.2 Mechanisms for Sorption on Iron (Hydr)oxides

The two main mechanisms by which elements sorb are surface complexation and ion exchange. Most of the radioelements of interest here are expected to sorb principally by surface complexation, the major exceptions to this being Sr, Cs and Ra which sorb by cation exchange. Other elements, notably nickel, exhibit both sorption mechanisms depending on the pH of the system.

Iron oxides, or hydrous iron oxides, in a variety of crystalline and amorphous forms, exhibit a strong capacity to sorb most cations, particularly in the close to neutral pH range being considered here. Typical data reveal a pH-adsorption edge in which the quantity of trace element removed increases substantially over an approximate two unit pH interval (Forbes et al., 1976).

Above the point of zero charge (PZC) of a substrate, the net charge on surfaces is negative, favoring the electrostatic attraction and subsequent sorption of cations or positively-charged species. Parks and DeBruyn (1962) cite the point of zero charge (PZC) for goethite in the range 7.6-8.1, hematite 6.5-8.6, and lepidocrosite (γ -FeOOH) 7.8-8.6. It should be noted that the PZC for hydrous iron oxides has been shown to vary depending on the method of preparation of the individual solid phases (Hiemstra and van Riemsdijk (1991). Zeltner and Anderson also showed that adsorbed CO₂ has a marked effect on the PZC of goethite. Thus, Fujuda et al. (1998) quote a PZC of 8.5 for goethite and experimental PZC values as high as 10 have been reported (Hiemstra et al., 1989).

The other aspect of iron (hydr)oxides favoring sorption is the relatively high surface area associated with these substrates, particularly for amorphous forms such as ferrihydrite. For example, measurements of the specific surface area of goethite (α -FeOOH) fall in the range 15 to 45 m²/g (Parks and de Bruyn, 1962; van Geen et al., 1994; Fukuda et al., 1998; Kohler et al., 1999), while a surface area of 600 m²/g has been cited for amorphous iron oxyhydroxide (Girvin et al., 1991).

Generally, surface complexation models have been developed to quantitatively describe adsorption of trace elements on hydrous oxide surfaces. Laboratory studies on pure metal

(hydr)oxides, e.g. on amorphous iron (hydr)oxide have shown that sorption processes can be described successfully by surface complexation (Dzombak and Morel, 1990). It is interesting to note that in the metal (hydrous) oxide literature, where sorption data have been interpreted in terms of surface complexation models for several decades, a linear correlation has been obtained between a cation's surface complexation constant and its first hydrolysis constant (Schindler, 1984; Dzombak and Morel 1990). The surface complexation constant indicates the extent of surface complexation and the hydrolysis constant indicates the tendency of a cation to hydrolyse.

Unfortunately, for natural systems, parameters and reactions necessary to characterize a surface complexation model are not always known or available (Honeyman and Santschi, 1988). Thus, sorption processes in natural systems are often modeled with an apparent overall surface reaction, and continue to be expressed in terms of a K_d value.

6.4.3.3 Recommendations of Specific K_d Values

Table 6-9 contains the recommendations for K_d values for specific elements, presented in terms of low (5% probability), median (90% probability) and high (5% probability) values. The emphasis in the table is on sorption on goethite/hematite/magnetite and, relative to amorphous iron (hydro) oxides, K_d values can be considered to be conservative. When interpreting experimental sorption data for iron (hydr)oxides, it is often difficult to distinguish between sorption, coprecipitation and redox processes (Grambow et al., 1996). In addition, for many radionuclides, pertinent data are not yet available, particularly for Fe(II) (hydr)oxides.

Where experimental work is used in support of values quoted, the appropriate reference has been included. In the absence of experimental data, reasoned argument and chemical analogs are reported to justify K_d selections.

Table 6-9
 Recommendations for K_d Values for Specific Elements. Revised values are shown in *bold italics*

Element	Recommended K_d Values (m^3/kg)			Comment/Reference
	Low (5% probability)	Median (90% probability)	High (5% probability)	
C	0	0	0.1	Maximum value revised based on results of Kohler et al. (1999) which indicate sorption of carbonate.
Cl	0	0	0	No change.
Ni	0.05	0.5	5	Wide range; pH of J-13 water close to adsorption edge for Ni (Siegel et al., 1993; Tamera and Furuichi, 1997; Marmier et al., 1999); therefore sharp rise in sorption close to pH of J-13 water (lognormal distribution preferable).
Se	0.005	0.05	5	Balistreri and Cao (1987; Fujikawa and Fukui, 1997; Parida et al., 1997; Hiemstra and Riemsdijk, 1999).
Zr	0.1	1	10	No change; strong hydrolysis; maximum increased in line with Pa.
Nb	0.1	1	10	No change; strong hydrolysis; maximum increased in line with Pa.
Sr	0.01	0.05	0.1	Fujikawa and Fukui (1997); 0.9 m^3/kg quoted for amorphous iron oxyhydroxide (Trivedi and Axe, 1999).
Tc	0	0	1	Although oxidizing conditions assumed, maximum value assumes reduction of Tc on iron oxide surface.
Pd	0.05	0.5	5	Ni used as chemical analog.
Sn	0.1	1	5	Pb used as chemical analog.
I	0	0	0.001	Maximum value based on observed sorption of I as IO_3^- on magnetite and goethite (Fuhrmann et al. 1998).
Cs	0.001	0.1	0.2	Cation exchange; reduced sorption below PZC of iron oxide; Marmier et al. (1999); Marmier and Fromage (2000); Fujikawa and Fukui (1997).
Pb	0.1	1	5	Adsorption edge pH 4-6 (Tamera and Furuichi, 1997); K_d amorphous iron oxides > 20 m^3/kg (Benjamin and Leckie 1980); also Hayes and Leckie (1981).

Table 6-9
 Recommendations for K_d Values for Specific Elements. Revised values are shown in **bold italics** (Continued)

Element	Recommended K_d Values (m^3/kg)			Comment/Reference
	Low (5% probability)	Median (90% probability)	High (5% probability)	
Ra	0.05	0.5	1	Cation exchange; Ra sorption expected to be > Sr sorption; Ames et al. (1983) data for oxyhydroxides.
Ac	1	10	20	Am used as chemical analog; also data for Eu (Fujita and Tsukamoto, 1997).
Th	1	10	20	No change; generally strong sorption on minerals (Allard, 1982); adsorption edge pH 2-5 (La Flamme and Murray, 1987); Hunter et al. (1988).
Pa	0.1	1	10	Strong hydrolysis; generally strong sorption observed; similar behavior to Nb and Zr.
U	0.05	1	10	Gupta and Venkataramani (1988); Sagert et al. (1989); higher maximum based on sorption on corrosion products by Grambow et al. (1996); K_d for sorption on amorphous ferrihydrite inferred at 900 m^3/kg (Payne et al., 1994). Sharp rise in sorption close to pH of J-13 water (lognormal distribution preferable).
Np *	0.0001 *	0.001 *	1 *	Np(V) considered; high values suggested by results of Kohler et al. (1999); also Combes et al. (1992) and Girvin et al. (1991). Sharp rise in sorption close to pH of J-13 water (lognormal distribution preferable).
Pu	1	10	20	Mixture of oxidation states possible; stronger sorption with Pu(V) (Sanchez et al., 1985);
Am	1	10	20	Generally strong sorption (Allard et al., 1984); also on site-specific samples (Triay et al., 1991).
Cm	1	10	20	Am used as chemical analog.

*: Median and low K_d values for Np reduced by ~ 2 orders of magnitude based on results of independent study [EdF Report, not yet published] which indicates that sorption of uranium species will dominate sorption sites.

Strictly, in order to realistically model trace element concentrations in a region of iron (hydr)oxide formation, such as a corroding steel canister, coprecipitation/solid solution models need to be developed (see earlier discussion in Section 6.3.3.2).

6.4.3.4 Other Considerations Relevant to Sorption on Corrosion Products

Several factors should be taken into consideration when making the decision to incorporate sorption on corrosion products of iron:

With regard to corrosion products from mild steel internals, radionuclides may not necessarily "see" the corrosion products in the transport path from fuel rod to beyond the waste package.

Corrosion products other than iron will exist, e.g. corrosion products from Mn or Ni, which tend to associate with iron oxides, and which are also capable of radionuclide sorption; note that Mn oxides are excellent scavengers of Ra as well as U and Th.

Over time and appropriate redox conditions, iron oxyhydroxides may convert to more crystalline phases, e.g. hematite. During such solid recrystallization processes, the adsorbed radionuclides may either become incorporated in the new phases (mineralization) or be released back into solution.

Iron oxyhydroxides formed from corrosion of steel are prone to form colloids (see next section).

6.4.3.5 Iron Oxyhydroxides as Colloids

Colloids formed from corrosion products could enhance radionuclide transport for those cases where sorption is strong. For example, Inagaki et al. (1998) noted that the presence of magnetite increased the colloidal material containing Pu and Np under both oxidising and reducing conditions. Similarly, Cromières et al. (1998) demonstrated strong sorption of thorium on hematite colloids. The specific surface area of these colloids (size ~50 nm) was measured at 19 m²/g, suggesting a non-porous structure. From a quantitative aspect, apart from the carbon steel within the waste package, the large amounts of steel planned for the repository will result in a large source capacity of colloids. Thus, in this respect, the benefits of corrosion products in sorbing radionuclides could be negated by the formation of colloids and increase in radionuclide migration.

In this regard, consideration of reliable mass-transport constraints on radio-colloid migration might be an appropriate and necessary consideration. Previously, such a colloid mass-transport barrier function was found for a Richards barrier (EPRI, 1994).

Alternatively, consideration of the extremely small localized failures (pinholes; see separate Monitor Scientific report, this year) that should characterize any early canister failures may provide a suitable mass-transport constraint on radio-colloid transport from within a failed container. With such a localized failure, any colloidal material formed from corrosion products, and containing adsorbed radionuclides, will be contained within the canister and unable to escape until the size of the pinhole increases.

6.5 References

Allard, B. (1982): Sorption of actinides in granitic rock. Swedish Nuclear Waste Management Co. (SKB) Technical Report TR 82-21. SKB, Stockholm, Sweden.

Allard, B., BU. Olofsson, B. Torstenfelt and H. Kipatsi (1984): Sorption behavior of well-defined oxidation states. Swedish Nuclear Waste Management Co. (SKB) Technical Report TR 83-61. SKB, Stockholm, Sweden.

Ames, L.L., J.E. McGarrah and B.A. Walker (1983): Sorption of trace constituents from aqueous solutions onto secondary minerals II. Radium. *Clays and Clay Minerals* **31**, 335-342.

Apted, M.J., Kozak, M., Stenhouse, M.J. and Zhou, W. (1998): Technical support to IMARC Phase 4 calculations. QuantiSci Report QSCI-9802-1 to Risk Engineering Inc., August 1998.

Balistreri, L.S. and T.T. Chao (1987): Selenium adsorption by goethite. *Soil Sci. Soc. Am. J.* **51**, 1145-1151.

Benjamin, M.M. and J.O. Leckie (1980): Multiple-site adsorption of Cd, Cu, Zn, and Pb on amorphous iron oxyhydroxides. *J. Colloid and Interface Sci.* **79**, 209-221.

Benson, L.V., J.H. Robison, R.K. Blankennagel and A.E. Ogard (1983): Chemical composition of groundwater and the locations of permeable zones in the Yucca Mountain area, Nevada. U.S. Geological Survey ACC: NNA.19870610.0028, Open File Report 83-854. USGS, Denver, Colorado.

Bowell, R.J. (1994): Sorption of arsenic by iron oxide and oxyhydroxides in soils. *Applied Geochemistry* **9**, 279-286.

Brady, P. (2000): Summary of in-package chemistry for waste forms. Office of Civilian Radioactive Waste Management Report ANL-EBS-MD-000050 Rev 00.

Bruno, J., J.E. Cross, J. Eikenberg, I.G. McKinley, D. Read, A. Sandino and P. Sellin (1991): Testing of geochemical models in the Poços de Caldas analogue study. Nagra Technical Bulletin NTB 90-29. Nagra, Wettingen, Switzerland.

Bruno, J. L. Duro, S. Jordana and E. Cera (1996): Revisiting Poços de Caldas: Application of the coprecipitation approach to establish realistic solubility limits for performance assessment. Swedish Nuclear Fuel and Waste Management Co. Report SKB TR-96-04. SKB, Stockholm, Sweden.

Chesnut, D.A., (2000): Engineered Barrier System Degradation, Transport and Flow Process Model, TDR-EBS-MD-000006 REV 00, March 2000.

Combes, J-M., C.J. Chisholm-Brause, G.E. Brown Jr., G.A. Parks, S.D. Conradson, P.G. Eller, I.R. Triay, D.E. Hobart and A. Meijer (1992): EXAFS spectroscopic study of neptunium (V) sorption at the α -FeOOH/water interface. *Environ. Sci. Technol.* **26**, 376-382.

Conca, J., and J. Wright, (1992), "Diffusion and Flow in Gravel, Soil, and Whole Rock", *Applied Hydrogeology*, Vol.1, No.1, 1992.

Cromières, L., V. Moulin, B. Fourest, R. Guillaumont and E. Giffaut (1998): Sorption of thorium onto hematite colloids. *Radiochimica Acta* **82**, 249-255.

Cross, J.E., A. Haworth, P.C. Lichtner, A.B. Mackenzie, L. Moreno, I. Neretnieks, D.K. Nordstrom, D. Read, L. Romero, R.D. Scott, S.M. Sharland and C.J. Tweed (1991): Testing models of redox front migration and geochemistry at the Osamu Utsumi mine and Morro de Ferro analogue study sites, Poços de Caldas, Brazil. Nagra Technical Bulletin NTB 90-30. Nagra, Wettingen, Switzerland.

Dzombak, D.A. and F.M.M. Morel (1990): *Surface Complexation Modeling: Hydrous Ferric Oxide*. John Wiley, New York, New York.

Efurd, D.W., W. Runde, J.C. Banar, D.R. Janecky, J.P. Kaszuba, P.D. Palmer, F.R. Roensch and C.D. Tait (1998): Neptunium and plutonium solubilities in a Yucca Mountain groundwater. *Environ. Sci. and Technol.* **32**, 3893-3900.

Electric Power Research Institute, (1996): *Yucca Mountain Total System Performance Assessment, Phase 3*, EPRI-TR-107191.

Electric Power Research Institute, (1998): *Alternative Approaches to Assessing the Performance and Suitability of Yucca Mountain for Spent Fuel Disposal*, EPRI-TR-108732.

Electric Power Research Institute, 1996, "Yucca Mountain Total System Performance Assessment, Phase 3", EPRI TR-107191, Palo Alto, CA.

Eriksen, T.E., P. Ndalamba, J. Bruno and M. Caceci (1992): The solubility of $TcO_2 \cdot nH_2O$ in neutral to alkaline solutions under constant pCO_2 . *Radiochimica Acta* **58-59**, 67-70.

Farmer, J.C. (2000): *Waste Package Degradation Process Model Report*, TDR-WIS-MD-000002 REV 00.

Forbes, E.A., A.M. Posner and J.P. Quirk (1976): The specific adsorption of divalent Cd, Co, Cu, Pb and Zn on goethite. *J. Soil Sci.* **27**, 154-162.

Fuhrmann, M., S. Bajt and M.A.A. Schoonen (1998): Sorption of iodine on minerals investigated by X-ray absorption near edge structure (XANES) and ^{125}I tracer sorption experiments. *Applied Geochem.* **13**, 127-141.

Fujikawa, Y. and M. Fukui (1997a): Radionuclide sorption on rocks and minerals: effects of pH and inorganic anions. Part 1. Sorption of cesium, cobalt, strontium and manganese. *Radiochimica Acta* **76**, 153-162.

Fujikawa, Y. and M. Fukui (1997b): Radionuclide sorption on rocks and minerals: effects of pH and inorganic anions. Part 2. Sorption and speciation of selenium. *Radiochimica Acta* **76**, 163-172.

Fujita, T. and M. Tsukamoto (1997): Influence of carbonate ions on europium sorption onto iron oxides. *Mat. Res. Soc. Symp. Proc.* **465**, 781-786.

Fukuda, T., S. Nagasaki, H. Satta, S. Tanaka and A. Suzuki (1998): Adsorption/ desorption of lanthanides on metal oxide interfaces. *Radiochimica Acta* **82**, 239-242.

Girvin, D.C., L.L. Ames, A.P. Schwab and J.E. McGarrah (1991): Neptunium adsorption on synthetic amorphous iron oxyhydroxide. *J. Colloid Interface Sci.* **141**, 67-78,

Glassley, B., (2000): in press.

- Grambow, B., E. Smailos, H. Geckeis, R. Muller and H. Hentschel (1996): Sorption and reduction of uranium (VI) on iron corrosion products under reducing saline conditions. *Radiochimica Acta* **74**, 149-154.
- Gross, M.B., (2000): *EBS Radionuclide Transport Abstraction*, ANL-WIS-PA-000001 REV 00, April 2000.
- Gupta, A.R. and B. Venkataramani (1988): Sorption of uranyl ions on hydrous oxides. A new surface hydrolysis model. *Bull. Chem. Soc. Japan* **61**, 1357-1362.
- Harrar, J.E., J.F. Carley, W.F. Isherwood and E. Raber (1990): Report of the Committee to review the use of J-13 well water in Nevada nuclear waste storage investigations. University of California Lawrence Livermore National Laboratory Report UCID-21867, ACC: NNA.19910131.0274. LLNL, Livermore, California.
- Hayes, K.F. and J.L. Leckie (1986): Mechanism of lead adsorption at the goethite-water interface. In (J.A. Davis and K.F. Hayes eds.) *Geochemical Processes at Mineral Surface*, pp. 114-141. Am. Chem. Soc., Washington D.C.
- Hiemstra, T. and W.H. Van Riemsdijk (1991): Physical chemical interpretation of primary charging behaviour of metal (hydr)oxides. *Colloids and Surfaces* **59**, 7-25.
- Hiestra, T., C.M. De Wit and W.H. Van Riemsdijk (1989): Multi-site proton adsorption modeling at the solid/solution interface of (hydr)oxides: a new approach. *J. Colloid Interface Sci.* **133**, 105-117.
- Honeyman, B.D. and P.H. Santschi (1988): *Environ. Sci. Technol.* **22**, 862-871.
- Hsi, C-K.D. and Langmuir, D. (1985): Adsorption of uranyl ions onto ferric oxyhydroxides: Application of the surface complexation site-binding model. *Geochim. Cosmochim. Acta* **49**, 1931-1941.
- Hunter, K.A., D.J. Hawke and L.K. Choo (1988): Equilibrium adsorption of thorium by metal oxides in marine electrolytes. *Geochim. Cosmochim. Acta* **52**, 627-636.
- Inagaki, Y., H. Sakata, H. Furuya, K. Idemitsu and T. Arima (1998): Effects of water redox conditions and presence of magnetite on leaching of Pu and Np from HLW glass. *Scientific Basis for Nuclear Waste Management XXI*, Mat. Res. Soc. Symp. **506**, 177-184.
- Jolley, D.M. (1999): In Drift Corrosion Products. Office of Civilian Radioactive Waste Management Report ANL-EBS-MD-000041, Rev 00, December, 1999. TCR No. T1999-0181.
- Kohler, M., B.D. Honeyman and J.O. Leckie (1999): Neptunium (V) sorption on hematite (α -Fe₂O₃) in aqueous suspension: the effect of CO₂. *Radiochimica Acta* **85**, 33-48.
- Krauskopf, K.B. (1979): *Introduction to Geochemistry*, 2nd edition. McGraw-Hill, New York, New York.

La Flamme, B.D. and J.W. Murray (1987): Solid/solution interaction: the effect of carbonate alkalinity on adsorbed thorium. *Geochim. Cosmochim. Acta* **51**, 243-250.

Langmuir, D. (1997b) *Aqueous Environmental Geochemistry*. Prentice Hall, Upper Saddle River, New Jersey.

Lee, J.H., J.E. Atkins and B. Dunlap (1997): Incorporation of "corrosion-time" and effects of corrosion-product spalling in waste package degradation simulation in the potential repository at Yucca Mountain. *Scientific Basis for Nuclear Waste Management XX*, Mat. Res. Soc. Symp. **465**, 1075-1082.

MacNeil, K., (2000): *EBS Radionuclide Transport Model*, ANL-EBS-MD-000034 REV 00, April 2000.

Marani, D., G. Macchi and M. Pagano (1995): Lead precipitation in the presence of sulphate and carbonate: testing of thermodynamic predictions. *Geochim. Cosmochim. Acta* **29**(4), 1085-1092.

Mariner, P. (2000): In-drift precipitates/salts analyses. Office of Civilian Radioactive Waste Management Report ANL-EBS-MD-000045, April 2000.

Marmier, N. and F. Fromage (2000): Sorption of Cs(I) on magnetite in the presence of silicates. *J. Colloid and Interface Sci.* **223**, 83-88.

Marmier, N., A. Delisée and F. Fromage (1999): Surface complexation modeling of Yb(III) Ni(II) and Cs(I) sorption on magnetite. *J. Colloid and Interface Sci.* **211**, 54-60.

Massari, J., (2000): personal communications.

McKinley, I.G., W.R. Alexander, C. McCombie and P. Zuidema (1992): Application of results from the Poços de Caldas Project in the Kristallin-1 HLW performance assessment. Proc. Second International High-Level Radioactive Waste Management Conf., Las Vegas, Nevada, pp. 357-361.

Nitsche, H., A. Müller, E.M. Standifer, R.S. Deinhammer, K. Bercraft, T. Prussin and R.C. Gatti (1992): Dependence of actinide solubility and speciation on carbonate concentration and ionic strength in groundwater. *Radiochimica Acta* **58-59**, 27-32.

Nowak, E.J. (2000): Physical and chemical environmental abstraction model. Office of Civilian Radioactive Waste Management Report ANL-EBS-MD-000046 Rev 00, April 2000.

Parida, K.M., B. Gorai, N.N. Das and S.B. Rao (1997): Studies on ferric oxide hydroxides. *J. Colloid and Interface Sci.* **185**, 355-362.

Parks, G.A. and P.J. DeBruyn (1962): The zero point of charge of oxides. *J. Phys. Chem.* **66**, 967-973.

Payne, T.E., J.A. Davis and T.D. Waite (1996): Uranium adsorption on ferrihydrite – effects of phosphate and humic acid. *Radiochimica Acta* **74**, 239-243.

Peters, C.A., I.C. Yang, J.D. Higgins and P.A. Burger (1992): A preliminary study of the chemistry of pore waters extracted from tuff by one-dimensional compression. In (Y.K. Kharaka and A. Maest eds.) *Proc. 7th International Symp. On Rock-Water Reactions*, pp. 741-745. A.A. Balkema, Rotterdam, The Netherlands.

Raman, A. and S. Nasrazadani (1990): Packing corrosion in bridge structures. *Corrosion* **46**, 601.

Runde, W. (2000): Pure phase solubility limits: LANL. Office of Civilian Radioactive Waste Management Report ANL-EBS-MD-000017, April, 2000.

Sagert, N.H., C.H. Ho and N.H. Miller (1989): The adsorption of uranium(VI) onto a magnetite sol. *J. Coll. Int. Sci.* **130**, 283-287.

Sanchez, A.L., J.W. Murray and T.H. Sibley (1985): The adsorption of plutonium IV and V on goethite. *Geochim. Cosmochim. Acta* **49**, 2297-2307.

Sandino, A. and J. Bruno (1992): The solubility of $(\text{UO}_2)_3(\text{PO}_4)_2 \cdot 4\text{H}_2\text{O}(\text{s})$ and the formation of U(VI) phosphate complexes: their influence in uranium speciation in natural waters. *Geochim. Cosmochim. Acta* **56**, 4135-4145.

Schindler, P. (1984): Surface Complexation. In (H. Siegel ed.) *Metal Ions in Biological Systems: Circulation of Metals in the Environment*, vol. 18. Marcel Dekker, New York, New York.

Siegel, M.D., P.L. Hopkins, R.J. Glass and D.B. Ward (1993): Design of an intermediate-scale experiment to validate unsaturated-zone transport models. *Proc. 3rd Annual International Conf. On High Level Radioactive Waste Management*, Las Vegas, Nevada, April 26-30, 1993, pp. 1972-1984. American Nuclear Society, La Grange Park, Illinois.

Stockman, C.T., (2000): *Waste Form Degradation Process Model Report*, TDR-WIS-MD-000001 REV 00, March 2000.

Stumm, W. and J.J. Morgan (1981): *Aquatic Chemistry*, 3rd edition. Wiley-Interscience, New York.

Tamura, H. and T. Furuichi (1997): Adsorption affinity of divalent heavy metal ions for metal oxides evaluated by modeling with the Frumkin isotherm. *J. Colloid and Interface Sci.* **195**, 241-249.

Triay, I.R., A. Meijer, M.R. Cisneros, G.G. Miller, A.J. Mitchell, M.A. Ott, D.E. Hobart, P.D. Palmer, R.E. Perrin and R.D. Aguilar (1991): Sorption of americium in tuff and pure minerals using synthetic and natural groundwaters. *Radiochimica Acta* **52-53**, 141-145.

Trivedi, P. and L. Axe (1999): A comparison of strontium sorption to hydrous aluminum, iron and manganese oxides. *J. Colloid and Interface Sci.* **218**, 554-563.

Van Geen, A., A.P. Robertson and J.O. Leckie (1994): Complexation of carbonate species at the goethite surface: implications for adsorption of metal ions in natural waters. *Geochim. Cosmochim. Acta* **58**, 2073-2086.

Vieno, T. and H. Nordman (1996): Interim Report on Safety Assessment of Spent Fuel Disposal. Finnish Nuclear Waste Disposal Management Co. Report TILA-96, Posiva-96-17.

Wilson, M.L., J.H. Gauthier, R.W. Barnard et al. (25 authors) (1993): Total-System Performance Assessment for Yucca Mountain – SNL Second Iteration (TSPA-1993). SANDIA National Laboratories Report SAND93-2675, Albuquerque, New Mexico.

Yang, I.C. (1992): Flow and transport through unsaturated rock – data from two test holes, Yucca Mountain, Nevada. In *Proc. Third International Conf. on High Level Radioactive Waste Management*, Las Vegas, Nevada, April 12-16, 1992, pp. 732-737. American Nuclear Society, La Grange, Illinois.

Yang, I.C., G.S. Davis, and T.M. Sayre (1990): Comparison of pore-water extraction by triaxial compression and high-speed centrifugation methods. *Proc. Am. Inst. Hydrology Conf. On Minimizing the Risk to the Hydrological Environment*, pp. 250-259. Kendall/Hunt Publishing Co., Dubuque, Iowa.

Zeltner, W.A. and M.A. Anderson (1988): Surface charge development at the goethite/aqueous solution interface: effects of CO₂ adsorption. *Langmuir*, **4**, 469-474.

Zhou, W., (2000): COMPASS2000, Source-Term Code for EPRI IMARC 2000 Calculation, Draft Report to EPRI, MSCI-2012C, 2000.

Zhou, W., J. Ahn, W. W.-L. Lee, P. L. Chambré, and T. H. Pigford; “Dissolution and Precipitation of a Two-Member Chain at a Dissolving Waste Matrix,” in *Proceedings of SPECTRUM '88*, an American Nuclear Society International Topical Meeting, Pasco, Washington, pp. 227, 1988.

Zhou, W., M.J. Apted and P. Robinson, (1994), “Comparison of international source-term codes”, in *Scientific Basis for Nuclear Waste Management XVII*, ed. A. Barkatt and R. Van Konynenburg, Materials Research Society, Pittsburgh, PA, 769-774.

7

UNSATURATED ZONE AND SATURATED ZONE FLOW AND TRANSPORT

This chapter examines details of flow and transport in the unsaturated zone (UZ) and saturated zone (SZ). It will describe modifications to the SZ code, and discuss changes to the input data for the SZ. An analysis is presented to illustrate how various processes and parameters control SZ transport. This chapter concludes with a discussion of conservatism or non-conservatism inherent in the overall modeling effort of the Yucca Mountain Project.

IMARC contains UZ and SZ flow and transport modules to calculate concentrations at a compliance boundary due to releases from a potential repository. The UZ is modeled as dual permeability continuum to represent the complex fracture/matrix interactions (EPRI, 1996, 1998). Flow and transport are assumed to occur in one or more vertical columns that can differ in terms of the infiltration rate and source concentrations. The UZ code is coupled to a three-dimensional SZ flow and transport code. It conceptualizes the SZ as a dual porosity system, assuming steady-state flow and transient mass transport. Thus, for computational efficiency it is assumed that within the SZ that the water-table configuration and recharge rates do not change as a function of changing climates. However, modifications have been made to the SZ code to enable flow and transport parameters to vary spatially. These changes are discussed in this chapter.

7.1 Description of the SZ Simulation Domain

The SZ zone model in IMARC has been extended to permit transport calculations at a regulatory boundary 20 km from the repository and a more general conceptualization of the geologic and hydrogeologic settings. This section describes the modifications in detail. Interest in a regulatory boundary 20 km from the repository has necessitated a revision to the simulation domain and the model grid. The domain is now 22 km long and 8.5 km wide (Figure 7-1). The source geometry is idealized as a rectangle 2500 wide and 700 m long and oriented at right angles to the direction of flow (flow direction is toward the bottom of Figure 7-1). In the real setting, flow is at somewhat of an angle to the repository. As is apparent in Figure 7-1, the edges of the repository are separated from the end and side boundaries to allow for the possibility of upstream and lateral dispersion.

The domain has a vertical thickness of 200 m. This value is smaller than those used previously (EPRI, 1996; 1998). It reflects our thinking that a plume would reach some limit in the vertical extent to which it would spread over 20 km of travel to the compliance boundary. The results of borehole flow meter surveys discussed in Section 7.5.2 suggest that open fractures in the SZ occur within a few hundred meters of the water table and are not as abundant deeper in the system. In effect, this modification restricts the ability of the plume to spread in the vertical

direction. However, the domain is sufficiently wide that transverse horizontal spreading would continue to reduce plume concentrations as a function of travel distance.

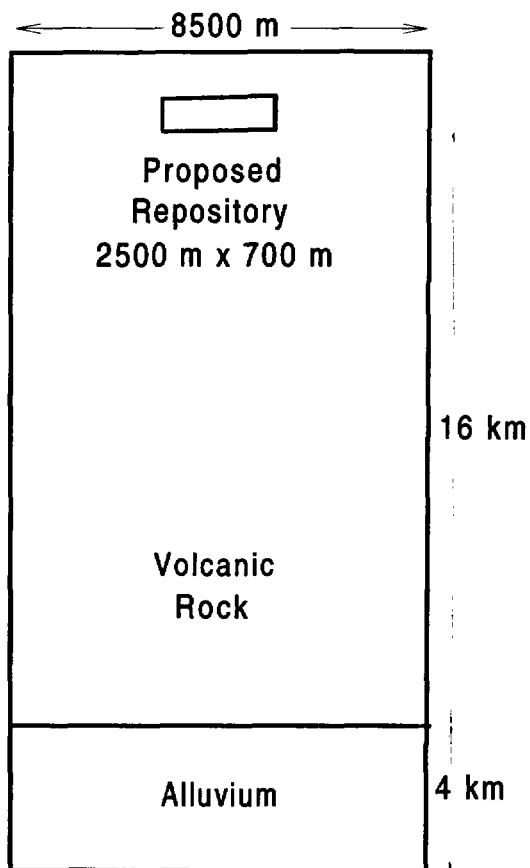


Figure 7-1
Sketch of the simulation domain in the SZ

7.2 Geologic Constraints on Flow in the SZ

7.2.1 Geologic Variability

One of the consequences of increasing the size of the simulation domain is that more than one geologic unit is involved. In particular, as ground water flows away from Yucca Mountain into the Amargosa Desert, it will eventually leave the various fractured tuff units and flow through alluvial deposits. Given the relatively limited geological information away from the immediate vicinity of the proposed repository, it is not clear where this transition in flow from fractured bedrock to alluvium might occur. According to CRWMS, M&O (2000a), the possibilities range from no alluvium along the 20 km path to as much as 9 km. As indicated in Figure 7-1, most model runs assume that the first 16 km of travel will be through fractured volcanic rocks and the remaining 4 km will be through alluvium.

Travel times through the SZ should be somewhat sensitive to where this boundary is located. The combination of relatively small advective velocities and enhanced sorption in the alluvium might reduce the rate of spreading as compared to the fractured rock units. Sensitivity analyses with IMARC will examine how uncertainty in knowledge concerning the distribution of alluvium will influence transport in the SZ.

7.2.2 Concept of a Flowing Interval

Phase 4 of the EPRI studies of flow and transport in the SZ (EPRI, 1998) considered the possibilities for channelized flow in the SZ and its implications for mass transport. In particular, as the flow becomes more channelized, the size of rock blocks increases. This increase in size of the rock blocks in a fractured medium reduces the potential for matrix diffusion and accordingly the travel time for contaminant migration. The Yucca Mountain Project has adopted this idea of channelized flow or as it is termed in CRWMS, M&O (2000a) *flowing intervals*.

A flowing interval is defined as a fractured zone that facilitates flow in the SZ. It is defined on the basis of borehole flow meter surveys. The flowing interval is characterized in terms of interval spacing, which is not the same as the fracture spacing. Figure 7-2 shows the difference between the flowing interval spacing and the fracture spacing. The flowing interval spacing is taken as the distance from the mid-point of the flowing interval to the midpoint of the next flowing interval. As the figure suggests, the flowing interval spacing is greater than the fracture spacing. This conceptualization for flow in the SZ is deemed to be more realistic than simply taking the fracture spacings in the SZ (CRWMS, M&O, 2000a).

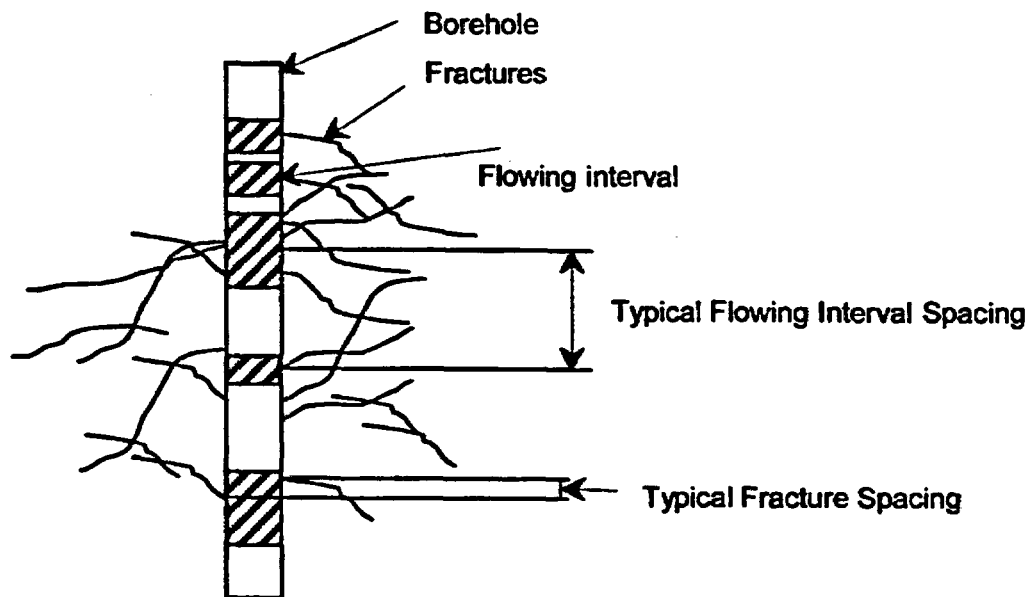


Figure 7-2

The flowing interval spacing is defined as the distance from the midpoint of one flowing interval to the next. The typical spacings between the flowing intervals are much greater than the fracture spacings (from CRWMS, M&O, 2000b)

The mean flowing interval spacings for the SZ is estimated to be 19.5 m (Figure 7-3). This value is significantly larger than the mean fracture spacing, which is a fraction of a meter (Figure 7-3). With large blocks, diffusion into the matrix is likely less effective in attenuating the rate of spread of contaminants than would be the case with smaller blocks. Figure 7-4 illustrates features of the flowing intervals defined in wells at Yucca Mountain for which flow-meter surveys were available. Generally, flowing intervals cannot be correlated between boreholes. The connection among these zones along the flow system is inferred. The flowing intervals represent a relatively small proportion of the total vertical section in each borehole (CRWMS, M&O, 2000b). Finally, there is a suggestion that with depth the number of flowing intervals and the proportion of the total flow being carried diminishes.

7.2.3 EPRI Approach to Modeling the Flowing Intervals

Many of the runs in this chapter consider that ground-water flow in the uppermost 200 m of the SZ is being carried in one-quarter of the vertical section. With the flowing intervals developed in this manner, linear flow velocities within the flowing intervals are four times higher than would be the case if flow were assumed uniform across the entire vertical section. We assume further that within the flowing interval that the fracture spacings and resulting block sizes will be much smaller than flowing-interval spacings and in keeping with fracture spacing measurements made from the SZ (Figure 7-3).

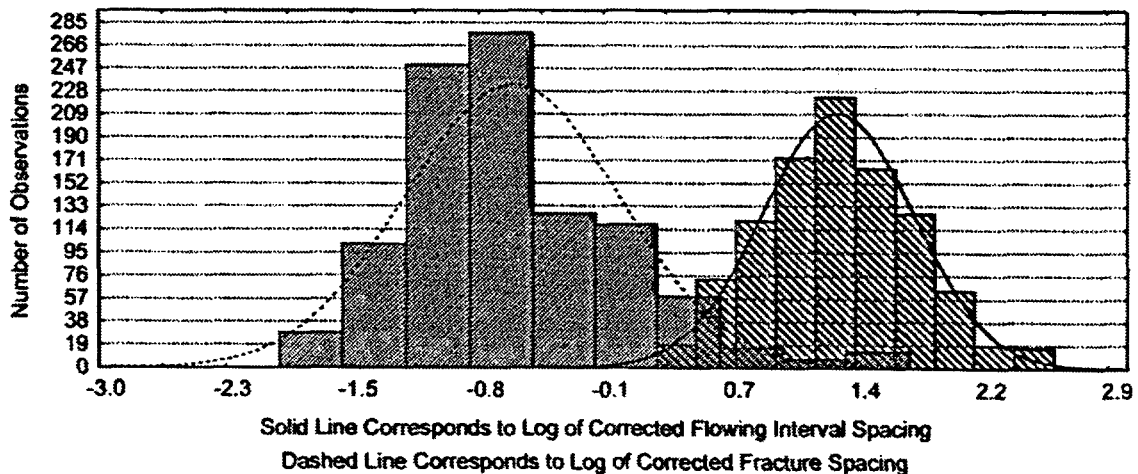


Figure 7-3
Comparison of the probability distributions of the log of corrected flowing interval spacing and corrected fracture spacing (from CRMWS, M&O, 2000b)

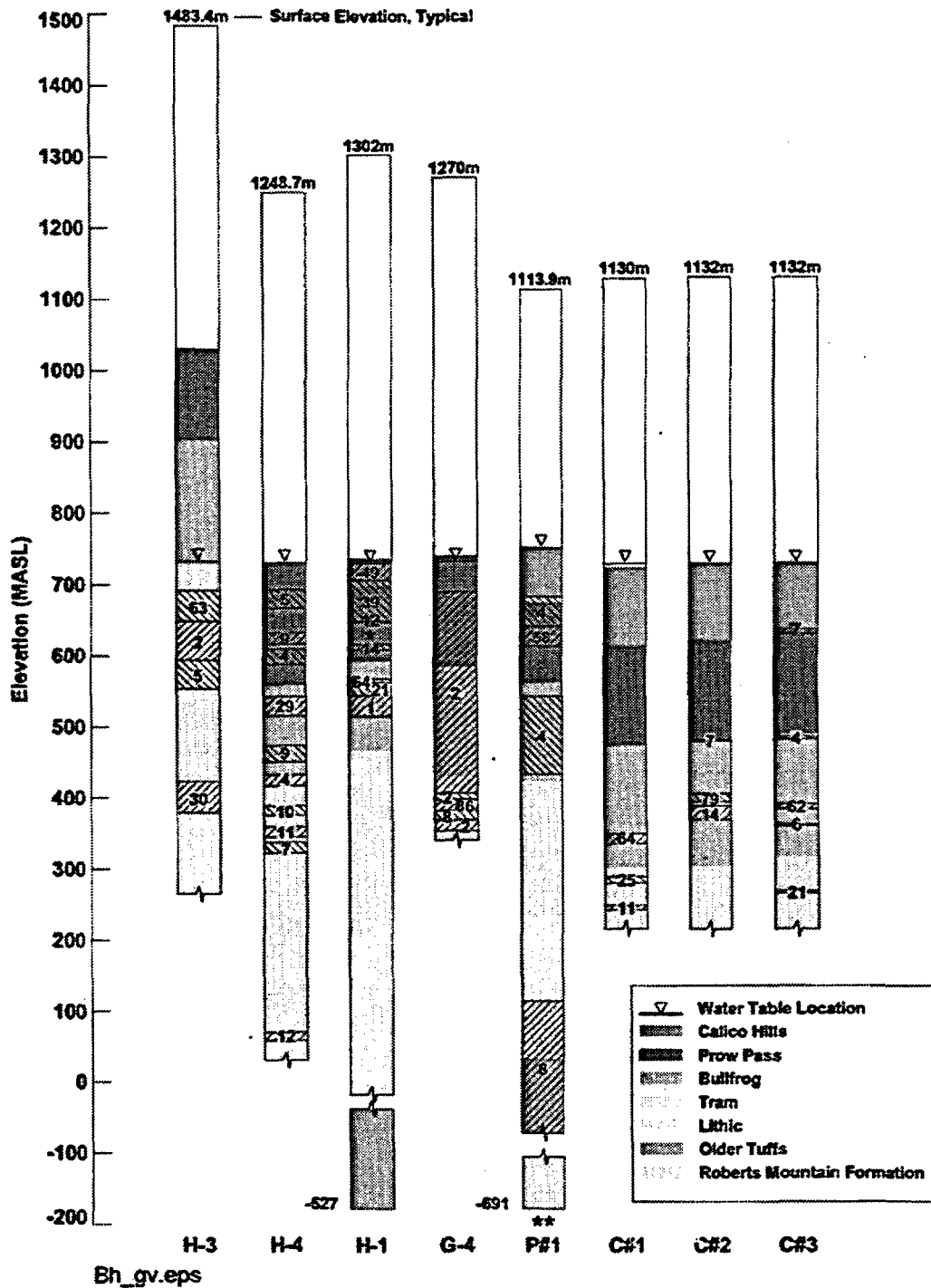


Figure 7-4 Comparison of the flow meter survey information among various boreholes. The shaded areas indicate the flowing intervals and the number within the flowing interval represents the percentage of total flow in that interval (from CRMWS, M&O, 2000b)

This conceptualization is probably more realistic than the more conservative approach used in GoldSim (M&O 2000c). From the description provided by CRWMS, M&O (2000a), it appears that the flowing interval is being modeled as an equivalent hydraulic fracture and the zone of intact rock between the flowing intervals is considered as a rock block. Representing the flowing zone as a fracture removes credit for matrix diffusion into the blocks along the flowing interval. In addition, the definition of the flowing interval spacing is made in such a way that the actual thickness of the intact rock block is exaggerated. Conceptualizing the SZ in terms of flowing intervals with rock blocks determined by the fracture spacings makes matrix diffusion more viable as a mechanism to attenuate the rate of contaminant migration.

7.3 Modifications to the SZ Flow and Transport Code

Revisions to the shape of the SZ simulation domain and the more complex geologic setting required changes to the SZ code within IMARC. Groundwater Simulations Group (GSG) made two basic modifications to the code. First, the saturated zone (SZ) transport module was modified to allow for different vertical and horizontal transverse dispersivity values. Second, the code was generalized to facilitate the representation of spatially distributed sets (zonation) of parameters. The parameters now capable of being zoned include hydraulic conductivity, porosity, retardation factors, dispersivity values, diffusion coefficients, and dual-porosity (matrix diffusion) parameters. The code now allows for single and dual porosity conditions to be represented together. For example, the revised model now has a major portion of the flow regime down-gradient from the repository footprint represented as a dual-porosity continuum (fractured tuff) with a smaller portion extending to the compliance boundary represented as a single porosity continuum (alluvium).

7.3.1 Verification of the Modified SZ Code

Two verification tests were run with the modified code to check the changes incorporating two transverse dispersivity values and material zonation. In the first test, the modified version of the code was compared to the previous (unmodified) version of the code for two cases, unrelated to Yucca Mountain. In the first case, the simulation domain was represented as a single unit with the horizontal and vertical transverse dispersivity both set to five meters. In the second case, the domain was represented by two zones having identical flow and transport properties with the two transverse components of dispersivity components again equal to five meters. In each case, the modified and unmodified version of the code produced identical results. Thus, changes to the array structures, input data formats, coefficient matrix formation etc. have not introduced coding errors.

A second cross-verification test involved the SZ module in the IMARC code and the numerical model FRAC3DVS (Therrien and Sudicky, 1996). FRAC3DVS has been verified against many different analytical solutions for a wide range of problems. The simulation domain for this test was 1000 m in the x-direction, 5000 m in the y-direction and 1000 m in the z-direction. The input data for this test are not related to Yucca Mountain. A uniform darcy flux of 9.136×10^{-3} m/day (3.3 m/yr) parallel to the x-axis was imposed. For the first trial, the longitudinal dispersivity was 20 m, while transverse horizontal and transverse vertical dispersivities were each 5 m. For the second trial, the longitudinal and transverse horizontal

dispersivity values were held at 20 m and 5 m, respectively, while the transverse vertical dispersivity was reduced to 0.05 m. This latter trial was designed to test the ability of the SZ flow and transport module to handle a second component of transverse dispersivity. The source for both of these trials was a 100 m by 100 m patch, which was oriented perpendicular to flow with a specified concentration of 1.0.

Figure 7-5 compares the results of the two cross-verification tests with FRAC3DVS and the SZ module in IMARC. The breakthrough curves for the two models at a hypothetical observation point 500 m down gradient are nearly identical with the sets of transverse vertical dispersivity values. Thus, the code modifications relating to dispersivity appear to be correct. The revised code is capable of treating situations involving differences in horizontal and transverse dispersivities. However, the use of small, vertical transverse dispersivities would require a highly resolved vertical discretization. For many regional problems, this resolution may not be practical.

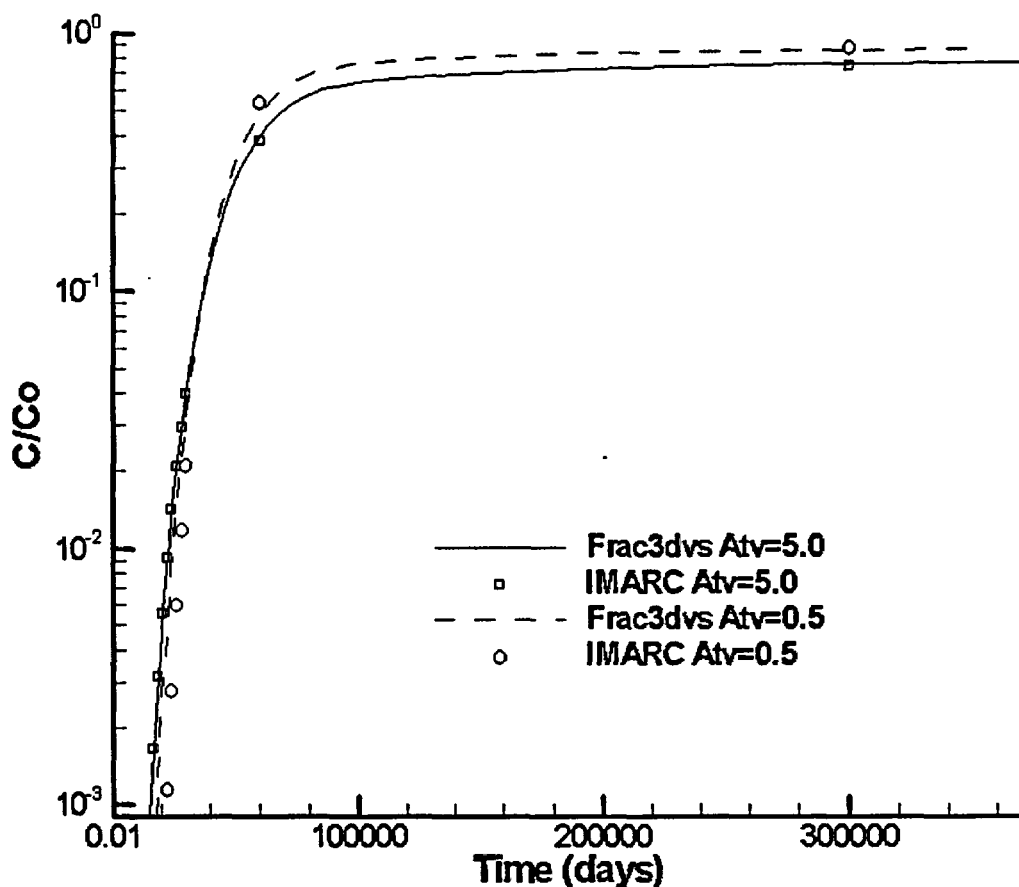


Figure 7-5
Comparison of concentration vs time at a point 500 m downgradient from the source for a transverse-dispersivity verification example

7.4 Design of Simulation Trials

Two series of simulations (F Series and S Series) are used to explore controls on transport in the SZ. The parameters of the F Series provide more expedited mass transport through the SZ, through a relatively large advective velocity and minimal matrix diffusion. In contrast, the parameters of the S Series provide slower rates of contaminant migration in the SZ through a reduced advective velocity and enhanced matrix diffusion.

A key difference between the parameters of the F and S Series is in the specific discharge value applied to the upstream boundary. This parameter, together with effective porosity and recharge rate, is important in determining the velocity of advective contaminant transport in the simulation domain.

In the Series F runs, the specific discharge is fixed at the upstream boundary at 0.60 m/yr, following CRWMS, M&O (2000a) and our previous work. We assume further that ¼ of the total vertical section is a flowing interval, based on a qualitative examination of data presented in CRWMS, M&O (2000b). With a base value of effective (fracture) porosity of 6.0×10^{-3} , the linear ground-water velocity is at least 100 m/yr in the fractured volcanic rocks and at least 3.3 m/yr in the alluvial materials (Table 7-1).

In the Series S runs, a smaller specific discharge value, 0.15 m/yr is applied to the boundary. This value is somewhat larger than the minimum suggested in CRWMS, M&O (2000a) (0.06 m/day). Our use of a smaller specific discharge was prompted by the observation that flowing intervals are not directly connected between boreholes (CRWMS, M&O, 2000b). The conceptualization of volcanic rocks in the SZ as small permeable zones of limited extent would imply that a lower value of specific discharge might be more realistic. Assuming again that ¼ of the interval is available for flow with an effective (fracture) porosity of 6.0×10^{-3} , the average linear velocity for the S Series would be at least 25 m/day in the fractured volcanic rocks and at least 0.83 m/yr in the alluvium.

The other key difference between the Series F and Series S trials is the extent to which matrix diffusion is operational in the volcanic rock blocks. Parameters with the F Series reduce the role of matrix diffusion by providing larger block sizes and smaller matrix diffusion coefficients than the S Series. The F Series of trials are based on a block-size radius of 0.75 m and a matrix diffusion coefficient of 3.2×10^{-12} m²/s. This diffusion coefficient is approximately two-orders-of- magnitude smaller than the free water diffusion coefficient. The diffusion coefficient is the mid-point of the conservative data range presented in CRWMS, M&O (2000a). The value for the block size is estimated, assuming that locally some of the fractures are not flowing. The S Series provides for more significant matrix diffusion, with a base block radius of 0.125 m (Figure 7-3) and a matrix diffusion value of 3.2×10^{-11} m²/s. This diffusion coefficient is similar to a value measured for tuff (CRWMS, M&O, 2000b).

Values of the parameters used to simulate flow and transport in the SZ are presented in Table 7-1. The base parameters for Series S and F are provided by Run 01 and Run 04, respectively. Values for the effective porosity, and bulk density are the mean values for the matrix properties presented in CRWMS, M&O (2000a). The diffusion coefficient for dissolved

mass in the fractures, 5×10^{-10} m²/s, is close to the free-water value, but reduced slightly from Phase 4 (EPRI, 1998) studies.

In the SZ simulation, the linear velocity is determined by the specific discharge applied at the upstream boundary. Thus, the mass transport simulations are not sensitive to the hydraulic conductivity values. What the hydraulic conductivity values will control is the distribution of hydraulic head along the 20 km flow system. Values of hydraulic conductivity in the SZ are not well known. Those values depicted in Table 7-1 come from ranges provided by Czarnecki et al. (1997).

The dispersivity values presented in Table 7-1 are the same as those used in the IMARC Phase 4 Studies (EPRI, 1998). The previous report justified a greater vertical transverse dispersivity than was previously considered by the Yucca Mountain Project. For the present study, restricting the vertical thickness of the simulation domain to 200 m reduces the opportunity for transverse mixing to dilute any potential plume moving through the SZ.

Table 7-1
Summary of base hydraulic and transport parameters for the SZ, used in Run 01: Series F and Run 04: Series S

Parameter Type	Parameters	Volcanic Rocks	Alluvium
Matrix	Effective Porosity	0.19	0.18
	Bulk density (kg/m ³)	1940	1270
	Diffusion Coefficient (m ² /s)	R 01: F 3.2×10^{-12} R04: S 3.2×10^{-11}	0
	Radius Matrix Block (m)	R 01: F 0.75 R 04: S 0.125	—
Flowing Interval	Effective Porosity	6.0×10^{-3}	—
	Diffusion Coefficient (m ² /s)	5×10^{-10}	—
	Bulk Hydraulic Conductivity (m/s)	1×10^{-4}	1×10^{-4}
Transport	Specific Discharge (m/yr)	R 01: F 0.60 R04: S 0.15	0.60 0.15
	Approximate Linear Ground-Water Velocity (m/yr)	R 01: F 100 R04: S 25	3.3 0.83
	Longitudinal Disp. (m)	20	20
	Transverse Disp. (m)	5	5

Assumes flowing interval: ¼ of section.

The following table presents base-case values for the distribution coefficients in the volcanic rocks and the alluvium in the SZ. Values apply to both the Series F and Series S runs. As has been the case in previous studies, it is assumed that radionuclides moving along the fracture system would not be retarded. The values come from data provided in CRWMS, M&O (2000a).

In cases where upper and lower bounds were provided for uniform distributions, the mid-point of the distribution is selected. Se is assumed to behave similarly to U. The values indicated for the volcanic rocks, apply to the rock blocks. Note that values provided for the alluvium are corrected (see Table 7-2) so that using the effective porosity in calculating retardation factors does not overestimate the actual retardation factor (discussion provided in CRWMS, M&O, 2000a). The calculation to provide the correction factor in Table 7-2 is shown below Table 7-2.

Table 7-2
Summary of K_d and dimensionless K_d values for volcanic units and alluvium in SZ used in Series F and Series S runs

Radionuclide	K_d (volcanics) (mL/g)	$K_d \times \rho_b$ (dimensionless)	$K_d \times c$ (alluv.) (mL/g)	$K_d \times \rho_b \times c$ (dimensionless)
Np	0.5	0.97	9.2	12
I	0.0	0.0	0.24	0.31
U	2.0	3.9	2.0	2.6
Tc	0.0	0.0	0.22	0.28
C	0.0	0.0	0.0	0.0
Am, Pu, Pa, Th	50	97	25.5	32
Cs, Sr	25	49	12.8	16
Se	2.0	3.9	2.0	2.6

$$\rho_{bv} = 1.94 \text{ g/cm}^3$$

$$\rho_{ba} = 1.27 \text{ g/cm}^3$$

$$c = \frac{\theta_e}{\theta_T} = \frac{0.18}{0.35} = 0.51; \text{ Rationale for correction described in CRWMS, M\&O (2000a)}$$

7.5 Sensitivity Analyses

This section reports the results of a sensitivity analyses with the UZ/SZ flow and transport code from IMARC. These model trials were designed to investigate how various hydrogeologic characteristics of the SZ influence transport. This analysis was purposely limited in scope to avoid the complexities of a full IMARC run. For this analysis, the properties of the UZ were taken from previous studies and remained constant for all model trials. The UZ is idealized in terms of four geologic units. The boundary conditions at the top of the UZ consisted of a constant rate of infiltration of 1.13×10^{-5} m/day (4 mm/yr) and a unit source with strength of 1.0. These conditions, along with the properties of the UZ, result in a water flux and breakthrough concentration curves at the water table, which are shown in Figure 7-6. These curves are used to define a third-type (Cauchy) boundary condition for the SZ simulation, which becomes constant after about 10^7 days (27,000 years). The first arrival of solute mass at the water table, defined here as a relative concentration equal to $(C/C_0) 10^{-5}$, occurs after approximately 1300 years. $C/C_0 = 0.5$ arrives at about 9300 years. This value is slightly higher but comparable to 1-D calculations provided in CRWMS, M&O (2000d) in a code comparison exercise. For all but one set of sensitivity analyses, the source size was fixed at 700 m by about 2500 m.

Following here are results of simulation trials involving the base parameters of Series F (Run 01) and Series S (Run 04), which help explain key factors influencing transport in the SZ. The first parameter of concern is the diffusion coefficient for the rock blocks in the flowing intervals.

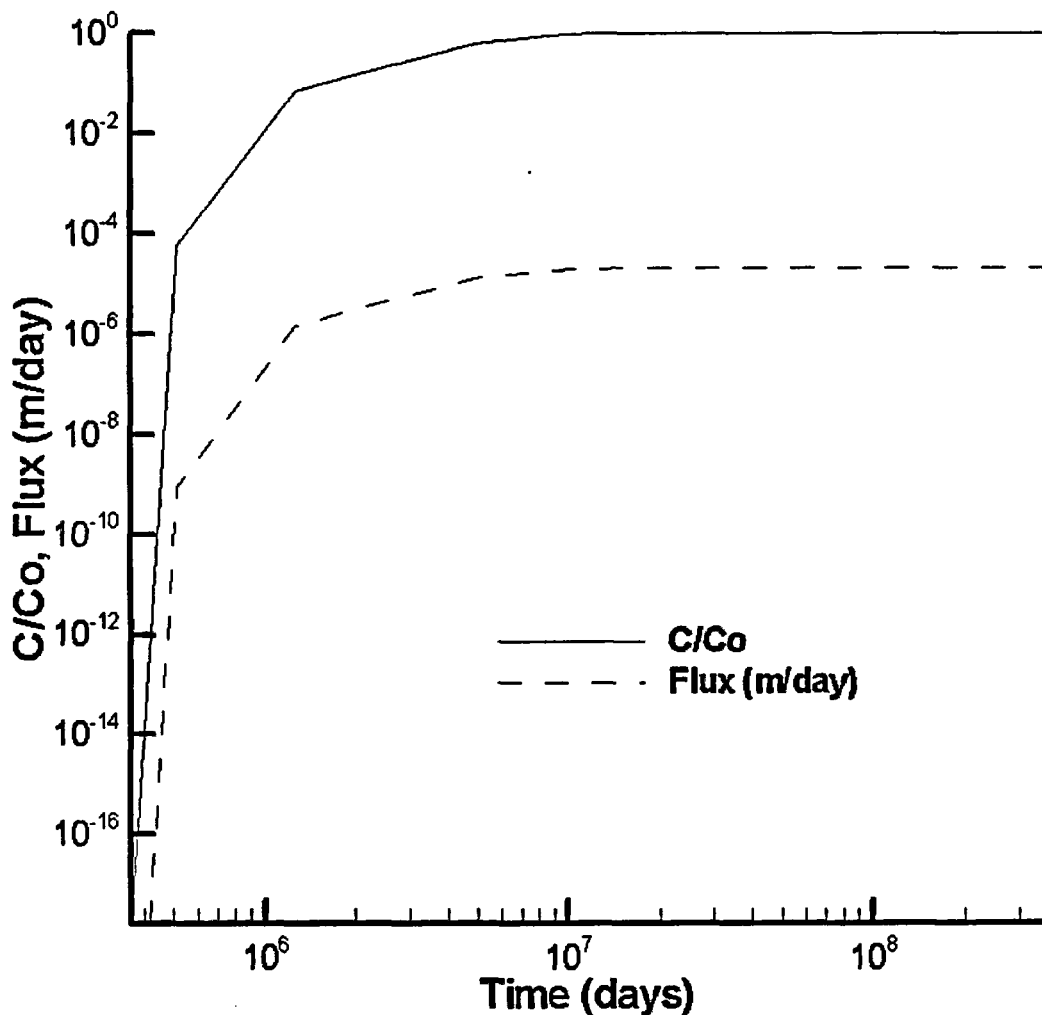


Figure 7-6
Breakthrough concentrations and water flux at the base of the UZ (water table)

7.5.1 Variation in the Diffusion Coefficient in the Volcanic Aquifer

The process of matrix diffusion in fractured rocks has the potential to control rates of contaminant spreading. A key-controlling variable in this respect is the diffusion coefficient in the matrix of rock blocks in the volcanic aquifer. As diffusion coefficients become larger, matrix diffusion is more effective in attenuating the rate of contaminant spreading.

The analysis here presents results from trials with the F and S Series parameters where values of the diffusion coefficients are varied. With the F Series, the diffusion coefficients for the rock blocks are varied from 10^{-10} to 10^{-13} m^2/s (8.6×10^{-6} to 8.6×10^{-9} m^2/day) in three model runs

(R 01, 02, 03; Figure 7-7), across the range of values provided in CRWMS, M&O (2000a). The base set of parameters is that of Run 01 (Table 7-1). With the S Series conceptualization, two sets of results are presented (R 04, 05). The base set of parameters in this series is that of Run 04 (Table 7-1).

Results of these runs are shown in Figure 7-7 with the maximum concentration at the outflow boundary plotted versus time in days. Note first how the F Series of runs provides a faster travel time than the S Series. Selecting a C_{max} value of 10^{-3} for comparison, breakthrough with R 01: Series F is at about 7700 years, while that for R 04: Series S is about 32,900 years. The steady-state concentrations at the outflow boundaries are lower with Series S as compared to Series F. The reason for this difference will be discussed in Section 7.5.7.

Changing the value of the matrix block diffusion coefficient in the volcanic aquifer has a noticeable effect with the F Series of runs (Figure 7-7). Approximately 4900 years, 7700 years and 8700 years are required for breakthroughs of the 10^{-3} relative concentration for the smallest to largest diffusion coefficients, respectively. As expected, the smallest values result in significantly faster breakthrough times at the compliance boundary. Considering the shortest residence time in the UZ is about 1300 years, matrix diffusion has only a marginal impact on travel times for R 03: Series F (smallest diffusion coefficient).

With the S Series, changes in the diffusion coefficient have little effect on the residence time in the system. This behavior is due to the fact that matrix diffusion is operating optimally given the relatively large diffusion coefficients in R 04 and R 05 (Figure 7-7) and the small block size associated with the S Series. It is possible to check this conclusion approximately by calculating the diffusion length, the distance that solutes can penetrate a matrix block in a given time. Mathematically, the diffusion length (d) is

$$d = (2 D_e t)^{1/2} \tag{Eq. 7-1}$$

where t = the reference time, which is taken here as the approximate residence time, 1×10^6 days for the F Series and 4×10^6 days for the S Series, and D_e is the effective diffusion coefficient. The results of the calculation are shown in Table 7-3.

Table 7-3
Calculated penetration by diffusion

Run Number	Time (days)	Diffusion Coefficient (m^2/d)	Penetration Distance (m)
R 01	1×10^6	2.8×10^{-7}	0.74
R 02	1×10^6	8.6×10^{-6}	4.2
R 03	1×10^6	8.6×10^{-9}	0.13
R 04	4×10^6	2.8×10^{-6}	4.7
R 05	4×10^6	8.6×10^{-6}	8.3

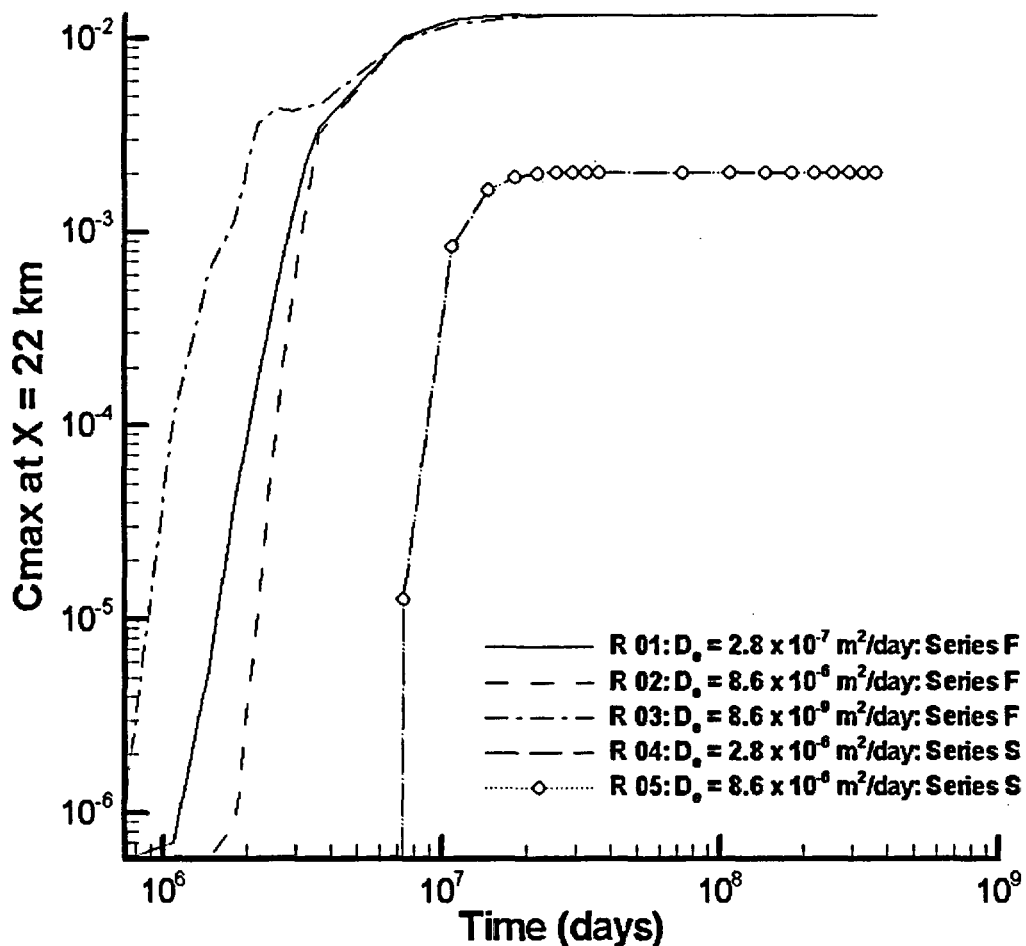


Figure 7-7
Time variation in maximum concentration at the compliance boundary for Series F and S runs as a function of the diffusion coefficient (D_0) of matrix blocks in the volcanic aquifer

If the block radius for the F series is 0.75 m and for the S series it is 0.125 m, then one would expect near-complete penetration of the blocks for all runs except R03. Because the characteristic diffusion distance for R01 is about the same as the block radius, it is reasonable to expect a minor variation between the curves for R01 and R02. With the S Series, diffusion is more than sufficient to penetrate the blocks. Thus, there should not be much sensitivity to changing diffusion coefficients in Series S.

7.5.2 Variation in the Size of the Rock Blocks

The process of matrix diffusion is also influenced by the block size. Unlike the M&O, we assume that block sizes are smaller than the flowing interval. The F Series of runs involves four different block radii 0.37 m, 0.75 m, 2.0 m, and 9.75 m. The base block radius with R 01 is 0.75 m, with 0.37 m and 2.0 m representing low and high variations on the base value. The 9.75 m radius provides a block size of 19.5 m, equivalent to the Project value for the mean

flowing interval spacing. These values again reflect the differences of scale between the fracture spacings and the flowing-interval spacings. The S series of runs involve much a smaller block radius. The base set of parameters with R 04 uses a mean block radius of 0.125 m. In R 09, a block size of 0.25 m is used with the S Series set of parameters.

Figure 7-8 illustrates the variation in C_{max} as a function of time for the runs of Series F and S. The basic differences noted previously between the F and S Series are again evident. The results of the F Series runs show that increasing the matrix block radius is similar to reducing the diffusion coefficient. With the largest block radius, breakthrough occurs in approximately 4100 years as compared to 7700 years for the base case. As expected, the larger blocks are less efficient at storing contaminant and breakthrough at the compliance boundary occurs more rapidly. With block sizes at scale of the flowing interval spacings, matrix diffusion is largely ineffective. These results make sense in terms of the diffusion lengths calculated in Table 7-3.

With the S Series (R 04, 09), peak breakthrough is at 32,900 years. This result is not apparently sensitive to doubling of the block radius (Figure 7-8). This result is surprising since the largest block size with the S series is still less than $\frac{1}{4}$ of the diffusion length. Again, it is likely that matrix diffusion is optimal with the combination of blocks sizes and diffusion coefficients being used. Thus, small changes in parameters do not affect the pattern of transport substantially.

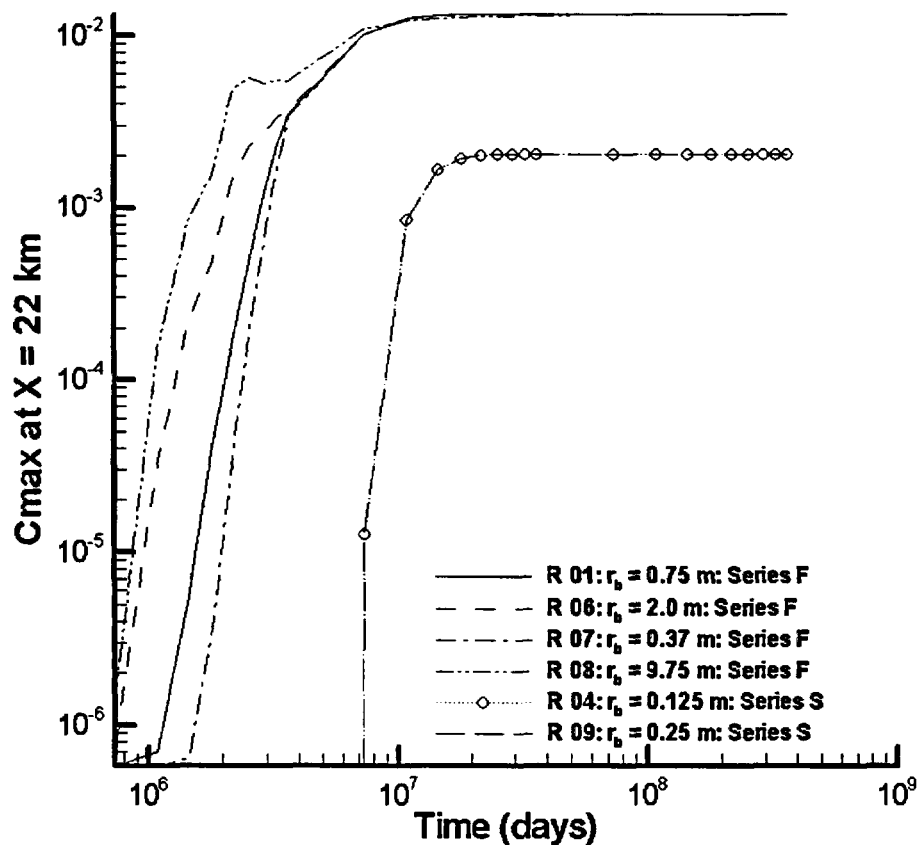


Figure 7-8
Time variation in maximum concentration at the compliance boundary for Series F and S runs as a function of the radius of matrix blocks in the volcanic aquifer (r_b)

7.5.3 Fraction of the Total Section that is Flowing

Another variable controlling the extent of matrix diffusion is the fraction of the total domain thickness available for flow. In the simulation experiments, maintaining the flux and changing the effective porosity adjust this variable. In effect, as the fraction of the total SZ cross-section composed of flowing intervals becomes smaller, the effective porosity becomes smaller and the linear ground-water velocity becomes larger. With the F Series of trials, three cases are examined. In the first, the flowing intervals comprise 1/2 of vertical section, providing an effective porosity of 1.2×10^{-2} and an average linear velocity greater than 50 m/yr. This value of effective porosity is the base case value (6.0×10^{-3}) multiplied by two reflecting the two times increase in the section available for flow. With the base value, the flowing intervals comprise 1/4 of total vertical section, providing an effective porosity of 6.0×10^{-3} and an average linear velocity greater than 100 m/yr. With a flowing interval comprising 1/10th of the vertical section, the effective porosity is 2.4×10^{-3} and the average linear velocity in the volcanic rocks is at least 250 m/yr. The S Series of runs (R 04, 12) involve flowing intervals of 1/4 and 1/10 of the section with the same matching effective porosity values.

Figure 7-9 shows how changing the effective porosity of the matrix blocks influences travel times. The results for the three F Series run are almost identical. The breakthrough curve for the high-effective porosity case (1/2 section a flow interval) is only slightly delayed compared to the low-valued case. The two S Series runs are also the same. It appears that for runs with Series F and S the fraction of the total section that is flowing has relatively little impact on the arrival of the peak concentration at the compliance boundary. The reason for this behavior is not clear at this time. One possibility is that the travel time through the fractured volcanic rocks is so fast with both the F and S Series runs that changing the advective velocity by adjusting the effective porosity will have a minor impact on the travel time. Another possibility is that matrix diffusion is able to compensate for differences in advective velocity.

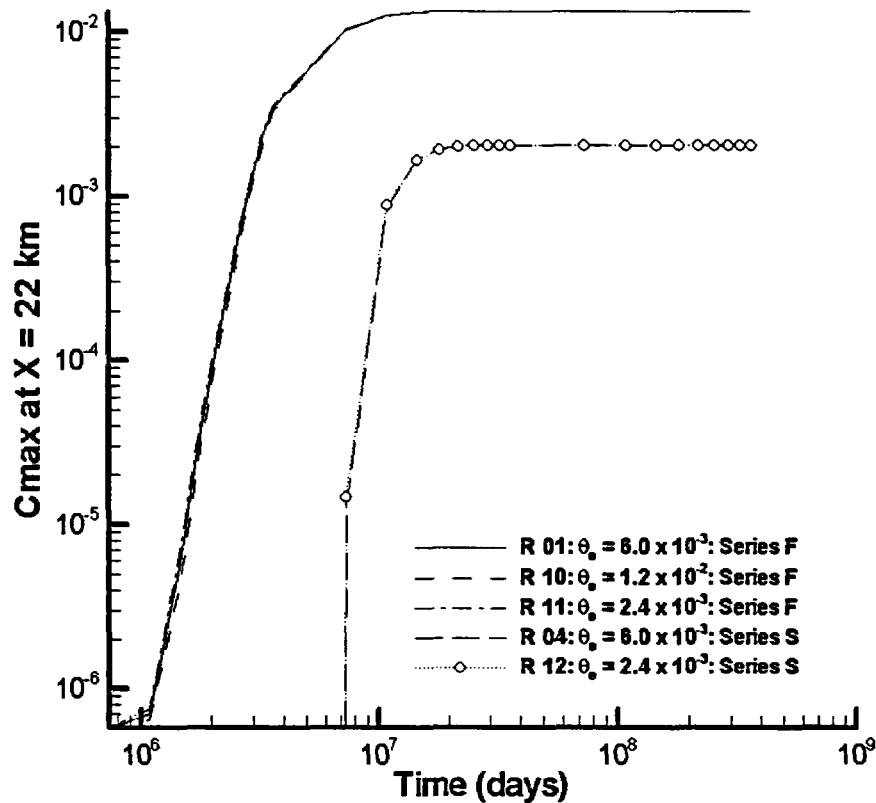


Figure 7-9
 Time variation in the maximum concentration at the compliance boundary for Series F and S runs as a function of the effective porosity (θ_e) of the flowing interval in the volcanic aquifer

7.5.4 Changes to the Boundary Between Volcanic and Alluvial Aquifers

There is some uncertainty as to how much of the potential travel path in the SZ to the compliance boundary will occur within the alluvial aquifer. The greater the distance of transport in the alluvium, the more favorable will likely be the performance, because of enhanced sorption and smaller advective velocities. Here, three cases are considered with the Series F parameters and two with Series S. The length of the volcanic unit varies from 11 to 19 km in the runs (see Figure 7-10).

With the F Series, the main impact is on the first contaminant arrivals. As expected, the best performance is achieved when the travel path through the volcanic rocks is a minimum (11 km). At a higher relative concentration (C_{max} value of 10^{-3}), there are only small differences among the results. In the S Series, there is no sensitivity to changes in the length of the fractured volcanic unit.

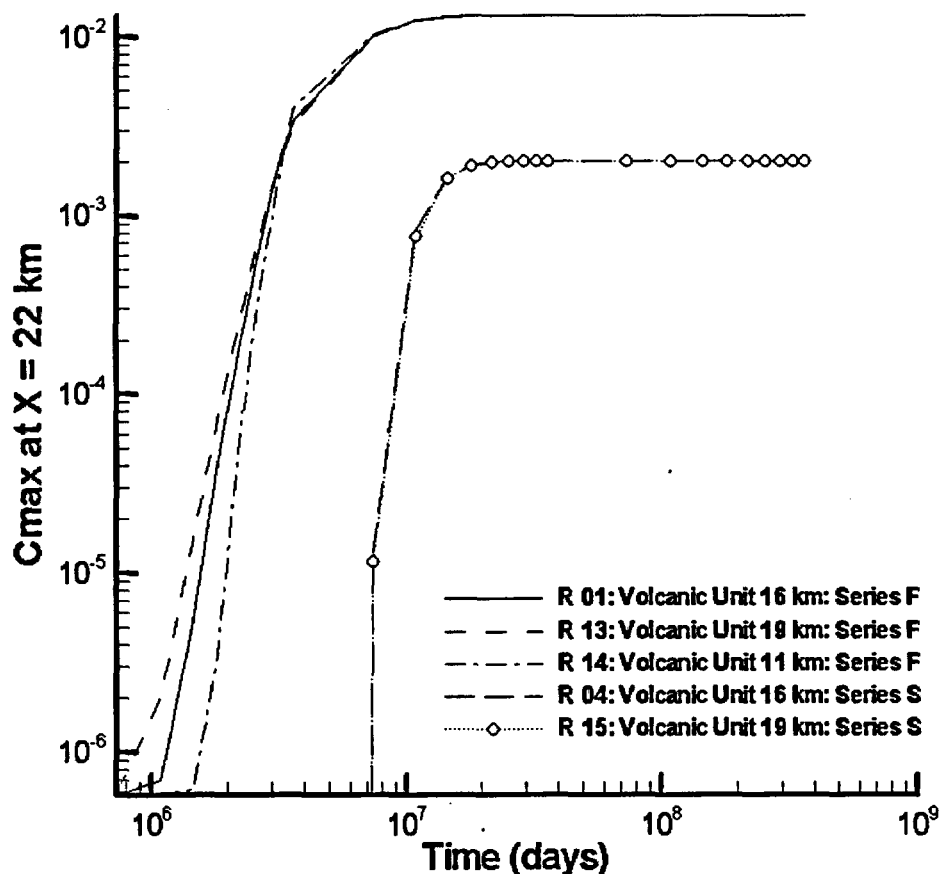


Figure 7-10
Time variation in the maximum concentration at the compliance boundary for Series F and S runs as a function of the length of the volcanic aquifer

7.5.5 Small Source Dispersion – Single Realization

It is well known that plume concentrations depend to a significant extent on source sizes. Most performance analyses to date have considered the source to be the same size as the repository footprint. However, with more robust containers being contemplated, it is possible that only a few containers might release radionuclides. This type of release will provide a source that is much smaller in size than the repository. The purpose of the following F Series runs is to assess how dispersion, particularly in the transverse direction, will reduce concentrations emanating from a small source during transport over a 20 km travel distance. In one case, the source was the size of the entire repository. In the other case (R 16), the source was 50 m by 50 m, representing a much more localized release.

Figure 7-11 shows a three-dimensional view of isoconcentration contours for the R 01: Series F plume at 1,000,000 years, which is steady state. Recall that for R01 the source dimensions are 700m (in the direction of flow) by 2500 m (perpendicular to flow). A unit source concentration provides a maximum concentration at the compliance boundary ($X=22000$ m) of 0.013, which is illustrated by the position of the 0.01 isosurface. At this time, the spreading front would be far

beyond 20 km. With a source concentration of 1.0 and the given source dimensions, there is a dilution for R 01 of about 75x between where the plume enters the SZ and 20 km. Figure 7-12 illustrates the comparable results for R 16 with the smaller (50 m x 50 m) source. The plume is illustrated using the same contour levels as in Figure 7-11. In this case, the plume is dramatically smaller and peak concentrations at the source are much lower, about 0.08 as opposed to 0.15 for the base case. Because the mass loading is provided by a third-type boundary, there is no requirement that concentrations in cells at the source be 1.0. For the small source case, the maximum concentration at the compliance boundary is reduced to a value less than the cutoff set in the IMARC code of 1×10^{-8} .

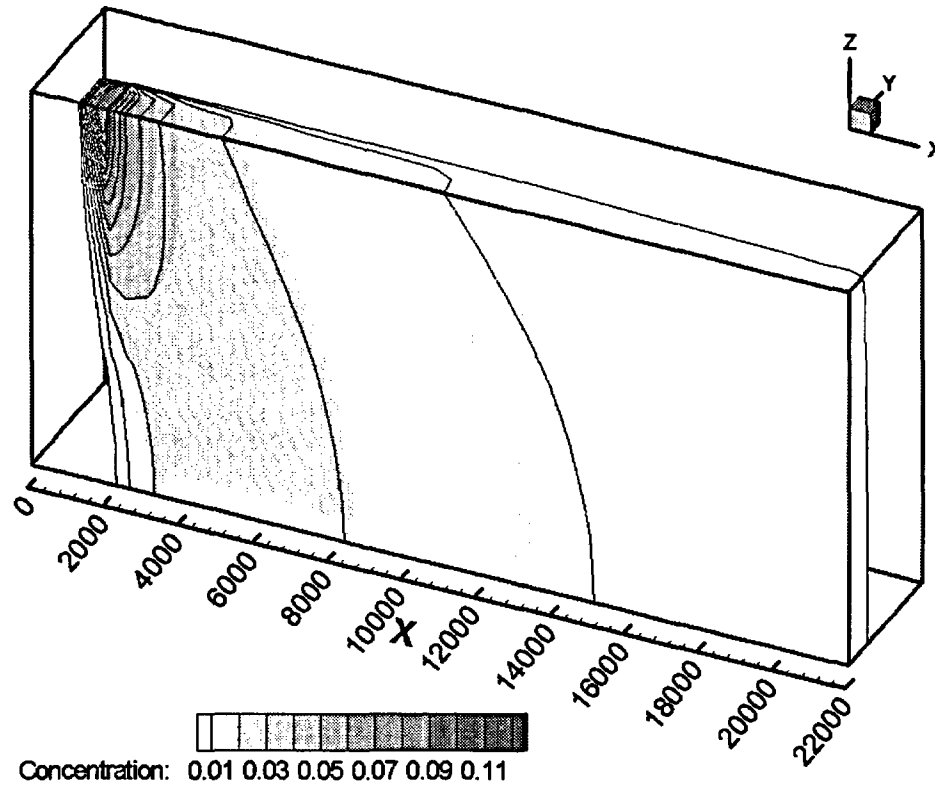


Figure 7-11
Isoconcentration contour for Run 01 Series F at $t=1,000,000$ years

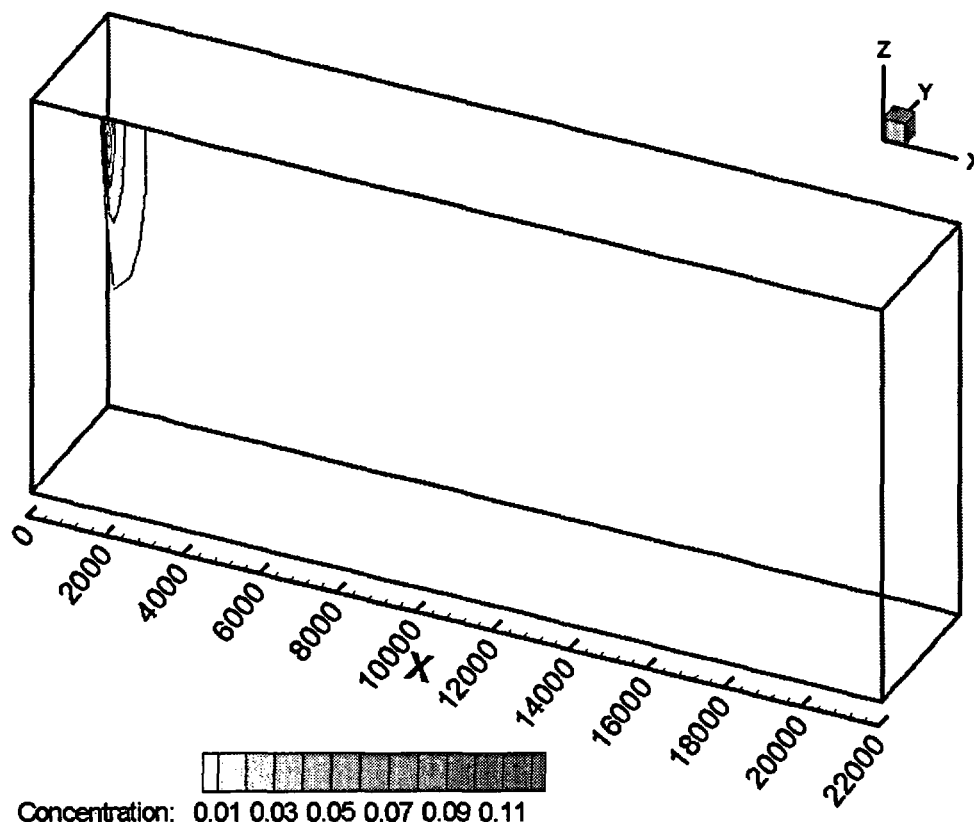


Figure 7-12
Isoconcentration contour for Run 16 with a 50 m x 50 m source at $t=1,000,000$ years

These results illustrate the importance of source size in controlling the contaminant concentrations. As the analyses in EPRI (1996, 1998) showed, the effectiveness of dispersion as an attenuation mechanism improves as the size of the source is reduced. When the source is the same size as the footprint of the repository, dispersion at best might provide several factors-of-ten concentration reductions. However, as the trials with R 16 show, more than five or more orders-of-magnitude in concentration reductions are possible with a smaller source. Thus, one of the indirect benefits of more robust containers is the likelihood of localized sources, which will enhance the performance of the geological system.

7.5.6 Changes in the Vertical Transverse Dispersion Coefficient

The selection of vertical transverse dispersivity values has been controversial. Some scientists think that a logical value of transverse, vertical dispersivity would be small, on the order of the coefficient of molecular diffusion. Other work (CRWMS, M&O, 2000e) indicates that larger values (0.2 to 2.4 m) are appropriate. Previous EPRI studies have argued that small dispersivity values apply to porous media and that values of vertical transverse dispersivity would be greater in fractured media. Thus, we still believe that transverse dispersivities on the order of 5 meters are appropriate for the fractured tuff rock in the Yucca Mountain vicinity. Analyses are presented here to illustrate how much the transverse vertical dispersivity value affects the transport of mass

within the SZ. The Series F parameter set is used for this purpose with vertical transverse dispersivities of 5.0, 0.5, and 0.1 m in Runs 01, 17, and 18, respectively.

Figure 7-13 shows the effect of changing the transverse vertical dispersivity on the maximum relative concentration at the compliance boundary (20 km). A reduction in the vertical transverse dispersivity does not change travel times significantly. More significantly, the steady-state peak concentration is only slightly higher with a smaller dispersivity, 0.018 as opposed to 0.015 for the base case.

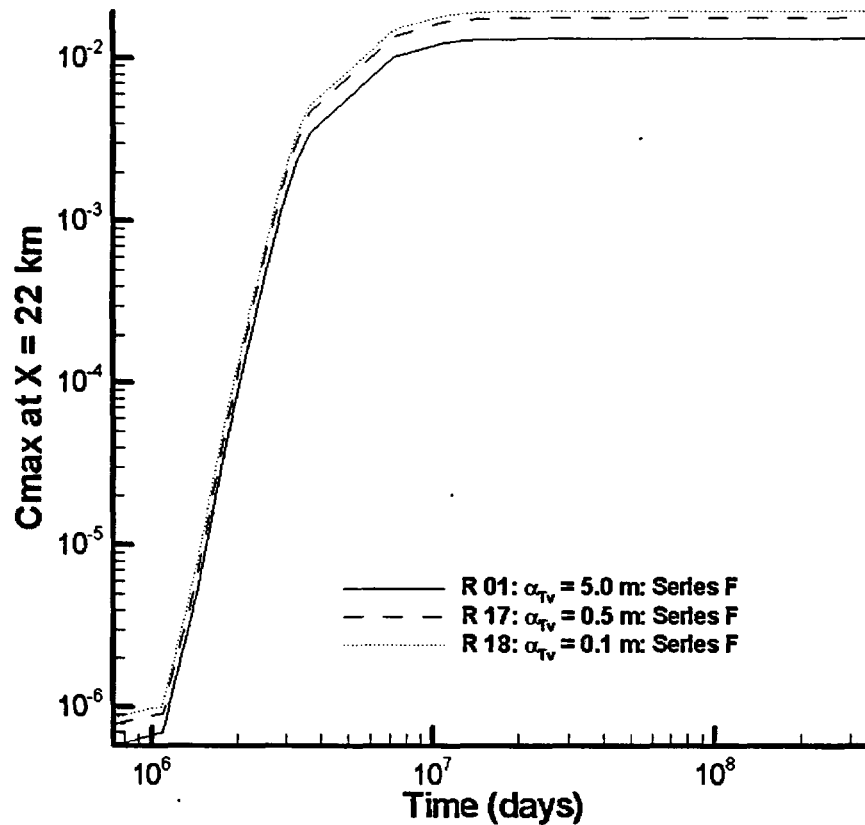


Figure 7-13
Sensitivity of maximum concentration at the compliance boundary to changes in the transverse vertical dispersivity

Figure 7-14 shows a three-dimensional view of the isoconcentration contours at a time of 1,000,000 years for R 17 with a transverse vertical component of dispersivity of 0.5 m, 10 times smaller than with R 01 shown in Figure 7-11. The plume is now much thinner in the vertical direction and the concentration for nodes adjacent to the mass inflow boundary is higher, 0.40 as opposed to 0.15 for the base case. Figure 7-15 shows isoconcentration contours at a time of 1,000,000 years for R 18 where the transverse vertical component of dispersivity was reduced to a value of 0.1, 50 times less than the base case. The plume is now even thinner in the vertical direction and the maximum concentration found for nodes in the vicinity of the mass-inflow boundary is higher, 0.69 as opposed to 0.15 for R 01. This result is expected given that a reduction in the dispersivity values provides a more concentrated, less disperse plume.

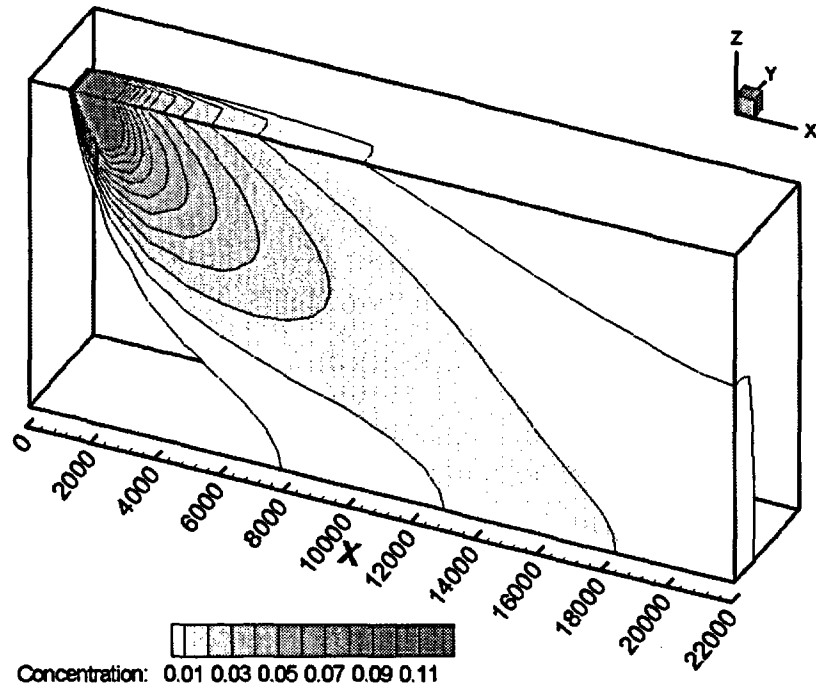


Figure 7-14
Isoconcentration contours at $t=1,000,000$ years for Run 17 Series F with a transverse vertical dispersivity of 0.5 m

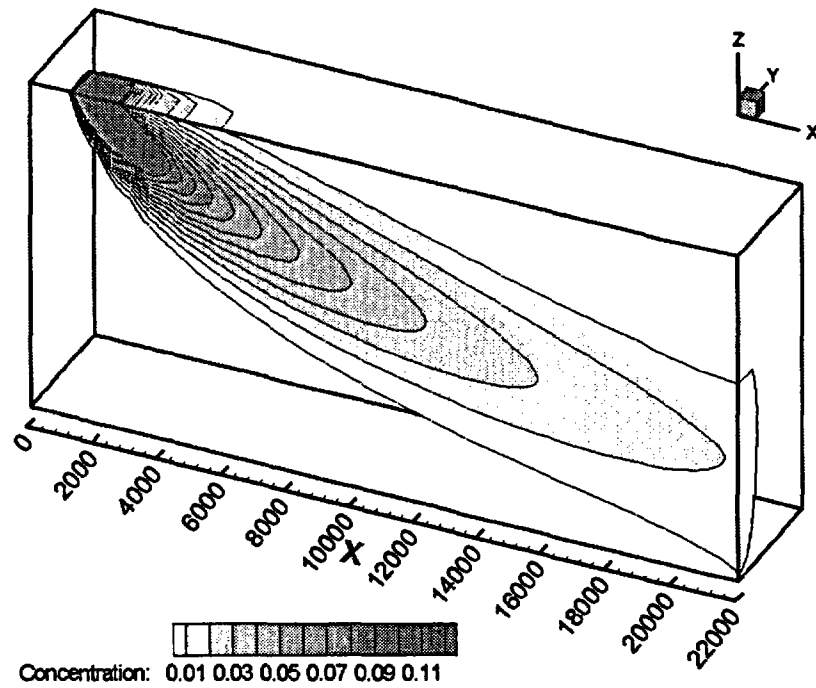


Figure 7-15
Isoconcentration contours at $t=1,000,000$ years for Run 18 Series F with a transverse vertical dispersivity of 0.1

The fact that vertical dispersion seems to be a relatively insensitive variable might be expected. The largest transverse dispersivity value is not particularly effective in mixing because the limited vertical extent of the simulation domain (200 m) constrains vertical spreading in this case. If the simulation domain had a greater z-dimension a greater difference among the simulation results would be evident.

These simulation trials show that the code is capable of incorporating small dispersivity values as necessary. However, to resolve the concentrations for such a small value of transverse vertical dispersivity, it was necessary to refine the mesh in the z-direction to meet the Peclet criteria (a function of dispersivity). For R 18, 135 rows of nodes were required in the z-direction. Runs 01 and 17 required 15 and 29 rows of nodes in the z-direction, respectively. This result is expected. While it is possible in the context of regional-flow simulations to provide accurate solutions for simulation trials with small, vertical transverse dispersivities, there is a significant computational burden. Most studies, however, end up avoiding 100,000+ node simulations.

7.5.7 Controls on Maximum Concentration

One of the obvious differences between the F and S Series of runs is in the maximum concentration values that were obtained. C_{\max} for the F Series of runs was approximately 1.4×10^{-2} . C_{\max} for the S series of runs was approximately 2.0×10^{-3} or about 7 times smaller (see, for example, Figure 7-9). It was not immediately obvious why this difference occurred. We examined this issue in detail by comparing concentration distributions for R 01 and R04 at long times when the concentration distribution was at steady state.

Figure 7-16 shows concentration profiles for R 01 and R 04 at 1,000,000 years, when this part of the plume was at steady-state. The concentration values were sampled at an elevation of 167 m (about 33 meters below ground surface). In each case, the mass loading on the SZ is the same. There are obvious differences in the simulated concentration profiles. With R 04: Series S, concentrations are high at the source and decrease markedly with distance. With R 01: Series F, concentrations are not as high at the source but decline less markedly with distance. There is apparently significant differences in the concentration distributions between the plumes. Plots of the 0.01 concentration isosurface make these differences more obvious (Figure 7-17). With the R 01: Series F parameters (Figure 7-17 upper), the 0.01 concentration isosurface extends to the outflow boundary on the right, whereas for Series S (Figure 7-17 lower) the isosurface extends only to about $X=14$ km.

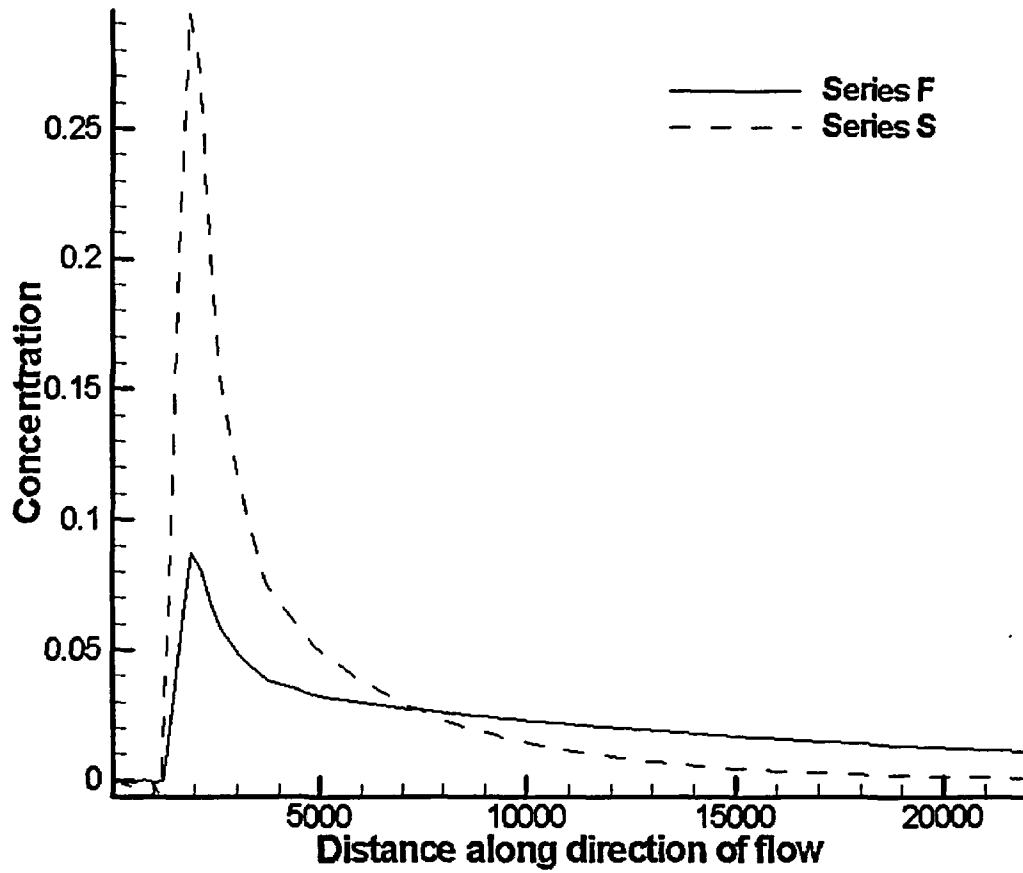


Figure 7-16
Relative concentration profiles for R 01: Series F and R 04: Series S at 1,000,000 years
down the flow system at 33 m below the top of the simulation domain

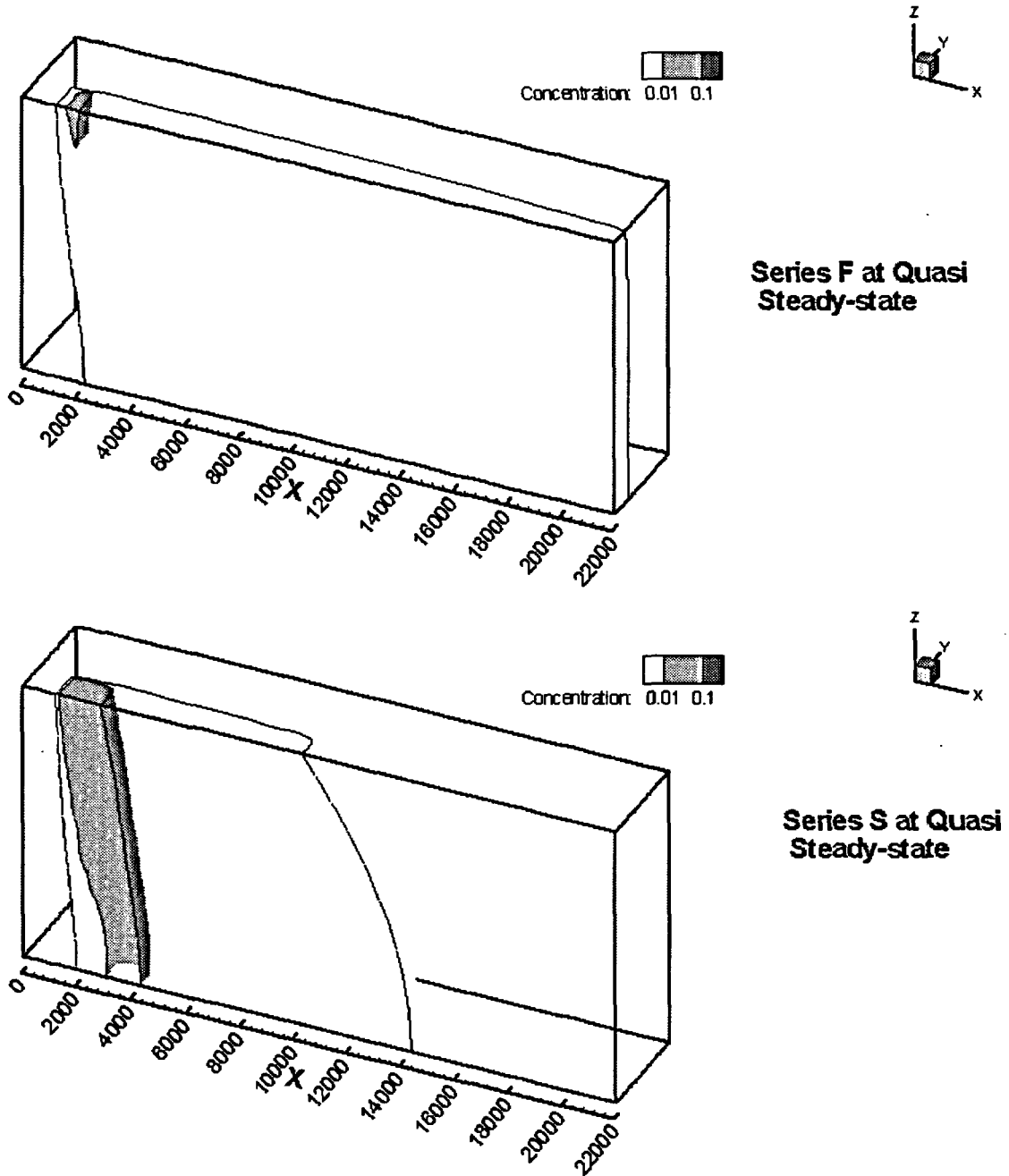


Figure 7-17
Three-dimensional plots of the 0.01 relative concentration isosurface at 1,000,000 years. The upper panel presents results for R 01: Series F. The lower panel presents results for R 04: Series S

The difference in the two concentration distributions is caused by a difference in the specific discharge at the vertical upstream boundary. Recall that water is provided to the simulation domain both through the upstream boundary as a specific discharge and recharge across the water table. With R 01 in Series F, the specific discharge is 0.60 m/yr. With R 04 in Series S, the specific discharge is 0.15 m/yr. This difference in the boundary condition changes the relative

proportions of inflows to the domain (inflow versus recharge). With the Series F trial approximately 10.2×10^5 m³/yr water flows in through the upstream boundary as compared to 7.7×10^5 m³/yr entering as recharge. In the Series S trial, three-times more water is provided from recharge (7.7×10^5 m³/yr) than from boundary fluxes (2.6×10^5 m³/yr). These changes impact the structure of the velocity field. For R 01, the average linear velocity in the x-direction increases from approximately 100 m/yr at the inflow boundary to approximately 175 m/yr at the compliance boundary. For R 04, the average linear velocity increases four times from about 25 m/yr to 100 m/yr. The vertical velocities with R 04 would be greater than with R 01.

Such changes to the velocity field are sufficient to produce differences in the plume architecture. These changes in plume shape contribute to differing C_{\max} values at the downstream compliance boundary.

7.6 Simulation Parameters for IMARC Runs

In subsequent chapters, simulation results are presented using IMARC. Generally, the parameter set for the SZ is the Series S parameters in Table 7-1 and the distribution coefficients presented in Table 7-2. The UZ, as in previous EPRI studies, is conceptualized in terms of four layers. The unsaturated flow parameters are summarized in EPRI (1998). Details of both the UZ and SZ flow and transport models, themselves, are also found in EPRI (1998).

7.7 Conservatism in the Concept of a Flowing Interval

The above sensitivity analysis showed that the extent to which the volcanic tuff portion of the SZ is able to impact mass spreading depends to an important extent on the size of the unfractured rock blocks. As the rock blocks become larger, matrix diffusion is reduced substantially (Figure 7-8). Presently, the Yucca Mountain Project conceptualizes the SZ in terms of flowing intervals with a mean spacing of approximately 19.5 m. As the simulation results showed, there is limited matrix diffusion with rock blocks of this size. The discussion in CRWMS, M&O (2000a) page 37 implies that this is the correct conceptualization and any analysis that involved *actual fracture spacings* would overestimate the effect of matrix diffusion.

This conceptualization is conservative and underestimates the impact of matrix diffusion for the following reasons. The definition of the flowing interval spacing (Figure 7-2) is itself nonconservative. The flowing-interval spacing needs to be specified as the actual thickness of the rock blocks between the flowing intervals. By moving from mid-point to midpoint of adjacent intervals, the spacings could end up being a factor of two or more larger than the intact rock blocks. In the example (Figure 7-2), all of the flowing interval spacings are larger than the intact rock between fracture zones. As is, this conceptualization would reduce the influence of matrix diffusion.

Assumptions concerning block size and the concepts related to the flowing interval can make a significant difference in terms of travel-time estimates. Our simulation experiments here (Figure 7-8) suggest that a less conservative conceptualization could lead to travel times an order-of-magnitude or more greater through the geologic system.

The concept of a flowing interval is a probably a reasonable picture of subsurface conditions. However, the way this concept is implemented in SZ modeling by the Yucca Mountain Project is overly conservative. Once there are several fractures in a flowing interval, any contaminants migrating in that interval will interact with the rock blocks present within that interval. These fractures would have spacings much less than the flowing interval spacings.

Likely, SZ transport occurs through a fractured medium with block sizes that are comparable to those in the UZ. Using actual fracture spacings would not overestimate matrix diffusion, as suggested in CRWMS, M&O (2000a) on page 37. There is little justification within the concept of a flowing interval to argue for large spacings and minimal matrix diffusion.

7.7.1 Implications

The existence of large non-flowing intervals in the SZ also has implications for the UZ. As presently implemented, there is one conceptualization for the UZ and a different one for the SZ. Pervasive fracturing in the UZ facilitates effective mass transport from the containers to the fracture network. In the SZ, the channelization model for transport (as it is presently implemented) expedites mass transport through the SZ. Thus, the most conservative model for each region has been selected at the expense of a consistent conceptual model for fractured tuff, in general. There is a need for a consistent view of fracturing to be developed for the UZ and SZ. If in fact, there are differences between the two systems, they need to be better explained.

The concept of a flowing interval for the SZ requires modification. At a minimum, the variable fracture-interval spacing needs to be defined more rigorously. More likely, the entire concept needs revisiting. First, the flowing interval needs to be considered to include more than one fracture. Transport through flowing intervals will likely be through sets of fractures with spacings less than flowing interval spacings and more similar to the actual fracture spacings. Second, if the fractured intervals are not correlated between holes, as Figure 7-3 would suggest, then it is likely that the fractured rocks in the SZ are much less permeable than current conceptualizations would suggest.

7.8 References

CRWMS, M&O, 2000a. Uncertainty Distribution for Stochastic Parameters. ANL-NBS-MD-000011. Las Vegas Nevada: CRWMS M&O.

CRWMS, M&O, 2000b. Probability Distribution for Flowing Interval Spacing. ANL-NBS-MD-000003. Las Vegas Nevada: CRWMS M&O.

CRWMS, M&O, 2000c. Input and Results of the Base Case Saturated Zone Flow and Transport Model for TSPA. ANL-NBS-HS-000030. Las Vegas Nevada: CRWMS M&O.

CRWMS, M&O, 2000d. Analysis Comparing Advective-Dispersive Transport Solution to Particle Tracking. ANL-NBS-HS-000001. Las Vegas Nevada: CRWMS M&O.

CRWMS, M&O, 2000e. Modeling Sub Gridblock Scale Dispersion in Three-Dimensional-Heterogeneous Fractured Media. ANL-NBS-HS-000022. Las Vegas Nevada: CRWMS M&O.

Czarnecki, J.B., C.C. Faunt, C.W. Gable, and G.A. Zyvoloski, 1997. Hydrogeology and Preliminary Finite-Element Ground-Water Flow Model of the Site Saturated Zone, Yucca Mountain, Nevada. U.S. Geological Survey, Milestone Report SP23NM3, 124 pp.

EPRI, 1996. Yucca Mountain Total System Performance Assessment, Phase 3. EPRI TR-107191, 3055-02, 17 Chapters.

EPRI, 1998. Alternative Approaches to Assessing the Performance and Suitability of Yucca Mountain for Spent Fuel Disposal. EPRI TR-108732, 18 Chapters.

Therrien R., Sudicky E.A., Three-dimensional analysis of variably-saturated flow and solute transport in discretely-fractured porous media, *J. Contaminant Hydrology*, 23(1-2) (1996) pp. 1-44.



8

BIOSPHERE

8.1 Introduction

It is likely that the quantitative measure of compliance for the candidate HLW repository at Yucca Mountain will be the “expected value” of dose to an average individual in a hypothetical group of highly exposed individuals termed a “critical group”. Doses or health risks to humans are only possible if the radionuclides released from the repository reach the biosphere. Potential exposure pathways in the biosphere can generally be classed into three broad categories: ingestion, inhalation, and external exposure. The actual pathway leading to exposure will be a function of many factors such as:

- Details of the assumed human behavior (e.g., where they live, what they do, what they eat and drink and where their food and water has been produced)
- Human physiology
- Radionuclide type
- The “geosphere/biosphere interface” (affects where and how radionuclides are transferred from the geosphere into the biosphere)
- A multitude of biosphere characteristics, many of which are similar to geosphere characteristics, but with many additional characteristics unique to the biosphere

For example, if it is assumed that the hypothetical critical group is engaged in agriculture where at least some of the water for irrigation is derived from contaminated groundwater, then possible exposure pathways via ingestion of contaminated agricultural products become numerous. Details of these factors that have been considered by EPRI in the past for Yucca Mountain TSPA were reported in Smith et al. [1996] and EPRI [1996].

8.2 Biosphere Model Used as Input to the IMARC-5 Calculations

The biosphere model used in these IMARC-5 analyses is the same as used in EPRI (1996), which was reported in full in Smith et al. (1996). The model is briefly summarized here.

For the purposes of the results of the dose calculations presented in this chapter, a farming “critical group” was considered. Data available in 1996 for values of dose per unit intake have been used [IAEA, 1994]. These take account of revisions to ICRP definitions of dose [ICRP, 1991], and other new recommendations on metabolism of the various elements. (ICRP sources available in 1996 for values of dose per unit intake, notably ICRP [1993])

and [1995], were not used since they only give ingestion data and then only for some of the relevant radionuclides.)

In deriving the above critical group information, the following assumptions have been made:

- the critical group consume only local produce derived exclusively from contaminated compartments;
- the components of the critical group's diet and life style are not extreme so doses received by members of the critical group should be summed across all relevant exposure pathways.

Dose conversion factors ($\text{Sv y}^{-1}/\text{mol y}^{-1}$) for peak total dose (summed over all pathways) and drinking water doses for unit flux of each radionuclide to the well are presented in Table 8-1. The factors can be used to convert radionuclide flux (mol y^{-1}) to a well derived from a groundwater transport code to annual individual doses to members of the assumed critical group. The conversion factors for a radionuclide includes the consequences arising from daughter in-growth in the biosphere, but not the consequences from the separate geosphere release of the daughters.

Care should be taken when analyzing and applying the conversion factors presented in Table 8-1. It must be remembered that they are only applicable to the biosphere and critical group described in EPRI [1996]. That is, they should only be applied to radionuclide concentrations in the groundwater entering the well (which is acting as the transfer agent between the geosphere and the biosphere). Applying the Table 8-1 values to radionuclide concentrations in groundwater at locations other than at the well would be inappropriate.

Table 8-2 presents information regarding the top three exposure pathways and the percentage contribution of each to the peak total dose. These results can be used to provide feedback concerning significant pathways and hence provide focus to further consideration of the validity of assumptions.

Table 8-1
Dose Conversion Factors for Unit Flux to the Well (from errata in Smith et al. [1996],
Table 5-20)

Flux to dose conversion factor (Sv y⁻¹/mol y⁻¹)

Radionuclide (1)	Total Dose	Drinking Water Dose
Se-79 ⁷	7.7E+1	1.4E-2
Nb-94	3.3E+1	2.5E-2
Tc-99	1.7E-2	9.0E-4
I-129	1.4E-2	2.1E-3
Cs-135	1.3E-2	2.6E-4
Pb-210	3.0E+5	2.6E+4
Po-210	2.9E+6	4.0E+5
Ra-226	7.3E+3	6.9E+1
Ra-228	8.0E+4	1.6E+4
Ac-227	9.7E+4	1.6E+4
Th-228	1.3E+5	2.6E+4
Th-229	1.1E+3	6.6E+1
Th-230	3.4E+2	8.6E-1
Th-232	1.1E-3	2.6E-5
Pa-231	5.1E+2	6.8E+0
Pa-233	2.1E+3	4.4E+2
U-233	1.9E+0	9.5E-2
U-234	9.4E-1	6.0E-2
U-235	3.2E-4	2.0E-5
U-236	3.5E-3	5.9E-4
U-238	2.8E-5	3.2E-6
Np-237	7.4E-2	1.6E-2
Pu-239	4.6E+1	3.1E+0
Pu-240	1.5E+2	1.2E+1
Pu-242	5.3E+0	1.9E-1
Am-243	1.5E+2	8.2E+0

Notes

(1) The contribution to dose from the in-growth of daughters in the biosphere is included in the factor given for the parent.

⁷ Editor's note: Since production of these dose conversions for Se-79, the half-life has been changed such that it is 20 times longer now. This should lower this dose conversion by a factor of 20, but should also increase the Se-79 inventory by a factor of 20. In IMARC-5 calculations, neither this dose conversion nor the inventory were updated. This should have no effect on results since the solubility of Se is relatively high.

Biosphere

Table 8-2
Top Three Exposure Pathways Contributing to Peak Total Dose (from errata in Smith et al. [1996], Table 5-21)

Radionuclide	Top Three Exposure Pathways	Percentage Contribution to Peak Total Dose
Se-79	Cow Liver	72.1
	Cow Meat	11.7
	Sheep Meat	3.53
	(Drinking Water)	(0.02)
Nb-94	External irradiation from soil	98.6
	Cow Milk	0.65
	Cow Meat	0.21
	(Drinking Water)	(0.1)
Tc-99	Fruit	30.2
	Root Vegetables	17.7
	Grain	14.8
	(Drinking Water)	(5.4)
I-129	Fruit	43.9
	Drinking Water	15.3
	Grain	13.7
Cs-135	Cow Meat	18.7
	Fruit	13.8
	Root Vegetables	10.7
	(Drinking Water)	(2.0)
Pb-210	Cow Liver	32.9
	Chicken Liver	24.3
	Fruit	20.4
	(Drinking Water)	(8.6)

Table 8-2
Top Three Exposure Pathways Contributing to Peak Total Dose (from errata in Smith et al. [1996], Table 5-21) (Continued)

Radionuclide	Top Three Exposure Pathways	Percentage Contribution to Peak Total Dose
Po-210	Chicken Liver	34.5
	Fruit	32.2
	Drinking Water	13.6
Ra-226	Chicken Liver	42.5
	Cow Liver	26.3
	Root Vegetables	5.83
	(Drinking Water)	(0.9)
Ra-228	Fruit	47.3
	Drinking Water	20.4
	Root Vegetables	10.8
Ac-227	Fruit	43.2
	Drinking Water	16.8
	Cow Liver	12.9
Th-228	Fruit	49.3
	Drinking Water	20.5
	Root Vegetables	11.7
Th-229	Inhalation of Dust	56.1
	Fruit	15.4
	Cow Liver	8.13
	(Drinking Water)	(6.1)
Th-230	Chicken Liver	40.8
	Cow Liver	25.3
	Inhalation of Dust	7.18
	(Drinking Water)	(0.3)

Table 8-2
Top Three Exposure Pathways Contributing to Peak Total Dose (from errata in Smith et al. [1996], Table 5-21) (Continued)

Radionuclide	Top Three Exposure Pathways	Percentage Contribution to Peak Total Dose
Th-232	Inhalation of Dust	40.1
	Fruit	11.1
	Root Vegetables	10.5
	(Drinking Water)	(2.4)
Pa-231	Inhalation of Dust	53.6
	Root Vegetables	12.5
	Fruit	10.1
	(Drinking Water)	(1.3)
Pa-233	Fruit	53.2
	Drinking Water	20.7
	Root Vegetables	11.9
U-233	Inhalation of Dust	62.0
	Fruit	13.1
	Cow Liver	6.16
	(Drinking Water)	(4.9)
U-234	Inhalation of Dust	29.9
	Chicken Liver	17.7
	Fruit	17.5
	(Drinking Water)	(6.4)
U-235	Inhalation of Dust	42.1
	Fruit	20.0
	Root Vegetables	10.9
	(Drinking Water)	(6.2)

Table 8-2
Top Three Exposure Pathways Contributing to Peak Total Dose (from errata in Smith et al.
[1996], Table 5-21) (Continued)

Radionuclide	Top Three Exposure Pathways	Percentage Contribution to Peak Total Dose
U-236	Fruit	43.2
	Inhalation of Dust	18.7
	Drinking Water	17.0
U-238	Inhalation of Dust	43.9
	Fruit	29.3
	Drinking Water	11.6
Np-237	Fruit	54.6
	Drinking Water	21.1
	Root Vegetables	12.3
Pu-239	Inhalation of Dust	57.2
	Fruit	17.5
	Cow Liver	8.91
	(Drinking Water)	(6.8)
Pu-240	Inhalation of Dust	53.5
	Fruit	20.1
	Cow Liver	8.84
	(Drinking Water)	(7.8)
Pu-242	Inhalation of Dust	76.5
	Fruit	9.39
	Cow Liver	5.10
	(Drinking Water)	(3.7)
Am-243	Inhalation of Dust	58.9
	Fruit	14.3
	Cow Liver	9.89
	(Drinking Water)	(5.5)

8.3 References

EPRI, 1996. Kessler, J., R. McGuire, J. Vlasity, A. Long, S. Childs, B. Ross, F. Schwartz, D. Bullen, M. Apted, W. Zhou, E. Sudicky, G. Smith, K. Coppersmith, J. Kemeny, and M. Sheridan, Yucca Mountain Total System Performance Assessment, Phase 3, EPRI TR-107191, Electric Power Research Institute, Palo Alto CA, December 1996.

IAEA, 1994. International Basic Safety Standards for Protection Against Ionising Radiation and for the Safety of Radiation Sources, Interim Edition. IAEA Safety Series 115-I, Vienna.

Smith et al., 1996. Smith, G., B. Watkins, R. Little, H. Jones, and A. Mortimer, Biosphere Modeling and Dose Assessment for Yucca Mountain, Electric Power Research Institute TR-107190, Palo Alto CA, December 1996.

9

VOLCANISM

9.1 Introduction

Over the past few years the repository design has improved to a point where volcanism has risen to one of the major contributors to the calculated release to the accessible environment. Very simply speaking, the scientific understanding of the natural and engineered barrier system has improved to the point where a very low probability event, such as a volcano is now a major contributor to the very small radionuclide release calculated. With this new importance, the debate over the anticipated type and frequency has increased between the US NRC and the US DOE. A Key Technical Issues (KTI) document has been generate to ensure all of the issues associated with volcanism are closed before waste receipt occurs. This chapter will review the differences some of the basic issues associated with volcanism. Further investigation is planned to support the Site Recommendation report, planned to be issued in mid to late 2001.

9.2 Magma Intrusion Scenario

Through the DOE and NRC interaction an agreed to magma intrusion scenario has been developed. The scenario notes that a magma dike intersects the drifts where the waste packages are emplaced. Three waste packages on either side of the dike fail and all of the radionuclides are now carried to the surface of the repository and blown out over the surface. The spent fuel is pulverized and is mixed with the volcanic material that is violently expelled.

9.3 Scenario Evaluation

The NRC has taken a very conservative approach to the development of the scenario. In fact the NRC has selected the worst attributes of each type of volcanic eruption and has applied them to the design basis scenario now in review. There are a number of issues that contribute to the scenario development, analog sites, magma composition, dike intrusion, dike geometry, dike contact temperature, dike pressure within the dike, rift-related eruptions, and eruption style. After the review of these items it will be clear that if a reasonable scenario where to be agreed upon, volcanism would not contribute to the already low release rate.

9.3.1 Analog Sites

The best analog scenario for basaltic dike intrusion and eruption within the Yucca Mountain Region should come from current environments that exhibit shallow crustal extension. Acceptable areas would include the flanks of large volcanoes such as Hawaii (Decker and

Wright, 1987) and Etna (Murray and Pullen, 1984) or regions of basaltic rift volcanism at divergent plate motions like Iceland (Hauksson, 1983; Bjornsson, 1985; Marquart and Jacoby, 1985) and the Afar (Ruegg et al., 1979). Areas of convergent plates along chains of cones formed by evolved magmas do not present good models and may perhaps be misleading. Many aspects of volcanism related to subducting plates are at odds with assumptions made about dike intrusion and formations scoria cone eruptions in the Yucca Mountain Region. For example, such eruptions, even of basaltic magma, are more violent than those of Hawaiian and Icelandic rift basalts. Because volcanism in rifting environments, in contrast to that at convergent plate margins, is the best models for future events at Yucca Mountain, Hawaii and Iceland (Rubin and Pollard, 1988) are the appropriate analog sites for basaltic eruptions in the Yucca Mountain Region.

9.3.2 Magma Composition

The likely composition of the intruded and extruded magma is that of a basalt. Typical analyses of basalt are given in Table 9-1.

Table 9-1
Chemical analyses of typical basalts (from Rogers and Hawkesworth, 2000)

	Tholeiitic basalt	Alkali basalt
Oxide	Wt %	Wt %
SiO ₂	48.77	47.52
TiO ₂	1.15	3.29
Al ₂ O ₃	15.90	15.95
Fe ₂ O ₃	1.33	3.16
FeO	8.62	8.91
MnO	0.17	0.19
MgO	9.67	5.18
CaO	11.16	8.96
Na ₂ O	2.43	3.56
K ₂ O	0.08	1.29
P ₂ O ₅	0.09	0.64
H ₂ O	0.30	1.16

From a qualitative view point, given the chemical makeup of the magma it can be noted that magma would not adversely affect the coupled processes present in the natural system and therefore is not anticipated to accelerate waste package nor the waste form corrosion characteristics significantly.

9.3.3 Dike Intrusion

Conceptual models for dike propagation, in-filling with magma, and eruption in rift settings provide important constraints for risk assessment at Yucca Mountain. Physical conditions of dike intrusion and eruption are well understood in Hawaii and Iceland and data from less studied areas like Etna and the Afar support the general model. Delaney and Pollard (1982) show that rapid injection is required to prevent freezing of relatively thin (0.5 to 5 m) dikes that extend over distances of 1 to 10 km. Spence and Turcotte (1985) demonstrate that for a 0.5-m wide basaltic dike the fracture propagation is about 1000 times faster than the magma flow within the dike. Thus they conclude that a propagating crack is a viable mechanism for the intrusion of magma in a dike. However, they conclude that magma viscosity is the key property that limits the fracture propagation and the fracture resistance of the elastic media (host rock) can be neglected.

The migration of seismic events allowed Moore and Krivoy (1964) to track the lateral dike propagation for the 1962 flank eruption of Kilauea with a velocity of 0.4 m/s. Using the same technique Jackson et al. (1975) estimate a dike velocity of 0.45 m/s for the 1968 east rift eruption. Once a dike is filled with magma near the surface it may erupt or it may freeze in place. Episodic influx of magma before complete solidification causes a dike to swell, producing a corresponding uplift of the overlying surface region. Conversely, an eruption will partially drain the dike leading to a surface deflation. Commonly such deflation is associated with normal faulting parallel to the dike and the formation of a shallow graben. The accurate measurement of surface deformation in erupting systems allows the geometry of the dike to be determined and the nature of fracture and flow in the subsurface to be understood. Such measurements associated with dike formation and surface eruption have been made at Hawaii, Etna, Iceland, and Afar.

Therefore the drifts where the waste packages are placed would not completely fill up with magma. With less magma in the drift the number of waste packages contacted by the magma is questionable. If the number of waste packages contacted by the magma were decreased then the probability of waste package failure would decrease and then the probability of the fuel mixing with the magma would decrease and then the probability of the magma reaching the surface and being expelled would also decrease. Thereby reducing the anticipated dose.

9.3.4 Dike Geometry

Hoffmann et al. (1990) used surface deformation measurements to model repeated dike intrusion and eruption associated with the Pu'u 'O'o eruption of Kilauea Volcano, Hawaii. The geometry of the model dike had a top at 0.4-km depth and a bottom at 2.9 km. The length was about 1.6 km and the width was 2.5-3.0 m. The average volumetric expansion of this dike during repose periods was about 500,000 m³, representing the influx of a new batch of magma. Delaney and Pollard (1982) made field and theoretical studies for such dike events and their subsequent eruptions. Rubin and Pollard (1987) give a theoretical basis for the propagation and geometry of dikes in the rift zones of Kilauea volcano and on Hawaii.

The scenario agreed to, assume a very large dike geometry which would allow the waste package emplacement drifts to fill up quickly with magma. If in fact there is a logical dike size it should

be included in the evaluation. Based on a Risk Informed methodology which is specified in the new Title 10 CR 63, the important parameters would be varied over the logical size distribution. Thereby reducing the probability of magma contact and reducing the anticipated radionuclides released.

9.3.5 Dike Contact Temperature

The AMR reviewing the waste package-magma contact temperature assumes that the contact temperature of the dike material and the containers will be at a very high temperature (1200 C). Turcotte and Schubert (1982) have considered the case of the cooling of a static dike. Using their equation (37) for 4 to 6 m-wide conduits, similar in scale to the drifts in the repository, would solidify in 10 to 20 days. However, cooling at the dike contact and solidification of the magma reduce the expected contact temperatures in the containers considerably. Delaney and Pollard (1982) show that the contact temperature at the wall of a basaltic dike would range from 50% to 60% of the initial magma temperature throughout the cooling history of the dike. They cite the lack of contact metamorphism observed at basaltic dike contacts as evidence for "a short duration of heat transfer and a small temperature increase in the wall rocks." They also calculate that a 2-m thick dike would completely solidify within a few hours. In Figure 9-1 below the calculated temperature profiles for a dike flowing at 1 m/s show a significant amount of solidification at the dike margin.

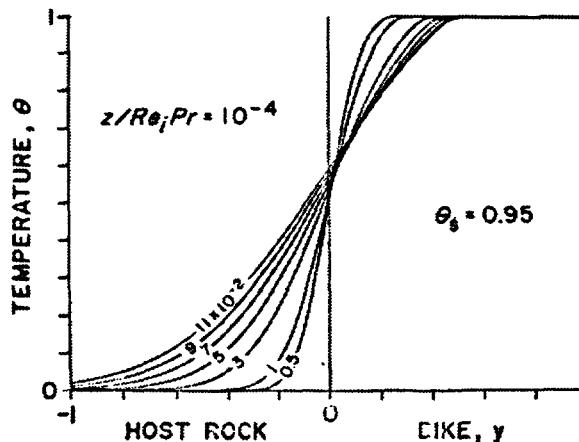


Figure 9-1
Temperature profiles across dikes and adjacent host rocks at various non-dimensional times. θ_s is the solidification temperature (fraction of temperature drop for solidification). Diagram from Delaney and Pollard (1982, p. 873)

If the reduced contact temperature were included in the release evaluation it would allow the waste package to act as a barrier and therefore reduce releases. At present, the contact temperature and force at which the magma is assumed to contact the waste packages are such that the waste packages fail on contact. With the temperatures associated with this data, the waste package probability of failure would be significantly reduced. This would lower the probability distribution for anticipated release to the environment. Looking at other natural analogs, the Hawaiian Islands, telephone poles, cars and other objects in the magma path are embedded in the magma, not melted.

9.3.6 Magma Pressure within the Dike

Turcotte and Schubert (1982) determined the driving pressures necessary to open cracks ranging in width between 1 mm and 10 m wide to be relatively low, in the range of 0.1-30 MPa. Because they consider the stress intensity factor (γ) to be zero they neglected the effect of crack propagation compared with the magma flow problem within the crack. They conclude that an injection pressure of 1 MPa is sufficient to supply magma for a 2.2 m wide dike that is 50 km long, neglecting the buoyancy factor. Hoffmann et al. (1990) calculated that the vent pressure of the Pu'u' 'O'o eruption of Kilauea Volcano increased by 0.38 MPa during repose periods.

Given these pressures it is not anticipated that the emplacement drift would fill very quickly or would the waste package have a significant relocation due to the magma intrusion.

9.3.7 Rift-Related Eruptions

The Pu'u' 'O'o eruption of Kilauea Volcano, Hawaii, being a long and well-studied event that includes repeated dike intrusions and eruptions (Rubin and Pollard, 1987), could be the preferred model for the next eruption in the Yucca Mountain Region. Here Parfitt and Wilson (1994) conclude that lava fountains erupt when the dikes system is wide and the flow rate is fast but gas pistoning with strombolian activity occurs when the rate is slow due to dike constrictions. They propose that the reduced width of the dike is due to local magma solidification. According to their model the pressure in the dike increases until the dike can expand to allow a rapid flow and renewed lava fountaining.

This section helps define the anticipated magma movement. From this, one can assume that the scenario developed by the DOE and NRC can be considered very conservative.

9.3.8 Eruption Style

Using Hawaiian or Icelandic basaltic volcanism as a model, the likely scenario for the next eruption in the Yucca Mountain Region might be a fissure opening with local lava fountains that rapidly focus ejection of pyroclasts into one or two main eruptive conduits. As a scoria cone builds above the conduit lava spreads around the base of the cones. The ratio of lava to scoria in the effusive products would be variable, but it likely would be about 50%. The explosive pulses would be episodic but the height of the general plume would be no more than a few hundred meters. Occasional bursts of dust could convectively rise to one or two km, but their deposits would be extremely thin. Beyond 10 km only a slight dust would accumulate. The 1965 eruption of Kilauea Iki would be a good model for the type event. A violent strombolian event (formerly called sub-plinian) would be an unlikely occurrence.

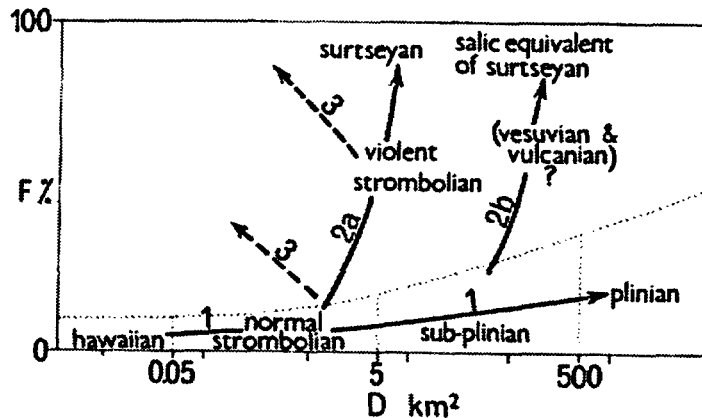


Figure 9-2
Fragmentation (F) vs. dispersal (D) for various types of explosive volcanic products.
 Diagram from Walker (1973). F represents the fraction of particles less than 1 mm where the deposit is 1/10 of its maximum thickness along the dispersal axis. D represents the area enclosed by an isopach line enclosing the area thicker than 1/100 of the maximum thickness.

Strombolian deposits are generally coarse having a median size of about 4 mm (Fisher, 1964; Sheridan, 1971; Walker, 1972). They are also characterized by a paucity of ash finer than 1 mm. Walker (1973) uses the low ash fraction (generally less than 10%) to characterize strombolian deposits and to differentiate them from other types such as plinian or violent strombolian (Figure 9-2).

Deposits from normal strombolian eruption are localized in the area proximal to the vent, extending only a few kilometers from the cone. These beds are rarely thick enough to measure at distances more than 5 kilometers. This is why Walker (1973) defined strombolian as the type cone-forming eruption. He contrasts this type of deposit to "sheet-forming" deposits that are associated with sub-plinian and plinian eruptions. Deposits from violent strombolian eruptions spread over a broader area ($D \sim 10 \text{ km}^2$) and are much more highly fragmented ($f \sim 50\%$) than normal strombolian beds. This type chosen by DOE for their expected event at Yucca Mountain does not represent the typical basaltic deposits that occur in the Yucca Mountain Region. Violent strombolian is a much more energetic type of eruption that would be expected. Such events are rare in extensional environments.

Given the technical information concerning the most probable eruption scenario, it is suggested that the DOE and the NRC revisit the agreed to scenario.

9.4 Conclusion

Having reviewed the different attributes associated with volcanism it is clear that the agreed to scenario, between DOE and NRC, may be considered conservative. Selectively choosing the most bounding attribute for each contributing affect may result in a non-realistic system resolution. Thereby, leading the DOE to implement design modifications that may effect the performance of the proposed repository in a negative fashion.

9.5 References

- Alidibirov, M. and Dingwell, D.B., 1996, Magma fragmentation by rapid decompression, *Nature*, 380:146-148.
- Bjornsson, A. 1985, Dynamics of crustal rifting in NE Iceland. *Journal of Geophysical Research*, 90:10151-10162.
- Decker, R.W., Wright, T.L., and Stauffer, P.H., editors, 1987, *Volcanism in Hawaii, U.S. Geological Survey Professional Paper 1350*.
- Delaney, P.T. and Pollard, D.D., 1982, Solidification of a basaltic magma during flow in a dike: *American Journal of Science*, 282:856-885.
- Fisher, R.V., 1964, Maximum size, median diameter, and sorting of tephra, *Journal of Geophysical Research*, 69:341-355.
- Gudmundsson, A., 1986, Possible effect of aspect ratios of magma chambers on eruption frequency, *Geology*, 14:991-994.
- Gudmundsson, A., 1987, Reply on "possible effect of aspect ratios of magma chambers on eruption frequency". *Geology*, 15:878-879.
- Hauksson, E., 1983, Episodic rifting and volcanism at Krafla in north Iceland: Growth of large ground fissures along the plate boundary. *Journal of Geophysical Research*, 88:626-636.
- Hoffmann, J.P., Ulrich, G.E., and Garcia, M.O., 1990, Horizontal ground deformation patterns and magma storage change during the Pu'u' 'O'o eruption of Kilauea Volcano, Hawaii, episodes 22-42. *Bulletin of Volcanology*, 52:522-531.
- Jackson, D.B., Swanson, D.A., Koyanagi, K.Y., and Wright, T.L., 1975, The August and October 1968 east rift eruptions of Kilauea Volcano, Hawaii. U.S. Geological Survey Prof. Paper 890, 33 pp.
- Kieffer, S.W., 1984, Factors governing the structure of volcanic jets, in *Explosive volcanism: inceptions, evolution, and hazards*, National Academy Press, p. 143-157.
- Mader, H.M., 1998, Conduit flow and fragmentation, in Gilbert, J.S. and Sparks, R.S.J., editors, *The physics of explosive volcanic eruptions*, Geological Society of London Special Publication no. 145, p. 51-71.
- Marquart, G. and Jacoby, W., 1985, On the mechanism of magma injection and plate divergence during the Krafla rifting episode in northeast Iceland. *Journal of Geophysical Research*, 90:10178-10192.
- Moore, J.G. and Krivoy, H.L., 1964, The 1962 flank eruption of Kilauea Volcano and structure of the east rift zone. *Journal of Geophysical Research*, 69:2033-2045.

- Murray, J.B. and Pullen, A.D., 1984, Three-dimensional model of the feeder conduit of the 1983 eruption of Mt. Etna Volcano, from ground deformation measurements. *Bulletin Volcanologique*, 47:1145-1163.
- Parfitt, E.A. and Wilson, L., 1994, The 1983-86 Pu'u 'O'o eruption of Kilauea Volcano, Hawaii: a study in dike geometry and eruption mechanisms for a long-lived eruption. *Journal of Volcanology and Geothermal Research*, 59:179-205.
- Rogers, N and Hawkesworth, C., 2000, Composition of magmas, in Sigurdsson, H., editor, *Encyclopedia of Volcanoes*, Academic Press, San Diego, p. 115-131.
- Rubin, A.M. and Pollard, D.D., 1987, Origin of blade-like dikes in volcanic rift zones, in Decker, R.W., Wright, T.L., and Stauffer, P.H., editors, *Volcanism in Hawaii*, U.S. Geological Survey Professional Paper 1350.
- Rubin, A.M. and Pollard, D.D., 1988, Dike-induced faulting in rift zones of Iceland and Afar. *Geology*, 16:423-417.
- Ruegg, J.C., Lepine, J.C., and Tarantola, A., 1979, Geodetic measurements associated with a seismo-volcanic crisis in Afar. *Geophysical Research Letters*, 6:817-820.
- Simkin, T. and Fiske, R.S., 1983, *Krakatoa 1883, The volcanic eruption and its effects*, Smithsonian Institution Press, 464 pp.
- Shaw, H.R., 1980, The fracture mechanism of magma transport from the mantle to the surface, in. Hargrove, A.R.B., editor, *Physics of Magmatic Processes*, Princeton University Press, Princeton, NJ. pp. 201-264.
- Sheridan, M.F., 1971, Particle-size characteristics of pyroclastic tuffs, *Journal of Geophysical Research*, 76:5627-5634.
- Spence, D.A. and Turcotte, D.L., 1985, Magma-driven propagation of cracks, *Journal of Geophysical Research*, 90:575-580.
- Turcotte, D.L. and Schubert, G., 1982, *Geodynamics*, John Wiley, New York.
- Vergnoille, S. and Mangan, M., 2000, Hawaiian and strombolian eruptions, in Sigurdsson, H., editor, *Encyclopedia of Volcanoes*, Academic Press, San Diego, p. 447-462.
- Wallace, P. and Anderson, A.T., 2000, Volatiles in magmas, in Sigurdsson, H., editor, *Encyclopedia of Volcanoes*, Academic Press, San Diego, p. 149-160.
- Walker, G.P.L., 1972, Characteristics of some basaltic pyroclasts, *Bulletin Volcanologique*, 35:303-317.
- Walker, G.P.L., 1973, Explosive volcanic eruptions - a new classification scheme, *Geol. Rundschau*, 62:431-446.

10

IMPLEMENTATION OF SUBSYSTEM MODELS INTO THE IMARC-5 CODE

10.1 Introduction

The methodology used to calculate distributions of radionuclide concentration and dose follow that used in previous EPRI studies (e.g. EPRI, 1998). The methodology is based on a “logic tree” approach that represents uncertainties in parameters and models with nodes and branches, each branch representing an alternative parameter or model and its credibility. Each end branch of the tree then represents a set of assumptions, models and parameters for which concentrations and doses can be calculated. The weight assigned to each calculation is the product of weights of the branches leading to that end branch. The *distribution* of concentrations and doses can be derived from the family of calculations, each with its calculated weight.

As will be shown below, there are very few branches in the current IMARC tree. The IMARC code in its present form represents a very high-level analysis tool, rather than a performance assessment code that carries along the full range of individual parameter uncertainties down to the lowest level. A very large degree of abstraction has gone into the production of the present version of IMARC, as has been described in previous chapters, and will be briefly summarized below. For example, many of the inputs to the assumptions being investigated have uncertainties already embedded into them – the failure curves for the drip shields, containers and cladding being the prime example of this.⁹ This is why container failure alternatives no longer appear in the IMARC logic tree. Alternative climate scenarios have been eliminated in IMARC-5, as well, for the reasons provided in Section 2.5.

The present version of the code is being used here to understand the dose impacts of a variety of assumptions about general system behavior. While the results are still probabilistic, there is no attempt to illustrate the extremes of consequences for the very lowest probabilities. Rather, the focus has been to capture the means of distributions. This does not imply that the extremes of the distributions have been neglected. Rather, they have been incorporated mostly indirectly in the results.

⁹ See Chapter 5 for a description of how uncertainties in EBS failure were incorporated into the failure distribution curves.

10.2 Discussion of the Implementation

The logic tree used in the current application (IMARC-5) consists of four nodes representing infiltration, focused flow factor, solubility/alteration time, and retardation. These nodes result in 54 different end branch combinations, and the structure of the logic tree is illustrated in Figure 10-1. Input values of infiltration rate, focused flow factor, solubility and alteration rate, and retardation for each radionuclide are summarized below and are documented in previous Sections.

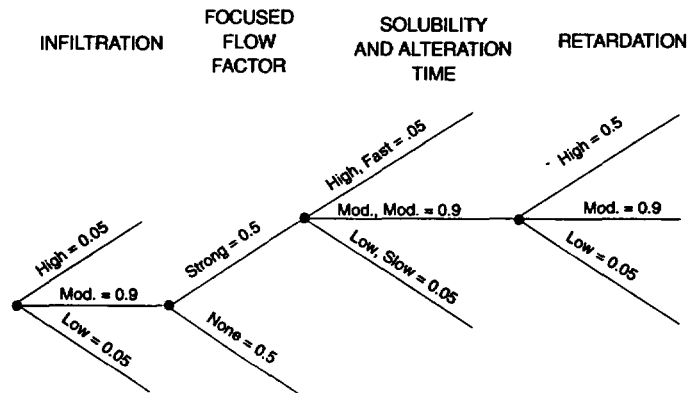


Figure 10-1
Logic tree for IMARC-5. Example connections are shown here for simplicity. There are 54 branches in total

Future Climate Change and Net Infiltration

Low, moderate, and high estimates of the average net infiltration are estimated for three different climate periods: the greenhouse climate, the interglacial climate, and the full glacial maximum climate. The greenhouse and interglacial climates are expected to last 1000 years each. The onset of the full glacial climate occurs in year 2000 (after present), and this climate continues for the remainder of the million year analysis. As might be expected, the first two climates have very little effect on the current dose calculations, especially given the robust container design being considered. These climates continue to be modeled in the event of possible future refinement of the climate node. Listed below are the infiltration rate branches (in mm/yr) for each of the climate periods.

	<u>Low</u>	<u>Moderate</u>	<u>High</u>
Greenhouse:	1.9	11.3	19.2
Interglacial:	1.11	7.2	9.6
Full glacial maximum:	6.8	19.6	35.4

Focused Flow Factors

There are two equally weighted scenarios of flow focusing in the full logic tree. The first presumes that no focusing occurs and that the average percolation flux is uniform throughout the repository. The second suggests that a strong focusing of 22 times the average percolation flux occurs in 4.5% of the repository while the remainder of the repository stays dry.

Solubility and Alteration Rate

Solubilities for each radionuclide are listed in Table 10-1 and are discussed fully in Section 6. Alteration rates continue to be linked to the solubility branches with fast alteration time corresponding to high solubilities and slow alteration rates to low solubilities. This is appropriate because, with a few exceptions, the dissolution of each nuclide into water is governed by either the solubility or the alteration rate, but not both. The estimated alteration rates have been reduced considerably from previous applications, ranging now from 1,000 years (0.05 probability) to 5,000 years (0.05 probability) with a 3,000 year median value.¹⁰

Table 10-1
Solubility limits employed in IMARC-5 (adapted from Table 6-7)

Element	Solubility Values (moles/liter)		
	Low (5% Probability)	Median (90% Probability)	High (5% Probability)
Se	1E-03	1E-02	7E+00
Tc	1E-08	1E-03	1E+01
Cs	9E-06	3E-03	1E-02
I	3E+00	1E+01	2E+01
Pb	5E-09	5E-06	5E-05
Ra	1E-10	1E-06	1E-05
Ac	1E-10	1E-09	3E-06
Th	1E-10	3E-09	1E-06
Pa	6E-07	3E-05	6.5E-04
U	1E-05	4E-05	5E-04
Np	6E-07	3E-05	6.5E-04
Pu	1E-10	2E-08	1E-06
Am	1E-10	1E-09	3E-06

Matrix Retardation

The four layer unsaturated zone retardation values remain unchanged from our previous (EPRI, 1998) study, IMARC-4. However, the saturated zone volcanic tuff retardation values were updated. The extension of the compliance boundary to 20 km also necessitated the addition of alluvium retardation values. A complete listing of all K_d is given in Table 10-2.

¹⁰ These three values of alteration time differ slightly from those described in Section 6. The alteration times were adjusted to be multiples of 1,000 years since IMARC-5 has time steps of 1,000 years at the earliest times.

Table 10-2
Kd values for sorption onto tuff and alluvium in the saturated zone

Radionuclide	K_{dv} (volcanics) (mL/g)	$K_{dv} \times \rho_b$ (dimensionless)	$K_{da} \times c$ (alluv.) (mL/g)	$K_{da} \times \rho_b \times c$ (dimensionless)
Np	0.5	0.97	9.2	12
I	0.0	0.0	0.24	0.31
U	2.0	3.9	2.0	2.6
Tc	0.0	0.0	0.22	0.28
C	0.0	0.0	0.0	0.0
Am, Pu, Pa, Th	50	97	25.5	32
Cs, Sr	25	49	12.8	16
Se	2.0	3.9	2.0	2.6

ρ_{bv} (volcanic tuff density) = 1.94 g/cm³

ρ_{ba} (alluvium density) = 1.27 g/cm³

Of course, in addition to the logic tree variables many other models and parameters must be specified in order to conduct a PA analysis. The following is a description of how the most critical of these models are abstracted into IMARC.

Waste Container Failures

In IMARC-5, three barriers must now all have failed before water is assumed to be able to contact the waste form itself. The titanium drip shield must first fail before flowing groundwater is assumed to be able to contact the waste package below.¹¹ Corrosion processes requiring flowing groundwater are assumed to start on the waste package surface once the drip shield has failed.

A third barrier has been added to IMARC for the first time – cladding. Although a small amount of cladding is assumed failed at the time of emplacement, a failure model for the bulk of the intact cladding has been adopted that requires the presence of water. Thus, part of the spent fuel waste form is assumed to be exposed to water immediately after the waste package has failed. The remainder of the cladding fails over time once water is present.

The waste container failure model is represented by two failure curves. The first assumes that the drip shield has failed on emplacement; this curve is assigned a 0.0001 fraction of all drip shields. The second scenario, applying to a 0.9999 fraction, infers an intact drip shield upon emplacement and represents failure of the waste containers after the drip shield has failed. Container failure is not dependent on the thermal history of the repository. Temperature had little effect on failure curves and was therefore neglected in order to simplify the analysis.

¹¹ Humid air corrosion of the waste package is assumed to start when the relative humidity is high enough whether or not the drip shield above the package is failed.

Waste packages fail by general corrosion and are assumed to be continuously dripped on, once the drip shield has failed. Source is initially released from the repository once more than 0.001 of a container fails. The time when this occurs depends on the fraction of the repository that is wet, which in turn depends on infiltration and flow focusing scenarios. The earliest release (7,000 years) occurs for the high infiltration/no-flow-focusing cases. Most other scenarios do not begin releasing until the 20,000 to 30,000 year range. The low infiltration/no-flow-focusing cases never produce a source since no dripping water is anticipated for these scenarios and diffusive transport is not considered for these calculations.

Fractions of Repository 'Wet'

The fraction of the containers above which liquid water is assumed to be dripping into the drifts is referred to as the fraction 'wet'. We have assumed that no release can occur without active dripping.¹² The fraction of the repository assumed 'wet' was taken from OCRWM (2000). A summary of the fractions wet is included as Table 10-3. These fractions depend on the degree of flow focusing (see Chapter 4 for a discussion of focusing) and the infiltration rate. Climate conditions are included in the table but have a negligible effect on the fraction wet since the now-simplified climate model anticipates the onset of a continuous glacial period after the first 2000 years. Thermal conditions are expected to persist for the first 1000 years. During this time the repository is assumed to be dry.

Table 10-3
Fractions of Waste Packages that are Wet

Un-focused Flow Area = 1.00 F = 1 prob. 0.50		Low	Base	High
	Thermal	0 (0)	0 (0)	0 (0)
	Current	0 (1.1)	0 (7.2)	0 (9.6)
	Glacial	0 (6.8)	0.04 (19.6)	0.14 (35.4)

Strong Focused Flow Area = 0.045 F = 22 Prob. 0.50		Low	Base	High
	Thermal	0 (0)	0 (0)	0 (0)
	Current	0.08 (24)	0 (158)	0 (211)
	Glacial	0 (150)	0.86 (431)	1.00 (779)

De-Focused Flow	Area = 0.955	F = 0	- Dry
-----------------	--------------	-------	-------

(#) - local percolation flux, mm/yr

¹² This is an optimistic assumption listed below in Table 10-4. A sensitivity study for diffusion-only release is presented elsewhere to investigate the degree of optimism.

Source Term

Radionuclides in the source are released immediately after the container fails. All of the water dripping on a failed waste package is allowed to enter the container and hence made available for waste dissolution. The amount of available water was estimated by interpolation of Table 11 in OCRWM [2000]: "Uncertainty in Seepage Parameters as Function of Percolation". Upon exiting the container the waste is mixed with all of the water flowing through the repository before being transported through the unsaturated zone.

Repository Configuration

The dimensions of the repository for the current analysis are 700 m in length by 2500 m in width. To simplify analysis, the repository was oriented so that its width is perpendicular to flow. On average about 4% of the repository is considered wet, with wet areas occurring in isolated locations. Since the UZ flow model used in IMARC-5 is one-dimensional, a series of vertical columns through the UZ were defined to accommodate alternatives to the fraction of the repository cross-sectional area considered wet. In order to represent widely dispersed failed containers, these columns were allowed to extend over the entire 2500 meter width of the repository (see Figure 10-2). This orientation is optimistic at early times when the possibility exists for a single container to fail directly upstream from an abstracting well. As modeled, the plume from a single container will be dispersed over the 2500 meter-wide column, making the dose to the average member of the critical group from that single container failure lower than it should be.¹³ Over longer periods of time when multiple failures are occurring over the entire repository, and when maximum concentrations and doses are calculated, representing failures over the entire width is reasonable.

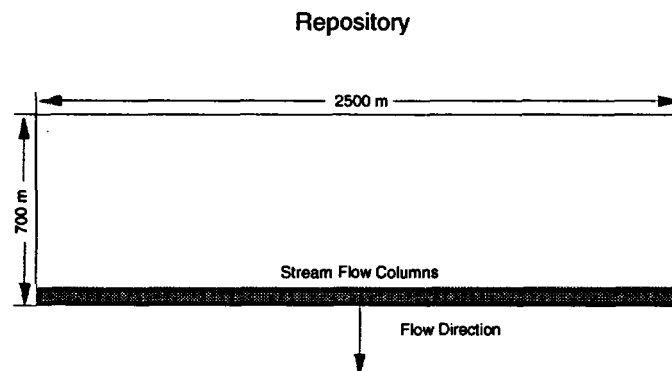


Figure 10-2
Configuration of the vertical flow columns through the unsaturated zone

¹³ Arguments were presented in Chapter 7 and in EPRI [1998] that suggest the degree of optimism is actually not all that large.

Conservatism and Optimisms in the IMARC-5 Code

While we have attempted to use 'best estimate' values and uncertainty distributions wherever possible, some necessary simplifications have resulted in the adoption of many conservatisms (model and parameter choices that tend to overestimate the dose rates) and a few optimisms (model and parameter choices that tend to underestimate the dose rates). These are listed in Appendix A. In general, it is felt that the conservatisms adopted in IMARC-5 outweigh the optimisms such that the overall estimate of the mean dose rates are not likely to be higher than those estimated using IMARC-5.

10.3 References

EPRI (1998). "Alternative Approaches to Assessing the Performance and Suitability of Yucca Mountain for Spent Fuel Disposal," EPRI TR-108732, Electric Power Research Institute, Palo Alto CA, November 1998.

OCRWM (2000). Document ANL-NBS-MD-000005, "Abstraction of Drift Seepage."



11

IMARC-5 RESULTS AND SENSITIVITY STUDIES

Performance assessments use calculations of radionuclide release and dose to evaluate a repository's performance, using several formats. The calculations presented in this Section concentrate on estimating dose to the average member of a critical group located 20 km downstream from the repository boundary (i.e. 20 km from the edge of the "accessible environment"). Most of these results and sensitivity studies are presented as doses to a maximally exposed individual for transport pathways considering water as the only means of ingestion; others present results for all pathways to ingestion.

11.1 Results Using All IMARC Branches

The first set of results is for calculations made using all 54 branches of the logic tree. Figure 11-1 is the annual dose contributed by the seven radionuclides that contribute the most to dose from all exposure pathways considered in the biosphere model – the "base case". This figure shows the annual dose from the drinking water pathway only. The general character of the dose curves shown in Figure 11-1 is as follows: ^{99}Tc , ^{237}Np , and ^{129}I dominate drinking water doses at the earliest times because they are available in adequate inventories, dose conversion factors are relatively high, and they are not significantly retarded in geologic units during transport.¹⁴ It was necessary to have the vertical axis on this plot start at an extremely small annual dose to show even the earliest breakthrough at 20 km before 100,000 years. This very long delay is caused by the very long combined lifetime of the engineered barriers considered in this model: the drip shield, container, and cladding. Delay is also caused by the relatively long travel times through the unsaturated zone (UZ) and the saturated zone (SZ). Peak annual drinking water doses occur at about 500,000 years and are on the order of 10^2 mrem – a very small fraction of the local natural background dose rates. Peak annual drinking water doses are dominated by ^{237}Np , ^{229}Th , and, to a lesser degree, ^{233}U .

¹⁴ In this case, retardation would have to cause delays of several tens of thousands of years to be noticeable on this log-log plot. Later sensitivities will show that retardation does occur for neptunium, but not over such long time scales.

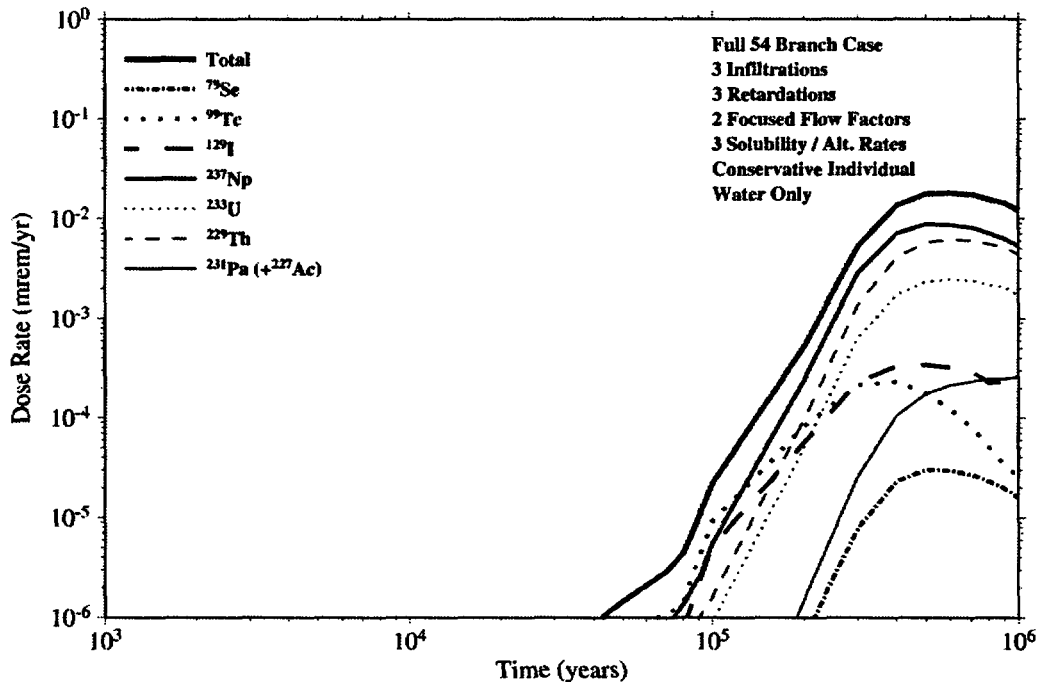


Figure 11-1
Expected Value of Annual Dose Versus Time 20 km Downstream, Drinking Water Pathway Dose Only

The IMARC5 “base case” results are significantly different from that calculated two years ago in IMARC-4 [EPRI, 1998, Figure 9-2]. Peak dose rates are significantly lower, there is now only one peak instead of multiple peaks, and the time of the peak is now somewhat earlier than the highest peak calculated in 1998. There are many reasons for these results, which will be illustrated further in subsequent sensitivity analyses. There are probably two major contributions to the lowering of the peak. We have assumed releases are spread out further across the width of the repository in the direction perpendicular to the flow direction in the saturated zone (SZ). This causes more dilution. A second contribution to a lower peak is that the container failure rate is lower than before. This means there are less containers contributing to release from the engineered barrier system (EBS) at any one time.

Figure 11-1 shows only one peak when there were three peaks in the results two years ago. One reason for this is because there is no early release due to failed EBS barriers at the time of repository closure. This change is a result of the major revision in the repository design DOE has made since 1998, as well as the incorporation of a new cladding degradation model in IMARC. Incorporation of a drip shield design in addition, to a more corrosion-resistant container design, means that one has to assume both the drip shield AND the container beneath it have both somehow failed shortly after emplacement. The likelihood of this combination now seems remote since both barriers are placed independently. Since both barriers are also designed to withstand a design basis rockfall event, and no geochemical conditions or thermal conditions are expected to exist that will fail both early, we considered early failure of both the drip shield and container *at the same location* to be negligible. Thus, the initial dose peak in the first 10,000 years we calculated two years ago has been eliminated.

The time of peak arrival in these, most recent calculations, is earlier than as was calculated two years ago. This is despite the fact that the location of our dose estimates two years ago was at 5 km whereas now it is at 20 km. The main reason why the peak is now occurring earlier is that we have lowered our estimate of sorption onto the SZ rocks from two years ago for many of the radionuclides contributing to this peak. This is based on new sorption data generated by the M&O in the intervening two years. Thus, the travel times through the SZ for these radionuclides is now estimated to be lower.¹⁵

Figure 11-2 shows the same "base case" annual dose versus time, but for all exposure pathways, not just the drinking water pathway as shown in Figure 11-1. When all pathways are considered, the peak annual dose to an individual in the critical group is calculated to be between 0.1 and 1 millirem – about 20 times higher than the peak annual dose from the drinking water pathway only. The major contributors to peak dose for all exposure pathways has also changed compared to those for just the drinking water pathway. The primary contributor is now ⁷⁹Se, followed in order by ²²⁹Th, ²³³U, and then ²³⁷Np. However, the dose contribution from ⁷⁹Se is only about a factor of four or five higher than that of ²³⁷Np.

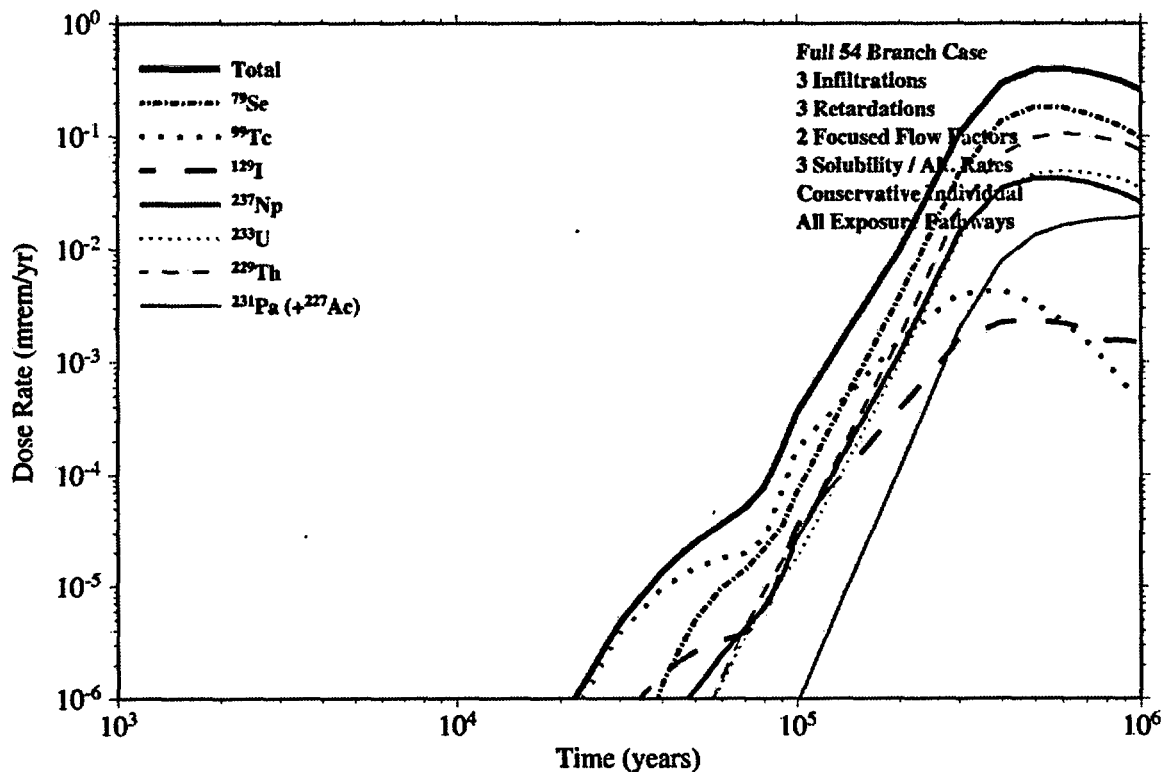


Figure 11-2
Expected Value of Annual Dose Versus Time 20 km Downstream, All Exposure Pathways Included

¹⁵ As will be shown later, we do not mean to imply radionuclide travel times through the SZ are negligible. They are still quite significant compared to the proposed regulatory period of compliance of 10,000 years.

This shift in primary contributors for all exposure pathways (compared to the radionuclides contributing the most to just the drinking water dose) is not surprising. These radionuclides have only a small portion of the dose contribution from the drinking water pathway. For example, the dose contribution for ^{79}Se from the non drinking water pathways is estimated to be about 5000 times that for the drinking water pathway alone [EPRI, 1996].¹⁶ One major reason ^{79}Se now dominates the dose is that the half-life for ^{79}Se has been updated based on newly available data. The new half-life is about 20 times longer than the older value. This means that, over the course of the 1,000,000-year modeling run there is no longer significant decay of ^{79}Se . With the lower half-life used two years ago, the ^{79}Se peak height was somewhat suppressed by radioactive decay.

It should be remembered that, like all of our radionuclide-specific dose conversion factors used, they are based on the assumptions made about the critical group and the models and parameters selected in the biosphere analysis [EPRI, 1996]. As an example, for ^{79}Se about 72% of the total dose is due to the consumption of cow liver. The estimate of this contribution is based on the annual consumption of 5 kg of cow liver, along with the host of parameters and assumptions in the biosphere model having to do with ^{79}Se concentration in the cow liver relative to uptake of all the other radionuclides in the array of exposure media. Furthermore, some conservative parameter values have been used for some of the radionuclides when estimating dose conversions that may have resulted in a conservative value for the ^{79}Se dose conversion factor [EPRI, 1996].

The logic tree format facilitates sensitivity studies on uncertainties included directly into the IMARC logic tree. Figures 11-3 through 11-9 explore the individual sensitivities to each of the sets of IMARC branches for ^{99}Tc and ^{237}Np . Figure 11-3 shows the sensitivity to the infiltration rate of individual dose due to ^{99}Tc from the drinking water pathway. Roughly only a factor of three to four in annual dose can be seen between the 'high' and 'low' infiltration rates. For the Full Glacial Maximum climate, the climate in effect at the time of radionuclide release from the engineered barrier system (EBS), the 'high' average infiltration (35.4 mm/yr) is about five times the 'low' average infiltration rate (6.8 mm/yr). Thus, the dose rate for ^{99}Tc seems only somewhat sensitive to infiltration rate – something that would be expected for a relatively high solubility species like Tc that would be more dependent on the alteration rate of the spent fuel waste form. The little dependence on infiltration rate may be the result of the 'low' solubility branch for Tc, since the 'low' Tc solubility value assumed is lower than even the 'low' Np solubility. Figure 11-4 shows the same sensitivity for ^{237}Np . In the case of ^{237}Np a somewhat greater sensitivity to infiltration rate can be seen at early times, somewhat more than an order of magnitude difference in the doses from the 'high' to 'low' infiltration rates. The fact that the sensitivity is more pronounced for Np than for Tc may be due to its generally lower solubility limits. It may be that at the lower infiltration rates, Np is somewhat solubility-limited whereas the release of Tc is likely to be governed by the alteration rate of the spent fuel.

¹⁶ The dose contribution for all exposure pathways for ^{229}Th , and ^{233}U is, respectively, about 17 times and 20 times that of the drinking water pathway alone.

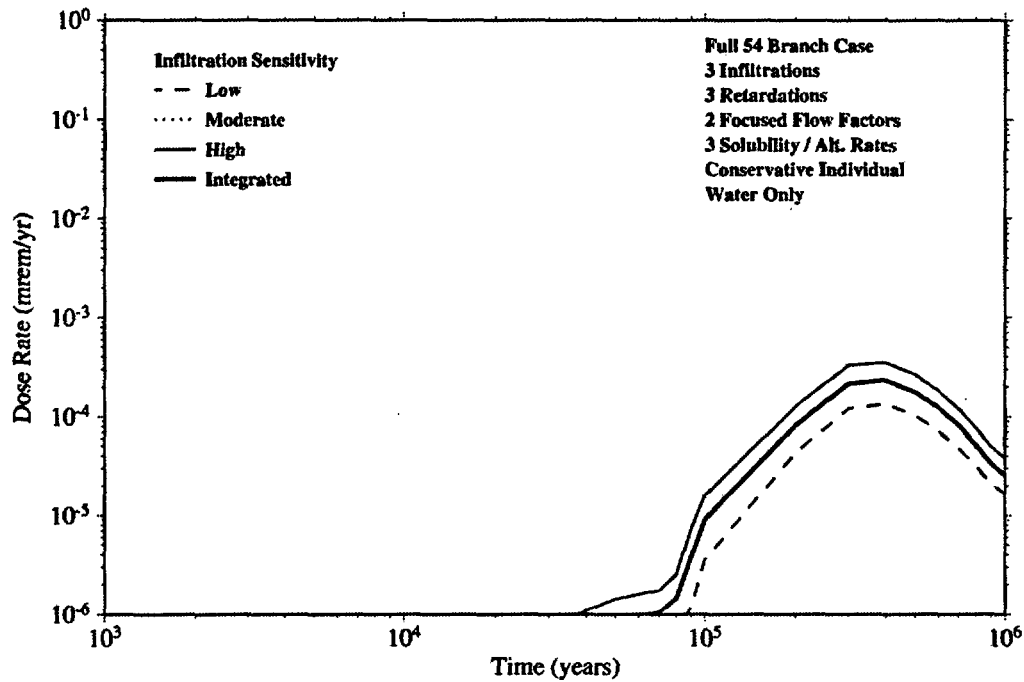


Figure 11-3
 Sensitivity of the Annual Drinking Water Dose from ⁹⁹Tc to Infiltration Rate

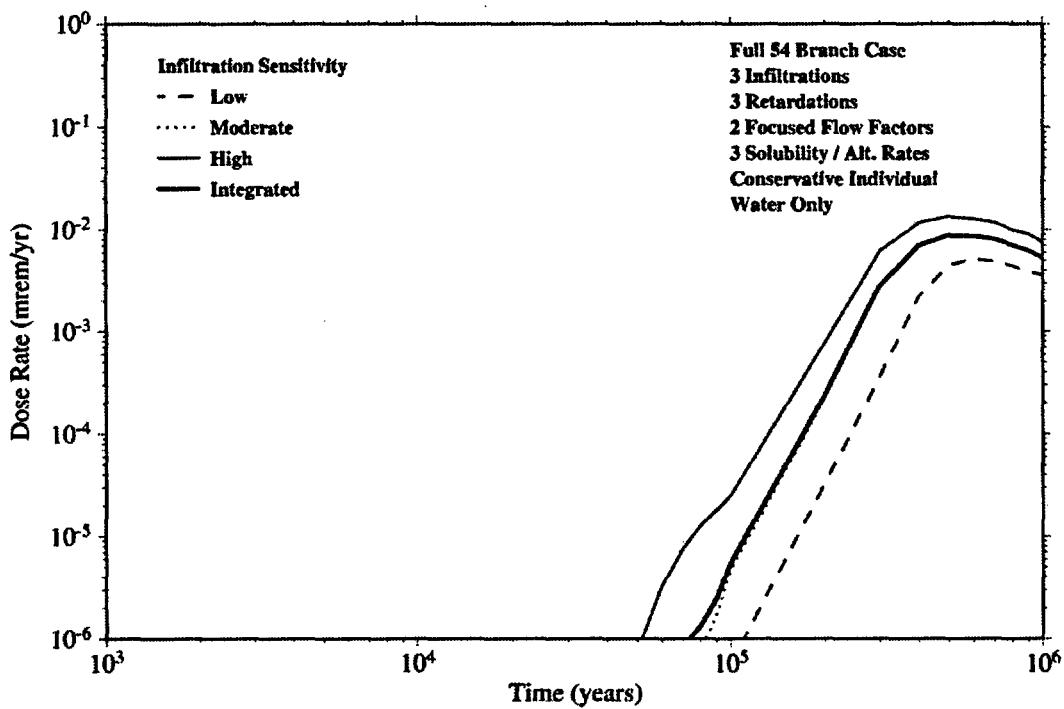


Figure 11-4
 Sensitivity of the Annual Drinking Water Dose from ²³⁷Np to Infiltration Rate

Figures 11-5 and 11-6 are the annual drinking water dose sensitivities from ^{99}Tc and ^{237}Np , respectively, due to variations in the focused flow factor. There is only a slight difference between the two cases. This is not surprising since the dose rates are highly dependent on the fraction of the repository that is 'wet'. In the no flow focusing case (focused flow factor of 1) it is assumed that, on average only 4% of the repository is 'wet' for the moderate infiltration scenario. This is conceptualized in IMARC as the probability of dripping for a given percolation rate. For no flow focusing the percolation rate is assumed equal to the net infiltration rate. For the case of focused flow with a flow focusing factor of 22, only $1/22^{\text{nd}}$ (4.5%) of the repository is assumed to have active flow within the region such that the average percolation rate in this active flow region is 22 times the average infiltration rate. For this higher percolation rate it is assumed about 86% of the containers would be dripped on such that, once again, about 4% of the entire repository is 'wet' for the moderate infiltration scenario. Thus, roughly the same number of locations are getting dripped on in both cases. The difference would be in the flow rates through each 'wet' region with the flow rate in the focused flow 'wet' region being 22 times that of the unfocused flow 'wet' region. This should give rise to slightly faster travel times through the UZ, but the travel time change is small enough such that it is not really seen well on this log-log plot. It is conceivable that if some other focused flow factor was used – perhaps an intermediate value – a larger difference would have occurred if the fraction wet were increased.

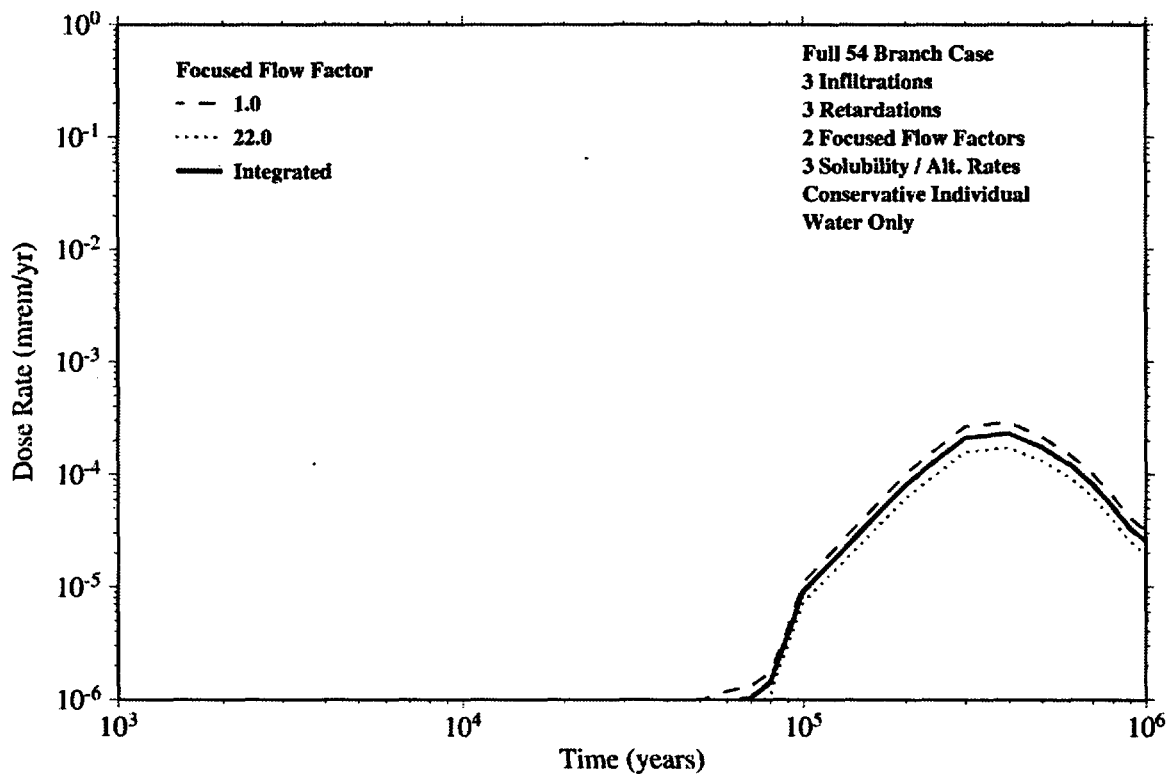


Figure 11-5
 Sensitivity of the Annual Drinking Water Dose from ^{99}Tc to the Focused Flow Factor

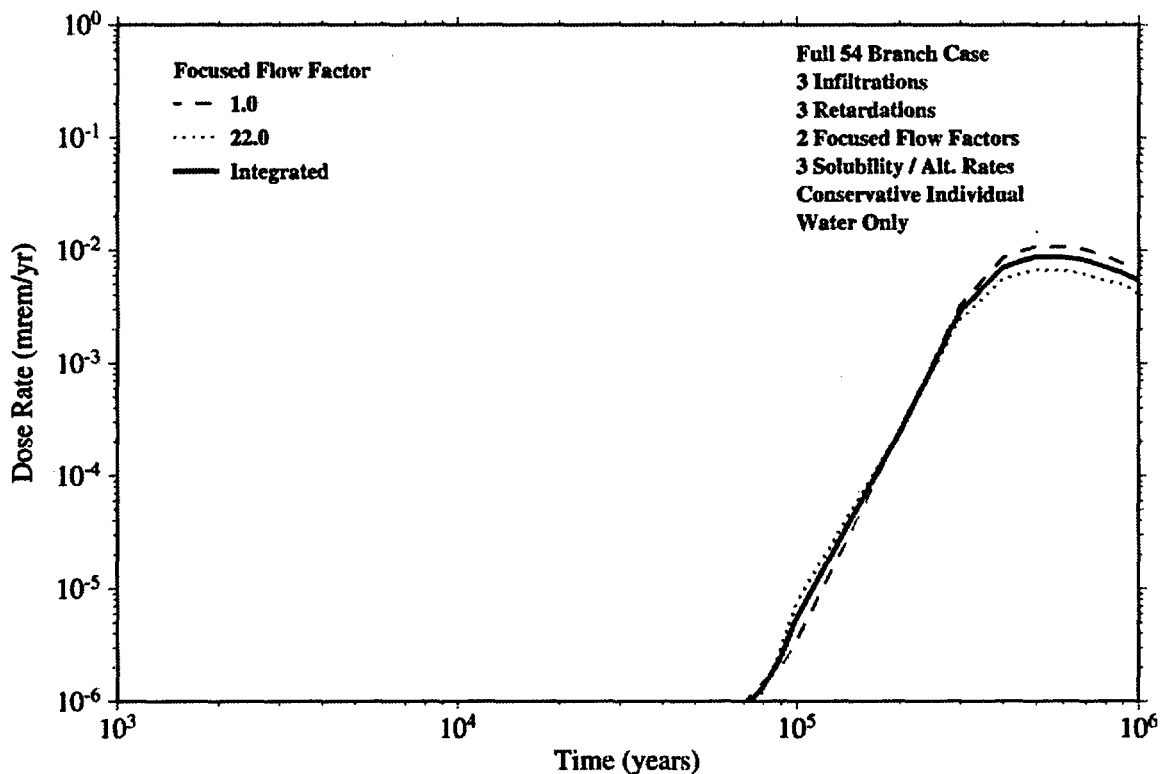


Figure 11-6
Sensitivity of the Annual Drinking Water Dose from ^{237}Np to the Focused Flow Factor

Figures 11-7 and 11-8 are the annual drinking water dose sensitivities from ^{99}Tc and ^{237}Np , respectively, due to variations in solubility and spent fuel matrix alteration time. Figure 11-7 shows the sensitivity of the annual dose to the 'low' Tc solubility/alteration time branch. As mentioned above, this is due to the fact that the 'low' Tc solubility value (10^{-8} moles/liter) is five orders of magnitude lower than the 'moderate' value. For this 'low' Tc solubility value, Tc is clearly much more solubility-limited than at the higher solubilities (where it is more alteration rate-limited). The sensitivity to solubility/alteration rate for Np is much less pronounced than for Tc. This is due to a much smaller range of solubilities for Np from the 'low' to the 'high' (only three orders of magnitude compared to nine orders of magnitude between the 'low' and 'high' Tc solubility). This suggests it would be useful to narrow the uncertainty range on Tc solubility further.

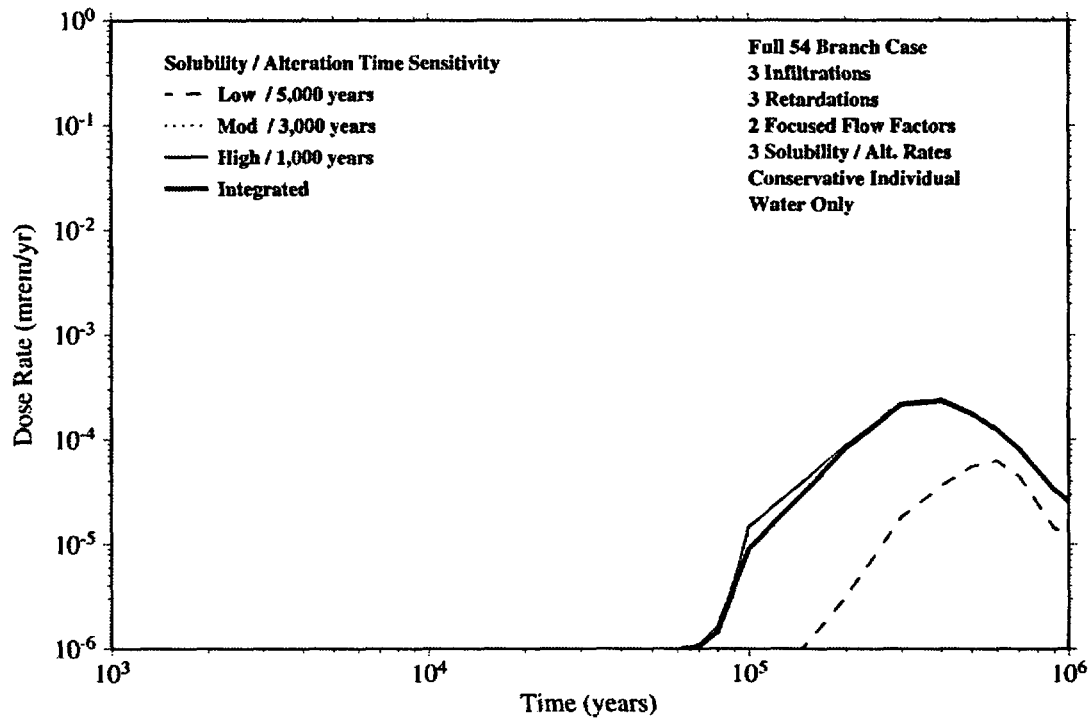


Figure 11-7
Sensitivity of the Annual Drinking Water Dose from ⁹⁹Tc to Solubility and Spent Fuel Matrix Alteration Time

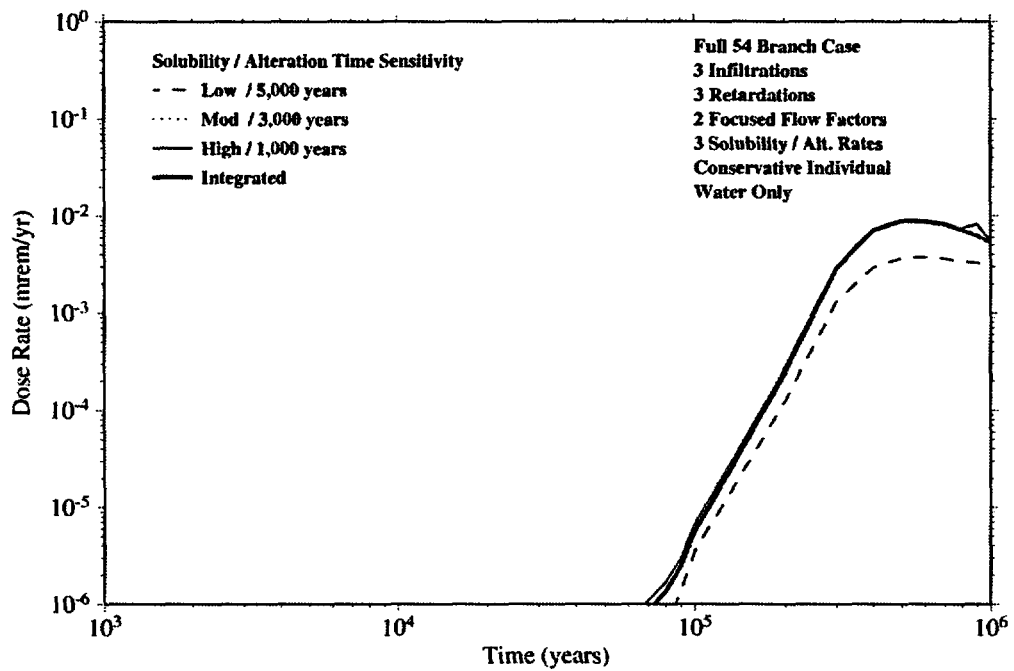


Figure 11-8
Sensitivity of the Annual Drinking Water Dose from ²³⁷Np to Solubility and Spent Fuel Matrix Alteration Time

The sensitivity to annual drinking water dose from ^{237}Np due to matrix retardation in the SZ is shown in Figure 11-9. In this case the time of the peak dose arrival varies by several hundred thousand years between the 'low' and 'high' matrix retardation case. This suggests that narrowing the uncertainty range on Np sorption may be of some use in narrowing the time of peak arrival – assuming one is interested in peak arrivals at times more than ten times beyond the likely period of regulatory compliance. Essentially no sensitivity of Tc to matrix retardation is noted since Tc has zero or near zero K_d 's on tuff matrix materials.

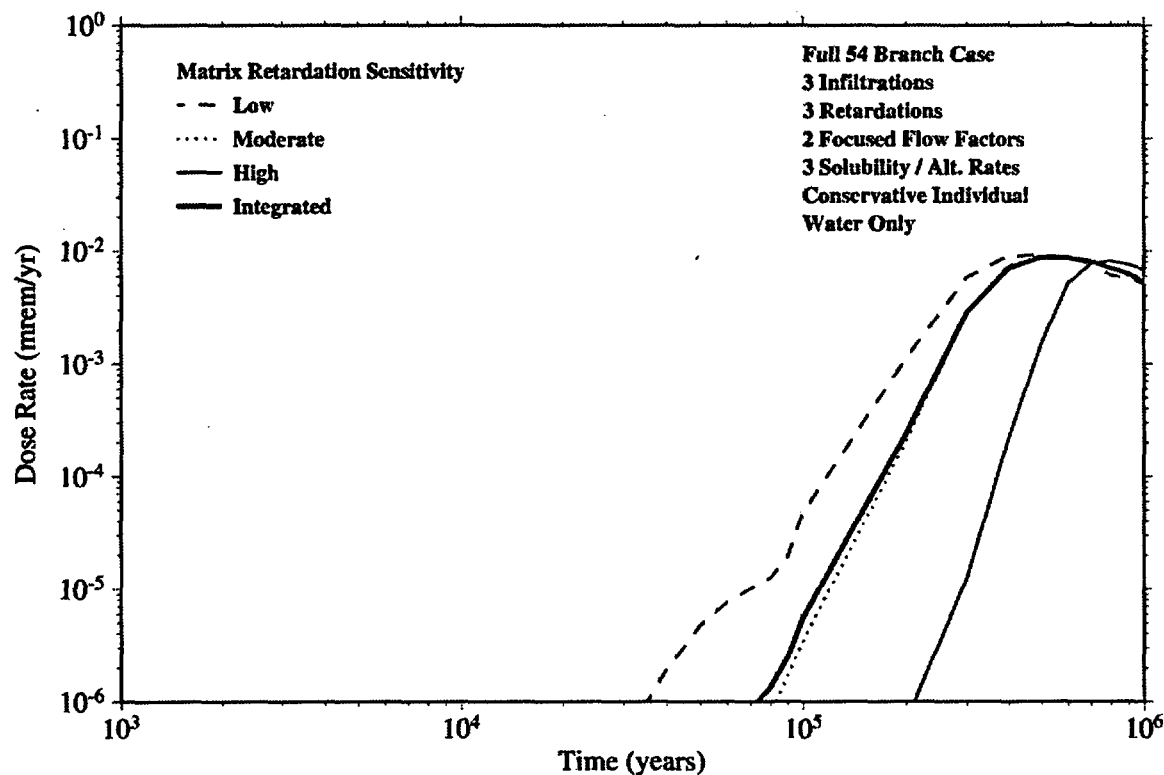


Figure 11-9
Sensitivity of the Annual Drinking Water Dose from ^{237}Np to Saturated Zone Matrix Retardation

11.2 Sensitivity Studies Involving a Single Branch

In addition to the sensitivity of calculated doses to alternatives in the logic tree calculations, it is instructive to examine the effect on doses of alternative assumptions to other input parameters. This allows for some additional combinations of effects that were and were not included directly into the IMARC logic tree.

Figure 11-10 shows the sensitivity of total annual drinking water dose for the eight radionuclides shown in Figure 11-1 to the assumed orientation of 'wet' zone in the repository. Since the UZ flow and transport model is 1-D, a vertical UZ 'source' column with these horizontal dimensions is what is employed in IMARC-5. The solid curve is the "base case" orientation where the 'wet' zone is assumed to span the entire 2500 meter width of the repository in the direction

perpendicular to flow in the SZ, but is only 28 meters long in the direction of SZ flow (see Figure 10-2).¹⁷ This sort of span would be appropriate at times where containers have failed throughout the repository such that the source term entering the UZ was well dispersed. The dashed curve in Figure 11-10 is for a source region of the same area as the solid curve, but is 100 meters wide (perpendicular to the SZ flow direction) by 700 meters long (in the SZ flow direction). One would expect a more compact plume with length and width dimensions more equal to each other to spread less in the SZ, which should cause higher concentrations, hence higher annual doses. Indeed this is observed. What may appear surprising is that changing the dimension in the direction perpendicular to SZ flow by a factor of 25 only changes the annual dose estimate by a factor of about three. This is because there is a sufficient amount of horizontal transverse dispersion occurring across the plume as it travels the 20 km downstream distance. For the IMARC-5 base case, horizontal and vertical transverse dispersivities of 5 meters have been adopted (see Chapter 7 for justification). This is high enough to significantly disperse a 100 meter-wide source such that there is less difference in the concentration at 20 km between the two significantly different source regions. It may be that some other intermediate source dimension would give a still higher concentration (and dose) at 20 km than the two source dimensions chosen in this sensitivity study. Yet, at the time of peak dose, one would expect container failures spread across the entire width of the repository such that it seems reasonable to use as the 'base case' the source region spanning the repository.

At earlier times when only a handful of containers are likely to be leaking assuming the radionuclides from these few containers were spread out across the entire width of the repository would be optimistic. That is, IMARC-5 would be overestimating the amount of dilution occurring in the UZ. However, EPRI conducted sensitivity studies on dispersion versus source dimensions and found that significant dilution in the SZ from a very small source representative of a single container failure is to be expected. This contrasts with the much smaller amount of additional dilution in the SZ from a UZ source size that already spans 2500 meters, such that the total amount of dilution due to spreading of the plume between the repository horizon, through the UZ, and 20 km downstream in the SZ may be not significantly different than for the smaller initial source size.

¹⁷ The 28 meter 'wet' zone dimension was chosen to represent about 4% of the repository dimension in the direction of SZ flow since about 4% of the repository is assumed 'wet' in most cases.

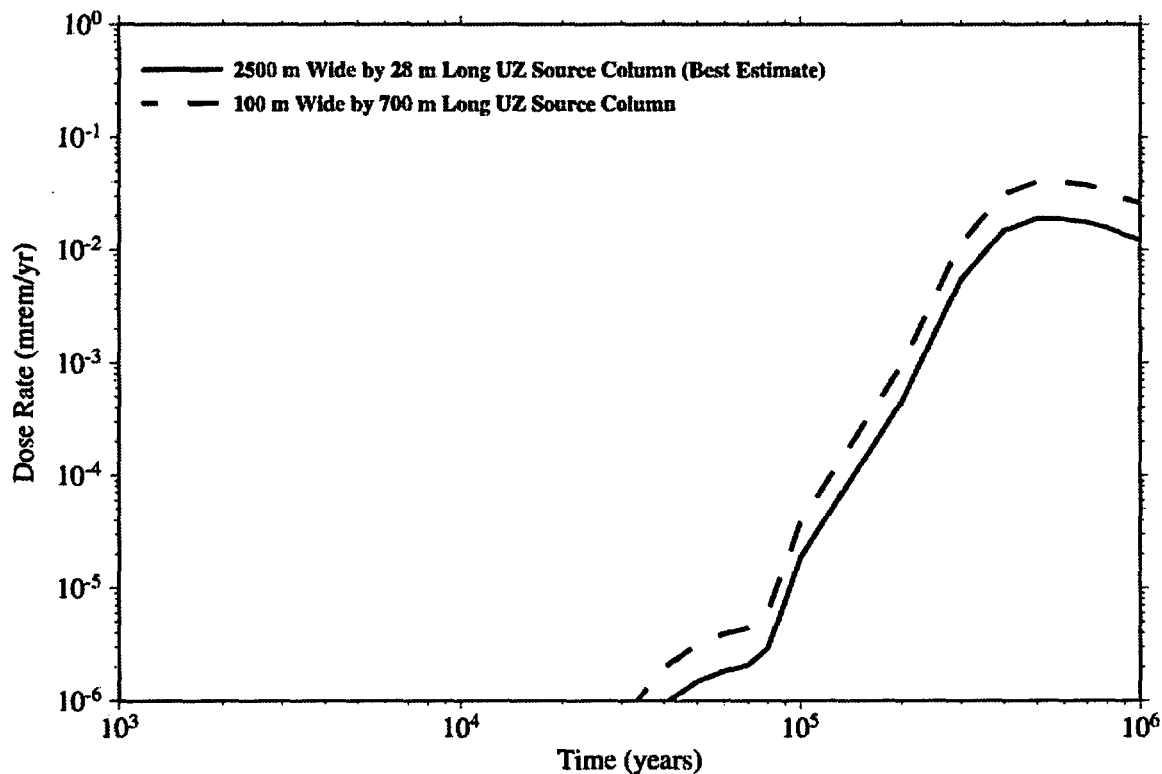


Figure 11-10
Sensitivity of the Annual Total Drinking Water Dose to Alternate Source Column Dimensions

Figure 11-11 shows the sensitivity to SZ flow velocity. Very little sensitivity to changes in SZ velocity can be seen. This seemingly counterintuitive result was explained in Chapter 7. In the IMARC-5 model, it was assumed the saturated zone flow is carried by the fractures even though the fracture porosity is a small fraction of the total SZ porosity that is mostly in the matrix blocks surrounding the fractures. The fracture velocity was altered by a factor of two by altering the fracture porosity by a factor of two. This assumes the SZ hydraulic gradient automatically adjusted such that total number of cubic meters of flow through the SZ did not change. Since radionuclides are free to diffuse out of the flowing fractures into the surrounding stagnant matrix, the amount of time the radionuclides spend in the flowing fracture is proportional to the fracture porosity. Thus, while halving the fracture porosity doubles the flow velocity, it also halves the amount of time, on average, the radionuclides spend in the fracture, such that there is almost no change in SZ travel time. If, on the other hand, the fracture porosity had been fixed while changing the hydraulic gradient by a factor of two (effectively varying the total SZ flux by a factor of two), the curves should diverge from each other.

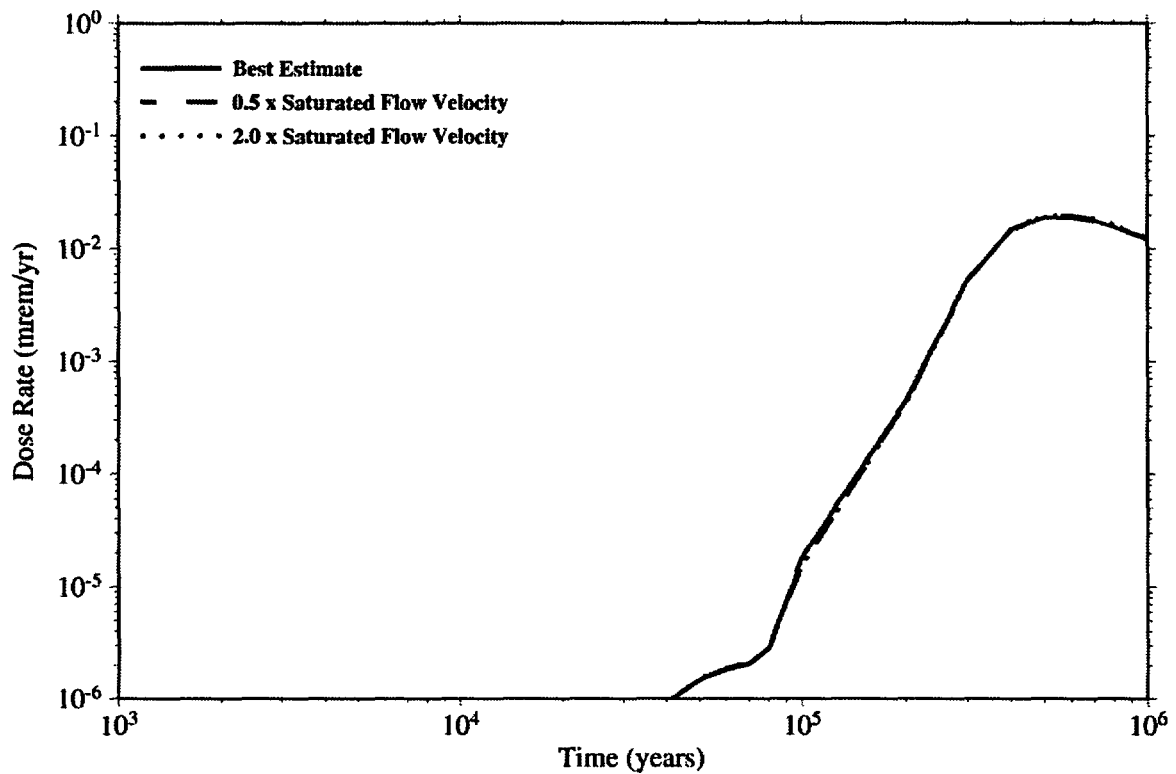


Figure 11-11
Sensitivity of the Annual Total Drinking Water Dose to Saturated Zone Velocity

Figure 11-12 shows the annual drinking water dose curves for the main, single “best estimate” branch of the 54 branches used in the current IMARC logic tree. This single branch, alone, has a probability of 0.365. This branch uses ‘moderate’ infiltration, no flow focusing, ‘moderate’ solubility and alteration time, and ‘moderate’ matrix retardation.¹⁸ Since this particular branch has such a high probability, it is not surprising that there is very little difference between this curve, and the full, 54 branch case presented in Figure 11-1.

¹⁸ A second branch, similar to this branch except for a flow focusing factor of 22 instead of 1, also has a probability of 0.365. However, for sensitivity study purposes, the no flow focusing branch was selected to represent the ‘best estimate’ case.

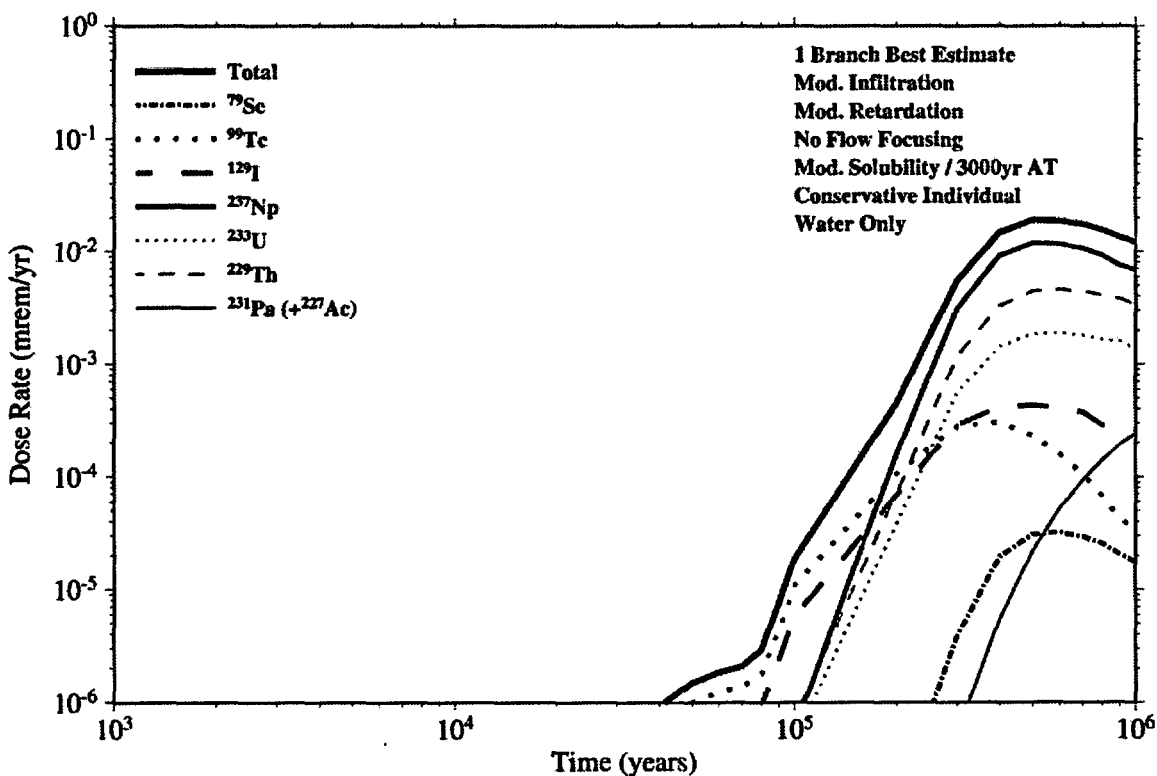


Figure 11-12
Annual Drinking Water Dose for the "Best Estimate" Single Branch: 'Moderate' Infiltration; No Flow Focusing; 'Moderate' Solubility; 3,000-Year Alteration Time; and 'Moderate' Matrix Retardation

Figure 11-13 shows the annual drinking water dose curves for the "worst case" branch: 'high' infiltration; no flow focusing; 'high' solubility and matrix alteration time; and 'low' matrix retardation. This branch has a probability of 6.25×10^{-5} . Compared to Figure 11-12, one can see earlier breakthrough of the plume due to somewhat earlier container failure and somewhat faster radionuclide travel time through the UZ and SZ. However, the dose rate at 10,000 years is still below 10^{-6} mrem/yr for this "worst case" branch.¹⁹ Interestingly, the peak dose is still located at roughly 500,000 years reflecting the continued integrity of the EBS barriers even for higher infiltration rates. The peak height in the "worst case" branch is also only about a factor of two higher than the "best estimate" branch.

¹⁹ As mentioned earlier, the current version of the IMARC code does not attempt to carry along, directly, the most extreme behavior cases. If we had, it is likely we would have found a few branches with more significant doses ahead of 10,000 years.

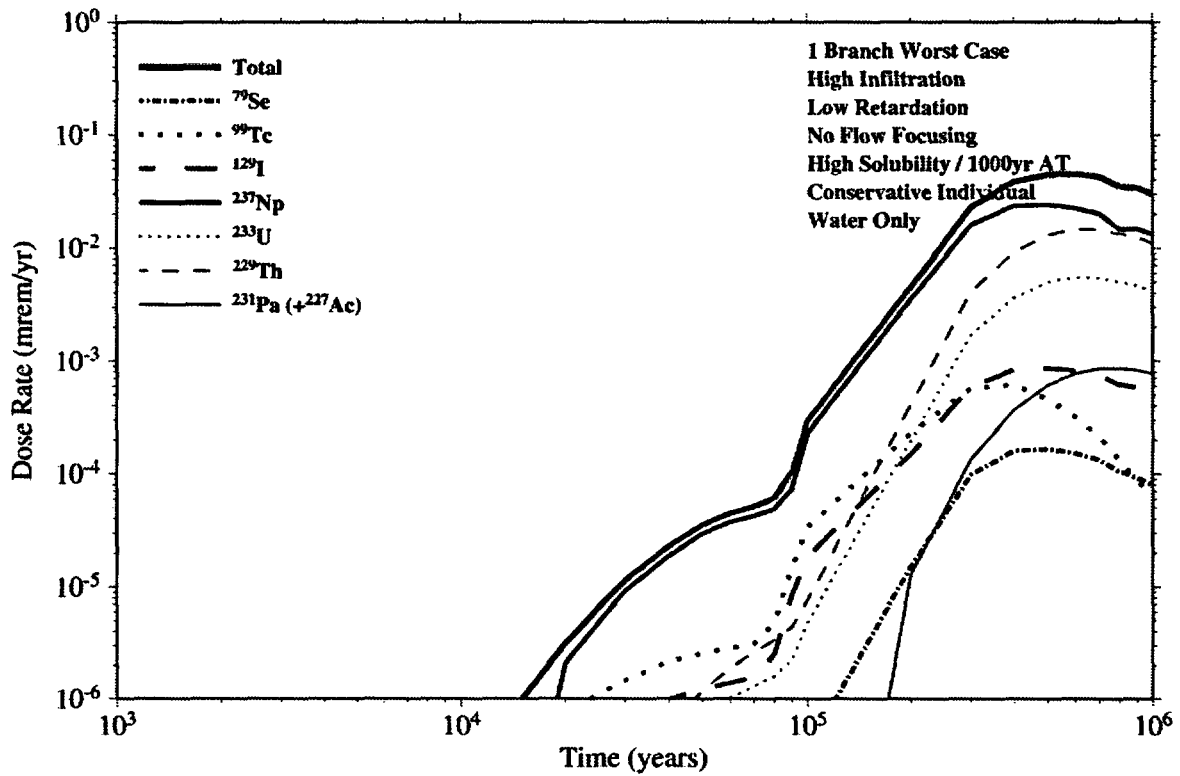


Figure 11-13
Annual Drinking Water Dose for the "Worst Case" Single Branch: 'High' Infiltration; No Flow Focusing; 'High' Solubility; 1,000-Year Alteration Time; and 'Low' Matrix Retardation

Figure 11-14 is an additional sensitivity on the combination of infiltration rate and flow focusing for the total annual drinking water dose. This figure suggests that, only for the combination of 'high' infiltration, and no focusing is there much of an effect on annual dose versus time. The reason this curve shows earlier breakthrough and somewhat higher dose rates is mostly related to the fact that the fraction of the repository assumed 'wet' for this particular combination is higher than for any of the other combinations.

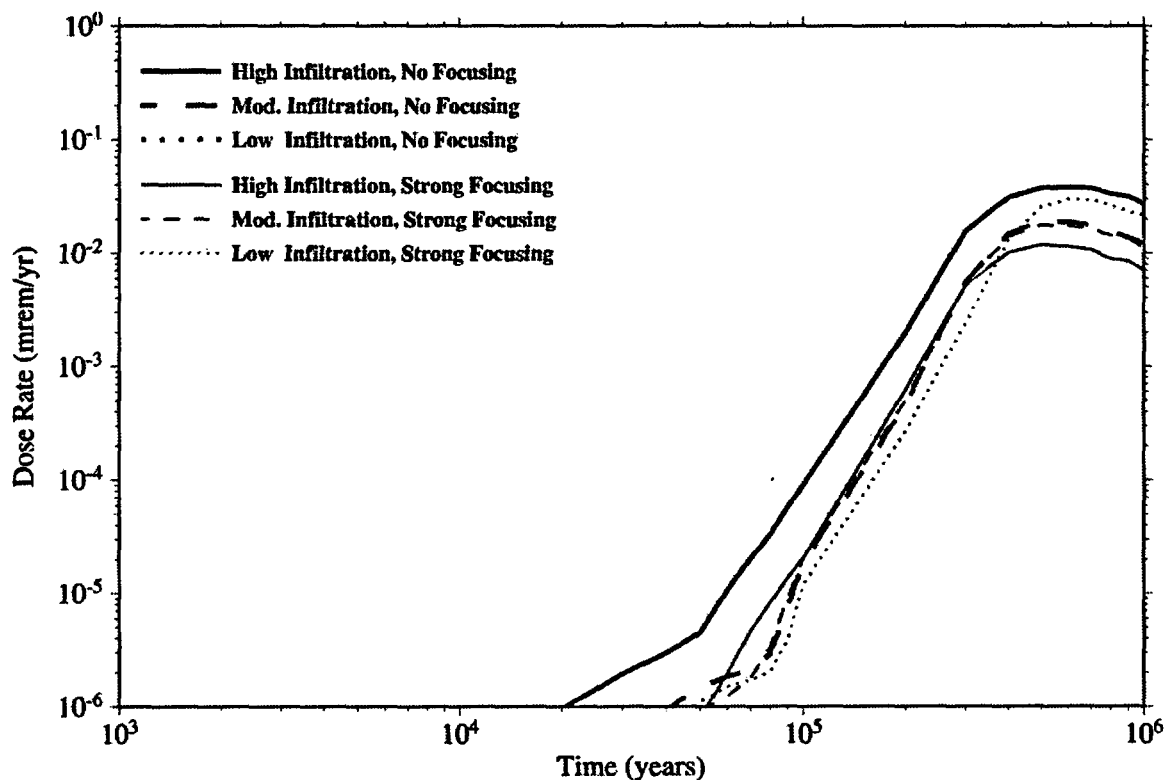


Figure 11-14
Annual Total Drinking Water Dose for the Six Combinations of Infiltration and Flow Focusing

Figures 11-15 and 11-16 partially explain why we combined solubility and spent fuel alteration time effects into a single branch. This figure shows a relative lack of sensitivity to just alteration time on total annual drinking water dose. This lack of sensitivity is further illustrated in Figure 11-16, which provides total annual drinking water dose curves for the nine combinations of solubility and alteration time. Only the three curves for 'low' solubility show later peak arrivals and lower peak heights. Given the time scale for EBS barrier failure is one or two orders of magnitude longer than the range of alteration times one should not expect to see much of an effect on just alteration time – at least not on a log-log plot as shown in Figure 11-15. The other reason why these two effects were combined into a single branch was that it is assumed that geochemical and temperature conditions that would cause a general elevation in solubilities would also cause a lowering of the spent fuel alteration time, and vice versa.

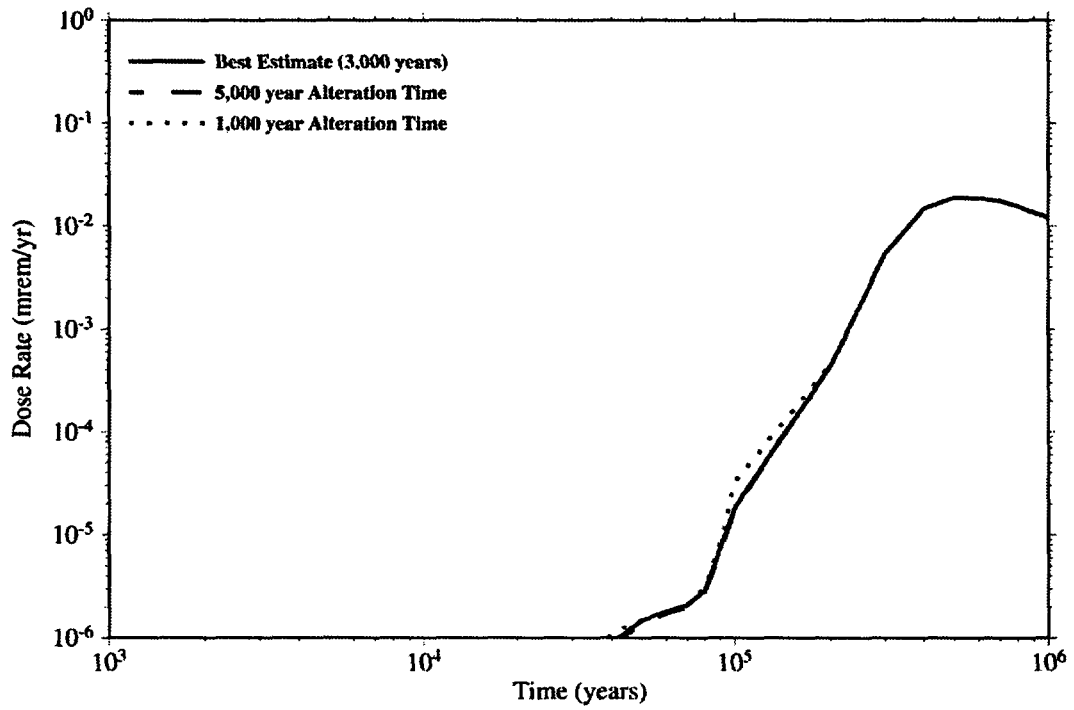


Figure 11-15
Sensitivity of Annual Total Drinking Water Dose to Spent Fuel Matrix Alteration Time

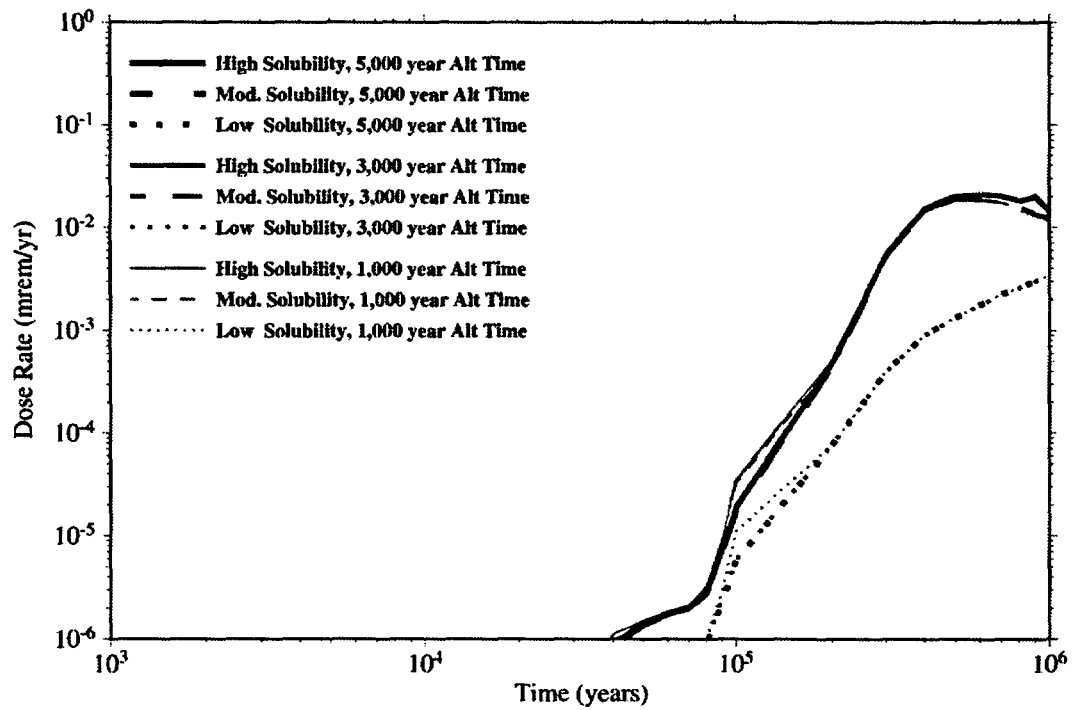


Figure 11-16
Annual Total Drinking Water Dose for the Nine Combinations of Solubility and Alteration Time

Figure 11-17 illustrates the lack of sensitivity to the assumed intensity of the next glacial climate stage. In all cases, the glacial climate is assumed to begin at 2,000 years and continues on for the rest of the modeling time (see Chapter 2). Figure 11-17 shows the total annual drinking water dose for a long-range glacial maximum intensity of 1/3, 2/3, and full. Peak heights differ by only about a factor of two. Since the peak arrival time for the Full Glacial Maximum (FGM) is earlier than the other two scenarios, this case was used in the main IMARC model.

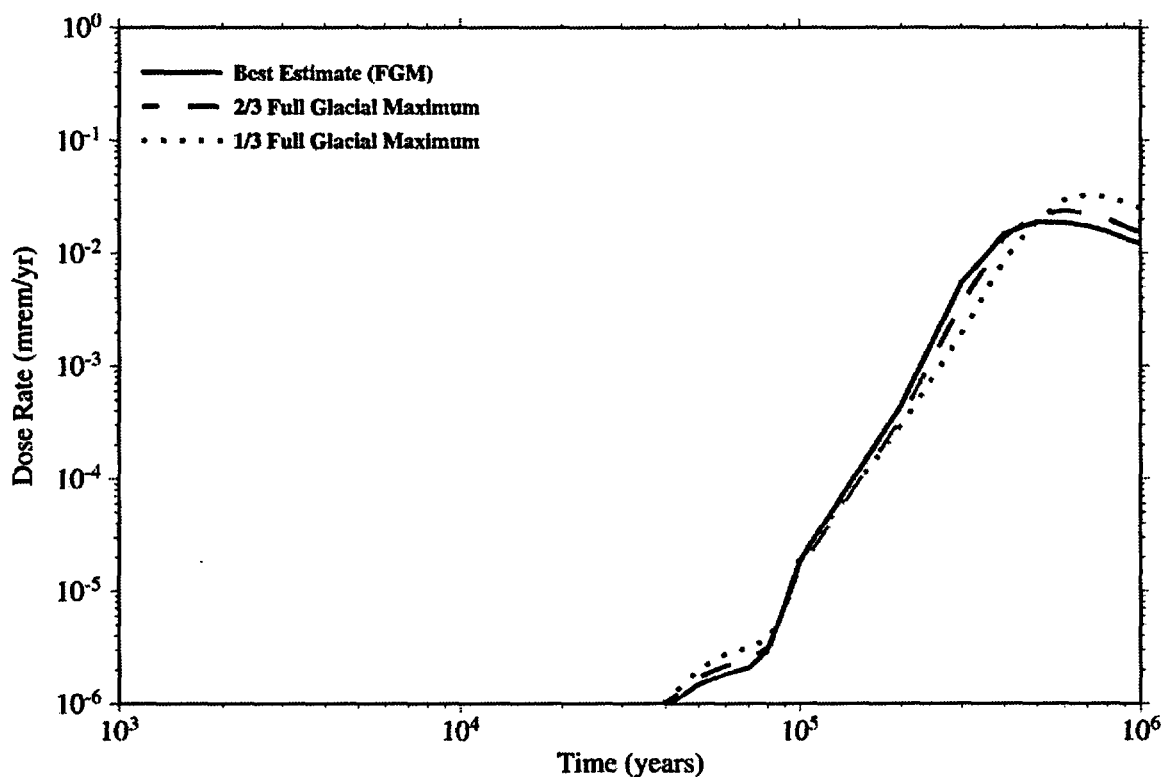


Figure 11-17
Sensitivity of Annual Total Drinking Water Dose to the Intensity of the Future Glacial Climate

Figures 11-18 and 11-19 show the lack of sensitivity to the details of radionuclide transport in the saturated zone. The SZ transport model is a dual porosity model in which flow in fractures is surrounded by tuff matrix 'blocks' into which radionuclides can diffuse. Figure 11-18 alters the matrix block size in the SZ. One would expect that for larger matrix block sizes there would be less total diffusion into the matrix and transport would be faster. On this log-log scale very little effect is seen. Thus, fracture-matrix interaction in the SZ is even effective even for matrix blocks as large as 50 meters – roughly comparable to the distance between flowing fractures in the M&O model. Figure 11-19 shows a similar lack of sensitivity to the rock matrix diffusion coefficient for a block size of 0.125 meter. One would expect earlier breakthrough for a lower diffusion coefficient. Yet even for a diffusion coefficient 320 times lower than the 'base case' fracture-matrix interaction is still effective. Additional sensitivity to SZ parameters are provided in Chapter 7.

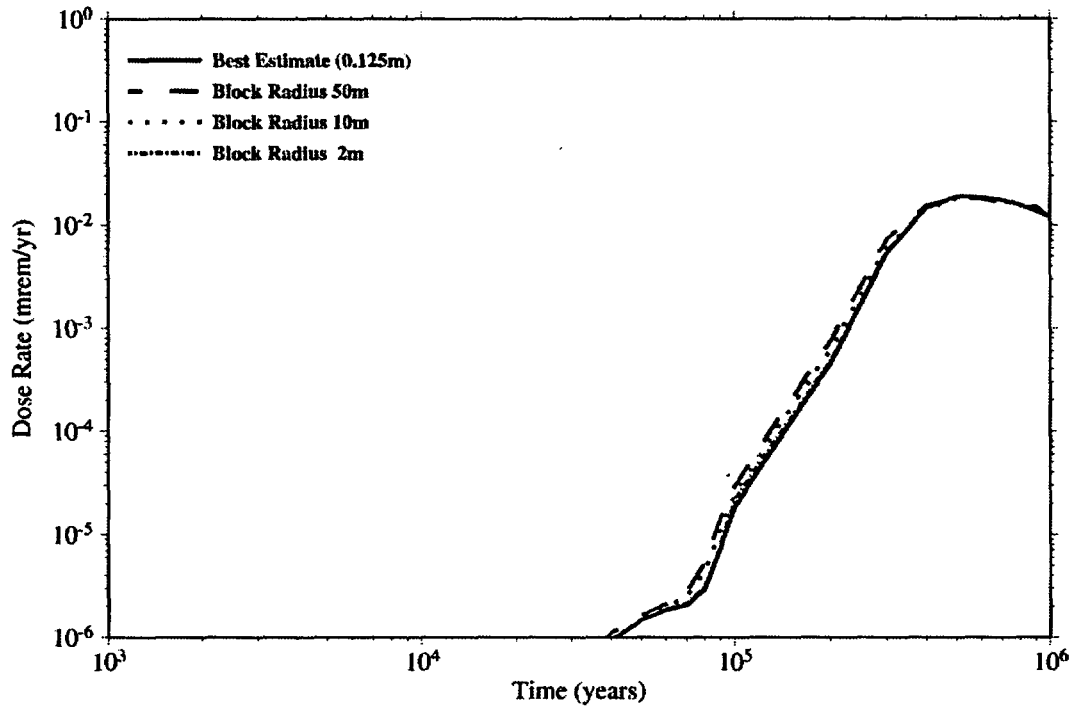


Figure 11-18
Sensitivity of Annual Total Drinking Water Dose to the Spacing Between Flowing Fractures in the Saturated Zone

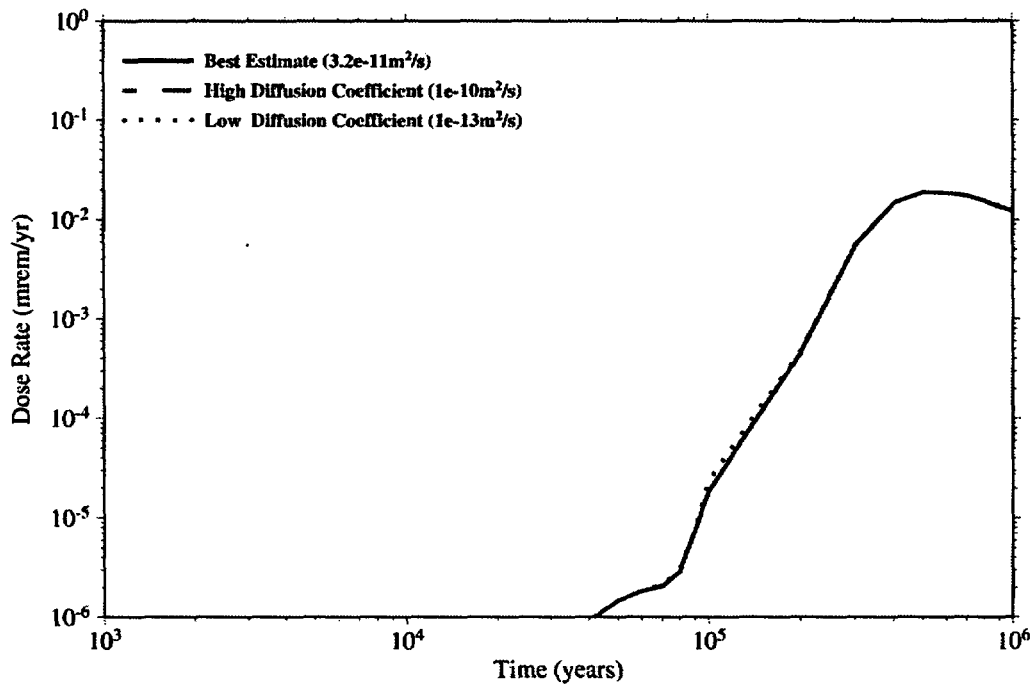


Figure 11-19
Sensitivity of Annual Total Drinking Water Dose to the Saturated Zone Matrix Block Diffusion Coefficient

It was thought that perhaps sorption of some species on container corrosion products would have a significant effect on doses. Figure 11-20 shows that container corrosion products themselves have little effect. Additional sensitivity studies of individual repository barriers, presented in Chapter 13, suggest that, in absence of other important barriers, corrosion product sorption can become important.

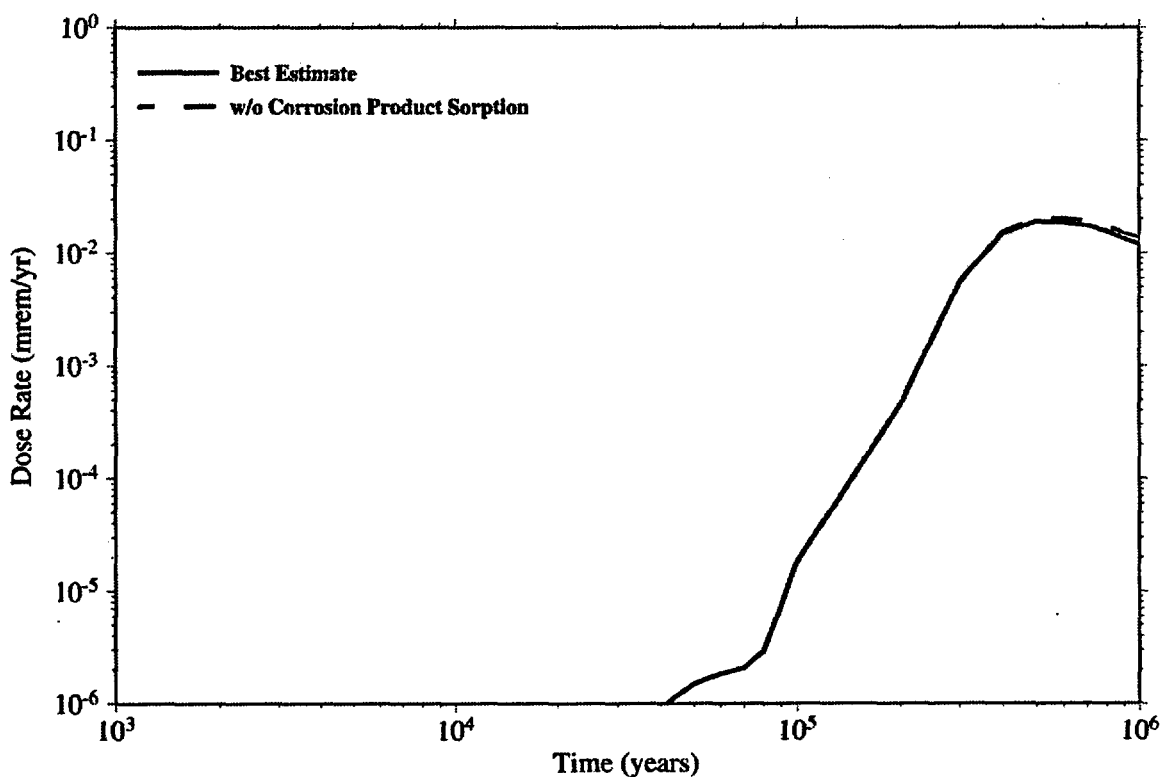


Figure 11-20
Impact on Annual Total Drinking Water Dose of Neglecting Sorption onto Container Corrosion Products

11.3 References

EPRI, 1996. Smith, G. M., Watkins, B. M., Little, R. H., Jones, H. M., and Mortimer, A. M. Mortimer, *Biosphere Modeling and Dose Assessment for Yucca Mountain*, EPRI TR-107190, Electric Power Research Institute, Palo Alto CA, December 1996.

EPRI, 1998. Kessler, J. H., McGuire, R. K., Vlasity, J. A., Long, A., Childs, S., Ross, B., Schwartz, F., Shoesmith, D., Kolar, M., Apted, M., Zhou, W., Sudicky, E., Smith, G., Kozak, M., Salter, P., Klos, R., Venter, A., Stenhouse, M., Watkins, B., and R. Little, *Alternative Approaches to Assessing the Performance and Suitability of Yucca Mountain for Spent Fuel Disposal*, EPRI TR-108732, Electric Power Research Institute, Palo Alto CA, November 1998.



12

REPOSITORY LICENSING STRATEGY

12.1 Introduction

In order for there to be general acceptance of the candidate spent fuel and high-level radioactive waste (HLW) repository at Yucca Mountain, decision makers and the public must have confidence that the repository adequately protects the public. Congress directed the US Department of Energy (DOE) to explore the Yucca Mountain site to determine its suitability as a HLW repository. Congress also directed the US Environmental Protection Agency (EPA) and the US Nuclear Regulatory Commission (NRC) to develop regulations for the candidate Yucca Mountain HLW repository that reflect limits on present and future radiological health impacts. A repository safety strategy, therefore, must take into account the intent of Congress, the regulations specified by EPA and NRC, and additional considerations that would help to provide confidence that public health protection will be adequately maintained.

12.2 Purpose

The purpose of the proposed safety strategy in this section is to summarize the essential issues related to evaluating whether or not the proposed Yucca Mountain repository is likely to comply with regulations similar to those proposed in the current draft standards. It will also provide a strategy for putting Yucca Mountain risks into perspective for the decision makers responsible for evaluating whether the proposed Yucca Mountain repository is sufficiently suitable for DOE to proceed into the licensing phase. In this section, the safety strategy will be limited to the postclosure time period. The safety strategy outlined here draws, as appropriate, from the most recent available DOE Repository Safety Strategy document – Revision 3 [DOE, 2000]. The DOE document is not intended to demonstrate compliance but indicate the roadmap to show compliance with the regulations.

While the EPA and NRC regulations provide significant guidance in shaping an appropriate safety strategy, the process to demonstrate compliance is not definitive. Therefore the detailed process is left to the DOE to develop. As with all complex natural systems, the engineering evaluations supported by science is as much art as it is technical. The art to engineering is to be able to model nature in a simplified way as to understand the trends and the uncertainties associated with the overall process.

The key to all scientific and engineering activities is to define the predominant features, events, and processes (FEPs) controlling overall performance.²⁰ Then sufficient biases can be applied to accommodate the effects on performance of the balance of the minor contributors without having to explore the minor contributors in detail. This is exactly what a 'risk informed' evaluation hopes to foster.

Coupling the probability of occurrence with the consequence of the event is the next step in understanding the importance of the event. NRC has provided guidance on events with very low probabilities that can be excluded from evaluation.

12.3 Regulatory Considerations

A draft of the new revision to the EPA standard for Yucca Mountain is in process, Title 40 Code of Federal Regulation (CFR) Part 197, "*Environmental Radiation Standards for Yucca Mountain, Nevada.*" The regulation specifies that a geological repository must meet given minimum nuclear dose standards at the accessible environment. EPA is obligated, under the Energy Policy Act (EnPA), to issue the final public health and safety standards for Yucca Mountain that "prescribe the maximum annual effective dose equivalent to individual members of the public" and that are "based upon and consistent with" the National Academy of Sciences (NAS) findings and recommendations. According to the EnPA, EPA's new health-based disposal standards "... shall be the only such standards applicable to the Yucca Mountain site."

In concert with the EPA the NRC is also developing their Yucca Mountain-specific federal regulation, Title 10 CFR Part 63, *Disposal of High-Level Radioactive Wastes in a Proposed Geologic Repository at Yucca Mountain, Nevada.* Like many of the recent regulations, Title 10 CFR 63 is risk based.²¹ Therefore there are no specific subsystem requirements called out in a risk-based regulation such as this one. This allows the applicant to perform a detailed system evaluation to determine and rank the design parameters to ensure that the regulations are met. This process will enable the applicant and the regulator to positively define the important design and natural attributes to the repository system and evaluate them individually and as a whole to optimize the facility and take advantage of the best features of the natural and engineered systems.

A risk based methodology also takes into account the uncertainties associated with each component and system with respect to time and operability. Therefore, given that the time horizon of the repository is 10,000 years, uncertainties associated with time can be accommodated. A risk based process carries two basic components within the evaluation, the probability of occurrence of a given event and the consequence of the event.²² Basing the development of the proposed repository on risk informed methodology ensures that all scenarios

²⁰ 'Performance' in this context is usually meant as the quantitative compliance measure, such as individual dose rate.

²¹ The draft EPA regulation for Yucca Mountain, 40CFR197, is only partially risk based: some components of Part 197 are risk based while others are not.

²² This is unlike a deterministic regulatory approach where only the consequences are restricted.

leading to release of contaminants to the biosphere are evaluated not only for the potential health consequences, but also that these consequences are put into an appropriate context by requiring an evaluation of their probability of occurrence.

Although final EPA and NRC standards were not available at the time of this writing, an individual protection criterion in the range of 15 to 25 millirem per year (0.15-0.25 Sv/yr) is being considered [40 CFR Part 197; 10 CFR Part 63]. The EPA is also considering adopting a separate groundwater protection set of criteria that would limit individual dose rates from drinking water to 4 millirem per year (0.04 Sv/yr) with concentration limits for individual radionuclides [40 CFR Part 197]. Both the EPA and NRC draft proposals apply these limits for 'preclosure' and 'postclosure' timeframes at Yucca Mountain. Preclosure activities include those required to transport High Level Waste (HLW) to Yucca Mountain, prepare it for disposal, build the disposal facilities, and emplace and monitor the waste.

The NRC has provided significant guidance related to the aspects of an appropriate safety strategy for Yucca Mountain. They noted that 10 CFR 63 will be based on a risk-informed, performance-based regulation approach in which risk insights, engineering analysis and judgement, and performance history are used to:

- Focus attention on the most important activities,
- Establish objective criteria based upon risk insights for evaluating performance,
- Develop measurable or calculable parameters for monitoring system and performance confirmation and
- Focus on the results as the primary basis for regulatory decision-making.

Thus, a safety strategy must, among other things, provide the guidance by which the scientist and engineers can focus their efforts to develop the Yucca Mountain system as they relate to overall performance of the Yucca Mountain system.

In their draft 10CFR63, NRC provides general direction on how to make a quantitative compliance assessment:

Demonstration of compliance with the postclosure performance objective specified at §63.113(b) requires a performance assessment that quantitatively estimates the expected annual dose, over the compliance period and weighted by probability of occurrence, to the average member of the critical group. Performance assessment is a systematic analysis of what can happen at the repository after permanent closure, how likely it is to happen, and what can result, in terms of dose to the average member of the critical group. Taking into account, as appropriate, the uncertainties associated with data, methods, and assumptions used to quantify repository performance, the performance assessment is expected to provide a quantitative evaluation of the overall system's ability to achieve the performance objective (§63.113 (b)).

Performance assessment shall include features, events, and processes (i.e., specific conditions or attributes of the geologic setting; degradation, deterioration, or alteration of the engineered barriers; and interactions between the natural and engineered barriers) considered for inclusion in the assessment should represent a wide range of beneficial and detrimental effects on performance. Features, events, and processes [FEPs] should be

considered in light of available data and current scientific understanding, and alternative conceptual models that are consistent with such data and understanding should be evaluated.

While there is a role for more qualitative information in providing additional confidence, it is necessary to be able to quantify them for the purposes of not only assessing compliance with regulatory limits, but also to help elucidate which Features Events and Processes (FEPs) require higher levels of confidence in their performance than others. Regarding the role for qualitative information, NRC notes that "...in reaching a determination of reasonable assurance, the Commission may supplement numerical analyses with qualitative judgments including, for example, consideration of the degree of diversity or redundancy among the multiple barriers of the geologic repository." Thus, in addition to the TSPA quantitative estimates, it is the degree of diversity or redundancy that lies at the heart of providing confidence that long-term risks will, indeed, not be too high.

In the new rule, the NRC makes it clear that the Natural system and the Engineered system shall work together to provide the performance of the repository, the major redundant systems. In fact the NRC goes to some length to make the point that an engineered system can not be the sole basis of compliance with the rule:

"The Commission firmly believes that the performance of the engineered and natural barriers must each make a definite contribution in order for the Commission to be able to conclude that the EPA standard will be met." [§VIII. Multiple Barriers and Defense in Depth]

NRC also notes a distinction between the concept of 'redundancy' in a passive system such as a geologic repository and an active system like a nuclear power plant:

Application of defense-in-depth principles for regulation of repository performance, for long time periods following closure, however, must account for the difference between a geologic repository and an operating facility with active safety systems and the potential for active control and intervention. A closed repository is essentially a passive system, and assessment of its safety over long timeframes is best evaluated through consideration of the relative likelihood of threats to its integrity and performance. Although it is relatively easy to identify multiple, diverse barriers that comprise the engineered and geologic systems, the performance of any of these systems and their respective subsystems cannot and should not be considered either truly independent or totally redundant.

The safety strategy should not be expected to quantify uncertainties, the task to quantify uncertainties should be left to another document like the License Application. The License Application Document will describe the system and the components in sufficient detail to demonstrate compliance with the regulations. Again the Safety Strategy is to define the process by which the License Application will be developed.

The NRC recognized that uncertainties will remain when estimates of performance over such long time frames are required. NRC notes, in draft Part 63, that although the performance objective for the geologic repository after permanent closure:

...is generally stated in unqualified terms, it is not expected that complete assurance that the requirement will be met can be presented. A reasonable assurance that the performance objective will be met is the general standard that is required. Proof that the geologic repository will be in conformance with the objective for postclosure performance is not to be had in the ordinary sense of the word because of the uncertainties inherent in the understanding of the evolution of the geologic setting, biosphere, and engineered barrier system. (§63.113)

12.4 Performance Assessment

One of the tools used to define the suitability is the Performance Assessment process. The ability of the repository to meet the performance objective, thereby providing waste isolation, will be determined through a risk-informed, performance based assessment. This assessment includes a quantitative performance assessment of the risk. The performance assessment takes into account all the factors, such as those described above, which determine postclosure performance of the natural and engineered barriers.

The performance assessment for a repository system is a risk assessment. That is, the quantitative assessment includes estimates of the consequences of potential release of radionuclides in possible scenarios, including scenarios for potentially disruptive processes and events, weighs these consequences by their probability of occurrence and provides an estimate of the overall risk to the public. The risk is expressed in terms of the expected annual dose, i.e., the mean value of the annual total effective dose equivalent to a member of the public. In this sense the estimate of mean annual dose is a probability-weighted measure that represents the risk. The estimate of expected annual dose is taken into account in assessing whether the postclosure performance objective is likely to be met.

12.5 Uncertainty

Critical to the assessment is the treatment of uncertainty. Uncertainties in the available scientific understanding, data, and models for the factors that determine barrier performance are inevitable due to system complexity and the large time and space scales involved. Many of these uncertainties are explicitly taken into account in the performance assessment. Alternate conceptual models and probability distributions to represent uncertainty and variability in model parameters are incorporated into the performance assessment so that variance around the mean of the annual dose can be considered in evaluating the likelihood the performance objective would be met.

Not all uncertainty can be represented explicitly in the performance assessment. Some uncertainties arise from complexities that prevent complete mechanistic understanding, validation of models, or practicable analysis. Other uncertainties are associated with unanticipated or unknown effects, such as failure mechanisms not yet revealed in spite of extensive testing. The postclosure safety case therefore employs additional measures. The aim of these measures is to provide a safety case in which, while acknowledging the presence of uncertainty, there is sufficient confidence in the postclosure safety that decisions by the DOE and the NRC to proceed to the next stage of repository development can be made. These measures include those that aim at increasing:

- The quality of the performance assessment and the treatment of quantified uncertainties
- The robustness of the system concept and the postclosure safety case for the system.

Both of these approaches are addressed within the postclosure safety case. The quality of the assessment is addressed through the technical basis for the process models and performance assessment models, comprehensive accounting of uncertainties within the performance assessment, the use of appropriate conservatism to account for uncertainties, and model validation activities. Robustness in the system concept and the postclosure safety case is addressed through adoption of sufficient engineered and natural barriers to provide safety margin and defense-in-depth and in providing information in a number of different areas to increase confidence in the postclosure safety case.

12.6 Evaluation Process

After all potentially relevant FEPs are identified, the next key is how the individual FEPs are coupled to each other and the finally to the system performance. To guide the activity, the NRC has issued a number of risk informed guidelines. Over the years the NRC and the industry have collaborated in the development of process, e.g., Reexamination of Spent Fuel Shipments Risk Estimates, NUREG/CR-6672.

To gain understanding of each FEP and then the system it is important to evaluate the components of the system using the near nominal conditions. It is clear that assumptions need to be made in order to simplify complex processes adequately to be modeled in a TSPA. In some cases conservative assumptions will have to be made in those cases where adequate data are not reasonably obtainable with which to, at the least, provide confidence that the uncertainty distribution is adequately understood. These conservative assumptions need to be documented to provide perspective on the quantification of system uncertainties.²³ It is simply too easy to make the argument that "If I chose the most bounding condition, then it will cover all other assumptions." This philosophy in the long run will cause confusion and misunderstanding and will lead to potentially misleading results. Therefore, it is recommended that, at least for the near-term Site Recommendation process, as many component evaluations as possible be performed using the near nominal inputs.

While one should avoid making conservative assumptions for the most important FEPs whenever it is feasible to do so, it is reasonable to apply a quantified and consistent assumption for regulatory purposes for less important FEPs and for those important FEPs that are very complex and involve large space and/or time scales. For SR, on the other hand, it would be very worthwhile to provide an alternative assessment substituting assumed 'best estimate' values or ranges in place of uncertainties to provide additional perspective to decision makers, in addition to the assessment where conservatisms are imposed.

²³ The substitution of conservatisms for 'best estimate' values or distributions skews the resulting risk analysis such that the 'expected value' (mean) of the results loses its traditional meaning. Rather, the results of a risk analysis incorporating conservatisms should provide confidence that the actual outcome will not be worse than the 'expected value'.

12.7 Defense-In-Depth

Defense-In-Depth (DID) has been part of the nuclear industry from the start. It is the process of providing redundant systems and/or components to ensure uncertainties are covered. Through the logical application of DID uncertainties can be managed. It is important to manage DID components very carefully, there is no other design component that can drive the complexity of the system faster than DID. Therefor DID should be implemented only after the uncertainties are defined and quantified. From the discussion section ahead of the draft 10CFR63, NRC noted that it has revised its original concept of DID, as originally expressed in 10 CFR 60:

“[In 10 CFR 60] the Commission opted to prescribe minimum performance standards for each of the major system elements (as they were envisioned at the time) as well as to require the overall system to comply with the primary performance objective, namely, whatever standards EPA would eventually establish. This approach was thought to have two advantages over the systems approach, if the barriers were chosen judiciously. It was argued that barriers could be prescribed, generically, which act “independently,” and that generic performance measures for these “independent” barriers could be selected that would reduce calculational uncertainty. Identification of such subsystem performance measures was expected to be helpful input to DOE’s design process, without being overly restrictive. It is now recognized that NRC attempted to define such criteria on the basis of limited, existing knowledge, without benefit of research and site-specific information that only later was acquired during characterization of a specific site at Yucca Mountain. ...”

The postclosure safety case regarding this standard also includes consideration of the resiliency of the repository system with respect to postclosure performance, that is, aspects that increase confidence the postclosure performance objective is met. These include number and diversity of the barriers of the system. In general, the risk-informed, performance-based approach used to assess postclosure safety of the system must rest on a firm foundation of safety margins, defense-in-depth, and other measures to enhance confidence that the regulatory standard is met. The NRC has traditionally relied on independent, redundant barriers to provide assurance of postclosure safety when quantitative estimates of system performance include significant uncertainties. This reliance is reflected in the following statements of consideration that accompany NRC’s proposed rule, 10 CFR Part 63:

The defense-in-depth principle has served as a cornerstone of NRC’s deterministic regulatory framework for nuclear reactors, and it provides an important tool for making regulatory decisions, with regard to complex facilities, in the face of significant uncertainties. NRC also has applied the concept of defense-in-depth elsewhere in its regulations to ensure safety of licensed facilities through requirements for multiple, independent barriers, and, where possible, redundant safety systems and barriers. Traditionally, the reliance on independence and redundancy of barriers has been used to provide assurance of safety when reliable, quantitative assessments of barrier reliability are unavailable. The NRC maintains, as it has in the past, that the application of the defense-in-depth concept to a geologic repository is appropriate and reasonable.

The portions of the proposed rule requiring a system of multiple barriers and an understanding of the resiliency of the geologic repository provided by those barriers are intended to ensure defense-in-depth and increase confidence that the postclosure performance objective will be achieved. To provide maximum flexibility in system design, the proposed rule does not place

specific requirements on the degree of defense-in-depth provided by multiple barriers. Nevertheless, the NRC expectation is that DOE will rely on a combination of barriers to enhance system performance and increase confidence in demonstrating that performance.

12.8 Review of DOE's Repository Safety Strategy, Revision 3

This section will review the DOE's Repository Safety Strategy, Revision 3 [DOE 2000].²⁴ It is hoped that through an independent review additional insights can be offered that will strengthen the document.

DOE's RSS3 follows the guidelines set forth in the regulations. The process is described as a 'Risk Informed' process which is based on a system requirement, not subsystem performance requirements. The DOE's RSS3 notes in "Section 1.3 Changes for This Revision,

"For the SR [Site Recommendation] considerations, the postclosure safety case must be sufficient to support the determination of the suitability of the site for repository development. The safety case will include representations of the important factors that are as realistic as possible. If the Yucca Mountain site is determined to be suitable for repository development and decision is made to submit a license application to the NRC, the postclosure safety case must be sufficient to enable the NRC to make a finding that there is reasonable assurance regarding postclosure public safety. To facilitate the regulatory review of the safety case the focus will be on those factors most important to postclosure safety."

The DOE has identified a number of systems and components as the primary barriers. Performance assessment sensitivity studies and barriers importance analyses suggest the overlying rock units, the waste package and other engineered barriers, and the unsaturated and saturated zone transport barriers are likely to play an important role in the repository's postclosure performance. For the purpose of this analysis, the key barriers are assumed to be those with the potential to inhibit water or radionuclide movement such that the fractional rate of transmission through the barrier is less than 10^{-4} per year or delay through it is 1,000 years or more. Those likely to satisfy these criteria include:

- Overlying unsaturated zone hydrologic units
- Drip shield
- Waste package barriers
- CSNF cladding
- Drift invert
- Underlying unsaturated zone hydrologic units
- Saturated zone.

²⁴ As of the development of this document Revision 4 has not been released to the public.

In the DOE's RSS specific components are called out as the barriers. It may be more appropriate for the RSS document to note the general system components and allow the supporting documents to define each of the component contribution and configuration. This would allow the reader to understand the difference between the License Application and the Strategy document. The RSS may want to include:

- Identification of major components of the system:
- For the most part the EPA and the NRC have helped define the major components to be considered:
- Waste Form, Pressurized Water Reactor (PWR) and Boiling Water Reactor (BWR) spent fuel. Due to the environment that the fuel must operate in, the fuel has a number of long term performance components, the ceramic fuel, the cladding and the fact that the relatively insolubility of the non-ceramic portion of the fuel.
- Waste Package, the waste package can be designed to accommodate virtually any environment.
- Engineered Barrier System, the engineered barrier system includes all of those design features needed to provide Defense-In-Depth (DID) in conjunction with the waste package.
- Near Field, the area rock and soil, just around the emplacement drifts.
- Far field, the far field can be subdivided into four areas:
 - Surface, those surface environmental effects that influence the spent fuel and its long term performance
 - Unsaturated Zone, the portion of the rock immediately beneath the repository footprint and above the water table.
 - Saturated Zone, the volcanic rock below the water table in which any radionuclides leaking through the unsaturated zone would enter and be transported downstream.
 - Alluvium, the solid material downstream of the hard, volcanic rock in the saturated zone through which it is thought any radionuclides exiting the hard volcanic rock will pass before entering the biosphere. Unlike the hard volcanic rock where radionuclide transport will be primarily through fractures, the alluvium is expected to behave more like a classic porous medium.
- Biosphere, that portion of the system in which radionuclides can encounter humans and other biota. The biosphere includes soils important to farming, drinking and irrigation water wells, and all aspects of the human community in which exposure groups are defined for the purposes of making dose estimates.

12.8.1 Uncertainties

The development and understanding of the uncertainties associated with the major factors are a key to the understanding of the system performance. The DOE's RSS3 notes that the focus will be on the development of the evaluations based on realistic factors [Section 1.3, DOE 2000]. At this point in time, it is clear that the DOE is struggling to understand all of the bounding assumptions that have been made throughout the evaluations. Therefore, the SRCR- TSPA can

only be considered conservative such that the anticipated repository performance is likely to be considerably better than will be reported in the SR-CR due to be issued in late 2000. Therefore, a major task for the DOE before the final issuance of the Site Recommendation report should be to identify and quantify the impact of the suite of assumptions and parameter values that are departures from a more 'best estimate' approach.

One example of unjustified conservatism was reviewed at the Carson City NWTRB meeting in June 2000. Through the presentation of the different components associated with the repository, the near field and the far field, it was discovered that there was an inconsistency between the two sub-systems. The far field evaluation indicated that there would be little moisture intrusion into the drift due to dripping water. Unfortunately the near field evaluation did not take this into consideration. The assumption that was made was that all of the emplacement drifts would be considered very humid and dripping water would always occur. Truly this is the most bounding assumption that could be used. But considering that the evaluation process is Risk Informed the evaluation should have taken into consideration the probability associated with the nominal suite of anticipated emplacement drift environments based on the far field results.

12.8.2 Defense-In-Depth

In Section 1.4 of RSS3 the DOE defines how they will address uncertainties. The RSS notes that "... it is expected that not all uncertainties will be explicitly included and because controversy could arise in areas not yet anticipated, the DOE's approach to safety case incorporates additional measures including margins and defense-in-depth."

The DOE has taken into consideration defense-in-depth (DID) throughout the repository design. For example, the natural system is another barrier to the engineered system. Each major barrier should not be considered redundant to one-another. Each barrier has their own performance characteristics, e.g., the unsaturated zone holds up and absorbs the proposed radionuclides differently than the saturated zone. But they are both considered important barriers. Paraphrasing the NRC, the natural barriers and engineered barriers shall work together to provide the basis for acceptance of the site. Due to the bounding assumption made with respect to the performance of the natural system the DOE's SRCR-TSPA is predominantly relying on the engineered barrier system to provide the performance. As is demonstrated in other sections of this report, basing the performance of the natural system on more realistic but still conservative assumptions, a balance between the natural and engineered system can be struck.

The DOE should continue to identify those features that not only provided quantitative DID but also qualitative DID. For instance, as it stands today the waste package internal basket was developed not only to withstand the thermal and structural loads but also to reduce the probability of moisture contacting the spent fuel and the basket materials are also selected to provide additional radionuclide retention. This would lower the release rate to the near field.

12.8.3 Natural Analog Systems

The DOE has noted that analogs are going to be used. In Section 2.4, Insights From Natural Analogues:

“Analogue studies may be most useful in analyses of transport and deposition of radionuclides, the stability and transport characteristics of alteration minerals, and the conditions in the shallow unsaturated zone. Some of this information could complement laboratory and field test conducted at Yucca Mountain.”

It is suggested that the project spend additional efforts in developing natural analogs, e.g., nickel base materials, unsaturated and saturated site moisture movement, drift openings.

12.9 Analytical Approach

Appendix C of the DOE's RSS provides an outline by which TSPA evaluation process should be performed. In concert with Appendix C or RSS Revision 3, noted below is a supplemental approach is proposed:

1. Identify all potentially relevant FEPs: describe your system qualitatively and introduce data as you have it. Incorporate the Risk Informed process to help rank and select the key FEPs components.
2. After defining the primary systems and subsystem features, develop the initial FEPs models and data sets to describe the system components mathematically, carrying along the known system variabilities and uncertainties. Develop a process to quantify the major uncertainties to support a Risk Informed process.
3. Provide FEPs screening arguments to rule out unimportant FEPs. Be as quantitative as practical. Looking at past NRC guidelines and licensing presidencies.
4. Through the Risk informed process the major system and subsystem can be ranked and selected. Based on the major system and subsystems, develop an understanding of performance at a system level. Perform sensitivities, etc. This process will further sort out the important FEPs and important variabilities and uncertainties.
5. Based on your initial TSPA work, identify candidate 'barriers'. Through out the process it is key to perform simple engineering evaluations, 'sanity checks' to ensure that the computer simulations are trending correctly. This will increase the confidence of the TSPA results.
6. Manage your important uncertainties and variabilities in these barriers. Use margin, DID, natural analogs, PC to bolster confidence. Use selective conservatism's to minimize seriously underestimate radiological consequences, when quantitative information is not directly applicable. It is also recommended that a 'best estimate' or near best estimate evaluation be performed. To provide an understanding of uncertainties and biases. At this point it very important to understand the uncertainties and how they have been applied. If for instance bounding evaluations have been applied to each subsystem/sub-model it will be very difficult to determine the system uncertainty. For the sub-model uncertainties will overwhelm the total system uncertainty.
7. Using the risk informed process develop a 'barriers importance analysis'. This step ensures that the barriers selected are truly providing the added retardation you expected and that they do not have a common mode failure with other the other barriers. This step should also

identify additional data that is needed. From this the Performance Confirmation plan can be generated and/or short-term data gathering (R&D programs) can be implemented.

8. The final step is to develop a License Application document based on a Safety Strategy that clearly demonstrates the Repository design compliance.

12.10 Summary of the Essential Elements of an Appropriate Repository Safety Strategy

The development of a Repository Safety Strategy is considered a key element in a successful licensing process. The RSS should be developed and used as the corner stone that guides the technical and licensing staffs to ensure that the licensing strategy is clearly defined and referenced. To this end, the RSS needs to consider all of the regulatory requirements and synthesize them so that the technical requirement documents can easily incorporate them. Through the established document structure the requirements will then flow down to the level of detail needed for each system and subsystem. The DOE should guard against the RSS becoming too detailed and providing direct guidance to the engineering and scientific staff.

To this end, Revision 3 of the Yucca Mountain Repository Safety Strategy provides a good start at developing a clear licensing strategy. The DOE document provides a clean review of the regulation. It is recommended that common regulatory interpretations be grouped together so that the organization responsible for developing the requirement document(s) can easily extract the common regulatory requirements. Since the RSS is a top-level guidance document it should not specifically specify a detailed design solution and then evaluate it, as it does in revision 3. For instance, the RSS goes into detail on the development of the specific barriers. If a Risk informed processes is implemented, the first step would be to evaluate all of the logical barriers and then issue a technical document ranking the proposed barriers. Revision 3, of the RSS takes this task on and makes it the central issue of the document. It would be clearer if the RSS focuses on the strategy and allow the processes to support the RSS.

12.11 References

10 CFR 60. 1998. Energy: Disposal of High-Level Radioactive Wastes in Geologic Repositories.

10 CFR 63. Disposal of High-Level Radioactive Wastes in a Proposed Geologic Repository at Yucca Mountain, Nevada.

40 CFR 191. Protection of Environment: Environmental Radiation Protect Standards for Management and Disposal of Spent Nuclear Fuel, High -Level and Transuranic Radioactive Waste.

40 CFR 197: Environmental Radiation Standards for Yucca Mountain, Nevada .

Repository Safety Strategy: Plan to Prepare the Postclosure Safety Case to Support Yucca Mountain Site Recommendation and Licensing Considerations, TDR-WIS-RL-000001 REV 03, January 2000.

13

BARRIER IMPORTANCE ANALYSIS USING IMARC

13.1 Introduction and Purpose

As discussed in the previous chapter on developing a repository safety strategy, a key aspect of that strategy is to identify the key barriers to radionuclide release in the repository system. In their draft regulation for Yucca Mountain, 10 CFR Part 63, the US Nuclear Regulatory Commission (NRC) states:

§63.102 (h): "*Multiple barriers.* §63.113(a) requires that the geologic repository include multiple barriers, both natural and engineered. Geologic disposal of HLW is predicated on the expectation that a portion of the geologic setting will be capable of contributing to the isolation of radioactive waste, and thus be a barrier important to waste isolation. ... It is intended that natural and the engineered barrier system work in combination to enhance the resiliency of the geologic repository and increase confidence that the postclosure performance objective ... will be achieved."

Thus, multiple barriers are required, some of which must be natural, and some must be engineered. The barriers important to waste isolation must be identified, quantified, and defended. For the purposes of analysis in this chapter, a "barrier" is assumed to be any single or readily distinguishable suite of features, events, and processes (FEPs) that act to:

- prevent or substantially delay²⁵ movement of the radionuclides to the biosphere; and/or
- substantially reduce their concentration²⁶ by action of either radioactive decay *or dilution*

The purpose of this chapter is to provide analyses using the IMARC code to potentially identify a set of natural and engineered 'barriers' upon which to build a safety case for Yucca Mountain. While admittedly artificial, the numerical device of barrier neutralization is useful for shedding light, in a conceptual manner, on the true importance of individual barriers. The analyses in this chapter use the barrier neutralization technique. Like a 'partial' neutralization or 'degraded' barrier performance analysis, none of these techniques represent the 'expected' behavior of the repository system, so they can all be considered artificial. The advantage of a full barrier neutralization approach is that it sometimes helps identify other barriers which are thought to be of only minor importance using more traditional sensitivity analyses, such as those presented in

²⁵ A 'substantial' delay may be on the order of 10⁴ years or longer since both EPA and NRC have proposed the time period of regulatory compliance be 10,000 years.

²⁶ A 'substantial' concentration reduction is arbitrarily assumed to be a factor of ten or larger.

Chapter 11. As will be shown in this chapter, this approach has identified potentially important barriers that may have otherwise been ignored.

The neutralization analyses presented in this chapter take on two forms. The first is the more common approach to barrier neutralization where a single or, at most, a handful of related barriers are assumed to be non functional. The second form is what we termed a "Hazard Index" approach when we first presented it two years ago [EPRI, 1998, chapter 14]. This second form is the successive addition of barrier after barrier until the entire suite of repository FEPs have finally been added. We note whether the magnitude or timing of the peak theoretical dose rate is changed by the addition of each barrier to gauge the potential importance of each of the barriers added.

13.2 'Traditional' Neutralization Analyses

Figure 13-1 shows the total drinking water annual dose at 20 km for the single 'best estimate' branch from the IMARC-5 logic tree. The second curve that assumes that, instead of the last four kilometers of the saturated zone (SZ) being alluvium, it is replaced with another four kilometers of volcanic tuff with the same properties as the volcanic tuff comprising the first 16 km of the SZ. This particular analysis suggests that whether or not there is alluvium present in the last four kilometers is not particularly important. This is because the presence of other barriers, particularly the engineered barriers in the drifts (the EBS), shifts the release so far back in time that the additional retardation in the SZ due to the presence of the alluvium is largely masked in this log-log plot. However, the figure does imply that the presence of four kilometers of alluvium shifts the time of peak arrival back by about 10^4 years. Given that the proposed regulatory compliance period is 10,000 years, the presence of alluvium can still be considered a potentially important barrier.

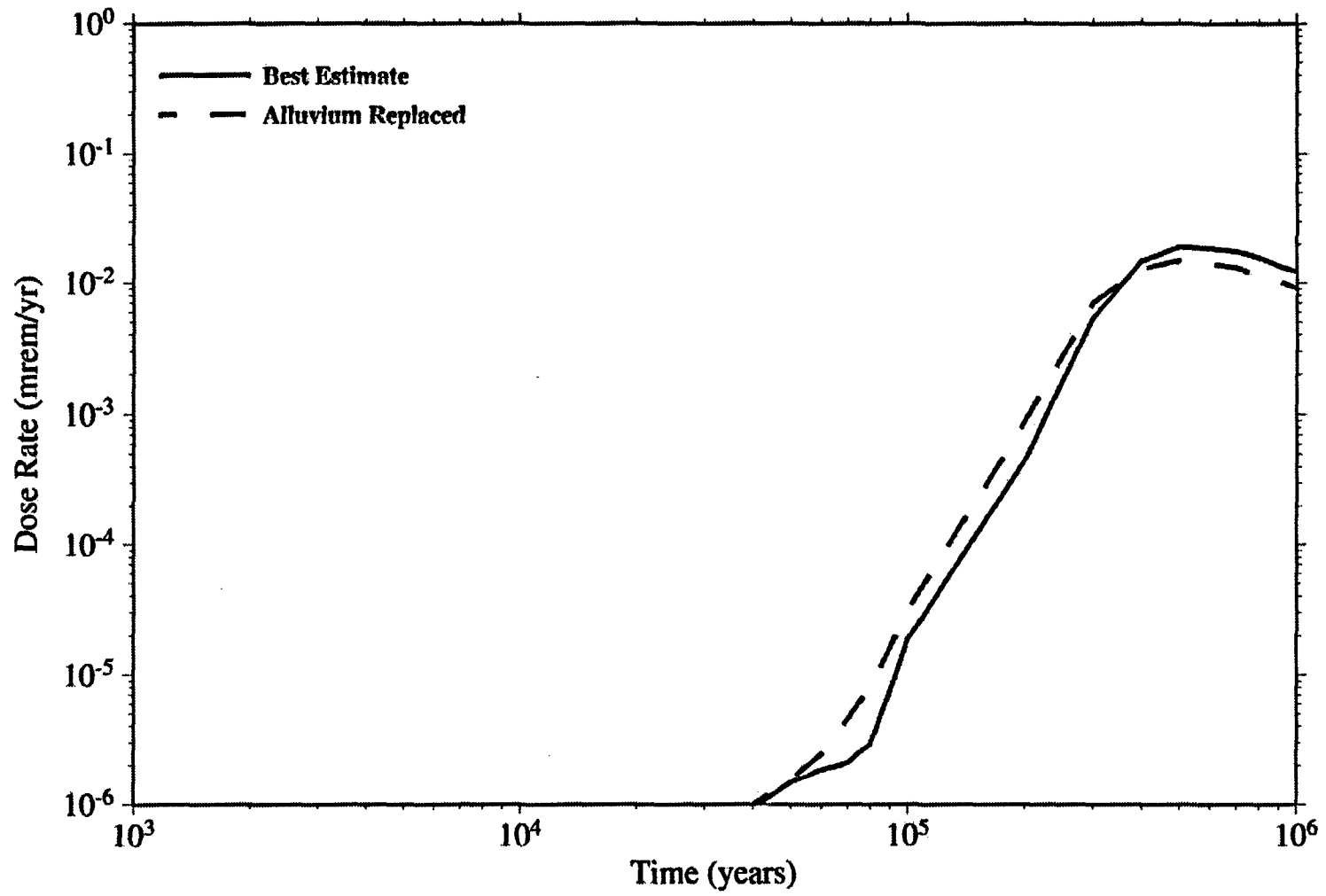


Figure 13-1
Impact on Annual Total Drinking Water Dose of Encountering No Alluvium

Figures 13-2 through 13-6 provide barrier neutralization analyses for the various components of the EBS. In the current repository design there are three main barrier components of the EBS (along with several other potential ones): the drip shields, waste containers, and the spent fuel cladding. The analyses presented here are intended to show that all three of these EBS barriers are of significance, not just the containers and drip shields.

The impact on total drinking water annual dose of removing the cladding barrier only is shown in Figure 13-2. As can be seen, if cladding is investigated in isolation, its impact on total dose does not appear large on a log-log plot.²⁷ But like alluvium, the presence of cladding delays the peak arrival time by roughly 10^4 years.

The neutralization of the two other major EBS barriers, the drip shield and the waste container, is shown in Figure 13-3. Removing the drip shield alone (the dashed curve in Figure 13-3) implies that the dose peak at 20 km is moved forward about 10^5 years – a very significant effect. However, neutralization of the drip shield alone has only a marginal impact on the magnitude of the peak dose rate. The dotted curve in Figure 13-3 shows the estimated performance with both the drip shield and the container barriers removed. The cladding barrier is still assumed to be present. With both the drip shield and container barriers removed the dose peak is shifted forward from about 400,000 years (drip shield-only removed) to about 20,000 years. The magnitude of the peak at 20,000 years is, however, not significantly different from that for the “base” case or the drip shield-only case.

The double peaks in the ‘No Drip Shield, No Container’ curve in figure 13-3 is caused by the nature of the cladding failure versus time. The first peak represents the time at which ^{99}Tc and ^{129}I dominate the dose. The second peak is when ^{237}Np dominates. The key result of this is that the cladding failing over time lower the peak release of ^{99}Tc and ^{129}I over 100,000 years as opposed to 3000 years without cladding credit.

Figure 13-4 also removes the cladding barrier so that the contribution cladding makes to safety is not masked by the presence of the container and drip shield barriers. Without ‘cladding credit’, the first dose peak is shifted forward in time to about 10,000 years. Furthermore, the dose at 10,000 years is now about an order of magnitude higher than with ‘cladding credit’. Thus, taking credit for the cladding barrier adds significantly to the defense-in-depth in the repository safety strategy.

The effect of removing all three of the major EBS barriers is shown in Figure 13-5. The major effect is to shift the time of peak dose at 20 km dramatically forward; the magnitude of the peak dose has increased by roughly an order of magnitude. This analysis confirms the obvious: the EBS barriers are important ones. What this analysis also showed, however, was that ‘cladding credit’ is also an important barrier in its own right (assuming the other two major EBS barriers are not present).

²⁷ The rather uneven nature of the early part of the ‘without cladding’ curve is a numerical artifact of the way the cladding failure versus time curve shown in Chapter 5 was implemented in the IMARC source term code (discussed in Chapter 6).

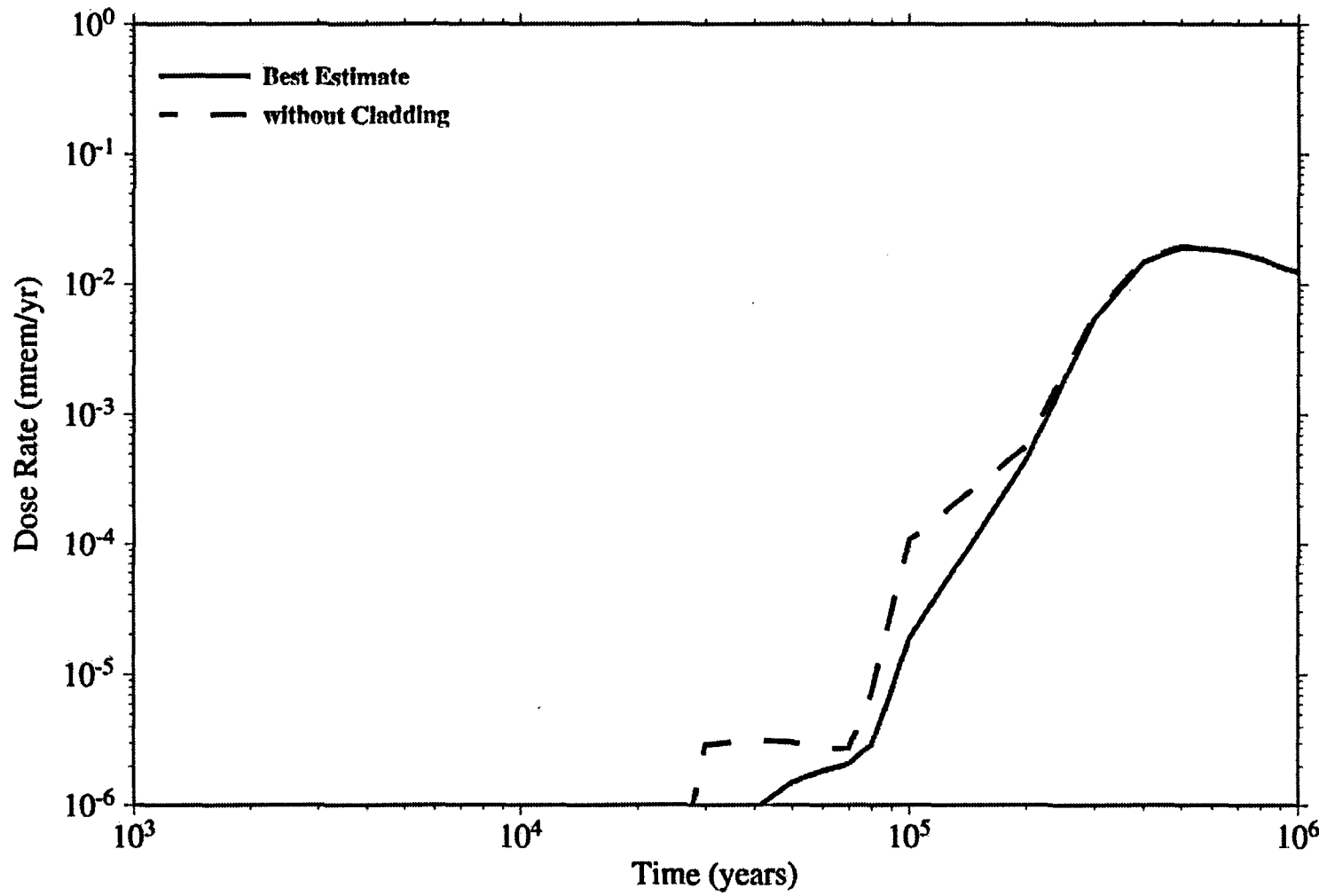


Figure 13-2
Impact on Annual Total Drinking Water Dose of Assuming No Cladding Effectiveness

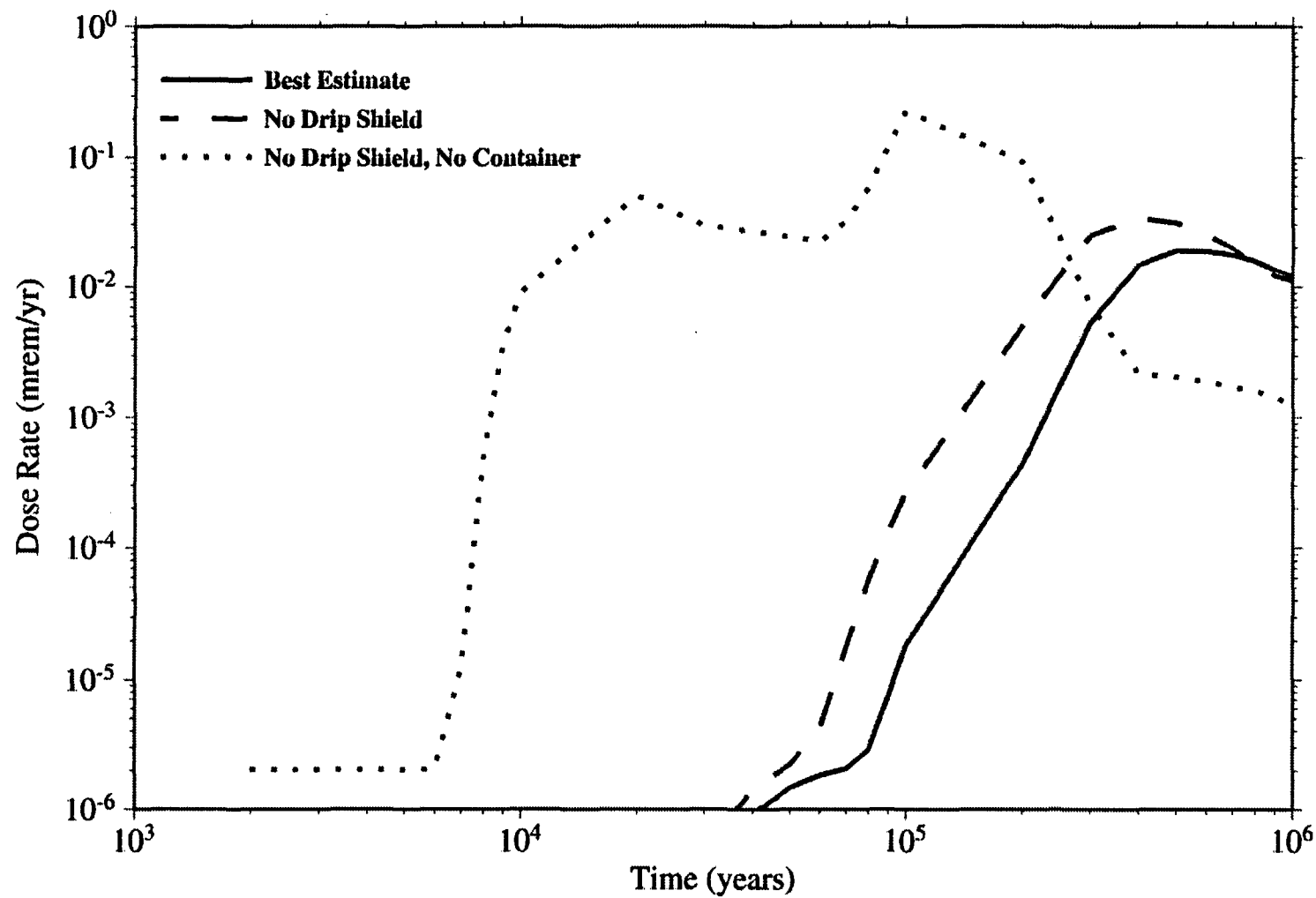


Figure 13-3
Impact on Annual Total Drinking Water Dose of Assuming No Drip Shield and No Container Effectiveness

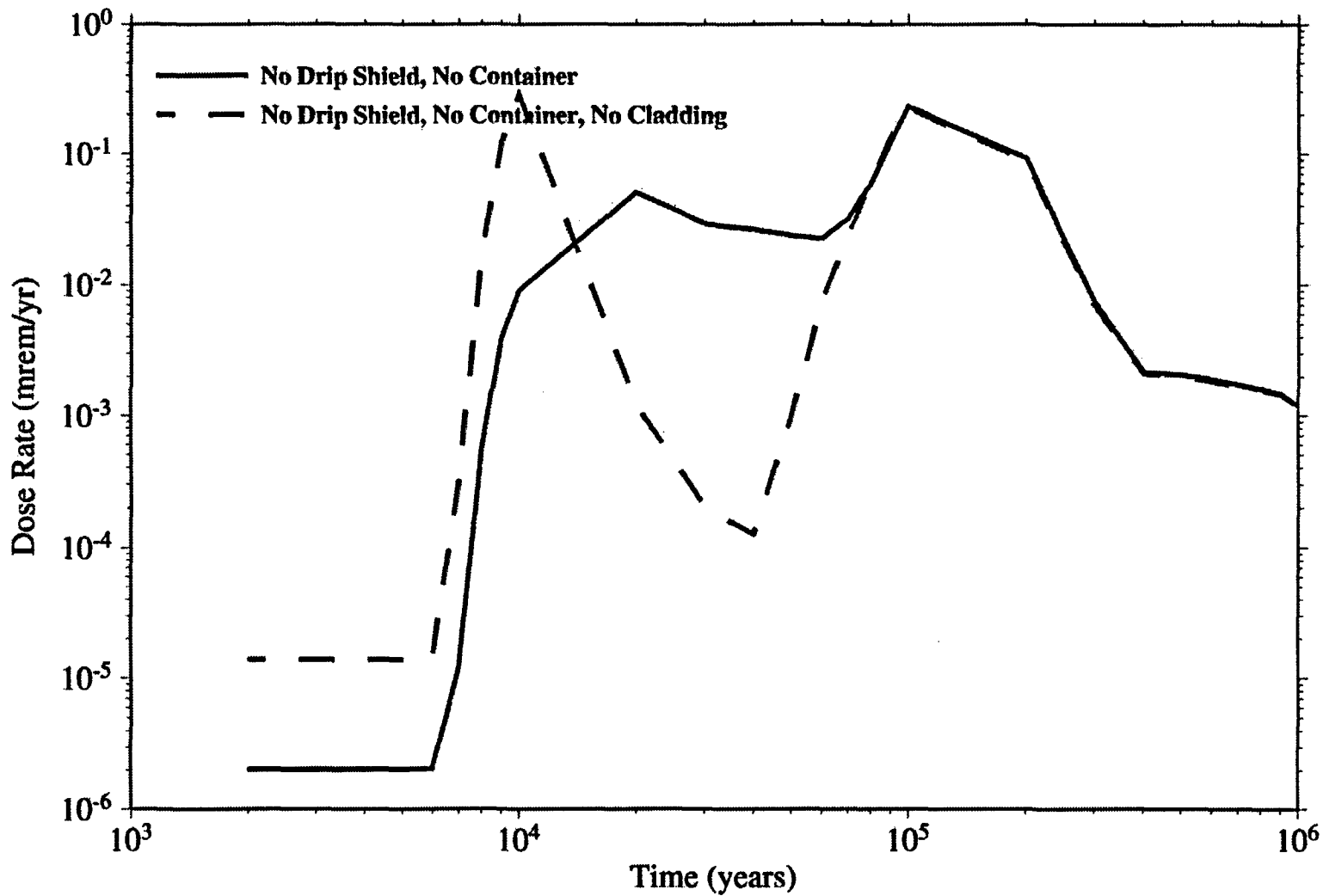


Figure 13-4
 Impact on Annual Total Drinking Water Dose of Assuming No Cladding, Container, or Drip Shield Effectiveness

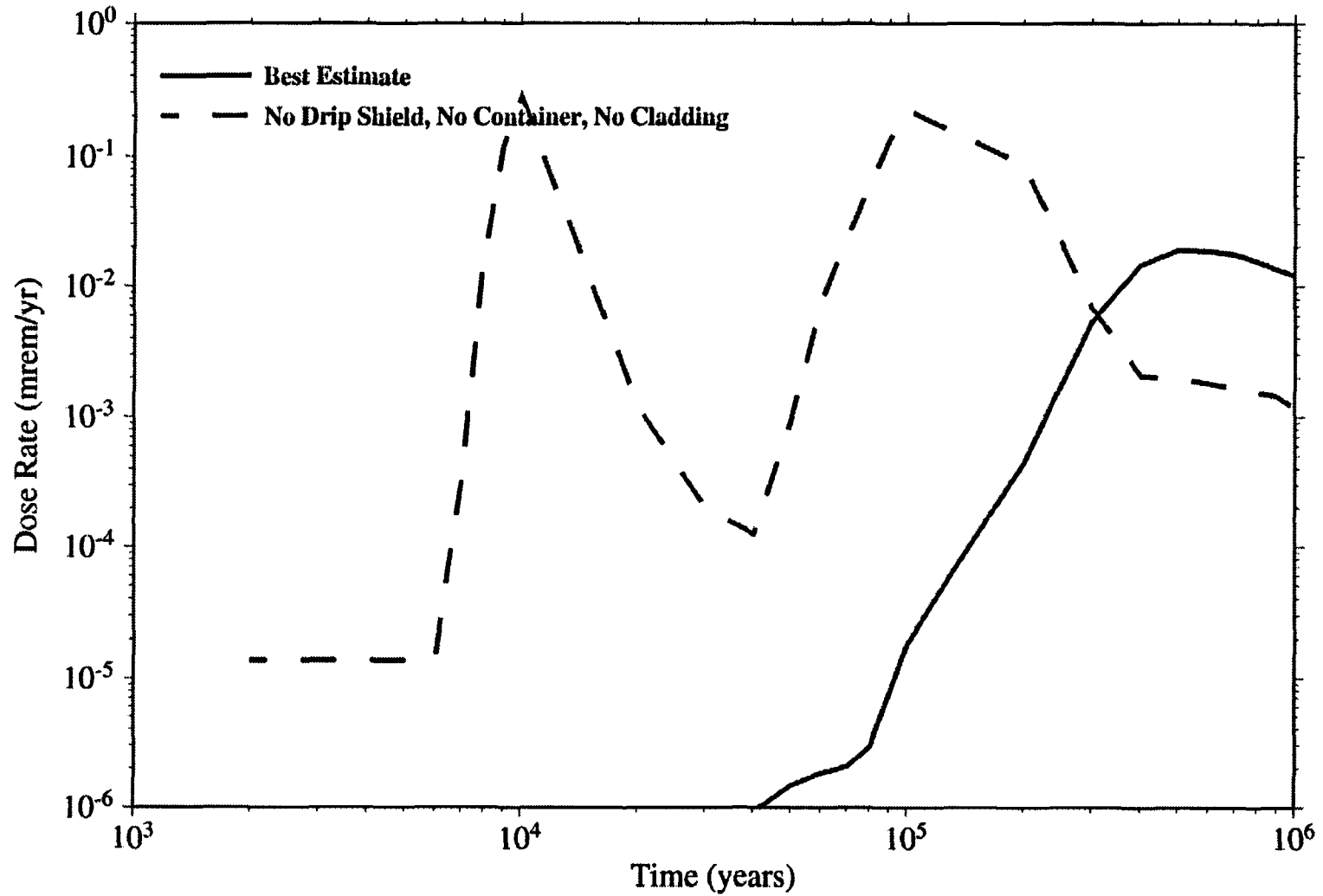


Figure 13-5
Impact on Annual Total Drinking Water Dose of Assuming No Drip Shield, Container, or Cladding Effectiveness

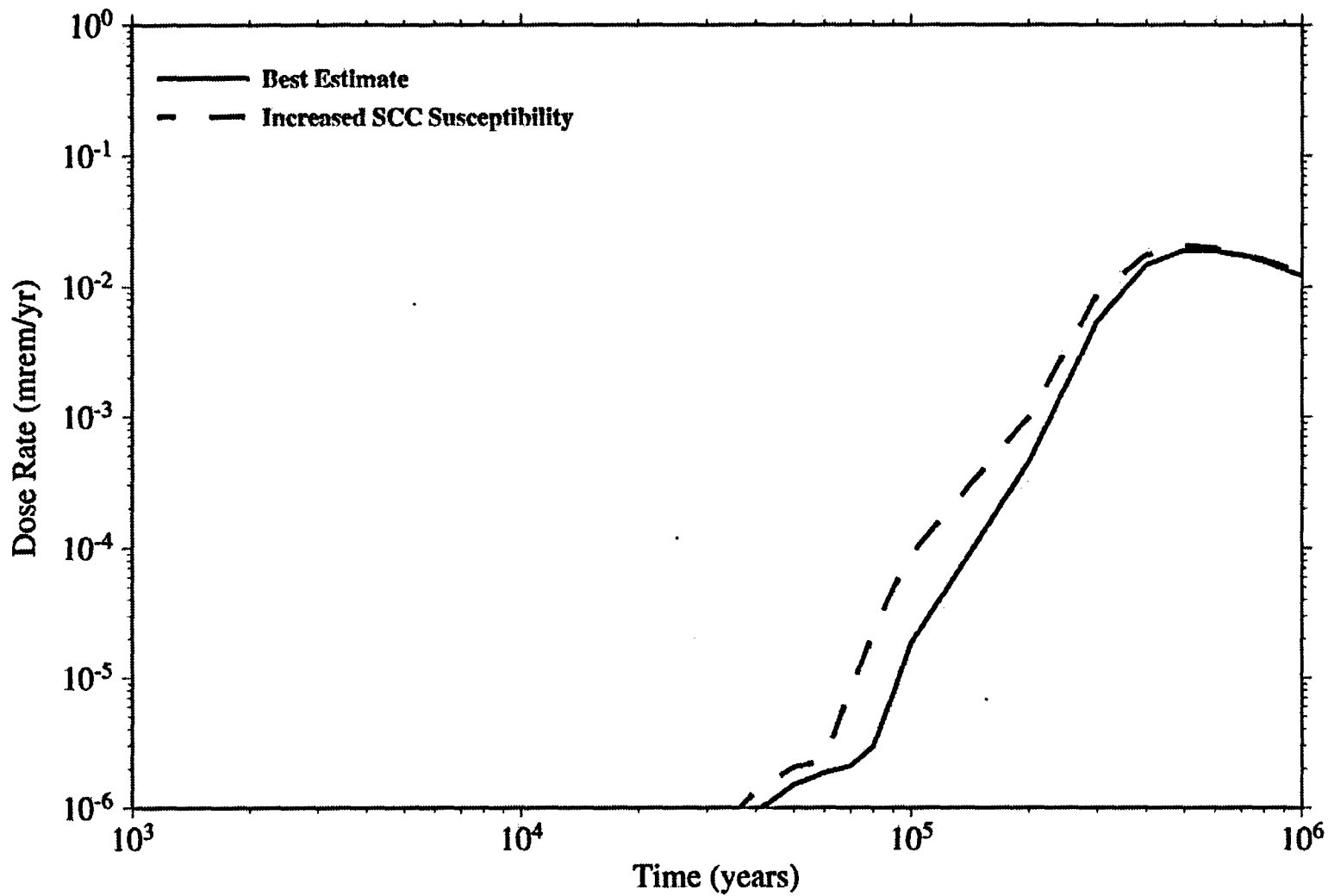


Figure 13-6
Impact on Annual Total Drinking Water Dose of Assuming Increased Container Susceptibility to Stress Corrosion Cracking

A final sensitivity study for the container barrier is shown in Figure 13-6. This provides an alternate analysis to the 'best estimate' model for container failure by assuming stress corrosion cracking in the container occurs more easily (see Chapter 5 for a complete description of this alternative model). This analysis suggests the more pessimistic model would cause the peak to be shifted forward in time by about 20,000 years.

13.3 'Hazard Index' Analyses

The purpose of the "Hazard Index" analyses provided in this section is to provide rough, quantitative estimates of the importance of the major Features, Events, and Processes (FEPs) in reducing the potential hazard due to the full inventory of disposed spent fuel and HLW disposed of at the candidate HLW disposal facility at Yucca Mountain. The approach used is to artificially "turn off" all FEPs initially, then add successive FEPs (in as logical an order as possible) one at a time to gauge their contribution to the total Hazard Index reduction. The FEPs will also be identified as being either due to "engineered" or "natural" features, or both.

13.3.1 Starting Point Assumptions for the IMARC Hazard Index Calculations

In order to "turn off" *all* of the FEPs involved with deep geologic disposal of HLW, the following, admittedly unrealistic starting assumptions are used:

- The repository contains 70,000 MTU spent fuel at some reasonable average burnup and a decay time of 2,000 years²⁸. The same inventory data used in the IMARC runs presented in earlier sections were used for the Hazard Index calculations, plus some additional inventory data for the additional radionuclides we added to illustrate the hazard reduction due to decay of some shorter-lived radionuclides;
- The entire inventory of radionuclides (from all 70,000 MTU) is assumed to be dissolved in 0.6 m³ of "drinking water". This assumes infinite solubility, and the entire inventory is concentrated in one small location;
- The 0.6 m³ (containing the entire 70,000 MTU inventory of dissolved radionuclides) is drunk by a single, adult individual over the course of one year at the beginning of their adult life (age 20);
- It is acceptable to use the drinking water pathway concentration-to-dose conversion factors found in EPRI [1996] - even for artificially high radionuclide concentrations.

Based upon the above assumptions, the starting Hazard Index for all radionuclides, HI_{in} , in the 70,000 MTU inventory is nearly 10^{17} mrem (Figure 13-14). Thus, the peak HI_{tox} will need to be reduced roughly 16 orders of magnitude to be in the range of the dose limits proposed by EPA and NRC. Since the "base case" dose rate versus time curve for the current IMARC analysis, Figure 11-2, does show that peak individual dose rates at 20 km have been lowered to

²⁸ IMARC starts with a decay time of 1,000 years, but requires its first single, 1,000-year time step to calculate the initial peak values.

10^{-0} mrem/yr it would be appropriate to be able to suggest what FEPs contribute to this dose reduction by 17 orders of magnitude.

The above starting point assumptions can be attacked for being extremely non physical. However, the intent is to neglect *all* barriers initially, such as solubility and dissolution rate constraints and the fact that it is impossible for all of the water to pass through the system and then flow into a small enough volume to be drunk by a single individual in a single year. Solubility and dissolution rate constraints are two of the many potential barriers to assign benefit to. Furthermore, the fact that engineering design can dictate how concentrated or spread out the waste is should also have a place in the calculations about how concentrated the water flow paths can get. To start with some more "real" set of assumptions would begin to neglect some of the FEPs that are in play. Since one of the purposes of these Hazard Index calculations is to show there are many barriers that contribute to hazard reduction, it is undesirable to exclude any initially. The introduction of Hazard Reduction Factors later on will allow the reader to start at a more "realistic" point if desired.

A starting time of 1,000 years was used to avoid difficulties with including shorter-lived radionuclides that would contribute greatly to the initial Hazard Index, such as Cs-137 and Sr-90. Because IMARC's smallest time step used is 1,000 years, this means that the initial calculation is actually made for 2,000 years.

13.3.2 Release Scenario

Because these represent scoping calculations, and because it is necessary to strictly control the FEPs that are introduced into the calculations, a single "scenario" was investigated having the same properties as the 'best estimate' IMARC branch shown in Figure 11-12: 'Moderate' Infiltration; No Flow Focusing; 'Moderate' Solubility; 3,000-Year Alteration Time; and 'Moderate' Matrix Retardation were considered in this "scenario". When the groundwater flux distribution through the distributed repository was included, a constant 19.6 mm/yr infiltration (moderate infiltration value for the full glacial maximum climate) was assumed in these calculations.

13.3.3 General Description

Results are presented in terms of "Hazard Index" versus time for a series of individual radionuclides, and a HI_{tot} for the total of 22 of the radionuclides contributing the most to long-term HI.

Figures 13-7 through 13-14 show the Hazard Index versus time for the starting case and for 13 sets of FEPs successively added that act to change the Hazard Index. Figures 13-7 through 13-13 are for individual radionuclides. Figure 13-14 is for the total Hazard Index summed over the 22 radionuclides contributing the most to the individual dose rate. The 14 curves shown on these figures are as follows:

- "Hazard Index" (starting case – all barriers "turned off"): All radionuclides from 70,000 MTU of spent fuel are assumed dissolved in 0.6 m^3 of water in year 1,000, which is

then drunk in a single year at year 2,000²⁹. An “alteration time”, the time required to dissolve the fuel, was set to one year to allow the IMARC code to calculate the dissolved inventory without becoming unstable. Since the fuel is dissolved in the first time step it does not affect the results.

The figure is artificial in the sense that the dose is calculated at 2,000 years only. Since all the radionuclides are assumed to be consumed in year 2,000 the curves go back to zero at the next time step (3,000 years). Thus, only the dose rates at the peak have meaning.

- “4% of Repository Wet”: This figure differs from the previous figure by a factor of 0.04. This accounts for the suite of individual FEPs that cause only a portion of the containers to come into contact with groundwater. The remaining 96% of the containers were assumed to remain dry due to the following assumptions:
 - For the smaller local percolation rates, the fact that the drifts are air-filled and curved causes the vast majority of the percolating water (for the lower local percolation rates only) to be diverted around the drifts;
 - Groundwater flow through the repository horizon is heterogeneous. So, on average, only 4% of the repository area has local percolation rates high enough to allow water to drip into the drifts and onto containers. Both of these processes were discussed in Section 5.

The FEPs contributing to the assumption that only 4% of the waste will ever be dissolved are mostly due to natural features of the repository (flow heterogeneity due to the presence of fractured, porous rock). However, the engineered feature of the drift being placed in the unsaturated zone with a drift radius small enough to divert low percolation rates around, rather than through, the drift also is an important FEP. These natural and engineered FEPs act in concert, so cannot be separated further.

For these FEPs, the “Hazard Reduction Factor” is 25 for all radionuclides. That is, these FEPs act to reduce the HI by a factor of 25.

- “3,000 yr Alteration Time”: This is representative of the barrier provided by the waste form itself. For this barrier addition it is assumed that the waste form dissolves uniformly over 3,000 years, and all radionuclides are released congruently. Because the dissolution rate has been increased by over three orders of magnitude from the previous cases, and because individuals are assumed to drink 0.6 m³ of water every year, peak concentrations have been reduced by a factor of 3000.

Again, alteration time is a function of both natural and engineered features acting in concert. That is, the dissolution rate is a function of “engineered” features, such as the waste form properties (e.g., the UO₂ matrix), and the degree to which the rest of the waste package and any other engineered materials in the engineered barrier system affect the chemistry or flow rate of the ingressing groundwater. The alteration time must also be considered a function of the “natural” features of groundwater chemistry and flow rate.

- “Moderate Solubility”: For these curves, solubility limits are added to those causing only 4% of the repository to be wet and a 3,000-year waste form alteration time. This ‘barrier’ can

²⁹ This neglects the roughly 100 years of decay time before final closure of the repository.

be considered due to the “natural” system in the sense that natural groundwater chemistry is assumed to control the solubility limits. An exception to this may be if an “engineered” feature, such as the presence of reducing or chelating agents, affected the local solubility limits. In the IMARC base case, three sets of solubility limits were considered. For the Hazard Indices presented here, the “moderate” solubility values were used.

- “Cladding Fails over Time”: This represents adding in the cladding barrier. It is assumed cladding begins to fail during the first time step. Mean cladding lifetime is several tens of thousands of years. This is considered a pure engineered barrier.
- “Containers Fail over Time”: This represents adding in the container barrier. As discussed in Section 5, containers are assumed to fail over many thousands of years. This is probably what most consider the primary engineered barrier.
- “Drip Shields Fail over Time”: This represents adding in the drip shield barrier. One drip shield is assumed failed at emplacement; the rest fail over many thousands of years. This is a new engineered barrier.
- “Dilution in the UZ”: In all the curves preceding this one, all of the flow was assumed to be limited to 0.6 m^3 per year. Furthermore, this flow was assumed to pass through ALL of the containers that were exposed to groundwater, then focused back into a small enough volume that it could be consumed by a single individual in one year.

In this curve, this assumption is removed. That is, it is assumed that the flow is no longer limited to 0.6 m^3 per year, nor refocused back into a small volume. Based on assumptions of a reasonable percolation rate over the base case repository area, actual annual flow volumes are roughly 10^4 times larger than 0.6 m^3 per year. This reduces ALL individual HI values uniformly by roughly 10^4 . The peak HI_{tot} is now reduced to approximately 10^4 .

This effective dilution factor of 10^4 is mostly due to an “engineering” decision to spread out the HLW over a large area (compared to the flow area associated with just $0.6 \text{ m}^3/\text{yr}$ flow rate). While this is not a ‘barrier’ per se, it does cause a major reduction in the hazard index, so is an important feature.

- “EBS Sorption”: These curves show that adding sorption on container corrosion products (iron oxyhydroxides) and backfill (crushed tuff) reduces the peak HI’s for those radionuclides that sorb. This can also be considered mostly an “engineered” FEP.
- “AE [Accessible Environment] at 5 km”: In all the previous curves, the HI’s at the repository exit were considered. In this figure, the travel time through the UZ and the first five kilometers of the SZ are considered. Sorption in the UZ and SZ are still neglected. This causes the peak HI_e to be reduced by another factor of over 10^2 due to additional dispersion in the SZ. This FEP can be considered mostly “natural”.
- “UZ/SZ Moderate Retardation”: These curves introduce “moderate” sorption values to the tuff. This can be considered a “natural” FEP.
- “AE in front of Alluvium”: These curves add in the effect of another 11 km of travel time in the SZ through volcanic tuff. The additional hazard reduction is about a half an order of magnitude due to additional dilution (and decay for some radionuclides). This is a natural barrier.

- “AE at 20 km”: The effect of moving the measurement point another 4 km downstream is to now include the 4 km of alluvium in the SZ. While the additional amount of dispersion on hazard reduction between 16 and 20 km is nearly negligible, the effect is more dramatic for those radionuclides that strongly sorb onto alluvium. This is a “natural” FEP.
- “Dose from All Pathways”: These curves *add* in all the non drinking water pathways to the total dose estimate (see Chapter 8 for a summary and EPRI [1996] for a detailed treatment of these other biosphere pathways). When this is done the HI’s *increase* rather than decrease. HI’s for Tc-99, I-129, and Np-237 increase by roughly a factor of 10^1 . HI’s for some of the U-235 and Np-237 daughters increase even more. The HI for Se-79 increases by a factor of roughly 10^4 . This suggests that the drinking water pathway may be a minor contributor to the total HI if subsistence agriculture making exclusive use of contaminated groundwater is assumed.

The effective positions at which the HI calculations are made change as more barriers are added:

1. Inside the container: “Hazard Index”; “4% of Repository Wet”; “3,000 yr Alteration Time”; “Moderate Solubility”
2. Immediately outside the containers: “Cladding Fails over Time”; “Containers Fail over Time”; “Drip Shields Fail over Time”
3. Just below the repository in the UZ: “Dilution in the UZ”; “EBS Sorption”
4. 5 km downstream in the SZ: “AE at 5 km”; “UZ/SZ Moderate Retardation”
5. 16 km downstream in the SZ: “AE in front of Alluvium”
6. 20 km downstream in the SZ: “AE at 20 km”; “Dose from All Pathways”

13.3.4 Presentation of Individual Hazard Index Estimates

⁷⁹Se (Figure 13-7)

Figure 13-7 presents the HI curves for ⁷⁹Se, one of the four most dominant radionuclides in the base case results for all pathways (see Figure 11-2). The initial HI for ⁷⁹Se starts at about 10^{12} , and is reduced by a factor of 25 for “4% of Repository Wet”, and another factor of 3000 when “3000 yr Alteration Time” is added. These HI reductions apply to all radionuclides as discussed earlier.

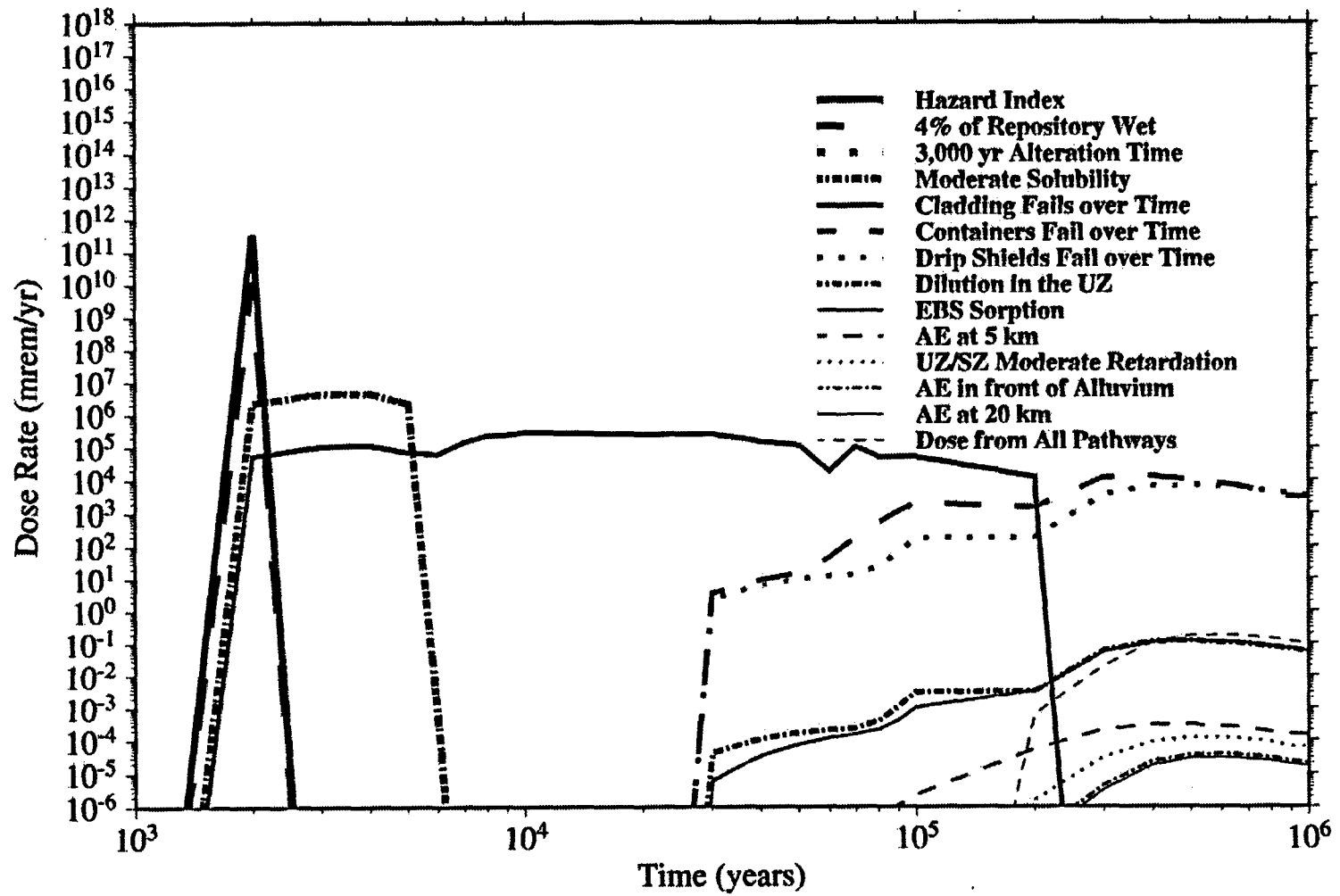


Figure 13-7
Hazard Index Curves for ⁷⁶Se

The “Moderate Solubility” curve for ^{79}Se lies directly on top of the “3,000 yr Alteration Time” curve because Se has a relatively high ‘moderate’ solubility. Thus, Se is alteration rate-limited.

Adding the cladding barrier lowers the HI by approximately two orders of magnitude, and also spreads out the HI in time.

Adding in the container barrier has the major effect of delaying the onset of radionuclide release to well beyond 10^4 years. The HI peak position is now pushed back to 300,000 years and the HI is reduced about another order of magnitude at this time. The rapid rise at 30,000 years in the HI curve for the container barrier added is a numerical artifact based on the IMARC model that doesn’t allow any radionuclides to release from the EBS until the container failure fraction exceeds 0.001.

Adding the drip shield also lowers the HI a little, perhaps as much as an order of magnitude at times of around 100,000 years. At later times, the drip shields do not have much additional effect as all the shields and containers have failed.

Adding the effect of dilution in the UZ has a dramatic effect in lowering the Hazard Index by more than four orders of magnitude. This is because it is now assumed radionuclides exiting the EBS are mixed with all the groundwater passing through 4% of the repository cross section.

Since there is a small amount of sorption of Se on container corrosion products, adding the EBS sorption barrier allows a small additional reduction in the HI. The reduction is about a factor of 10 at early times, and diminishes at later times.

Adding in transport through the UZ and the first five kilometers in the SZ (“AE at 5 km”) lowers the HI by about another three orders of magnitude and delays the arrival of the ^{79}Se plume. The HI reduction is largely due to dilution in the SZ.

Including the barrier of sorption on the UZ and SZ (“UZ/SZ Moderate Retardation”) further delays the ^{79}Se plume by another 200,000 years and lowers the HI by about an order of magnitude.

Extending the SZ to 16 km (“AE in front of Alluvium”) further delays the ^{79}Se plume by another 100,000 years and lowers the HI another factor of 5 or so. This is because there is not much additional dilution between 5 km and 16 km.

For ^{79}Se adding in the 4 km of alluvium (“AE at 20 km”) has almost no additional effect since sorption of Se on alluvium is not significant.

The last set of FEPs considered, “Dose from All Pathways” raises the HI by a factor of 5000. This is because the agricultural pathways in the assumed biosphere provide more dose than simply the drinking water pathway used in all the previous FEPs.

Table 13-1 provides a summary of the Hazard Reduction factors (HR) for ^{79}Se at both 10,000 years and at the time of peak HI (whenever the peak occurs). This table suggests that the total hazard reduction is approximately 16 orders of magnitude and that several ‘natural’ and

'engineered' barriers (dilution also considered a 'barrier' in this case) contribute to the hazard reduction. The range of Hazard Reduction factors shown for the "engineered" and "natural" FEPs toward the bottom of the table are determined by assuming the hazard reduction to those FEPs that are a combination of engineered and natural are either all engineered or all natural. The HI is increased by almost four orders of magnitude when one considers all the other biosphere exposure pathways rather than just the drinking water pathway.

Table 13-1
Hazard Reduction Factors for ^{79}Se

10,000 Years	At Time of Peak	Time of Peak [yr]	FEPs	"Engineered" or "Natural"?
10^1	10^1	2000	4% of repository wet	both
10^3	10^3	3000	3,000 year alteration time	both
10^0	10^0	3000	Moderate solubility	natural
10^2	10^2	8000	Cladding fails over time	engineered
∞	10^1	300,000	Containers fail over time	engineered
	10^0	400,000	Drip shields fail over time	engineered
	10^4	400,000	Dilution in the UZ	both
	10^0	400,000	EBS sorption	mostly engineered
	$10^{2.5}$	500,000	AE at 5 km	natural
	10^{-1}	600,000	UZ/SZ moderate retardation	natural
	10^{-1}	600,000	AE in front of alluvium	natural
	10^{-0}	600,000	AE at 20 km	natural
∞	10^{-16}		Total Hazard Reduction	
	10^{-11}		Hazard reduction due to "engineered" features	
	10^{-13}		Hazard reduction due to "natural" features	
$10^{-3.7}$	$10^{-3.7}$		Hazard "reduction" (i.e., increase) due to all pathways	

^{99}Tc (Figure 13-8)

Figure 13-8 shows the Hazard Index curves for ^{99}Tc , another of the dominant radionuclides at earlier times. The trends are similar to those for ^{79}Se with a few exceptions. There is a slight change in the HI curve for "Moderate Solubility" compared to the "3,000 yr Alteration Time" curve, which suggests a very slight solubility limitation. In addition, Tc has zero or near-zero sorption on all of the solids considered (EBS, volcanic tuff, and alluvium). Thus, adding these sorption barriers has no effect on the ^{99}Tc HI sorption curves. Adding in the dose from all pathways only increases the dose by a factor of ten for ^{99}Tc .

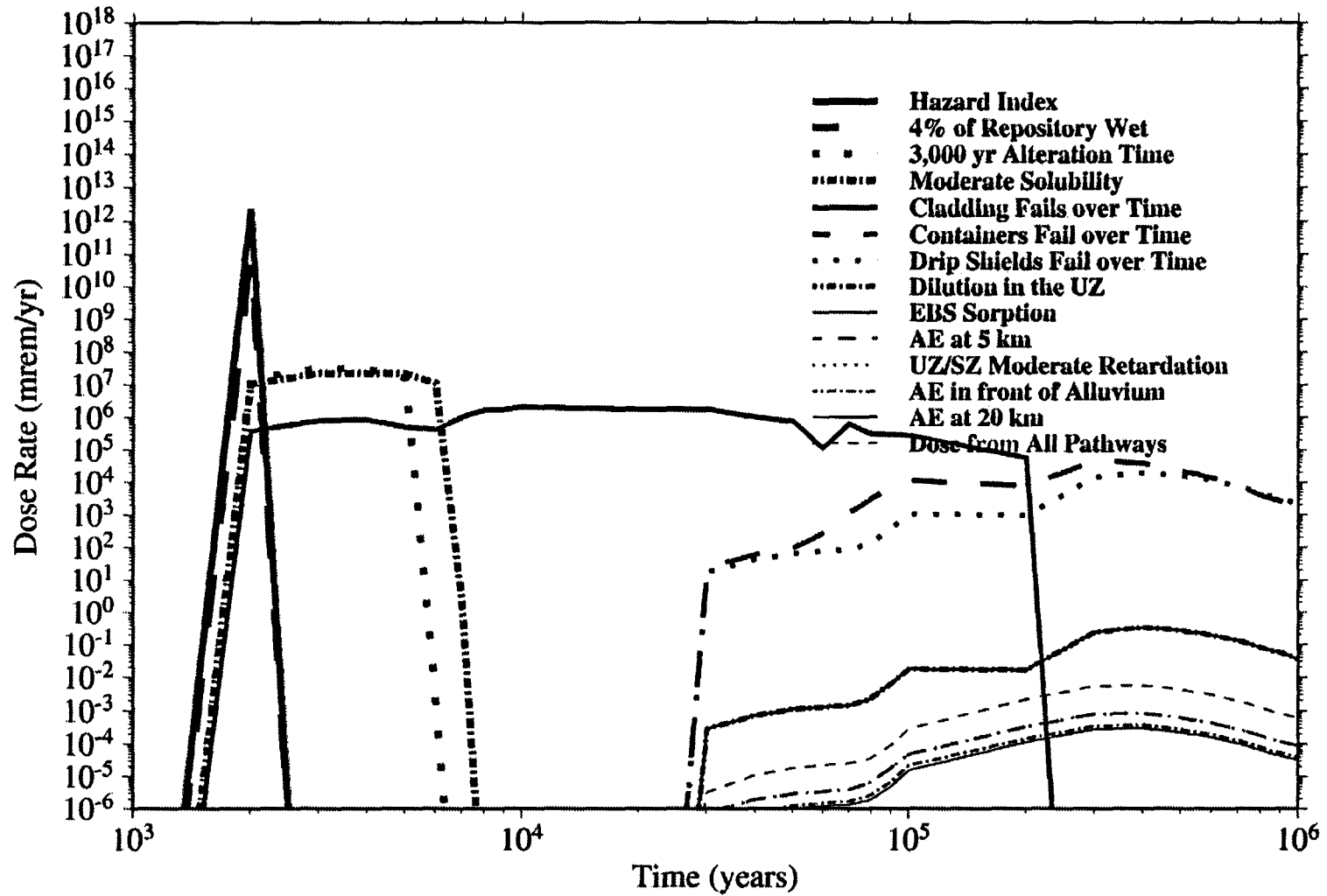


Figure 13-8
Hazard Index Curves for ^{99}Tc

Table 13-2 provides a summary of the Hazard Reduction factors for ^{99}Tc at the time of the HI peak, whenever the peak occurs.

Table 13-2
Hazard Reduction Factors for ^{99}Tc

Hazard Reduction	Time of Peak [yr]	FEPs	"Engineered" or "Natural"?
10^{-1}	2000	4% of repository wet	both
10^3	3000	3,000 year alteration time	both
10^0	3000	Moderate solubility	natural
10^2	8000	Cladding fails over time	engineered
10^{-1}	300,000	Containers fail over time	engineered
10^{-0}	400,000	Drip shields fail over time	engineered
10^5	400,000	Dilution in the UZ	both
10^0	400,000	EBS sorption	mostly engineered
10^2	400,000	AE at 5 km	natural
10^0	400,000	UZ/SZ moderate retardation	natural
10^{-1}	400,000	AE in front of alluvium	natural
10^{-0}	400,000	AE at 20 km	natural
10^{-17}		<i>Total Hazard Reduction</i>	
10^{-9-12}		<i>Hazard reduction due to "engineered" features</i>	
10^{-9-12}		<i>Hazard reduction due to "natural" features</i>	
10^{-1}		<i>Hazard "reduction" (i.e., increase) due to all pathways</i>	

^{129}I (Figure 13-9)

Figure 13-9 shows the Hazard Index curves for ^{129}I , another of the dominant radionuclides at earlier times. The trends are similar to those for ^{99}Tc . Both are relatively high solubility and low sorbing. Adding in the dose from all pathways only increases the dose by a factor of ten for ^{129}I .

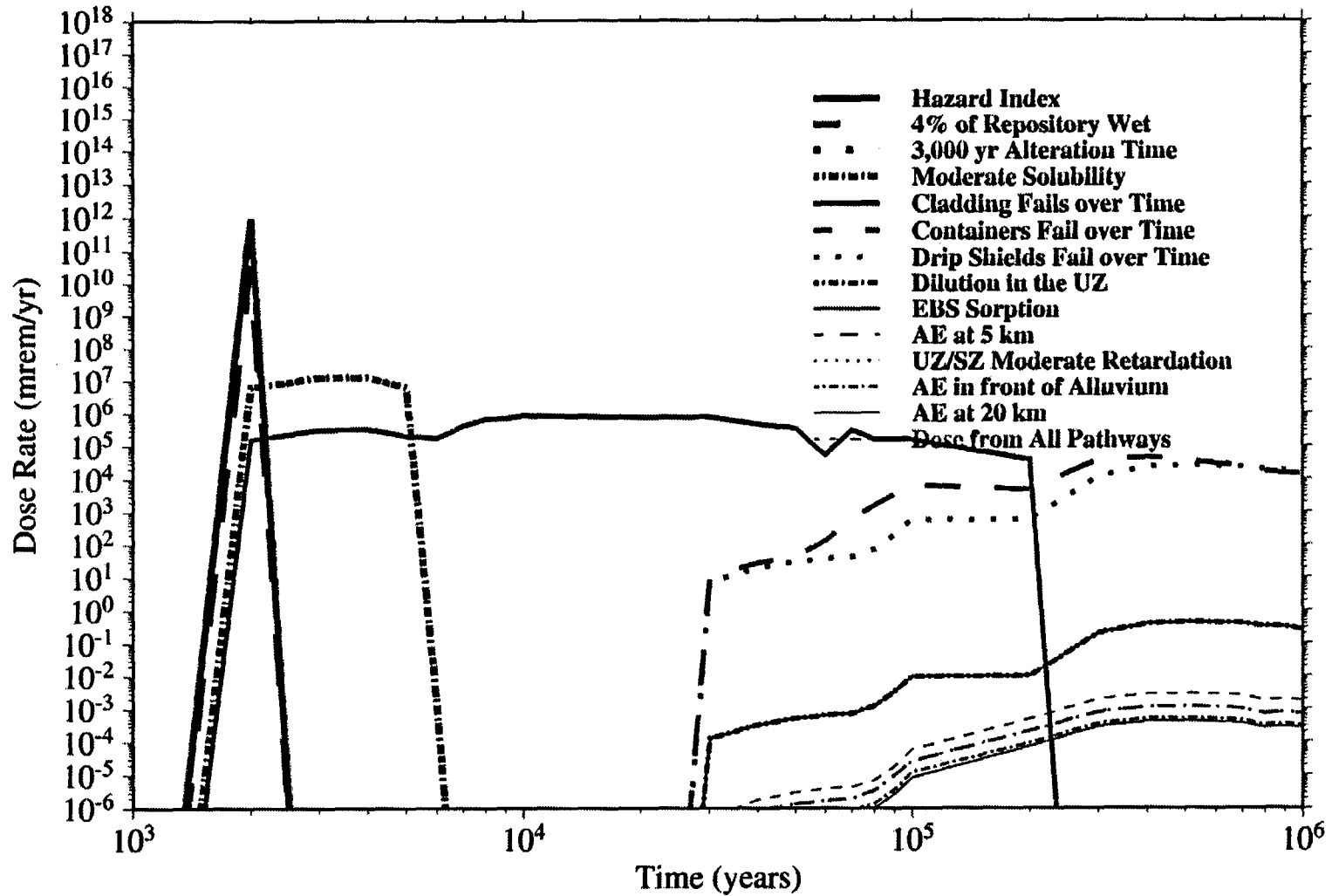


Figure 13-9
Hazard Index Curves for ¹²⁹I

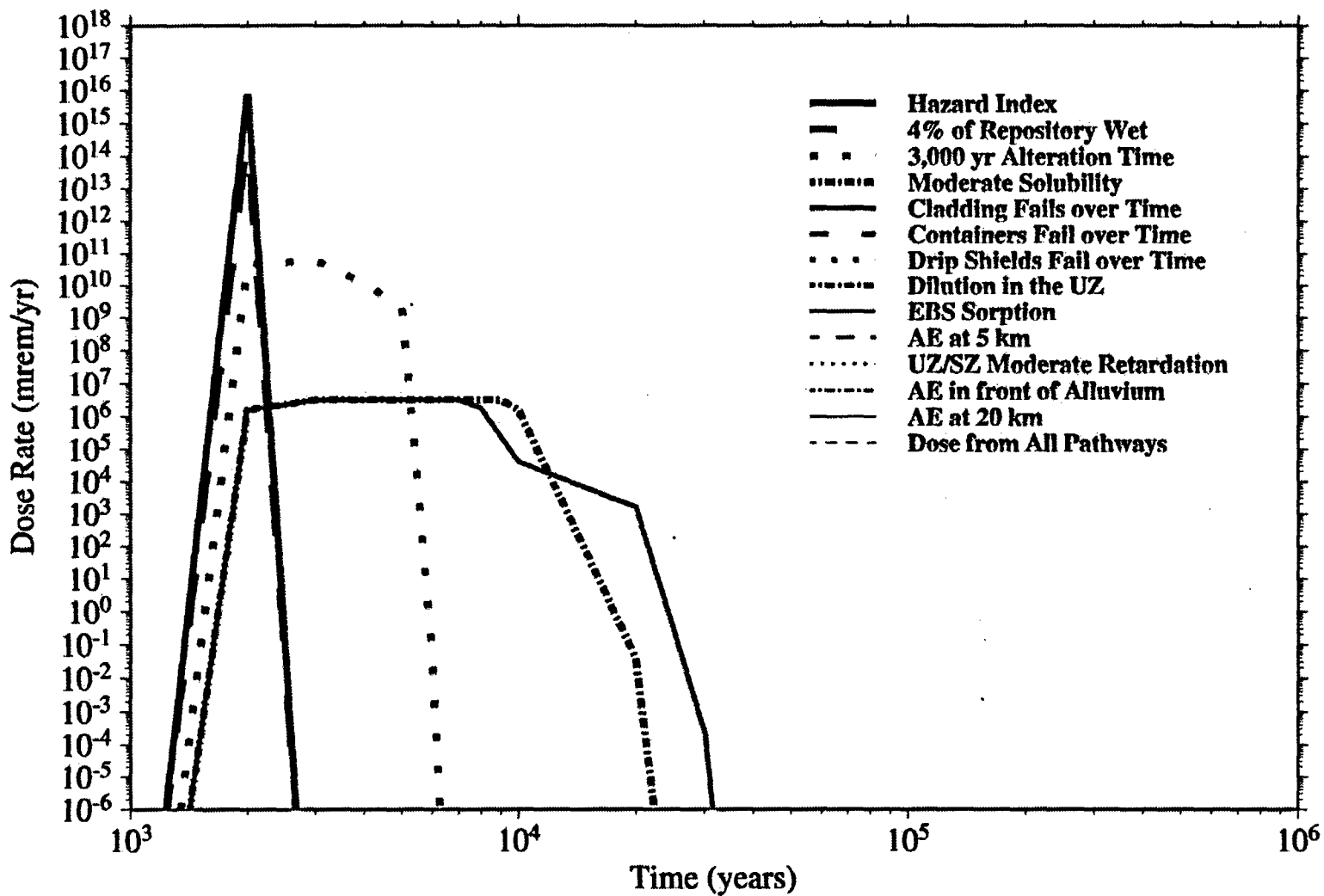


Figure 13-10
Hazard Index Curves for ²⁴¹Am

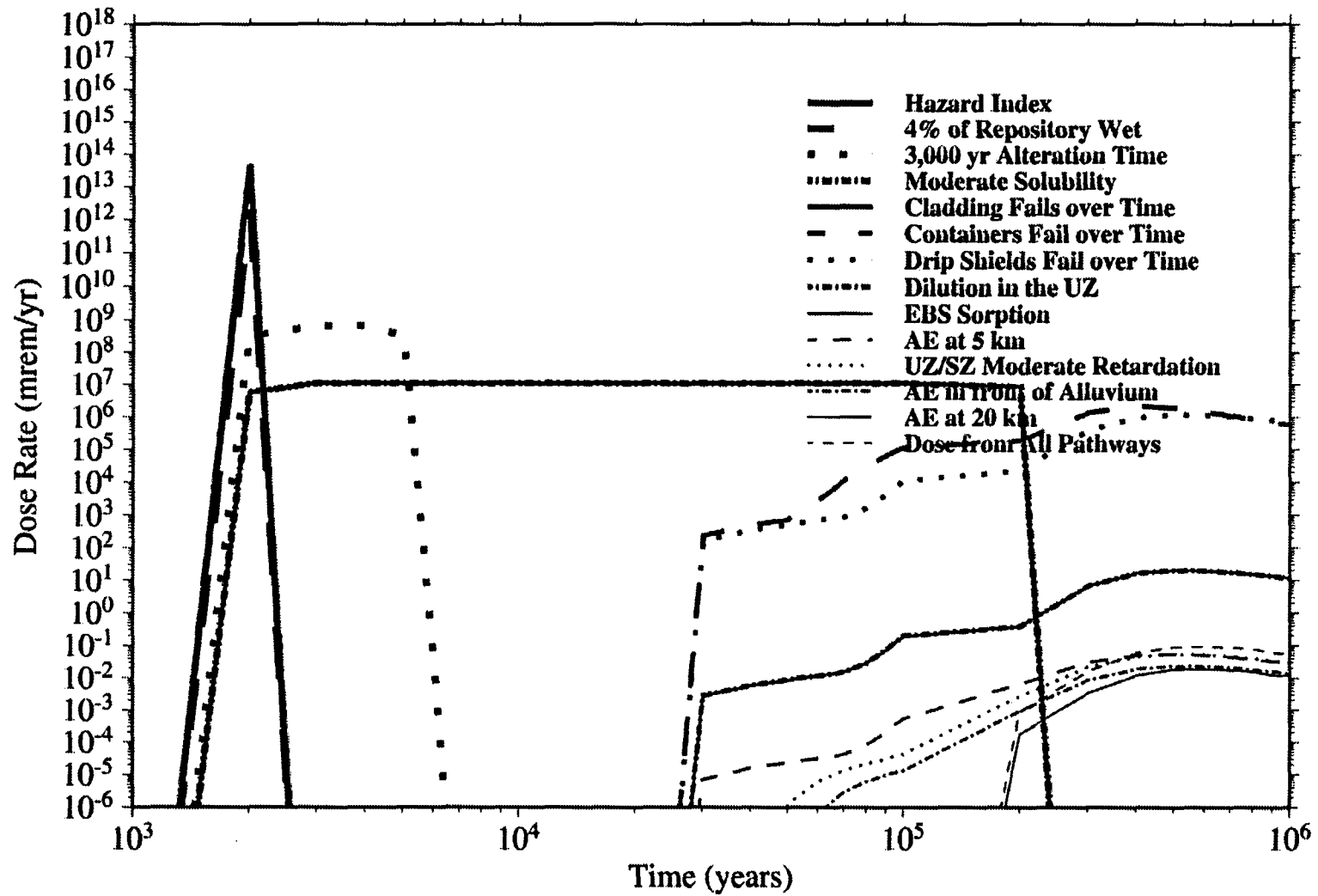


Figure 13-11
Hazard Index Curves for ²³⁷Np

Figures 13-10 through 13-13 are the Hazard Index curves for each successive member of the decay chain: $^{241}\text{Am} \rightarrow ^{237}\text{Np} \rightarrow ^{233}\text{U} \rightarrow ^{229}\text{Th}$.

^{241}Am (Figure 13-10)

The Hazard Index curves for ^{241}Am are shown in Figure 13-10. This radionuclide has a relatively short half-life, 432 years. It also has a relatively low solubility, so the Hazard Index curves show that even just adding the solubility limit is enough to show the effect of decay on the HI curve. With the addition of the cladding barrier, decay of ^{241}Am is complete.

^{237}Np (Figure 13-11)

Figure 13-11 shows the Hazard Index curves for ^{237}Np . A few aspects of the Hazard Index curve is of note for this moderately soluble, slightly sorbing species. Adding in "Moderate Solubility" for ^{237}Np lowers the HI from the previous curve by about 10^2 . However, after about 200,000 years of flow the inventory of ^{237}Np has been depleted. The solubility of Np is low enough that adding in cladding failure does not alter the HI curve. This suggests that the cladding fails fast enough that the available inventory of Np is sufficiently maintained to keep Np at its solubility limit. Only by the addition of the container barrier is the source term lowered enough to keep Np below its solubility limit. The ^{237}Np dose from all pathways is roughly ten times the drinking water dose. Table 13-3 shows the Hazard Reduction factors for ^{237}Np .

Table 13-3
Hazard Reduction Factors for ^{237}Np

Hazard Reduction	Time of Peak [yr]	FEPs	"Engineered" or "Natural"?
10^{-1}	2000	4% of repository wet	both
10^3	3000	3,000 year alteration time	both
10^2	3000	Moderate solubility	natural
10^{-0}	3000	Cladding fails over time	engineered
10^1	300,000	Containers fail over time	engineered
10^{-1}	400,000	Drip shields fail over time	engineered
10^{-6}	400,000	Dilution in the UZ	both
10^0	400,000	EBS sorption	mostly engineered
$10^{2.5}$	500,000	AE at 5 km	natural
10^{-0}	500,000	UZ/SZ moderate retardation	natural
$10^{-0.5}$	500,000	AE in front of alluvium	natural
10^{-0}	500,000	AE at 20 km	natural
10^{-16}		<i>Total Hazard Reduction</i>	
10^{-11}		<i>Hazard reduction due to "engineered" features</i>	
$10^{-5.5}$		<i>Hazard reduction due to "natural" features</i>	
10^{-1}		Hazard "reduction" (i.e., increase) due to all pathways	

²³³U (Figure 13-12)

The Hazard Index curves for ²³³U, a slightly soluble, moderately long lived radionuclide, show signs of ingrowth from its parent, ²³⁷Np. The Hazard Index curve for “Moderate Solubility”, initially about a factor of 10³ lower than the previous curve, initially rises slightly with time, before finally falling at very long times due to radioactive decay. The initial rise is caused by the ingrowth of additional ²³³U inventory from its parent. Since ²³³U shares its solubility with the other uranium species, the fractional inventory of ²³³U increases with time initially, causing its shared solubility to increase, too. Table 13-4 shows the Hazard Reduction Table for ²³³U.

Table 13-4
Hazard Reduction Factors for ²³³U

Hazard Reduction	Time of Peak [yr]	FEPs	“Engineered” or “Natural”?
10 ⁻¹	2000	4% of repository wet	both
10 ³	3000	3,000 year alteration time	both
10 ³	200,000	Moderate solubility	natural
10 ⁻⁰	200,000	Cladding fails over time	engineered
10 ⁻⁰	500,000	Containers fail over time	engineered
10 ⁻¹	700,000	Drip shields fail over time	engineered
10 ⁻⁵	700,000	Dilution in the UZ	both
10 ⁰	700,000	EBS sorption	mostly engineered
10 ²	600,000	AE at 5 km	natural
10 ⁻¹	600,000	UZ/SZ moderate retardation	natural
10 ^{-0.5}	600,000	AE in front of alluvium	natural
10 ⁻⁰	500,000	AE at 20 km	natural
10 ⁻¹⁵		<i>Total Hazard Reduction</i>	
10 ⁻¹⁰		<i>Hazard reduction due to “engineered” features</i>	
10 ⁻¹³		<i>Hazard reduction due to “natural” features</i>	
10 ⁻¹		Hazard “reduction” (i.e., increase) due to all pathways	

²²⁹Th (Figure 13-13)

Figure 13-13 presents the Hazard Index curves for ²²⁹Th. This radionuclide is interesting because it has a fairly low solubility, is a fairly strong sorber, and has a half-life of only 7300 years. Yet its behavior in this figure is strongly influenced by the decay of its parents. The initial set of HI curves are similar to that of its parent, ²³³U. However, adding in EBS sorption lowers the HI for ²²⁹Th significantly – about two orders of magnitude. Yet when the next barrier is added, “AE at 5 km” the HI for ²²⁹Th is seen to increase, a very non intuitive result. This is because Th is strongly retained in the EBS while its parent, ²³³U, is not retained nearly as much. Adding in the travel time through the first 5 km of SZ allows sufficient time for some of the inventory of ²²⁹Th to grow back in from its parent that managed to get into the UZ and SZ.

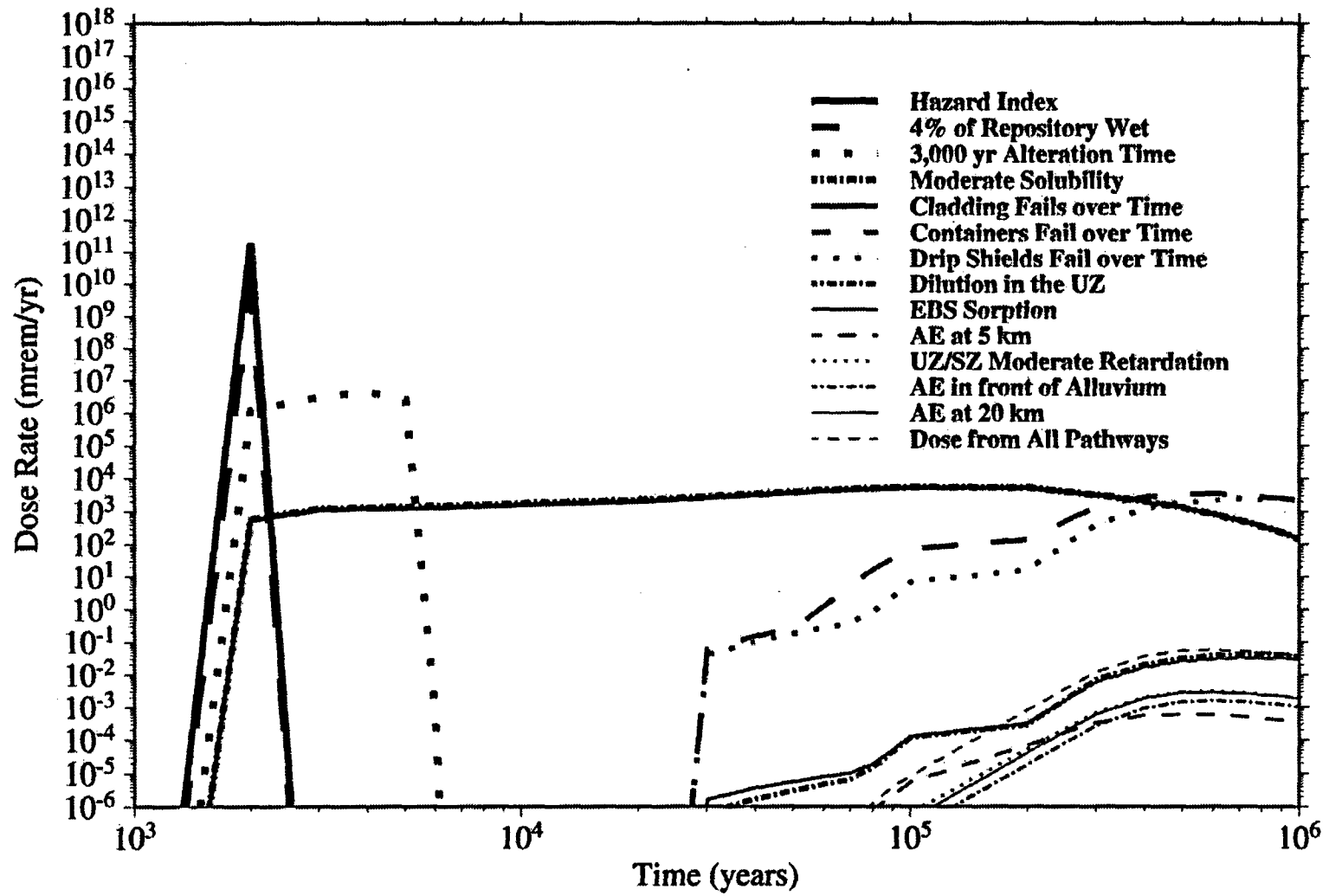


Figure 13-12
Hazard Index Curves for ^{233}U

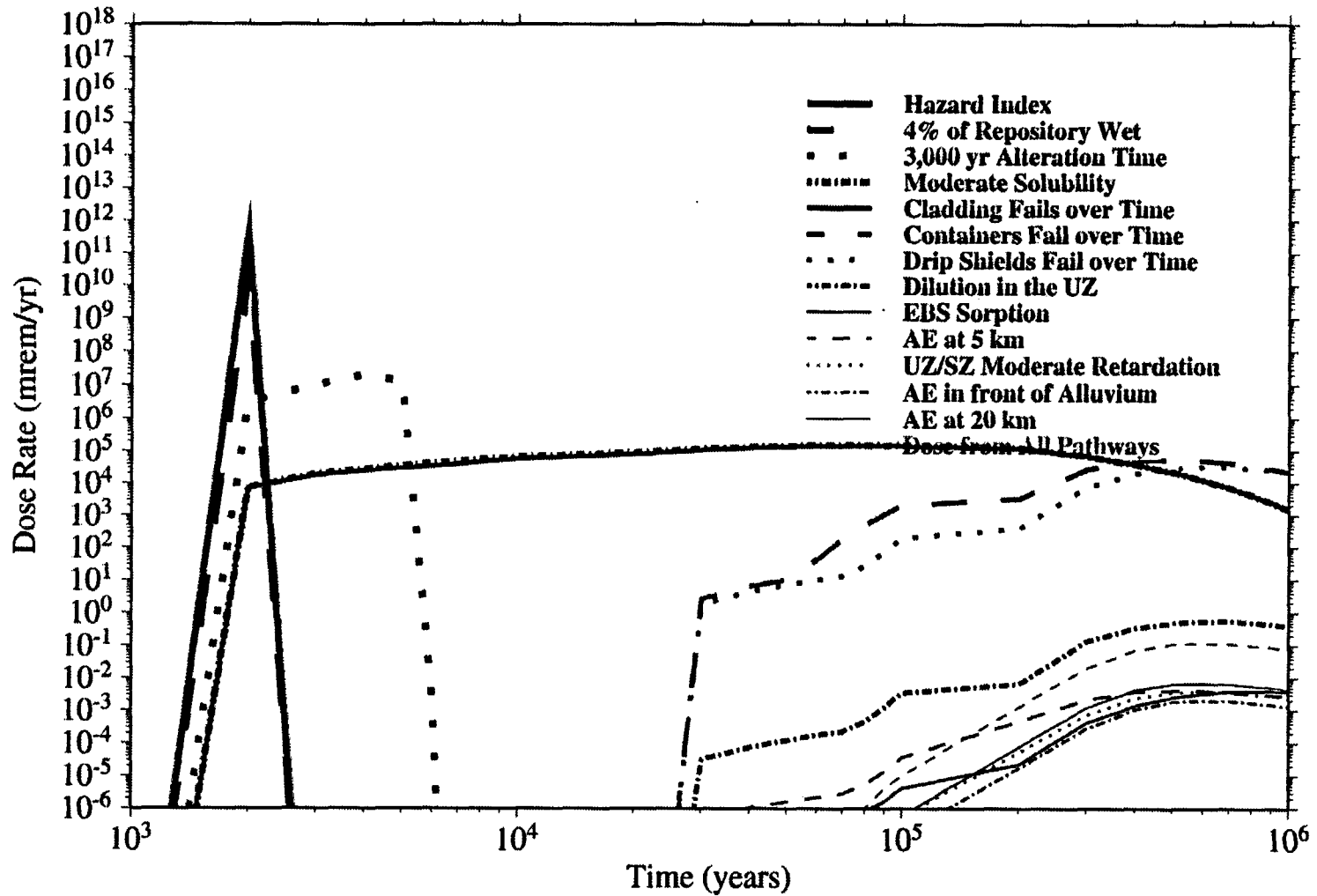


Figure 13-13
Hazard Index Curves for ^{220}Th

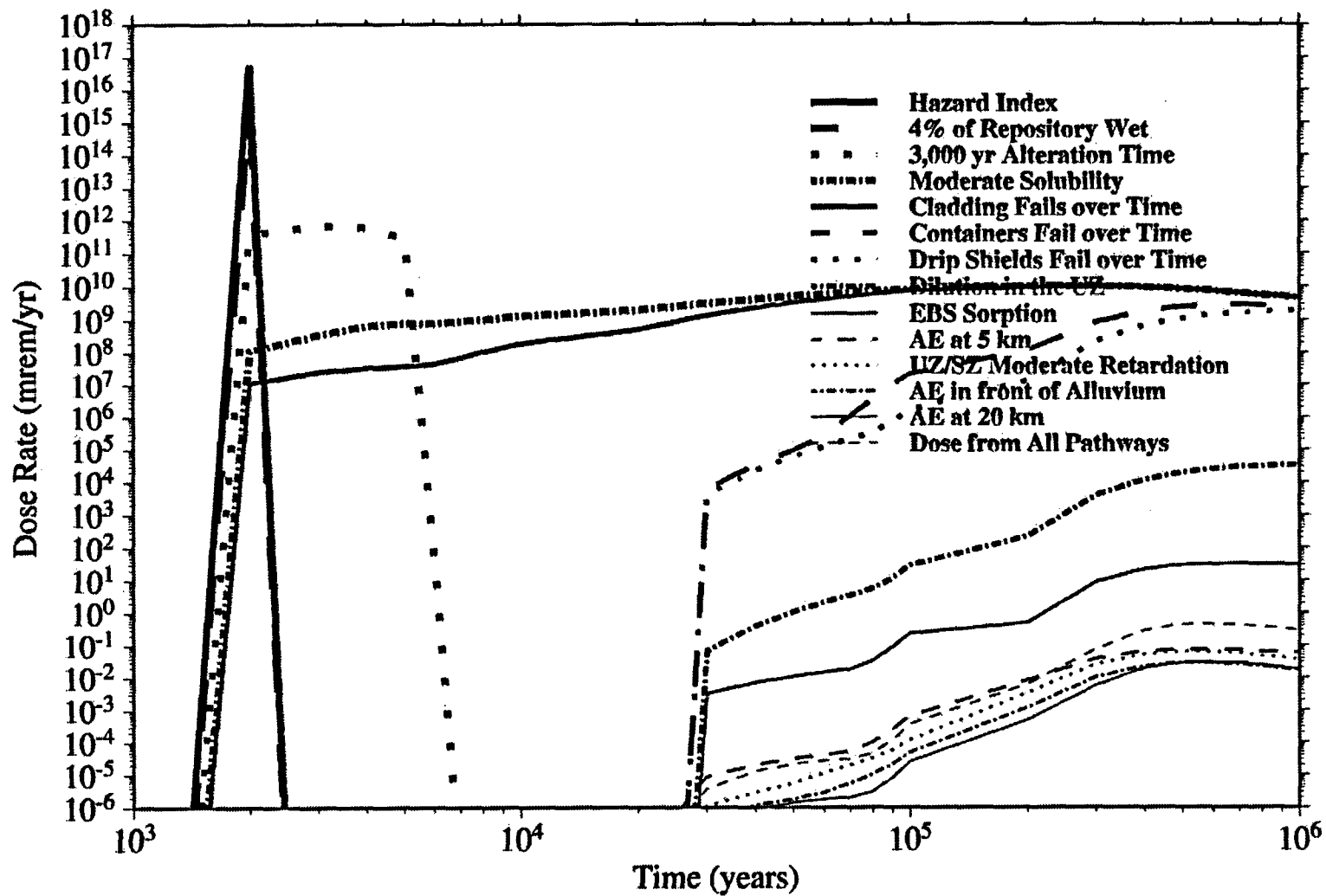


Figure 13-14
Hazard Index for 22 Radionuclides

Hazard Index Curves Summed for 22 Radionuclides (Figure 13-14)

Figure 13-14 shows the HI curves for the summed contribution of the 22 most important radionuclides to dose. Some of the most important radionuclides were shown individually earlier. The relative magnitude of the hazard reduction caused by adding each set of FEPs in succession shows significant time dependence for many of the FEPs. This is to be expected as the radionuclides dominating the total HI change with time.

This figure shows that the initial HI is approximately 10^{17} millirem. The three radionuclides contributing the most to the total initial HI are Pu-239, Pu-240, and Am-241. Thus, all FEPs will need to reduce this initial HI_{tot} by a factor of about 10^{16} to meet regulatory limits in the 10^1 mrem/yr range.

As in all of the previous figures, the “4% of Repository Wet” and “3,000 yr Alteration Time” curves lower the total HI by factors of 25 and 3000, respectively. Adding “moderate solubility” lowers the HI by about 10^3 at early times. The HI reduction benefit derived from distributed cladding failure is seen to diminish from about one order of magnitude at 2,000 years to near zero at 100,000 years. Similarly, the huge initial benefit of adding containers and drip shields at early times is nearly gone by one million years as all containers and shields have failed by that time. On the other hand, EBS sorption is seen to increase in importance at longer times since the actinides sorb more than Tc-99 and I-129 that contribute the most to the HI at earlier times.

Table 13-5 provided the Hazard Reduction factors for the combined 22 radionuclides case. As in the previous figures, many FEPs help to reduce the Hazard Index. At least several orders of magnitude HI reduction are contributed by both ‘engineered’ and ‘natural’ barriers.

**Table 13-5
Hazard Reduction Factors for the Combined 22 Radionuclides Case**

<u>Hazard Reduction</u>	<u>Time of Peak [yr]</u>	<u>Barrier</u>	<u>“Engineered” or “Natural”?</u>
10^{-1}	2000	4% of repository wet	both
10^3	3000	3,000 year alteration time	both
10^2	200,000	Moderate solubility	natural
10^{0-1}	200,000	Cladding fails over time	engineered
10^{-1}	600,000	Containers fail over time	engineered
10^{-0}	700,000	Drip shields fail over time	engineered
10^{-5}	700,000	Dilution in the UZ	both
10^3	700,000	EBS sorption	mostly engineered
10^2	500,000	AE at 5 km	natural
$10^{0.5}$	600,000	UZ/SZ moderate retardation	natural
$10^{-0.5}$	600,000	AE in front of alluvium	natural
10^{-0}	600,000	AE at 20 km	natural
10^{-18}		<i>Total Hazard Reduction</i>	
10^{5-14}		<i>Hazard reduction due to “engineered” features</i>	
10^{5-14}		<i>Hazard reduction due to “natural” features</i>	
10^{-1}		<i>Hazard “reduction” (i.e., increase) due to all pathways</i>	

The relative hazard reduction for each of these barriers is meant to be illustrative. If we had added the barriers in a different order we would have, in many cases, obtained different values of hazard reduction for them. Yet this analysis suggests there are many natural and engineered barriers that strongly contribute to overall performance. With respect to Figure 13-14, which shows the Hazard Indices for the 22 radionuclides, Table 13-6 provides a summary of their behavior as a barrier using the criteria described in Section 13.1.

Table 13-6
Assessment of Barrier Action for the 12 Candidate Barriers

<u>Candidate Barrier</u>	<u>Prevents or Delays Movement?</u>	<u>Reduces Concentration?</u>
4% of repository wet 3,000 year alteration time		Yes
'Moderate' solubility	Yes	Yes
Cladding fails over time	Yes	Yes
Containers fail over time	Yes	Yes
Drip shields fail over time	Yes	Yes
Dilution in the UZ		Yes
EBS Sorption	Yes	Yes
AE at 5km	Yes	Yes
UZ/SZ moderate retardation	Yes	
AE in front of alluvium ³⁰	Yes	
AE at 20 km ³¹	Yes	

Thus, all of the proposed 'barriers' meet the somewhat arbitrary criteria set out above as making a significant contribution. Probably the two strongest contributors to overall hazard reduction, however, are the containers and dilution in the UZ and SZ. The first is primarily an 'engineered' feature while the latter has both engineered and natural components.

For the purposes of licensing DOE may choose to fully defend only a subset of the total number of candidate barriers. This will depend on the case that can be made for 'reasonable assurance' of each candidate barrier. For the purpose of providing insight for Site Recommendation, however, the entire suite of candidate barriers should be presented to decision makers – along with information about the uncertainty in performance of each barrier over at least 10,000 years.

13.4 References

EPRI, 1996. Smith, G. M., Watkins, B. M., Little, R. H., Jones, H. M., and Mortimer, A. M. Mortimer, *Biosphere Modeling and Dose Assessment for Yucca Mountain*, EPRI TR-107190, Electric Power Research Institute, Palo Alto CA, December 1996.

³⁰ This represents the potential barrier of an additional 11 km of volcanic tuff in the SZ

³¹ This represents the potential barrier of 4 km of alluvium in the SZ

EPRI, 1998. Kessler, J. H., McGuire, R. K., Vlasity, J. A., Long, A., Childs, S., Ross, B., Schwartz, F., Shoesmith, D., Kolar, M., Apted, M., Zhou, W., Sudicky, E., Smith, G., Kozak, M., Salter, P., Klos, R., Venter, A., Stenhouse, M., Watkins, B., and R. Little, *Alternative Approaches to Assessing the Performance and Suitability of Yucca Mountain for Spent Fuel Disposal*, EPRI TR-108732, Electric Power Research Institute, Palo Alto CA, November 1998.

14

CONCLUSIONS AND RECOMMENDATIONS

There is general consensus that a risk-based approach to estimating future health consequences from the candidate spent fuel and HLW repository is appropriate. Scientific information should be considered in this light. For example, the Committee on Technical Bases for Yucca Mountain Standards (TYMS Committee) within the National Research Council noted, in their recommendations to the US Environmental protection Agency (EPA):

Implicit in setting Yucca Mountain Standard, is the assumption that EPA, USNRC [US Nuclear Regulatory Commission], and DOE [US Department of Energy] can, with some degree of confidence, assess the future performance of a repository system for time scales that are so long that experimental methods cannot be used to confirm directly predictions of the behavior of the system or even of its components. This premise raises the basic issue of whether scientifically justifiable analyses of repository behavior over many thousands of years in the future can be made. We conclude that such analyses are possible, within restrictions noted in this report. [TYMS, 1985]

Both regulatory agencies, the EPA and NRC also recognize the limitations of scientific understanding over very long time frames, and the importance of risk-based approaches in their draft regulations for Yucca Mountain. For example, in paragraph 63.101(a)(2) of NRC's draft regulation for Yucca Mountain, NRC notes:

Although the performance objective for the geologic repository after permanent closure specified at §63.113 is generally stated in unqualified terms, it is not expected that complete assurance that the requirement will be met can be presented. A reasonable assurance, on the basis of the record before the Commission, that the performance objective will be met is the general standard that is required. Proof that the geologic repository will be in conformance with the objective for postclosure performance is not to be had in the ordinary sense of the word because of the uncertainties inherent in the understanding of the evolution of the geological setting, biosphere, and engineered barrier system. For such long-term performance, what is required is reasonable assurance, making allowance for the time period, hazards, and uncertainties involved, that the outcome will be in conformance with the objective for postclosure performance of the geologic repository. [NRC, 1999]

Thus, total system performance assessments (TSPAs), such as the one presented in this report, do not, nor need not achieve scientific 'purity'; it need not match, for example, every little wobble in the climatic and infiltration record or track the corrosion process in every inch on the container surface. Rather, we attempt to achieve a 'stylized' estimate of future reality such that we can model things with reasonable amounts of data and still achieve confidence that future radiological impacts will be reasonable. As described above in the quote from the NRC, it is confidence that future populations will be adequately protected that is the main goal of

TSPA- not scientific purity. The abstractions of features, events, and processes made in TSPA need to be viewed in this light.

The iterative TSPA process, if used wisely, can become an important management tool, guiding the allocation of future resources toward those components of the repository system with the greatest impact on overall performance, and away from those components that do not affect performance. This is a central role for TSPA. As a management tool a TSPA is less dependent on the ability to correctly “predict” future doses. Rather, it is only important to assess the relative effect of various management decisions regarding what additional site information needs to be collected or what process models need to be developed.

14.1 Suitability of Yucca Mountain as a Permanent Repository

The current preferred approach to the disposal of HLW and spent fuel is deep geologic disposal. Yucca Mountain is being developed as a candidate site. The adequacy of Yucca Mountain as a host site must be assessed in the face of uncertainty. As discussed above, quantitative compliance assessments will most likely require an examination of the absolute values of the dose rates (or health risks). It will be necessary for the regulators to provide detailed feedback to the performance assessor on the acceptable approaches for dealing with issues containing a large degree of uncertainty. This is especially true for issues regarding future human behavior which are completely unknown, yet can have a huge impact on calculated doses.

If the candidate repository at Yucca Mountain is built and filled with spent fuel and HLW according to the repository design upon which our TSPA model was based we are confident that very low doses to hypothetical individuals living in the vicinity of Yucca Mountain due to the presence of the repository can be reasonably assured for many thousands of years into the future. The time period of low doses is likely to exceed 100,000 years – ten times longer than the recorded history of human civilization. If this is considered an appropriate measure of performance, then Yucca Mountain is suitable as a permanent HLW repository. While we have not yet considered volcanism quantitatively, our qualitative evaluation of the consequence analysis prepared by the M&O for TSPA-SR is that it is very conservative (see Chapter 9 and Appendix A). Thus, while there is a low probability of a volcanic event in the first 10,000 years from volcanism, our opinion is that the consequences have been overestimated by the M&O such that volcanism – in terms of risk (with the probability of volcanism factored in) – does not result in a high dose risk.

Beyond 10^4 years, our TSPA model of the ‘normal release scenario’ suggests the dose rate to a “conservative” individual³² will never be more than a fraction of natural background levels. Dose rates to an average individual living in the vicinity of Yucca Mountain will be even lower. If the regulatory limit is a dose rate on the order of natural background levels then the existing IMARC model shows compliance for even the conservative individual for time periods beyond 10^4 years, as well. It is likely that further site development work and TSPA model refinements to eliminate some large conservatisms can be made that would further reduce projected dose rates (see Appendix A). A wide uncertainty band will be associated with any dose projection that far

³² Roughly equivalent to the average member of a critical group.

into the future, however. A large portion of that uncertainty band in the TSPA will remain and will have to be integrated into a performance confirmation plan.

The Yucca Mountain site has several beneficial features that act to limit the potential health consequences of waste disposal.

- It is in an enclosed basin, so groundwater flow is limited.
- The fact that the region is (and will likely remain) fairly arid means the population that can be supported by *exclusive* use of potentially contaminated groundwater is limited;
- The fact that the repository is located in the unsaturated zone means that the majority of the waste containers are likely to remain dry. No other candidate HLW disposal site has this very beneficial feature.

We believe there is much merit to the current repository design compared to the design in place at the time of the Viability Assessment two years ago. The incorporation of another engineered barrier, in this case a titanium drip shield, was judicious. It significantly diminishes the impact of the large uncertainty, in the amount and distribution of groundwater flow at the repository horizon, on our confidence that doses during the first 10,000 years will, indeed, remain low.³³ The change of the container design itself was another great improvement related to both improved performance and uncertainty reduction. By putting the Alloy 22 on the outside, instead of keeping it on the inside of carbon steel, DOE eliminated a major uncertainty in performance of the older container design having to do with chemical and mechanical conditions at the surface of the Alloy 22. This change in container design vastly extends the container lifetime. Incorporation of the drip shield not only extends the container lifetime further, but also reduces the impact of any 'early' container failure by making it very unlikely that both the drip shield and the container would fail early in the same location.

The current repository design for the proposed repository at Yucca Mountain has received some criticism for placing too much reliance on a single barrier – the waste container. If this *were* true, although our own analyses suggest it is not, then this would be inconsistent with the very sensible NRC requirement for multiple barriers. Analyses presented in Chapter 11, but especially Chapter 13, suggest there are multiple natural and engineered barriers that significantly delay the release of radionuclides into the biosphere and/or significantly reduce the concentration of those radionuclides. While the container barrier is certainly very important, our analysis suggests that the safety case for Yucca Mountain would not fall apart if some, as yet undiscovered, flaw in the container design is found in the future. It is recommended, however, that DOE work to further bolster confidence in some of the natural barriers.

Our analysis of the current M&O TSPA-SR (based on the available M&O Analysis Model Reports and Process Model Reports at the time of this writing) suggest that a few optimisms and a great many conservatisms were incorporated in their models.³⁴ These are discussed in

³³ EPRI advocated the use of an additional barrier capable of diverting groundwater around the container some time ago [see, for example, EPRI 1996a].

³⁴ As discussed in Chapter 12, adoption of conservative models and parameter values is sometimes justified. For example, if certain parameters or models have less effect on overall repository performance, then it is justifiable to

Appendix A. On the whole, the conservatisms in the M&O models outweigh the handful of optimisms such that the result of the M&O analyses probably overestimate annual doses by a wide margin. In the IMARC analyses presented in this report we have attempted to eliminate some, but not all of these conservatisms.³⁵ In doing so we estimate significantly lower peak annual doses over the very long term compared to recent DOE estimates presented to, for example, the US Nuclear Waste Technical Review Board. Our estimates of peak doses beyond 10,000 years are two to three orders of magnitude lower than those presented by DOE. This provides confidence that the proposed Yucca Mountain repository is likely to have significantly better performance than DOE is now giving it credit for. In particular, we find that the performance of many of the natural barriers is likely to be very much better than some of the current DOE models suggest.

Thus, there is reason to expect that Yucca Mountain will be suitable as measured against a variety of potential performance criteria. Yucca Mountain should continue to be developed and a License Application should be prepared. This does not mean to imply we feel additional R&D is not needed. Rather, as described in the next section, some additional R&D is justified prior to the decision to begin repository loading, and certainly before repository closure. However, we feel sufficiently confident in the currently available information and conservative analyses to think that Yucca Mountain is, indeed, a suitable site. Additionally, specific R&D over the course of the next few years to decades should help provide the necessary confidence to proceed to repository loading and ultimate closure in a licensing environment.

14.2 Recommendations for Future Work

14.2.1 General Comments

We have assumed the ultimate goal of activities at Yucca Mountain is to provide reasonable assurance that the site is suitable - and licensable - for safely and permanently disposing of spent fuel and HLW. Thus, additional site development work must be geared to provide sufficient confidence that this can be achieved. Supporting confidence in the regulatory decision will be critical to the successful licensing of any HLW disposal facility. Part of this confidence will be the demonstration of multiple barriers. Thus, future work should be geared toward:

1. Identifying which barriers contribute to performance, and the demonstration that those barriers function at least as well as predicted. The current Repository Safety Strategy effort by DOE is certainly appropriate in that regard. It may be useful, however, to identify a somewhat smaller set of barriers for which quantitative estimates of their contribution to performance can be made. Chapter 13 presents such a set of candidate barriers. A 'Hazard Index' approach of quantifying their contribution to overall performance was also suggested

use conservative values instead of embarking on additional, sometimes costly research. In addition to these, DOE has, in some cases, applied conservative values and models to some FEPs that *do* have a significant influence on overall performance. Some, but not all conservatisms of this second variety in the DOE model could be reduced through additional research. This will be discussed in a companion EPRI report on performance confirmation and an appropriate long-term, committed R&D program for Yucca Mountain.

³⁵ See Appendix A also for a discussion of the optimisms and conservatisms identified for the IMARC code.

in Chapter 13. It is recommended that both DOE and NRC conduct a similar analysis. DOE has partially done so with their 'neutralization' and 'degraded barrier' analyses. We encourage DOE to continue to make appropriate use of such analyses since they provide a significant amount of insight.

2. Exploring alternative indicators of performance as additional input for regulatory insight. Chapter 15 of EPRI [1998] provided a few suggestions of such alternative indicators. Although quantitative analysis of these indicators are not appropriate as the primary compliance measure, they can be useful to put some of the primary analyses into perspective. Alternative indicators of performance also includes natural analogs. DOE has already made partial use of natural analogs in the development of some of their performance assessment models. Direct, quantitative use of natural analog information is often difficult to apply to the specifics of the Yucca Mountain candidate repository. Yet more can be done to make use of a larger amount of natural analog information to further bolster confidence in results of TSPAs.
3. Making a better case for the existing barriers – especially natural barriers. We encourage DOE to pursue efforts to, for example: provide better estimates of the long-term solubilities of key radionuclides; provide reasonable estimates of fracture/matrix interaction in both the unsaturated and saturated zones under natural flow conditions; and demonstrate that closure welds can be made and stress-relieved reliably.
4. Providing perspective on the suite of mostly conservative assumptions in the current DOE analyses. While a conservative approach may be appropriate for licensing, it would be useful for the Site Recommendation to give decision makers a better appreciation for the magnitude of some of the major conservatisms (or optimisms) in the TSPA-SR.

14.2.2 Specific Recommendations

Several possible recommendations for future work can be made based on the sensitivity and other ancillary studies presented in this report.

Flow Heterogeneity

We support further field and modeling work to narrow the range of uncertainty regarding the fraction of the repository that may experience active dripping under various conditions. Specifically, work to reduce the reasonable upper bound on the fraction of the repository experiencing active dripping will be of significant value to overall performance.

Drip Shield/Container/Cladding

These three barriers within the EBS are shown to have very significant importance in mitigating radiological consequences of the candidate Yucca Mountain HLW repository. Thus, the current performance of these three barriers must be shown to be adequately reliable. Some of the fundamental assumptions about constructability, and long-term corrosion behavior certainly warrant additional R&D. We encourage the continuation of the work at the Long Term

Conclusions and Recommendations

Corrosion Test Facility and continued review of the test plan for this facility to make sure a sufficiently wide range of thermal, mechanical, and chemical conditions are used.

Furthermore, considerable reliance on the integrity of the closure welds is assumed in making the safety case for Yucca Mountain. It is assumed that the remote welding and stress-relief operations can be tightly controlled and the properties of the resulting welds are adequately known and consistent. It may be useful to develop a weld test and demonstration facility to provide further assurance the welds will be at least as good as presently assumed. Such a test facility may also help in improving the welding procedures, and could result in eliminating some of the potentially conservative assumptions now being made by both DOE and EPRI.

We encourage DOE to develop alternative lines of reasoning regarding the very long-term passivity of the corrosion layer on Alloy 22. Chapter 5 of this report provides some of the same and some additional arguments about why we feel very long-term passivity will probably be maintained. This issue should be included in a long-term research program.

Solubility/Sorption Data

The M&O has noted that one of the most significant conservatisms leading to their current dose projections over the very long term is that they do not assume some radionuclides are incorporated into secondary phases. This results in higher solubility estimates for neptunium, for example, than actually might exist. Since neptunium is the leading contributor to very long-term dose in the DOE model, and one of the major contributors in the EPRI model, it would be useful to do additional work to make a case for incorporation of neptunium, and other similar radionuclides into secondary phases.

Unsaturated and Saturated Zone Fracture/Matrix Coupling and Dilution

The IMARC analyses assume considerable credit for fracture/matrix interaction in slowing the migration of all species be they nonsorbing or sorbing. We provide analyses in Chapter 7 that back up this claim and points out the potential conservatisms in the current M&O approaches on this issue. Additional work to determine the degree of fracture/matrix interaction under natural flow conditions would prove valuable.

Another very important 'barrier' – of a sort – that was identified in the work presented here is the considerable amount of dilution thought to occur between the repository and the accessible environment. We estimate concentrations between the bottom of the EBS and the accessible environment to be lowered by at least five orders of magnitude. This estimate is based on assumptions about the amount of dispersion that can be expected mostly in the saturated zone (see Chapter 7). Improving our estimates of dispersion in the SZ will require well thought out, large scale (in both space and time) testing. This could be another important aspect of a long-term research program.

Biosphere/Human Behavior

It has also been noted in previous IMARC reports [e.g., EPRI, 1998, Chapter 18; EPRI 1996b] that the current plans to use a critical group are highly conservative – or at least misleading if decision makers are inadvertently led to believe the *entire* downstream population would receive doses as high as the critical group. Even if the critical group concept is preserved for compliance purposes, it is recommended that individual dose distributions in the local population be estimated to provide insight to decision makers and public confidence.

Volcanism

Given the projected robust, long-term performance of the EBS components of the new repository design, only the volcanism and human intrusion scenarios have the potential to contribute substantially to the dose projections during the first 10,000 years after repository closure. EPRI has not reviewed the human intrusion scenario the M&O uses. The volcanism consequence analyses have been partially reviewed in Chapter 9. The current M&O and NRC volcanism consequence models are thought to be significantly conservative. Given that volcanism consequences appear to dominate dose estimates during the likely regulatory compliance period, it would be very useful if more reasonable dose consequence analyses were available to augment the current conservative analyses. More can and should be done to provide projections of performance that are more 'best estimate' and less 'bounding'. Such projections should and can be made available to Site Recommendation decision makers.

14.3 References

EPRI, 1996a. Zhou, W., Conca, J., Arthur, R., and M. Apted, *Analysis and Confirmation of Robust Performance for the Flow-Diversion Barrier System within the Yucca Mountain Site*, EPRI TR-107189, Electric Power Research Institute, Palo Alto CA, December 1996.

EPRI, 1996b. Smith, G. M., Watkins, B. M., Little, R. H., Jones, H. M., and Mortimer, A. M. Mortimer, *Biosphere Modeling and Dose Assessment for Yucca Mountain*, EPRI TR-107190, , Electric Power Research Institute, Palo Alto CA, December 1996.

EPRI, 1998. Kessler, J. H., McGuire, R. K., Vlasy, J. A., Long, A., Childs, S., Ross, B., Schwartz, F., Shoemith, D., Kolar, M., Apted, M., Zhou, W., Sudicky, E., Smith, G., Kozak, M., Salter, P., Klos, R., Venter., A., Stenhouse, M., Watkins, B., and R. Little, *Alternative Approaches to Assessing the Performance and Suitability of Yucca Mountain for Spent Fuel Disposal*, EPRI TR-108732, Electric Power Research Institute, Palo Alto CA, November 1998.

NRC, 1999. *Disposal of High-Level Radioactive Wastes in a Proposed Geological Repository at Yucca Mountain, Nevada; Propose Rule, Federal Register*, 64(34), 22 February, 1999.

TYMS, 1995. *Technical Bases for Yucca Mountain Standards*, Committee on Technical Bases for Yucca Mountain Standards, National Research Council, National Academy Press, Washington DC, 1995.



A

APPENDIX A – CONSERVATISMS AND OPTIMISMS IN THE DOE AND EPRI TSPA MODELS

This appendix provides a summary of some of the 'departures from reality' - conservatisms and optimisms (or non conservatisms) - found in the current version of the DOE TSPA-SR models as found in the Analysis Model Reports (AMRs). It also documents some of the major conservatisms and optimisms in IMARC-5. When we use the term 'conservative' we mean that, by adopting a particular parameter value of conceptual model, overestimates of radiological impact or the severity of conditions within the system will be made. The converse defines 'optimistic' or non conservative.

Section A.1 provides the listing of conservatisms and optimisms found in the DOE models. Section A.2 does the same for the IMARC-5 model.

The summary of conservatisms and optimisms in this appendix is not meant to be comprehensive. Rather, the ones listed appeared during the limited review of AMRs and appeared most significant. Thus, there are many other conservatisms, and a few optimisms that have not been listed below.

A.1 Conservatisms and Optimisms Found in DOE's Current TSPA-SR Models

The list compiled in this section is taken from the review of the DOE AMRs as well as from general presentations made by DOE or the M&O.

A.1.1 Future Climate and Net Infiltration

- Average annual precipitation is too high for glacial transition conditions. This is conservative in that it overestimates net infiltration. The M&O relies on ostracode data from distant locations for establishing future climate whereas EPRI relies on more local, and probably more reliable indicators based on Spaulding's work for USGS. In addition, the M&O glacial and monsoon climates have substantial summer precipitation that is not characteristic of past Yucca Mountain glacial climates. Since net infiltration depends on winter precipitation, net infiltration estimates are likely to be closer to EPRI estimates than the average annual precipitation values would suggest. The effect of additional summer precipitation on net infiltration modeling is not well understood. Modern climate net infiltration used by the M&O is lower than other measured/estimated values provided by the M&O, USGS, and others.

A.1.2 Near Field Processes

- **Use of conduction-only heat transfer on the mountain scale in the MSTHM** – This is conservative for temperatures (i.e., it overestimates temperatures), so will be optimistic regarding the time for temperatures to drop to below boiling (so onset of EBS corrosion is artificially delayed).
- **Modeling convection on a north-south cross-section** – The mountain-scale model modeled convection along a north-south cross-section. In three dimensions, the center of the repository is much closer to the edge than it appears to be in a north-south section. As a result, the possibility that edge effects will penetrate to the center of the repository is underestimated by the north-south cross-sectional model. Thus, temperatures are likely overpredicted.
- **Geometric mean of measured fracture permeability** – Permeability is a spatially variable parameter. The hydrologic properties analysis adopts the geometric mean of measured fracture permeability as the baseline value for modeling, and this is the value used in the MSTHM. But the geometric mean may not be the most appropriate average. The permeability value that will correctly predict the flow is the arithmetic mean, which is larger than the geometric mean. Use of the geometric mean will therefore tend to under predict water flows. Therefore, this is optimistic.
- **Surface needle effect** - Water can be forced to seep into drifts when fractures dead-end at a drift with no connections to other fractures that could provide pathways for lateral diversion. This “surface needle effect” is discussed in the seepage modeling report but not included in the numerical calculations. Neglect of the surface needle effect is recognized by the project as being non-conservative with respect to moisture and further work is planned to address it. The surface needle effect does not alter temperatures.
- **Seepage flux into the drifts** – All seepage is assumed to start at the crown of the drift or drip shield so that all groundwater entering the drifts is assumed to contact the EBS barriers. This is conservative since a significant portion of the dripping water may miss or just glance the drip shields or containers.

However, another aspect of seepage into and back out of the drifts may or may not be optimistic in the sense that no changes to near-field permeability due to coupled thermal-hydrologic-chemical processes have been assumed. At present, it is felt that this is a reasonable assumption based on the relevant AMR.

Major assumptions that are conservative with respect to water flux but not with respect to temperature are:

- High inverse-alpha value.
- Neglect of ventilation dry-out - Removal of moisture from the host rock by ventilation is mentioned in reports, but not considered in numerical models. This is conservative with respect to flow since, after closure, it may take longer to rewet the rock immediately surrounding the repository than would be predicted by neglecting this phenomenon.
- Rescaling of time - The times corresponding to temperature fields calculated by the LDTH model are rescaled at each location to correspond to the temperature decay curve calculated by the SMT model. This rescaling reduces the calculated temperature difference between

pillar and drift wall because the calculated package temperatures correspond to a later time when radioactive decay has reduced the heat output. This assumption is thus non-conservative with respect to waste package temperature. It is conservative with respect to moisture because in the real situation the center of the pillar will be cooler than the model predicts and thus will have a greater tendency to drain condensate out of the system.

- Adjustment of thermal loading – The thermal loading in the LDTH model is reduced, based on a comparison between the SMT and SDT models. The main value of this step seems to be that it creates a one-to-one correspondence between the SMT and LDTH temperature curves that allows time to be rescaled without leaving any gaps. Like rescaling of time, this assumption reduces the temperature contrast between waste package and pillar, and therefore it is conservative with respect to moisture and non-conservative with respect to temperature.

Thermal Performance

- **Thermohydrologic model** – The underlying governing equations for flow and heat transfer in TOUGH and NUFT is the same, yet these models have largely been validated against each other. The impacts of any possible model validation problems are paramount in determining the performance of the repository. A clear understanding and benchmarking of computer codes are required. Industry accepted and proven computational tools should be used instead of laboratory-generated, unproven computer codes.
- **Neglect of dependence of radiative heat transfer on drift-wall temperature** - A conduction/radiation model is used in the MSTHM to calculate temperature differences within the drift. Since radiative heat transfer, unlike conduction, is not linear in temperature, the magnitude of temperature differences depends on temperature as well as on the heat output of the packages. Industry accepted and proven computational tools should be used instead of laboratory-generated, unproven computer codes.
- **Latent heat removal by ventilation** – Thermal models include ventilation by simply assuming 70% heat removal during the ventilation period. Ventilation models calculate how much ventilation air is needed to achieve 70% heat removal, considering only sensible heat. Latent heat will also be removed; it is unclear whether the intention is to ventilate the repository at the calculated rates and remove more heat than predicted, or to use the minimum airflow capable of removing 70% of the generated heat.

A.1.3 Engineered Barrier System

- In the EPRI corrosion model, it is assumed that humid air conditions can be established on all corrodable surfaces within the repository while the establishment of aqueous conditions requires that groundwater, in the form of seepage drips, contact the surface. This assumption is consistent with assumptions made in USDOE models and clearly defines that the primary function of the drip shield will be to protect the waste package from seepage drips leading to the evaporative cycles which will establish potentially aggressive aqueous conditions.
- Evaporative cycles on aqueous chemistry and its influence on the relationship between RH and waste package surface temperature. Despite studies the specification of a contact water composition, threshold relative humidity (RH_{thres}) and associated surface temperature is not clearly defined. The value of RH_{thres} will depend on the nature of the hygroscopic salts

introduced into the repository either as soluble groundwater species or as aerosols and dust transported in air during the early period of forced ventilation. Bounding assumptions were made by the USDOE without an understanding how conservative they are.

- The assumption that aqueous conditions can be established at 120°C is conservative, since it shortens the dry-out period when oxidation of the metals will be negligible and lengthens the period over which aqueous corrosion processes can occur.
- Groundwater concentration process will not occur in the absence of seepage drips onto the DS/WP surfaces. Consequently, under the generally prevailing humid air conditions, it is likely that this threshold relative humidity (50%) will be even more conservative.
- Groundwater concentration process will not occur in the absence of seepage drips onto the DS/WP surfaces. Consequently, under the generally prevailing humid air conditions, it is likely that this threshold relative humidity (50%) will be very conservative.
- The USDOE eliminates localized corrosion of the drip shield as a degradation mechanism. Although it is stated that localized corrosion could simply be included by modification of the general corrosion model. In the IMARC model, localized corrosion is not excluded in this fashion.
- The model for hydrogen absorption on the titanium drip shield can be considered very conservative since it assumes that all the hydrogen absorbed during general corrosion will remain in the residual wall thickness and will not be consumed by the consumption of titanium as general corrosion progresses through the drip shield wall. This constitutes a very conservative assumption, since it is highly likely that absorbed hydrogen will be retained at the surface through which it is absorbed and hence consumed (i.e., re-released) as the corrosion process proceeds.
- The EPRI model for crevice corrosion is considerably less conservative in some regards but more conservative in others than the model used by the USDOE. As in the EPRI model, the USDOE assumes that localized corrosion will only occur as a consequence of dripping directly onto the waste package through a failed drip shield. The US DOE's criterion for initiation is not based on a temperature threshold but a potential threshold measured electrochemically (this test process is not designed to provide this threshold). Based on these measurements it is predicted that crevice corrosion will not initiate, a less conservative conclusion than used in this IMARC model.
- The USDOE model for crevice propagation, if it were to initiate, is extremely conservative. This will yield non-mechanistic failures that may allow moisture ingress into the waste package.
- The initiation of stress corrosion cracking (SCC) in the annealed final closure weld is a conservative assumption. Understanding the material properties and the stress-state the waste package will experience can only lead to one conclusion. The probability of SCC initiating is negligible, approaching zero.
- For conservatism, it has been assumed that a waste package under a failed drip shield would essentially be unprotected from dripping water. Therefore, the time to penetrate the outer barrier of the waste package is conservatively calculated. No probabilistic distribution is applied.

- The cladding is assumed to be in an extremely aggressive environment that is considered to be non-realistic. It is assumed that fluoride enters the waste package and comes in contact with only the cladding. Clearly the basket internals would buffer most of the fluoride entering the waste package. In addition for fluoride to enter the waste package, the water flowing through the crack in the waste package would need to be significant. Thereby diluting the concentration of the fluoride, again reducing the fluoride contact. The USDOE also assumes that the fluoride contacts the cladding in a limited area, which is extremely conservative.

A.1.4 Source Term and EBS transport

- The model for the degradation rate of the spent fuel waste form conservatively neglects the potential for reducing conditions and the presence of secondary phases.
- Colloid generation is assumed plentiful with significant amounts of irreversible sorption occurring. Given that the colloid transport model DOE uses is conservative, these assumptions compound the overestimated importance of colloid-aided transport.
- No secondary phase generation is assumed for Np. By including this possibility, Np solubility limits could be lowered. Independent analyses by EPRI suggest that solubility limits could be lowered by about an order of magnitude.
- Release is assumed to begin immediately upon penetration through the container by stress corrosion cracking. This is assumed since there is, theoretically, a water pathway that can be established at that point. However, there is a huge conservatism applied regarding the diffusive and advective pathway inside the breached container. All of the waste form is assumed to be in contact with the inside of the container so that seepage flux can contact the waste form immediately. No film flow or the likelihood of more tortuous diffusive pathways has been considered. These conservative assumptions are likely to vastly overestimate release under these conditions.
- The diffusive barrier presented by the container pedestal and other features have been conservatively ignored. Instead, it is assumed the container is in intimate contact with the invert such that there is no additional resistance to diffusive flux.
- Sorption onto degraded EBS materials and the invert are ignored. See Chapter 13 for a sensitivity study on the magnitude of this conservatism. Ignoring it can increase dose by at least an order of magnitude.
- Evaporation of water from inside the failed container at early times when significant decay heat is still available has been neglected. Analysis presented in Chapter 5, however, suggests this is a minor conservatism.
- Diffusion through the invert has been overestimated by using a bounding diffusivity versus invert saturation correlation. Actual diffusivities at lower saturations may be an order of magnitude lower.

A.1.5 Unsaturated Zone and Saturated Zone Flow and Transport

- Fracture/matrix interaction in both the UZ and SZ are underestimated. These two conservatisms, along with the potential magnitude of the conservatisms, are discussed in

detail in Chapter 7. These include conservatisms with respect to flowing intervals spacing in the SZ, and deliberate inconsistencies in the conceptualization of the UZ versus SZ fractures such that the maximum radionuclide travel times are maintained. It was concluded that UZ travel times are likely underestimated by as much as two orders of magnitude. SZ travel times are also being significantly underestimated.

- No sorption on fracture surfaces in the SZ is assumed. This is conservative – especially since the DOE model is conservative with respect to the amount of fracture/matrix interaction.
- The effective diffusion coefficient in the SZ volcanic blocks is set conservatively low. This prevents even more diffusion from the fractures into the stagnant matrix blocks. Depending on the assumed size of the matrix blocks, fracture flow velocity, and flowing interval spacing, this conservatism ranges from insignificant to significant.
- Colloid filtration in the UZ has been neglected. This is likely conservative. The degree of conservatism is a function of saturation in the UZ, and can be estimated from colloid transport experiments reported in EPRI [1999].

A.1.6 Biosphere

- Use of the critical group concept is meant to be conservative. The critical group is designed to be living at the worst place with respect to the plume location. The average dose rate to the entire population of individuals living immediately downstream will be much lower.
- Fraction of water that is contaminated: 100% of the local groundwater used by the local community is assumed contaminated. This is conservative since it is more likely that at least some of the groundwater needs for drinking, household use, and agricultural purposes will be met from non contaminated areas. The degree of conservatism is unknown, but thought to be large – perhaps an order of magnitude or more.
- In general, the worst chemical form is assumed when estimating radionuclide uptake in humans.
- General conservatisms in a host of parameters throughout the GENII-S code that cause the biosphere dose conversion factors to be overestimated.

A.1.7 Volcanism

- Selections of eruptive type overly bounding. The violent strombolian phase should not be assumed in all cases. Volcanic behavior in the Yucca Mountain area is more similar to the Hawaiian Islands than the Cascade volcanoes type of volcanoes, e.g., Mt. St. Helens. In terms of their behavior of the local Yucca mountain volcano's, the eruptions can be regarded as intermediate in character between Plinian and Strombolian. For example, the median and maximum magma conduit diameters are based on data from the much larger volcanoes than would be expected in the Yucca Mountain vicinity. Dose consequences are very sensitive to conduit diameter.
- Magma contact temperatures, studies show that magma temperature decreases by 40% when contacting objects. This leads to a reduced waste package temperature and waste form contact temperature. However, no credit for these processes in reducing magma temperatures was considered. Thus, more container damage than might otherwise occur may be predicted.

- Magma viscosity and velocity are over estimated. This assumption is bounding since it is assumed that sufficient magma enters the emplacement drift to contact between 6 to 18 waste packages and move them around causing the waste packages to fail.
- Waste form particle size assumption very conservative. When the waste form is exposed to the erupting magma it is assumed that the spent fuel is pulverized into very fine particles. The shearing forces involved in magma eruption are unlikely to be able to cause enough grinding of the relative hard ceramic fuel to actually pulverize the majority of the fuel into a fine powder. This is conservative because a fine powder is more easily dispersed long distances.
- The fuel particles are assumed to be on or near the top of all of the magma and eruptive material as it falls back to earth. This assumption is conservative since the majority of the dose from the eruptive scenario is via the inhalation pathway. Waste buried deeper within the fallen ash is less likely to be resuspended by the wind.
- A realistic wind distribution should be taken into consideration. As it stands, the recorded wind directions are being ignored. The present approach is to conservatively assume the wind always blows toward Amargosa Valley, thereby ensuring the ash fall lands on the greatest local population. The current approach is somewhat optimistic in that winds aloft are usually of higher speed.
- In general, the volcanism evaluation assumes the most bounding value for each parameter. A Risk Informed process should be correctly applied.
- A magma conduit is always assumed to be centered on a drift. This is likely to be conservative since a conduit not centered on a drift should intersect less waste containers.
- All drip shields, containers, and other EBS components are assumed partially or completely destroyed such that the entire inventory of the waste package is available for immediate release. This is conservative.
- The major faults on either side of the repository have the potential to divert any magma around the repository. This has been conservatively ignored.

A.2 Conservatism/Optimisms in IMARC-5

A.2.1 Climate Scenarios

- We assume a “greenhouse” climate begins immediately. This scenario has higher net infiltration values than the present “interglacial” climate.
- We assume a constant “full glacial maximum” climate beginning 2,000 years after repository closure. Thus, this assumption is conservative in that higher infiltrations allow for more radionuclide release. For those solubility-limited radionuclides, however, a higher flow rate associated with the full glacial maximum may result in a slight lowering of the concentrations such that this assumption will be slightly optimistic for those radionuclides. It may be optimistic in the sense that, by maintaining a constant climate, we do not alter the water table elevation after 2,000 years. Any rapid water table rise might cause a temporary “flushing” of radionuclides out of part of the UZ that was swamped by the water table rise.

- IMARC modeling uses Spaulding climate characterizations based on local paleoclimate information. Climates are markedly different from those used in M&O analyses. Because they are lower in average annual precipitation, IMARC may incorporate optimism (see net infiltration comments below).

A.2.2 Net Infiltration Issues

- IMARC calculated net infiltration is higher than M&O for modern climate; and is equal for glacial/glacial transition conditions. The IMARC mean net infiltration estimate is in the range of other site estimates while the M&O value is lower.

A.2.3 Near-Field Coupled Processes Issues

- Rather than taking a range of 'flow focusing' values for the distribution of groundwater flow at the repository horizon, we assign equal probabilities to the ends of the flow focusing distribution suggested by the M&O. Since it is likely that either one end or the other of the flow focusing distribution will result in the worst case results, assigning a 50% probability to each end probably overestimates dose consequences. Thus, this assumption is likely to be somewhat conservative.

A.2.4 EBS Drip Shield, Container, and Cladding) Degradation Issues

- Pure NaNO_3 governs the boiling point on surfaces with evaporites. Conservative since this species has the highest boiling point, and a more plausible mixture of species would have a lower boiling point. Thus the presence of liquid water is assumed to occur as high as 120°C . In all likelihood, liquid water will not be present except at lower temperatures. The effect of this conservatism is to initiate corrosion at earlier times and higher temperatures.
- The general corrosion rate on drip shields exposed to seepage drips will be higher than on those free of drips. This is likely to be more realistic than the more conservative DOE assumption that non-dripping corrosion is just as fast as dripping corrosion.
- We use a uniform distribution of $[0, 0.04]$ for f_h , the fractional efficiency for hydrogen absorption into Ti-7 during corrosion reactions involving water. This is conservative since plausible arguments can be made that hydrogen absorption will not occur. Allowing for hydrogen absorption allows the possibility of HIC in Ti-7.
- All hydrogen initially absorbed into the Ti-7 remains in the base metal, rather than some being removed during general corrosion. This is conservative since it is likely that the majority of any hydrogen absorbed into the Ti-7 will be subsequently removed from the base metal during general corrosion. This assumption also leads to another conservative conclusion, that the hydrogen is immediately dispersed throughout the Ti-7, rather than being concentrated near the corrosion front.
- Failure of the drip shield by HIC is assumed to occur at the time the hydrogen concentration equals the 'critical' concentration. This is conservative lower threshold and it is likely that HIC would occur until higher hydrogen concentration levels are achieved.
- We neglect local HIC due to the possibility of galvanic contact between Ti-7 and the carbon steel used in the roof support after the roof support collapses. This is optimistic. It is unlikely

that this will be a significant effect, but, to date, no meaningful data is available to quantitatively assess the consequences. On the whole, the conservatism employed in the IMARC model for HIC of Ti-7 are considered to outweigh this potential optimism.

- For SCC of the waste package, we use the Stress Intensity Threshold model (STM) with a threshold stress intensity factor of $8 \text{ MPa m}^{1/2}$. This is conservative since this parameter value represents a near-bounding value.
- The probability of having a radially oriented flaw in the lid weld is 0.01. This is conservative based on one set of data. This results in 25% of the waste packages having a radial flaw in the outer lid.

A.2.5 Source Term Issues

- The COMPASS model calculates the solubilities and fluxes based on the saturation values in each of the compartments. The saturation in the container compartment is 20%. i.e., water is assumed to fill 20% of the entire cavity inside the container. For a flow-through scenario, like the one being used here, it may be that the container saturation should be less than 1%. For a diffusion-only scenario, where containers are assumed filled with only humid air, the effective saturation will be a fraction of one percent. This conservatism is likely to cause the release rate of potentially solubility-limited species (e.g., Np, U, Pu, and maybe Se) to be overestimated since more water is assumed available into which dissolution can occur, than would actually be expected.
- We don't yet consider colloid release or any disruptive scenario. This is optimistic. The degree of optimism is not thought to be large since the M&O colloid transport model – itself a somewhat conservative model – shows only limited radiological importance to colloid transport.
- The current IMARC conceptualization ignores diffusive release from the EBS in zones without active dripping. This is an optimistic assumption. Sensitivity studies we conducted show that in most, but not all instances, diffusion-only from non dripping areas can be neglected. For some high solubility, low sorbing species, however, diffusion-only transport was calculated to be significant. Our calculations for diffusive release, however, are conservative in the sense that we assume excellent diffusive connection between the waste container, the invert, and the surrounding rock – condition that is not likely to be met, but is difficult to rule out completely. It is felt that the current M&O model of diffusive release is very conservative.

A.2.6 Unsaturated Zone (UZ) and Saturated Zone (SZ) Flow and Transport Issues

- UZ transport model: conservative. Recent, alternative analysis by the M&O reviewed in Chapter 7 suggests travel times through the UZ are longer than the IMARC model predicts.
- Dilution in UZ: non-conservative early; realistic when there are many container failures. Most of the conservatism is diminished by the time the plume reaches 20 km. See pages 7-15 to 7-17 in EPRI [1998].

A.2.7 Biosphere Issues

- Use of a critical group with fairly high consumption rates for a variety of foodstuffs. Conservative in the sense that it is unlikely that: (1) all of the foodstuffs assumed to have been grown using groundwater with the highest contamination levels at the accessible environment will actually have been grown under such conditions; and (2) assuming all the foodstuffs *are* grown using groundwater at the highest contamination levels, any one individual will actually consume all of these particular foodstuffs. While the regulator requires the use of a critical group concept (to make sure almost all individuals are likely to have doses no higher than that of the average individual in the critical group), this required conservatism should not be forgotten by decision makers evaluating the appropriateness of Yucca Mountain as a HLW disposal site.
- Due to lack of resources, the parameters going into the IMARC biosphere model have not been treated with uncertainty. Yet it is known that significant uncertainties in some of these parameters exist. Rather, where significant uncertainties exist in these parameters, discrete values have been chosen from that end of the range of literature values that will result in higher dose conversion factors. This is discussed in detail in EPRI [1996]. The conclusion of this exercise, considering the full range of the parameters reviewed in EPRI [1996] was that, depending on the particular radionuclide dose conversion factor, the ‘actual’ dose conversion factor could be up to about one order of magnitude larger and up to four orders of magnitude smaller than the dose conversion factors selected for use in IMARC.³² While it is appropriate to use conservative parameter values when uncertainties are poorly known, it is not appropriate to use the absolutely highest possible combination of parameter values if one wishes to adopt a risk-informed approach. Rather, EPRI advocates the sort of ‘reasonably bounding’ approach used here for biosphere modeling.

A.3 Summary of Sensitivity Studies on Waste-Form Saturation and Diffusive Release for Varying Near-Field Rock Lengths

In this sensitivity study, radionuclide EBS release rates are calculated with the waste-form water saturation and the near-field rock length as sensitivity parameters. The purpose of these studies is to estimate the quantitative effect of assuming: (1) a large amount of water is inside the waste container in the IMARC source term model; and (2) diffusive release in the IMARC model is negligible.

The “waste-form water saturation” is defined as the water saturation of the “waste compartment”. In EPRI compartment-model source-term, the “waste compartment” represents waste solid and void space inside the canister. Hence, the “waste-form saturation” determines the amount of water inside the failed waste canister.

Once liquid water flows through a breached waste canister, some amount of water is believed to stay inside the canister and forms a continuum pathway for radionuclides to escape. This water amount defines the liquid water volume that first receives dissolved radionuclides. Within this volume, some radionuclides are subject to solubility limit, depending on the magnitude of this

³² The dose conversion factors for some radionuclides will have a narrower range than this.

volume. This volume determines aqueous concentrations of soluble radionuclides and the total amount of dissolved nuclides for solubility-limited nuclides. Therefore, this quantity is an indispensable parameter in PA calculations.

The amount of water inside the waste package, however, is difficult to quantify, and depends on conceptual models. For example, in M&O’s model, a thin film of water liquid with 1-mm thickness is assumed to cover the entire waste-solid surface. In order to determine radionuclide aqueous concentrations, the quantitative knowledge on waste solid surface area is required.

In EPRI IMARC-5 calculations, a waste-form saturation of 0.2 is assumed. Together with total void volume inside the canister, aqueous concentrations of radionuclides can be determined. In unsaturated repository, assuming that 20% of void volume is filled with water will be conservative, especially in humid air, and no-seepage conditions. The question of how this parameter will affect PA results motivates the first sensitivity study to be summarized in this section.

Another potentially important parameter used in IMARC source-term calculations is the “length of near-field host rock”. This parameter defines the distance from the EBS edge to the rock fracture entrance where a zero radionuclide concentration is considered reasonable due to advection. Clearly, this parameter should be the distance from the EBS edge to the nearest fracture along the flow zone. With heterogeneous rock and non-uniform distributions of fractures, it is unlikely that this parameter can be the same for all waste packages. How this parameter may impact the EBS release rate is the motivation for sensitivity study on the near-field rock length, to be discussed below.

A.3.1 Sensitivity Cases

Six cases have been constructed for the source-term calculations using the IMARC-5 source term submodel, COMPASS2000. These cases and the reference case using IMARC-5 data (called IMARC) are defined in Table A-1. In these cases, the waste-form saturation varies from 0.001 to 0.1, and two near-field rock lengths of 1 m and 20 m are used.

Table A-1
Cases in the Sensitivity Study

Parameters	IMARC	Case 1	Case 2	Case 3	Case 4	Case 5	Case 6
Waste-form water saturation S_{waste}	0.2	0.001	0.01	0.1	0.001	0.01	0.1
Near-field rock length [m] δ_r	5.0	1.0	1.0	1.0	20.0	20.0	20.0

Radionuclides considered in this study include:

Se-79, Tc-99, I-129,

Pu-239 → U-235 → Pa-231,

Np-237 → U-233 → Th-229, and

Pu-242

Moderate parameters used in IMARC calculations are adopted for data other than two sensitivity parameters in this sensitivity study. For illustration, solubilities of the radioelements are listed in Table A-2.

**Table A-2
Solubility Data**

	Se	Tc	Pu	U	Np	Th	Pa
Solubility [mol/l]	10^2	10^3	2×10^8	4×10^6	3×10^5	3×10^9	3×10^5

A.3.2 Results with Diffusion-only Transport

The calculations are conducted with diffusion-only transport mechanism. Release rates of all nuclides increase as the near-field rock length decreases. A shorter intact rock presents a smaller mass transfer resistance – enhancing radionuclide release rates from the EBS.

Response of release rates to different waste-form saturations varies amount radionuclides. To demonstrate, results of some nuclides will be presented and discussed below.

Se-79

The release rate of Se-79 is not sensitive to waste-form water saturations, as shown in Figure A-1. Se-79 has a relatively high solubility (see Table A-2). Varying waste-form saturation does not alter the amount of dissolved Se-79. However, for a given dissolved amount of Se-79, increasing saturation (or liquid volume) decreases its aqueous concentration, which has a negative impact on diffusive flux. On the other hand, increasing saturation increases effective diffusion coefficient for nuclides to migrate out of the waste compartment in the absence of advection, which is a positive impact to diffusion. Overall, the two opposite impacts on diffusion of Se-79 out of the waste canister are just canceled. This explains why Se-79 release rates are insensitive to the waste-form water saturations.

For the same reason, release rate of soluble/ non-sorbing I-129 is also insensitive to waste-form saturations.

It can be seen that the IMARC-5 case result is enveloped by these sensitivity case results.

Pa-231

Similar to Se-79, release rate of Pa-231 is shown not sensitive to waste-form water saturations (see Figure A-2). Although Pa-231 has a lower solubility (Table A-2) compared with Se-79, it is unlikely that Pa-231 could reach solubility inside the waste package due to its initially small inventory (3×10^9 mol) and fast decay rate. Hence, the release of Pa-231 out of the waste package is controlled by in-growth rate from parent nuclide U-235.

The Pa-231 release rate predicted by the current IMARC data is in between of those calculated by the sensitivity cases.

Pu-239

As shown in Figure A-3, Pu-239 release rate increases as the waste-form water saturation increases. Sharing a low solubility with isotope Pu-242, aqueous concentration of Pu-239 inside the waste canister reaches its solubility limit. When water saturation increases, the aqueous concentration does not change. The effective diffusion coefficient, however, does increase as the saturation increases, which increases diffusive flux out of the waste package. The net effect, hence, is to increase the release rate in the absence of advection.

The similar behavior is also observed in the release of Pu-242 who shares solubility with Pu-239, U-235 and U-233 who share the same solubility, and Th-229 who has an extremely low solubility limit. For these nuclides, the IMARC release rates are higher than most sensitivity case release rates.

Note, although aqueous concentrations for these nuclides are limited by solubility, the total amount of dissolved nuclides increases with the waste saturation, resulting in a narrower release curve. Because diffusion-only transport greatly delays radionuclide release, for most nuclides, the complete release curve cannot be observable within a million years.

Np-237

Figure A-4 shows that solubility-limited Np-237 release rate is sensitive to the waste-form water saturation, a behavior similar to Pu-239. Compared with Pu-239, Pu-242, U isotopes and Th-229, Np-237 is less sorbing and moderately constrained by solubility limit (see Table A-2). Faster mass transfer removes previously sorbed and precipitated nuclides more rapidly. For less sorbing and/or less solubility-limited nuclides, there is a less amount of nuclides to be discharged from solid/ or solid phase due to enhanced mass transfer. This explains why Np-237 release rate is not as sensitive as Pu-239, to the waste-form water saturation.

Similar behavior is also observed for moderately solubility-limited and non-sorbing Tc-99. For these nuclides, the corresponding IMARC release rates are higher than most sensitivity case results.

A.3.3 Results with Both Diffusion and Advection

Results with advection and diffusion under varying waste-form saturation and near-field rock length are shown in Figures A-5 through A-7 for a few typical nuclides: Se-79, Pu-239, and Np-237. Overall, with advection, the release rates are controlled by advective rate, and hence, are not sensitive to both the waste-form saturation and the near-field rock length.

Figures A-5 and A-6 show that the release rates are not sensitive to both parameters for soluble/less-sorbing Se-79 and solubility-limited/less-sorbing Np-237. For solubility-limited and sorbing Pu-239, its release rate is only slightly increased when increasing the waste-form saturation, as shown in Figure A-7.

Because advection is so dominant, intact rock length does not impact the EBS release rates for all nuclides.

The degree of optimism in the IMARC-5 calculations with respect to neglecting diffusion-only release depends on the radionuclide being considered. It is not always possible to make the case the diffusive transport is negligible. This is because diffusive release can, theoretically, occur from 100% of the waste packages, whereas advective release is occurring from, on average, about 4% of the waste packages at very long times. Thus, diffusive fluxes, at long times, would have to be $\ll 4\%$ of the advective fluxes to say diffusive release is negligible. Depending on which figure one considers in this appendix, one can or cannot reach this conclusion. Examples of the relative importance of diffusive release by radionuclide is as follows:

- Se-79: comparing Figure A-1 (diffusion only) with Figure A-5 (advection and diffusion combined), diffusive releases *from a single package* range from $\sim 1\%$ (20 meter rock diffusion distance) to $\sim 10\%$ (1 meter rock diffusion distance) of total releases. Thus, diffusive releases *are* potentially important for the suite of parameters and diffusion models used in IMARC-5. However, one would expect that diffusive release would not contribute much more than about a factor of 4 more than advective release.
- Np-237: comparing Figure A-4 with Figure A-6, diffusive releases from a single container vary from about 0.1% to about 5% of total releases. Thus, diffusive release of Np seems negligible.
- Pu-239: comparing Figure A-3 with Figure A-7, diffusive releases are always less than about 5%, so again, Pu diffusive releases are negligible.

It is likely, then, that diffusive release from other high solubility species (e.g., Tc and I) would not be negligible, whereas other solubility-limited species would have negligible diffusive releases. Furthermore, it is likely that the diffusive distances to the nearest flowing fracture for the containers in the 'dry' zones are likely to be longer than the distance to the nearest flowing fracture in the 'wet' zones (in which advection takes place). This would also tend to reduce the importance of diffusion-only releases from these 'dry' zones that has been neglected in IMARC-5. Finally, the assumptions we make in IMARC-5 about how well connected the diffusive pathways are through the entire container to and through the invert are quite conservative. If these conservatisms are taken into account, diffusive release would become even less important. Given that the potential diffusive releases we neglected in IMARC-5 seem to be

less than an order of magnitude, it seems, then, that neglecting diffusive release from the 'dry' zones is not a significant optimism.

A.3.4 Summary

This sensitivity study reveals that with advection, the EBS release rates for all nuclides are not affected by the magnitude of the waste-form water saturation and the near-field rock length if the system is defined using moderate IMARC data.

With the absence of advection, the EBS release rates of all nuclides are sensitive to the length of intact near-field rock. The release rate is almost inversely proportional to the near-field rock length.

In the absence of advection, whether or not the release rate is sensitive to the waste-form saturation depends on the solubility of the nuclide. While soluble nuclides are not, solubility-limited nuclides are, sensitive to this parameter. This sensitivity can be further aggravated if the nuclide has a high sorption coefficient.

This sensitivity study reveals that using the current IMARC value for the waste compartment saturation, the EBS release rates could be overestimated by several orders of magnitude, primarily, for sorbing and solubility-limited nuclides. If considering an intact near-field rock longer than the currently assumed in IMARC calculations, the release rate could also be overestimated.

A.4 References

EPRI, 1996. Smith, G. M., Watkins, B. M., Little, R. H., Jones, H. M., and Mortimer, A. M. Mortimer, *Biosphere Modeling and Dose Assessment for Yucca Mountain*, EPRI TR-107190, Electric Power Research Institute, Palo Alto CA, December 1996.

EPRI, 1998. Kessler, J. H., McGuire, R. K., Vlasity, J. A., Long, A., Childs, S., Ross, B., Schwartz, F., Shoesmith, D., Kolar, M., Apted, M., Zhou, W., Sudicky, E., Smith, G., Kozak, M., Salter, P., Klos, R., Venter, A., Stenhouse, M., Watkins, B., and R. Little, *Alternative Approaches to Assessing the Performance and Suitability of Yucca Mountain for Spent Fuel Disposal*, EPRI TR-108732, Electric Power Research Institute, Palo Alto CA, November 1998.

EPRI, 1999. Kaplan, D.I., and A. P. Gamerdinger, *Colloid Transport and Deposition in Water-Saturated and Unsaturated Sand and Yucca Mountain Tuff*, EPRI TR-110546, Electric Power Research Institute, Palo Alto CA, December 1999.

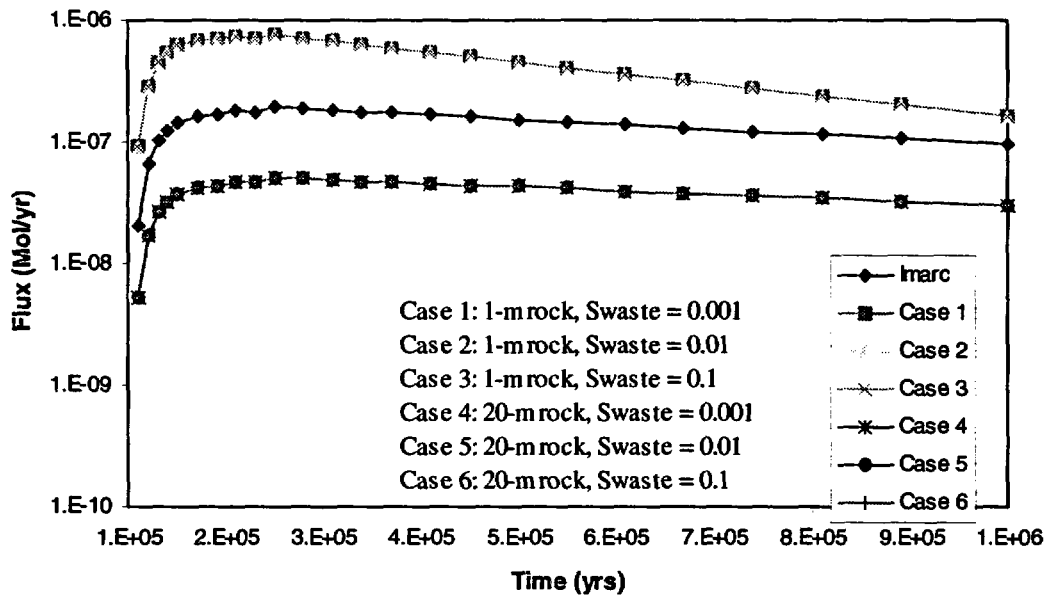


Figure A-1
Sensitivity study results for Se-79 without advection

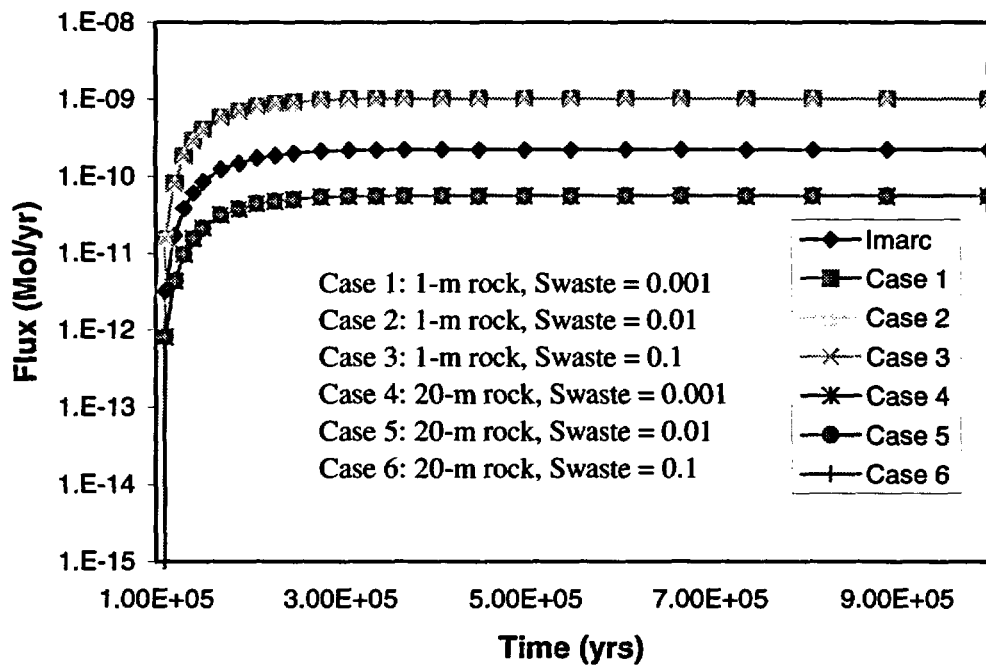


Figure A-2
Sensitivity study results for Pa-231 without advection

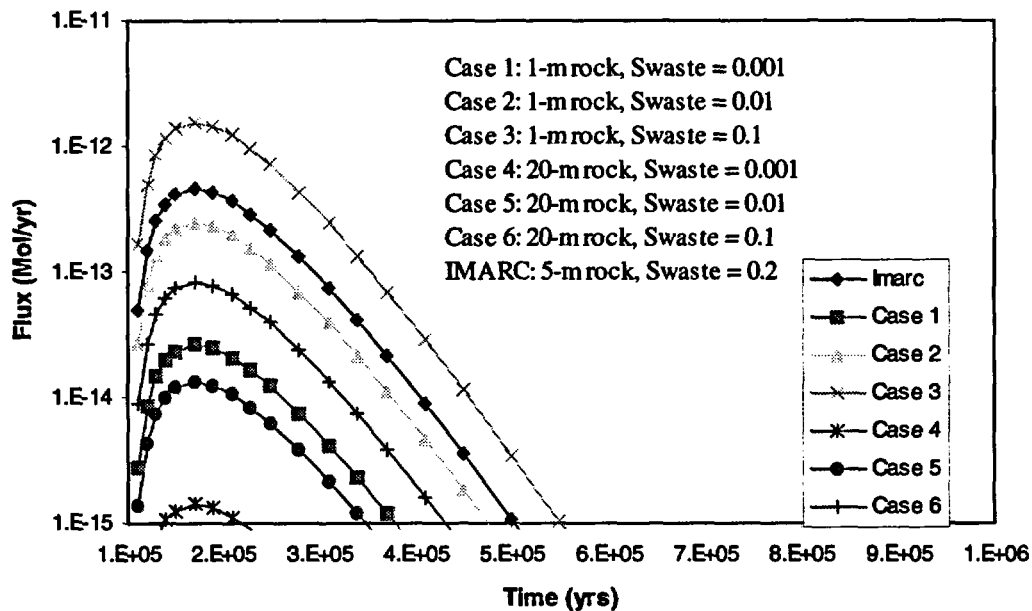


Figure A-3
 Sensitivity study results for Pu-239 without advection

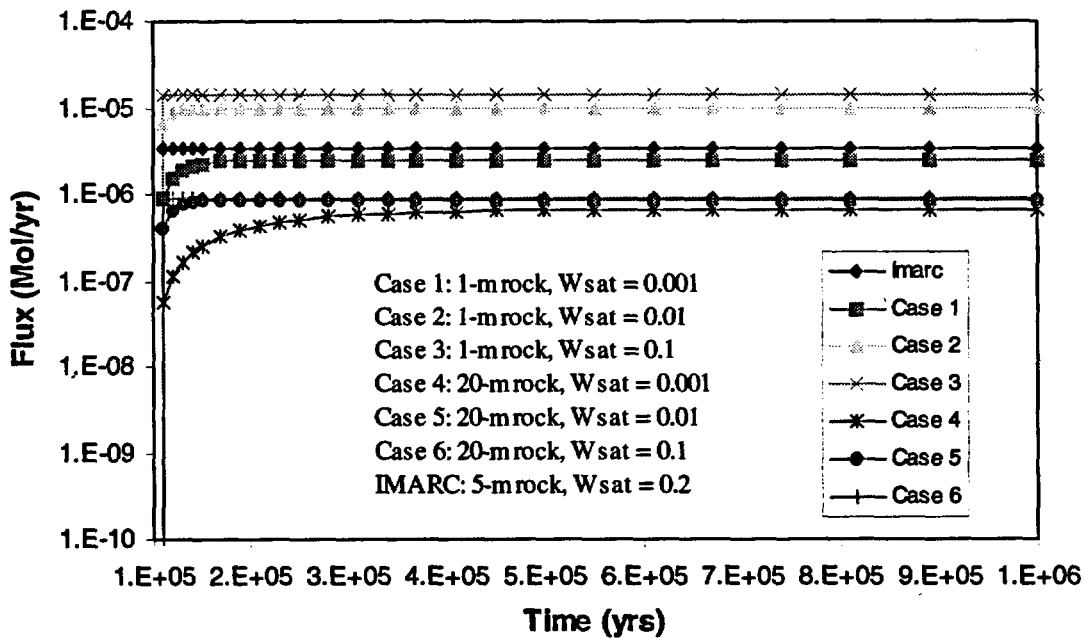


Figure A-4
 Sensitivity study results for Np-237 without advection

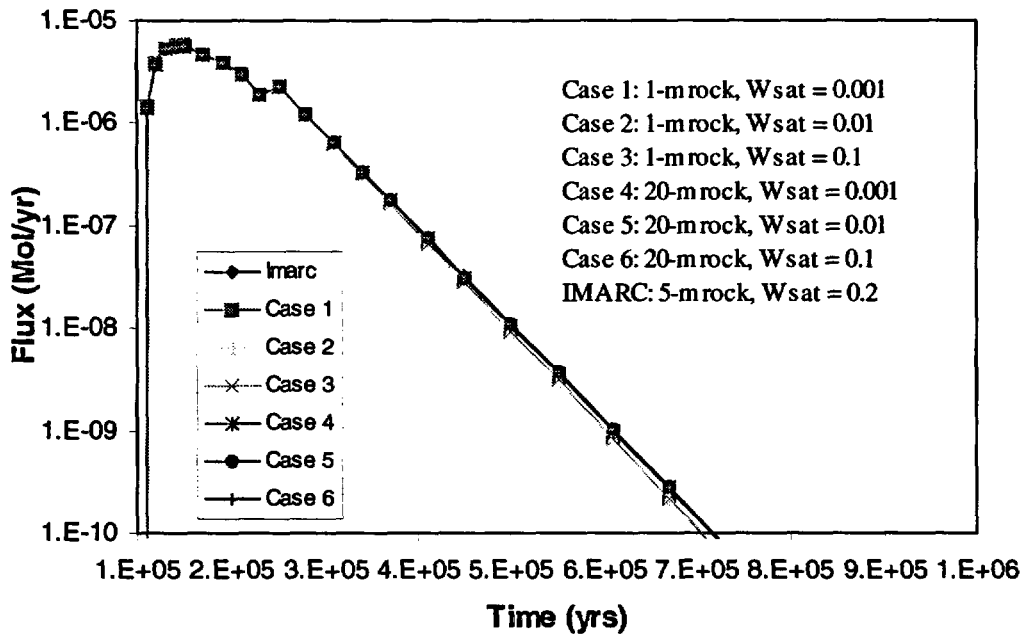


Figure A-5
Sensitivity study results for Se-79 with advection

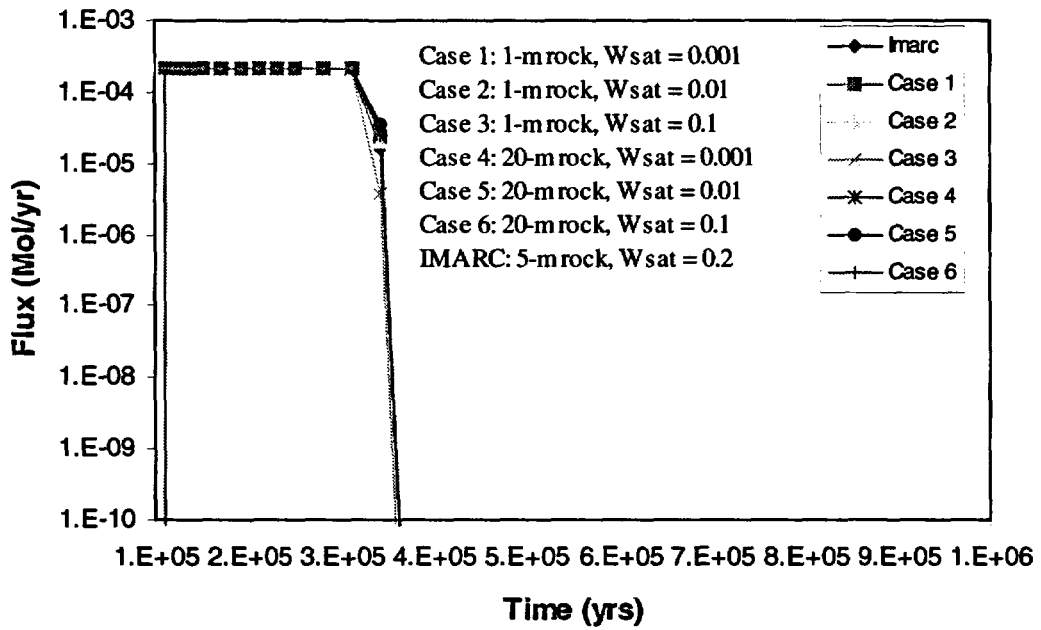


Figure A-6
Sensitivity study results for Np-237 with advection

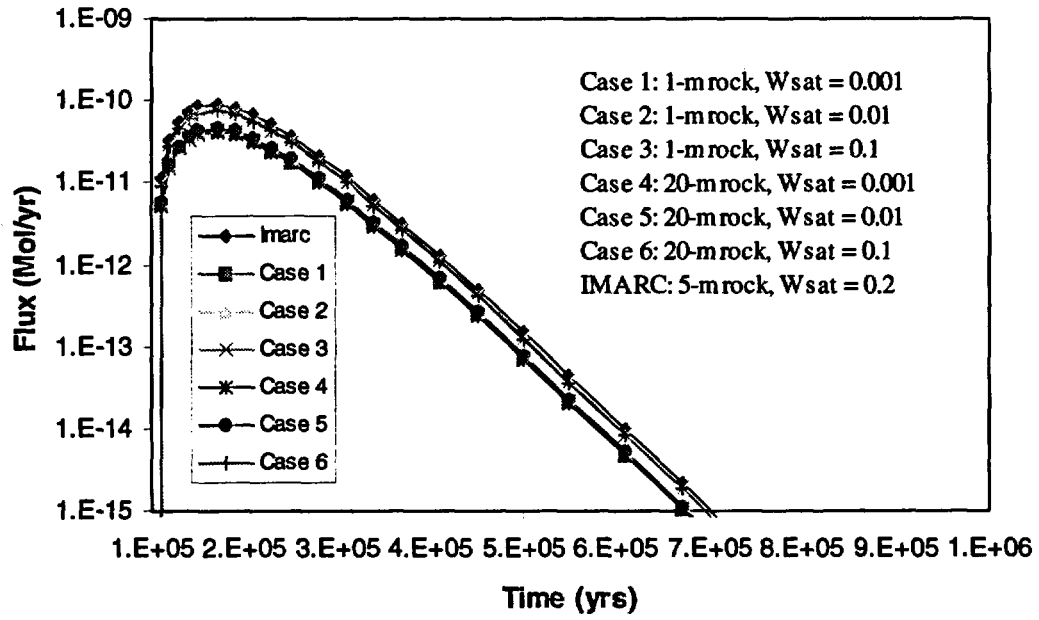
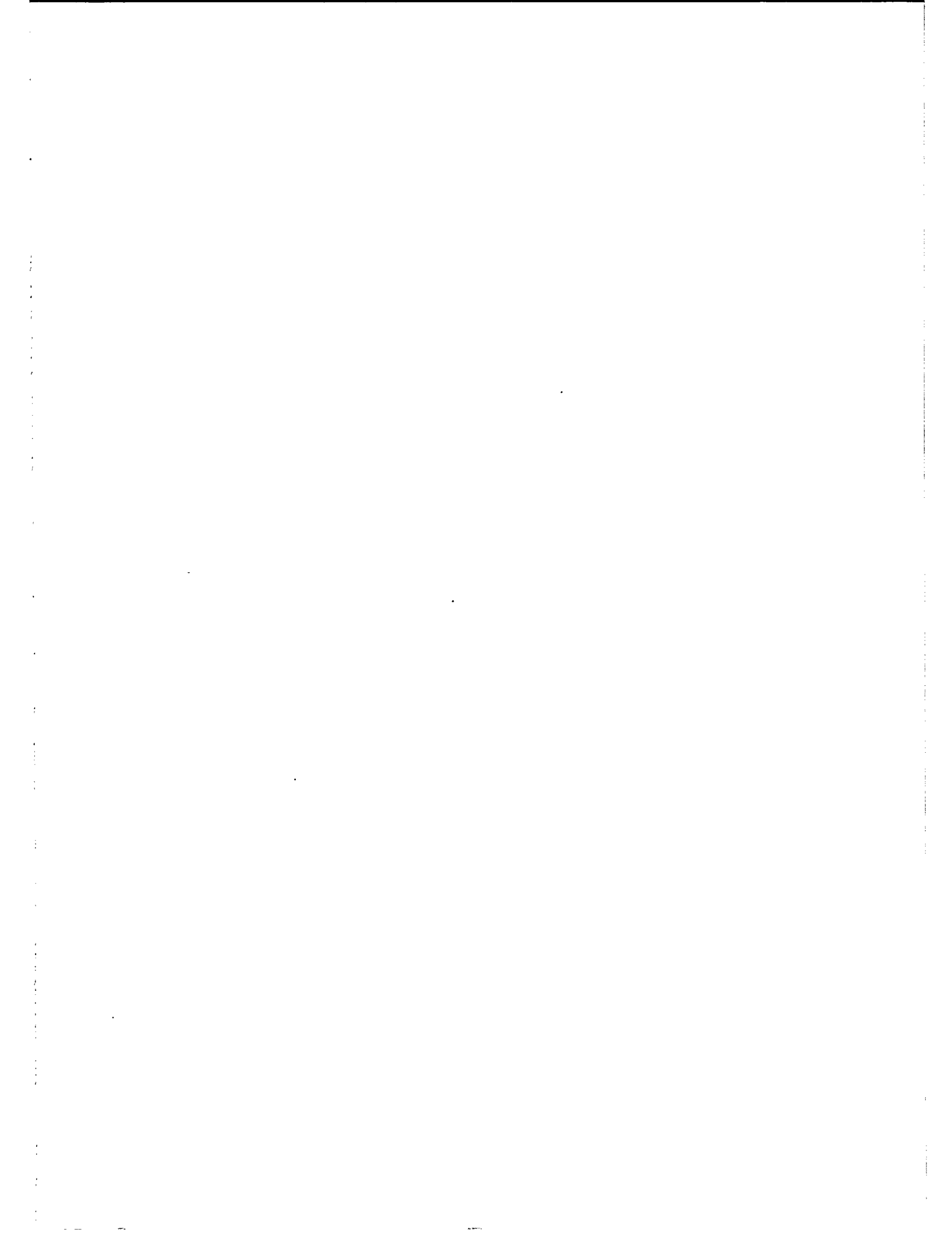


Figure A-7
Sensitivity study results for Pu-239 with advection






About EPRI

EPRI creates science and technology solutions for the global energy and energy services industry. U.S. electric utilities established the Electric Power Research Institute in 1973 as a nonprofit research consortium for the benefit of utility members, their customers, and society. Now known simply as EPRI, the company provides a wide range of innovative products and services to more than 1000 energy-related organizations in 40 countries. EPRI's multidisciplinary team of scientists and engineers draws on a worldwide network of technical and business expertise to help solve today's toughest energy and environmental problems.

EPRI. Electrify the World

© 2000 Electric Power Research Institute (EPRI), Inc. All rights reserved. Electric Power Research Institute and EPRI are registered service marks of the Electric Power Research Institute, Inc. EPRI. ELECTRIFY THE WORLD is a service mark of the Electric Power Research Institute, Inc.

 Printed on recycled paper in the United States of America

1000802